

Electrochemical Processing of Metal Chalcogenides in Deep Eutectic Solvents

Thesis submitted for the degree of
Doctor of Philosophy
at the University of Leicester

By

Francesca Rose Bevan

Department of Chemistry
University of Leicester
August 2019



UNIVERSITY OF
LEICESTER

Electrochemical Processing of Metal Chalcogenides in Deep Eutectic Solvents

Abstract

The increased need for metals in all aspects of life has resulted in attempts to make both primary extraction and secondary recycling of metals more efficient. This project investigates the use of DESs as an alternative to aqueous solutions for the dissolution of metal chalcogenides specifically, both in the form of minerals and synthetic semiconductors. The metals studied include silver, cadmium, zinc and lead with the biggest focus on copper. These compounds exhibit a wide range of properties and ultimate applications. Cd and Zn selenides and tellurides are important compounds in the ever-growing solar energy industry due to their small band gaps and high conductivities. Copper, in particular the sulphide minerals are an important source of Cu which is one of the most used metals worldwide.

This study has demonstrated a novel method of investigating the electrochemical properties of minerals in DESs using paint casting. The currents observed are semi-quantitative for the metal content of the mineral. Signals for both the metal and the chalcogenide could be distinguished in the voltammetry and these were similar to those for the individual components. The electrochemical signals for the minerals were similar to those for the pure compounds.

Numerous sulfide, selenide and telluride compounds were studied in both the pure and mineral forms. It was found that during bulk electrolysis both components were solubilised, the speciation of the metals in solution were generally identified using UV-Vis spectroscopy coupled with EXAFS analysis. In most cases the metal speciation was dominated by the chloro-complexes and the chalcogenide was oxidised to an oxygen containing species. In all cases the solubilised metals could be recovered electrochemically by bulk electrolysis without cross contamination from the chalcogenide. The final part of the study showed that copper could be selectively won in a pure state from complex minerals like chalcopyrite.

Publications

Parts of this work have already been published in the following paper:

- Abbott, A. P., Bevan, F. B., Baeuerle, M., Harris, R. C., Jenkin, G. R. T., (2017) Paint Casting: A Facile Method of Studying Mineral Electrochemistry, *Electrochem. Comm.*, **76**, 20-23 (data in Chapter 3).
- Anggara, S., Bevan, F., Harris, R. C., Hartley, J. M., Frisch, G., Jenkin, G. R. T., Abbott, A., (2019) Direct Extraction of Copper from Copper Sulfide Minerals using Deep Eutectic Solvents, *Green Chem.*, **21**, 6502-6512 (data in Chapter 3 & 5)

Parts of this work have also been presented in oral and poster form at the following conferences:

- Mineral Processing with Deep Eutectic Solvents (oral presentation), *26th EUICHEM on Molten Salts and Ionic Liquids*, 3rd to 8th July 2016, Vienna.
- Mineral Processing with Deep Eutectic Solvents (oral presentation), *21st Meeting of the ELECTROCHEM conference series*, 17th to 19th August 2016, Leicester.
- Mineral Processing with Deep Eutectic Solvents (oral and poster presentation), *Midlands Electrochemistry Group Meeting (MEG)* 26th April 2017.
- Mineral Processing with Deep Eutectic Solvents (poster presentation) *STEM for Britain*, 12th March 2018, London.

Statement of Originality

The experimental work in this thesis has been carried out by the author in the material centre at the University of Leicester between October 2015 and August 2019. The work has not been submitted, and is not presently submitted, for any other degrees at this or any other university.

Signed.....

Date.....

**Material Centre
University of Leicester,
University Road,
Leicester, LE1 7RH.**

Acknowledgments

I begin by thanking my supervisors, Andy Abbott, Gawen Jenkin and Dan Smith for your guidance throughout my project. I have had a lot of opportunities since being at Leicester and I need to thank Andy for not only supporting those opportunities but encouraging me when I did not think I had the confidence. I must also thank NERC for funding the work in this project.

There are several people across both geology and chemistry departments that have helped me throughout my PhD, Dr. Tom Knott and Lin Marvin from geology have given me so much guidance over the four years so thank you. I also want to thank everyone in the materials centre for making my time there enjoyable, there are too many of you to mention personally but I hope you know who you are. I want to give special thanks to Dr. Jenny Hartley, although you only arrived back in Leicester in my final year, I could not have finished without your guidance. I would also like to thank Syahrie Anggara for his hard work and huge smile during his time at the materials centre.

There are a few people who I need to give special thanks to, for supporting me with writing tips and proof-reading in the final stages. Natasha Leo, Dr. Andrea Severson and Graham Bevan you have all helped in so many ways, even if you live thousands of miles away!

Finally and most importantly, my family. I want to thank every member of my family for surrounding me with love and support through my entire life. Mum, Dad and Georgina, thank you for always being there for me, celebrating with me and picking me up when I fail. I hope you know how much you help and how grateful I am for everything. James, my partner and best friend, I do not even know where to start thanking you, you have believed in me and encouraged me every step of the way. From listening to every presentation, proof reading every poster and helping brainstorm cell designs! I quite simply could not have done this without you.

This thesis is dedicated to Jacqueline Bevan, my wonderful Nanny Bevan, thank you for watching over me while I was writing. Seeing you cooking and dancing around the kitchen in your lab coat all those years ago must have inspired me.

Contents

Abstract	ii
Publications	iii
Statement of Originality	iv
Acknowledgements	v
Contents	vii
Abbreviations	xi

Chapter 1: Introduction

1.1 Overview	2
1.2 Chalcogens and chalcogenides	4
1.2.1 Chalcogen Redox Chemistry	4
1.2.2 Chalcogenide Minerals	13
1.3 Metallurgy and the Environment	14
1.4 Chalcogenide Processing	18
1.4.1 Selenium and Tellurium Processing	20
1.5 Solvometallurgy	22
1.6 Ionic Liquids and Deep Eutectic Solvents	24
1.6.1 Properties of DESs	28
1.6.2 Metal Processing with ILs and DESs	30
1.6.3 DES viscosity	31
1.7 Research Objectives	32
1.8 References	34

Chapter 2: Experimental and Methodology

2.1 Materials	46
2.1.1 Deep Eutectic Solvent Preparation	47
2.2 Electrochemical Methods	47
2.2.1 Cyclic Voltammetry	49
2.2.2 Chronopotentiometry	52
2.2.3 Chronocoulometry	52
2.3 Bulk Dissolution	53

2.3.1 <i>UV-Vis</i>	54
2.3.2 <i>ICP-MS</i>	54
2.3.3 <i>EXAFS</i>	55
2.4 Recovery	56
2.4.1 <i>EDX</i>	57
2.4.2 <i>XRD</i>	58
2.4.3 <i>Scaled up recovery</i>	59
2.5 References	61

Chapter 3: Electrochemistry of Copper Chalcogenides

3.1 Introduction	64
3.1.1 <i>Metallurgy of copper ores</i>	65
3.1.2 <i>Copper reprocessing</i>	69
3.1.3 <i>Aims</i>	70
3.2 Paint Casting	71
3.2.1 <i>Paint casting sulfur and sulfides</i>	72
3.2.2 <i>Paint casting copper sulfides</i>	77
3.2.3 <i>Quantifying paint casting</i>	79
3.2.4 <i>Effect of water</i>	85
3.3 Electrochemistry of copper sulfide minerals	86
3.3.1 <i>Paint casting copper sulfide minerals</i>	86
3.4 Electrochemistry of chalcogens and other copper chalcogenides	92
3.4.1 <i>Paint casting copper selenide and telluride compounds</i>	96
3.5 Electrochemical studies of copper chalcogenide compounds	98
3.5.1 <i>Chronocoulometry</i>	99
3.5.2 <i>UV-Vis analysis</i>	100
3.5.3 <i>EXAFS</i>	104
3.6 Conclusions	108
3.7 References	110

Chapter 4: Electrochemistry of Transition Metal Chalcogenides

4.1 Introduction	116
4.1.1 <i>Transition metal chalcogenides</i>	116

4.1.2 <i>Naturally occurring transition metal chalcogenides</i>	117
4.1.3 <i>Uses of metal chalcogenides</i>	119
4.1.4 <i>Aims</i>	122
4.2 <i>Paint casting</i>	123
4.2.1 <i>Zinc Chalcogenides</i>	124
4.2.2 <i>Silver Chalcogenides</i>	131
4.2.3 <i>Cadmium chalcogenides</i>	134
4.2.4 <i>CV comparison</i>	137
4.3 <i>Speciation in solution</i>	139
4.3.1 <i>Electrochemical dissolution</i>	139
4.3.2 <i>Rate of dissolution</i>	141
4.3.3 <i>Chalcogen speciation analysis</i>	143
4.3.4 <i>Recovery/ Extraction</i>	148
4.4 <i>Conclusions</i>	149
4.5 <i>References</i>	151

Chapter 5: Electrochemical Processing of Chalcopyrite

5.1 <i>Introduction</i>	156
5.1.1 <i>Chalcopyrite</i>	156
5.1.2 <i>Current chalcopyrite processing methods</i>	157
5.1.3 <i>Challenges and improvements in chalcopyrite processing</i>	158
5.1.4 <i>Aims</i>	161
5.2 <i>Analysis of chalcopyrite</i>	162
5.2.1 <i>Chalcopyrite sample analysis</i>	162
5.2.2 <i>Paint casting chalcopyrite</i>	165
5.3 <i>Cell design</i>	173
5.4 <i>Hybrid DESs</i>	181
5.4.1 <i>Reline and Oxaline</i>	182
5.5 <i>Analysing the experiment design</i>	186
5.5.1 <i>Green metrics</i>	186
5.5.2 <i>Cell design problems/improvements</i>	188
5.6 <i>Conclusions</i>	191

5.7 References	193
Chapter 6: Conclusions and future work	
6.1 Conclusions	198
6.2 Suggestions for future work	202
Chapter 7: Appendix	
	204

Abbreviations

AFM:	Atomic Force Microscopy
CE:	Counter Electrode
CV:	Cyclic Voltammetry/Voltammogram
DES:	Deep Eutectic
EXAFS:	Extended X-ray Absorption Fine Structure
GC:	Glassy Carbon (electrode)
HBD:	Hydrogen Bond Donor
HPLC:	High Performance Liquid Chromatography
ICP-MS:	Inductively Couple Plasma-Mass Spectrometry
IL:	Ionic Liquid
RE:	Reference Electrode
RTIL:	Room Temperature Ionic Liquid
SEM/ED(A)X:	Scanning Electron Microscopy/Energy Dispersive (Analysis) by X-ray
WE:	Working Electrode
XANES:	X-ray Absorption Near Edge Structure
XRD:	X-Ray Diffraction

CHAPTER 1: INTRODUCTION

Table of Contents

1.1 Overview	2
1.2 Chalcogens and chalcogenides	4
<i>1.2.1 Chalcogen Redox Chemistry</i>	<i>4</i>
<i>1.2.2 Chalcogenide minerals.....</i>	<i>13</i>
1.3 Metallurgy and the environment	14
1.4 Chalcogenide Processing.....	18
<i>1.4.1 Selenium and Tellurium Processing</i>	<i>20</i>
1.5 Solvometallurgy	22
1.6 Ionic Liquids and Deep Eutectic Solvents	24
<i>1.6.1 Properties of DESs.....</i>	<i>28</i>
<i>1.6.2 Metal Processing with ILs and DESs</i>	<i>30</i>
<i>1.6.3 DES Viscosity.....</i>	<i>31</i>
1.6 Research Objectives	33
1.7 References	34

1.1 Overview

Metal ores are commonly defined as “deposits in the Earth’s crust that contain sufficient amounts of valuable metal that are worth extracting.”^{1, 2} Ores or mineral deposits are the main source of the majority of metals. These are processed by a variety of different techniques, including pyrometallurgy (roasting and smelting) and hydrometallurgy (leaching and electrowinning) in order to obtain the pure metals. However, current extraction processes create large amounts of aqueous and tailings waste. Consequently, metal manufacture is one of the industries with the biggest production of low grade waste and is also deemed one of the largest users of energy of any industrial sector.³ There are several categories of ores, the most common being oxides, sulfides, sulfates and silicates.² The main focus of this investigation is on the chalcogenide minerals and compounds; in particular, the processing of materials containing S, Se and Te. Sulphide ores are processed purely for their metal content and are one of the most common and important sources of high value metals such as Au, Ag and Cu.⁴ Selenide and telluride ores on the other hand are typically a lot rarer and far more widely dispersed than their sulfide analogues. The Te and Se is also more valuable than the S and therefore requires extraction from other sources (e.g. anode slimes).

The metal complexes that form with S, Se and Te are called chalcogenides and they provide a number of important and interesting applications. Sulfides, specifically carbon disulphide, is used in the manufacture of cellophane and rayon.⁵ One of the leading uses of selenides and tellurides is in photovoltaic (PV) solar cells. Mercury cadmium telluride is an important compound that has been used in thermal imaging and IR sensors, and cadmium sulfoselenides have been used as pigments in various applications from ceramics, to paints and plastics.⁵

The emphasis on processing Se and Te has increased in recent years due to the interest in low CO₂ technologies, such as solar cells. Of the current solar cell market, photovoltaic thin films occupy a fairly small field. However, they are increasingly being trialled because of their cost effectiveness due to cheaper and more efficient substrate materials and better space efficiency (thin films).⁶ There are three main types of photovoltaic thin films: amorphous silica, cadmium telluride (CdTe) and copper indium gallium diselenide (CIGS), of which two require a substantial source of Te or Se. Se and Te are reasonably rare, lying

66th and 73rd overall in element abundance. The key issue that arises in the processing of these elements is how widely dispersed they are in the Earth's crust,⁵ in fact it is reported that Te is eight times less abundant than Au.⁷ The metals are present in such low concentrations that direct mining is neither effective nor practicable. Instead they are recovered as by-products from pyrometallurgical refining of other metals. Hence, the supply of these elements is directly proportional to production of the primary product, in most cases Cu, and to a lesser degree Au, Pb and Ni.⁷

In this investigation, the sulfide ores that have initially been explored are simple 2-element compounds, such as CuS (covellite) and Cu₂S (chalcocite). However, CuFeS₂ (chalcopyrite) is a significantly more interesting mineral to investigate. It is currently the most abundant source of Cu,^{8,9} with an estimated 70 % of the world's Cu residing in chalcopyrite deposits.⁴ The most common methods of processing chalcopyrite and other ores in general are hydrometallurgy and pyrometallurgy.¹⁰ Both require extreme conditions, concentrated acid and heat, respectively, in order to overcome the strong sulphide bonds that are present.^{11,12}

Pyrometallurgy and hydrometallurgy, have been optimised throughout their development to minimise the emission of H₂S and SO₂, which are significant hazards in the metal processing industry. An alternative method which has been proposed, uses Ionic Liquids (ILs) as alternative solvents to the current acid leaching processes. This technique is referred to as ionometallurgy and provides the basis for the review in this introduction.¹²

Previous research has been conducted on the use of Deep Eutectic Solvents (DESs) for the extraction and recovery of metals such as Fe and Pb from sulfide minerals.^{13,14,15} In this project, the extraction of Cu from the more complex ore, chalcopyrite, will be investigated. Along with an investigation into the chemical and electrochemical behaviours of other chalcogens and chalcogenides, such as Cd, Ag, Zn, Pb and Cu sulfide, selenides and tellurides.

1.2 Chalcogens and chalcogenides

The term 'chalcogen' has been used to describe the elements in Group 16 of the periodic table since the 1930s.⁵ This group consists of S, Se, Te, as well as O and Po. However, the 3 former elements are the ones most commonly discussed together in the literature. All 3 elements are solid at room temperature and their boiling points increase with atomic number. The metallic properties of the elements also increase. Elemental S is yellow in colour and does not exhibit any metallic properties, Se is quite often found as a red or black amorphous solid with semi metallic features. Finally, Te is classed as a metalloid (or occasionally a metal) and often appears with a silvery metallic lustre, frequently described as similar to Sn.⁵

Sulfur is highly abundant in comparison to Se and Te. It is often mined directly from native S, but large amounts are also recovered from roasting metal sulphides, as well as during oil refining. The uses of S are extensive; large amounts are used in the manufacture of fertilizers or are converted into sulfuric acid and then used in applications such as waste water processing and hydrometallurgical metal extraction.^{16,17} S can be used directly to vulcanise rubber but can also be used indirectly in the synthesis of a variety of chemicals such as gunpowder, detergents and fungicides.⁵

Te has many different uses, e.g. as additives to enhance machinability in Cu and improve resistance to vibration in Pb.⁵ Te also finds uses in thermoelectric cooling and, when alloyed with Cd, it can form a compound that presents heightened electrical conductivity, making it a useful material in the manufacturing of photovoltaic (PV) solar cells. Se is classed as one of the most significant semiconductors finding uses in solar cells and photographic exposure meters. Se can also be used as an additive in casting alloys of Fe, Cu, Pb and steel, where the addition of Se improves machinability and casting properties. Se can further be used in catalysts in plating solutions to improve the appearance and resilience.⁵

1.2.1 Chalcogen Redox Chemistry

The chalcogens, most specifically S, participate in a large number of redox reactions due to their ability to be stable in a wide range of different oxidation states. For example, S can be present in a mineral as elemental sulphur, monosulphides, disulphides, or

Table 1.1: The redox reactions and standard potentials of sulfur in water.⁵

Half-reaction	E° / V
$S_2O_8^{2-} + 2 H^+ + 2e^- \rightarrow 2HSO_4^-$	+2.123
$S_2O_8^{2-} + 2e^- \rightarrow 2SO_4^{2-}$	+2.01
$SO(g) + 2H^+ + 2e^- \rightarrow S(s) + H_2O$	+1.507
$S_2Cl_2 + 2e^- \rightarrow 2S(s) + 2Cl$	+1.23
$2 SO_3^{2-} + 6H^+ + 4e^- \rightarrow S_2O_3^{2-} + 3 H_2O$	+0.705
$4 HSO_3^- + 8H^+ + 6e^- \rightarrow S_4O_6^{2-} + 6 H_2O$	+0.581
$S_2O_6^{2-} + 4H^+ + 2 e^- \rightarrow 2H_2SO_3$	+0.57
$4SO_2(g) + 4H^+ + 6e^- \rightarrow S_4O_6^{2-} + 2 H_2O$	+0.51
$4H_2SO_3 + 4H^+ + 6e^- \rightarrow S_4O_6^{2-} + 6 H_2O$	+0.51
$H_2SO_2 + 2H^+ + 2e^- \rightarrow S(s) + 2H_2O$	>+0.5
$2HSO_3^- + 4H^+ + 4e^- \rightarrow S_2O_3^{2-} + 3 H_2O$	+0.491
$S_5O_6^{2-} + 12H^+ + 10e^- \rightarrow 5S(s) + 6H_2O$	+0.484
$S_2O_3^{2-} + 6H^+ + 4e^- \rightarrow 2S(s) + 3H_2O$	+0.465
$S_2O_6^{2-} + 2H^+ + 2 e^- \rightarrow 2HSO_3^-$	+0.455
$SO_2(g) + 4H^+ + 4e^- \rightarrow S(s) + 2H_2O$	+0.451, +0.470
$H_2SO_3 + 4H^+ + 4e^- \rightarrow S(s) + 3 H_2O$	+0.45
$2 SO_3^{2-} + 4H^+ + 2 e^- \rightarrow S_2O_4^{2-} + 2 H_2O$	+0.416
$S_4O_6^{2-} + 12H^+ + 10e^- \rightarrow 4S(s) + 6H_2O$	+0.416
$2H_2SO_3 + 2H^+ + 4e^- \rightarrow S_2O_3^{2-} + 3 H_2O$	+0.40
$SO_4^{2-} + 8 H^+ + 6 e^- \rightarrow S(s) + 4 H_2O$	+0.357
$HSO_4^- + 7 H^+ + 6 e^- \rightarrow S(s) + 4 H_2O$	+0.339
$5S_2O_3^{2-} + 30H^+ + 24e^- \rightarrow 2S_5^{2-} + 15H_2O$	+0.331
$SO_4^{2-} + 10H^+ + 8 e^- \rightarrow H_2S(g) + 4H_2O$	+0.311
$SO_4^{2-} + 10 H^+ + 8 e^- \rightarrow H_2S(aq) + 4 H_2O$	+0.303
$3H_2SO_3 + 2 e^- \rightarrow S_2O_6^{2-} + 3H_2O$	+0.30
$S_5^{2-} + 10H^+ + 8e^- \rightarrow 5H_2S(g)$	+0.299
$HSO_4^- + 9 H^+ + 8 e^- \rightarrow H_2S(aq) + 4 H_2O$	+0.289
$SO_4^{2-} + 9 H^+ + 8 e^- \rightarrow HS^- + 4 H_2O$	+0.252
$SO_3^{2-} + 6H^+ + 6e^- \rightarrow S^{2-} + 3H_2O$	+0.231
$S_2O_3^{2-} + 8H^+ + 8e^- \rightarrow 2HS^- + 3H_2O$	+0.200
$S(s) + 2H^+ + 2e^- \rightarrow H_2S(g)$	+0.171
$SO_4^{2-} + 4 H^+ + 2 e^- \rightarrow H_2SO_3 + H_2O$	+0.17
$SO_4^{2-} + 8 H^+ + 8 e^- \rightarrow S^{2-} + 4H_2O$	+0.149
$SO_4^{2-} + 4 H^+ + 2 e^- \rightarrow SO_2 + 2 H_2O$	+0.138
$S(s) + 2H^+ + 2e^- \rightarrow H_2S(aq)$	+0.141
$S_3^{2-} + 3H^+ + 4e^- \rightarrow 3HS^-$	+0.097
$2HSO_3^- + 3H^+ + 2 e^- \rightarrow HS_2O_4^- + 2 H_2O$	+0.060
$S_4^{2-} + 4H^+ + 6e^- \rightarrow 4HS^-$	+0.033
$S_2O_6^{2-} + 2e^- \rightarrow 2SO_3^{2-}$	+0.026
$S_4O_6^{2-} + 2e^- \rightarrow 2S_2O_3^{2-}$	+0.08, +0.219, -0.10
$S_5^{2-} + 5H^+ + 8e^- \rightarrow 5HS^-$	+0.003
$S_2O_3^{2-} + 6H^+ + 8e^- \rightarrow 2S^{2-} + 3H_2O$	-0.006
$2 HSO_3^- + 2H^+ + 2 e^- \rightarrow S_2O_4^{2-} + 2 H_2O$	-0.013, -0.009
$S(s) + H^+ + 2e^- \rightarrow HS^-$	-0.065
$2H_2SO_3 + H^+ + 2e^- \rightarrow HS_2O_4^- + 2H_2O$	-0.08, -0.056
$2 SO_4^{2-} + 4H^+ + 2 e^- \rightarrow S_2O_6^{2-} + 2H_2O$	-0.22
$4S(s) + 2e^- \rightarrow S_4^{2-}$	-0.33

$5S(s) + 2e^- \rightarrow S_5^{2-}$	-0.340, -0.315
$4S_5^{2-} + 2e^- \rightarrow 5S_4^{2-}$	-0.441
$S_2^{2-} + 2e^- \rightarrow 2S^{2-}$	-0.48, -0.524
$S(s) + 2e^- \rightarrow S^{2-}$	-0.48 to -0.58 V
$S_3^{2-} + 2e^- \rightarrow S^{2-} + S_2^{2-}$	-0.49
$2S_3^{2-} + 2e^- \rightarrow 3S_2^{2-}$	-0.506
$S_4^{2-} + 2e^- \rightarrow S^{2-} + S_3^{2-}$	-0.52
$S(s) + H_2O + 2e^- \rightarrow HS^- + OH^-$	-0.52
$2 SO_3^{2-} + 3 H_2O + 4e^- \rightarrow S_2O_4^{3-} + 6OH^-$	-0.58
$SO_3^{2-} + 3H_2O + 4e^- \rightarrow S(s) + 6 OH^-$	-0.66
$SO_4^{2-} + H_2O + 2 e^- \rightarrow SO_3^{2-} + 2OH^-$	-0.93
$2SO_3^{2-} + 2H_2O + 2e^- \rightarrow S_2O_4^{2-} + 4OH^-$	-1.12

The Pourbaix diagrams in Figures 1.1, 1.2 and 1.3 are fairly complex and discussions in the following section provide a general description of species that we could expect to find in the DES systems. The diagram for S, in Figure 1.1 reveals that in aqueous environment, elemental S is only stable in a very narrow window and only in an acidic environment, making it unstable above pH 8. The chemistry of S is dominated by sulfate and sulfide species; in a reductive environment (0 V to -1.8 V) the sulfide species governs, whereas in an oxidative environment (0 to 1.8 V) sulfate is prevalent. Sulfur is poorly soluble in water ($1.9 \times 10^{-8} \text{ S}_8\text{kg}^{-1}$)¹⁸ and therefore analysing its electrochemical behaviour, specifically reduction, is complex. However it has been predicted that during the oxidation of sulfide to S, reduction back to sulphide proceeds via a polysulfide intermediate species.¹⁹

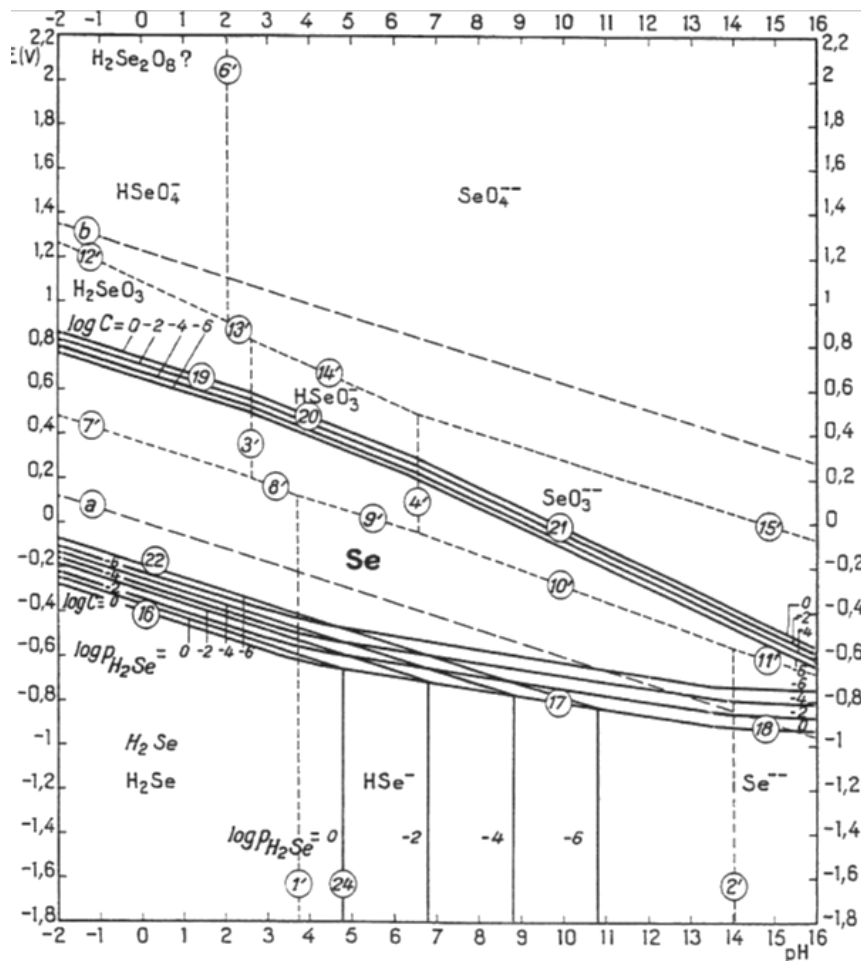


Figure 1.2: The Pourbaix diagram for the selenium-water system.⁵

A similar analysis can be carried out for the other two chalcogens of interest, Se and Te. The types of redox reactions, oxidation states, and potential species formed are somewhat similar, however significantly fewer reactions are present.

Table 1.2: The redox reactions and standard potentials of selenium in water.⁵

Half-reaction	E° / V
$\text{SeO}_4^{2-} + 4\text{H}^+ + 2\text{e}^- \rightarrow \text{H}_2\text{SeO}_3 + \text{H}_2\text{O}$	+1.15
$\text{Se}_2\text{Cl}_2 + 2\text{e}^- \rightarrow 2\text{Se(s)} + 2\text{Cl}^-$	+1.1
$\text{HSeO}_4^- + 3\text{H}^+ + 2\text{e}^- \rightarrow \text{H}_2\text{SeO}_3 + \text{H}_2\text{O}$	+1.090
$\text{SeO}_4^{2-} + 3\text{H}^+ + 2\text{e}^- \rightarrow \text{HSeO}_3 + \text{H}_2\text{O}$	+1.075
$\text{SeO}_4^{2-} + 2\text{H}^+ + 2\text{e}^- \rightarrow \text{SeO}_3^{2-} + \text{H}_2\text{O}$	+0.880
$\text{SeO}_3^{2-} + 6\text{H}^+ + 4\text{e}^- \rightarrow \text{Se(s)} + 3\text{H}_2\text{O}$	+0.875
$\text{Se}^{4+} + 4\text{e}^- \rightarrow \text{Se(s)}$	+0.846
$\text{HSeO}_3^- + 5\text{H}^+ + 4\text{e}^- \rightarrow \text{Se(s)} + 3\text{H}_2\text{O}$	+0.778
$\text{H}_2\text{SeO}_3 + 4\text{H}^+ + 4\text{e}^- \rightarrow \text{Se(s)} + 3\text{H}_2\text{O}$	+0.740
$\text{SeO}_3^{2-} + 7\text{H}^+ + 6\text{e}^- \rightarrow \text{HSe}^- + 3\text{H}_2\text{O}$	+0.414
$\text{HSeO}_3^- + 7\text{H}^+ + 6\text{e}^- \rightarrow \text{H}_2\text{Se} + 3\text{H}_2\text{O}$	+0.386
$\text{H}_2\text{SeO}_3 + 6\text{H}^+ + 6\text{e}^- \rightarrow \text{H}_2\text{Se} + 3\text{H}_2\text{O}$	+0.360
$\text{HSeO}_3^- + 6\text{H}^+ + 6\text{e}^- \rightarrow \text{HSe}^- + 3\text{H}_2\text{O}$	+0.349
$\text{SeO}_3^{2-} + 6\text{H}^+ + 6\text{e}^- \rightarrow \text{Se}^{2-} + 3\text{H}_2\text{O}$	+0.276
$\text{SeO}_4^{2-} + 2\text{e}^- + \text{H}_2\text{O} \rightarrow \text{SeO}_3^{2-} + 2\text{OH}^-$	+0.05
$\text{SeO}_3^{2-} + 4\text{e}^- + 3\text{H}_2\text{O} \rightarrow \text{Se(s)} + 6\text{OH}^-$	-0.366
$\text{Se(s)} + 2\text{H}^+ + 2\text{e}^- \rightarrow \text{H}_2\text{Se(g)}$	-0.369
$\text{Se(s)} + 2\text{H}^+ + 2\text{e}^- \rightarrow \text{H}_2\text{Se}$	-0.40
$\text{Se(s)} + \text{H}^+ + 2\text{e}^- \rightarrow \text{HSe}^-$	-0.510
$\text{Se(s)} + 2\text{e}^- \rightarrow \text{Se}^{2-}$	-0.92

In comparison to the S Pourbaix diagram, elemental Se is stable in a much larger region spanning a wide range of pHs. Interestingly, selenide species continue to form in the reductive environment (-0.3 V to -1.8 V) with selenites and selenous acid forming in the oxidative environment (0.8 V to 2 V) analogous to the behaviour of sulfur. Bouroushian et al.⁵ noted that the electrochemistry of S and Se is similar in several ways. In particular, the formation of elemental S/Se monolayers that passivate electrode surfaces during electrochemical analysis being common across both elements.⁵ Finally, the redox reactions of Te are shown in Table 1.3.

Table 1.3: The redox reactions and standard potentials of tellurium in water.⁵

Half-reaction	E° / V
$\text{TeO}_4^{2-} + 4\text{H}^+ + 2\text{e}^- \rightarrow \text{TeO}_2(\text{s}) + 2\text{H}_2\text{O}$	+1.509
$\text{TeO}_4^{2-} + 4\text{H}^+ + 2\text{e}^- \rightarrow \text{TeO}_2\text{aq}(\text{s}) + 2\text{H}_2\text{O}$	+1.343
$\text{HTeO}_4^- + 3\text{H}^+ + 2\text{e}^- \rightarrow \text{TeO}_2(\text{s}) + 2\text{H}_2\text{O}$	+1.202
$\text{HTeO}_4^- + 3\text{H}^+ + 2\text{e}^- \rightarrow \text{TeO}_2\text{aq}(\text{s}) + 2\text{H}_2\text{O}$	+1.036
$\text{H}_2\text{TeO}_4 + 2\text{H}^+ + 2\text{e}^- \rightarrow \text{TeO}_2(\text{s}) + 2\text{H}_2\text{O}$	+1.020
$\text{TeO}_3(\text{s}) + 2\text{H}^+ + 2\text{e}^- \rightarrow \text{TeO}_2(\text{s}) + \text{H}_2\text{O}$	+1.020
$\text{H}_2\text{TeO}_4 + 3\text{H}^+ + 2\text{e}^- \rightarrow \text{HTeO}_3 + 2\text{H}_2\text{O}$	+0.953
$\text{H}_2\text{TeO}_4 + 6\text{H}^+ + 2\text{e}^- \rightarrow \text{Te}^{4+} + 4\text{H}_2\text{O}$	+0.920
$\text{TeO}_4^{2-} + 2\text{H}^+ + 2\text{e}^- \rightarrow \text{TeO}_3^{2-} + \text{H}_2\text{O}$	+0.892
$\text{H}_2\text{TeO}_4 + 2\text{H}^+ + 2\text{e}^- \rightarrow \text{TeO}_2\text{aq}(\text{s}) + 2\text{H}_2\text{O}$	+0.854
$\text{TeO}_3(\text{s}) + 2\text{H}^+ + 2\text{e}^- \rightarrow \text{TeO}_2\text{aq}(\text{s}) + \text{H}_2\text{O}$	+0.850
$\text{TeO}_3^{2-} + 6\text{H}^+ + 4\text{e}^- \rightarrow \text{Te}(\text{s}) + 3\text{H}_2\text{O}$	+0.827
$\text{HTeO}_4^- + 2\text{H}^+ + 2\text{e}^- \rightarrow \text{HTeO}_3 + \text{H}_2\text{O}$	+0.813
$\text{HTeO}_3^- + 5\text{H}^+ + 4\text{e}^- \rightarrow \text{Te}(\text{s}) + 3\text{H}_2\text{O}$	+0.713
$\text{H}_2\text{TeO}_4 + \text{H}^+ + 2\text{e}^- \rightarrow \text{HTeO}_3^- + \text{H}_2\text{O}$	+0.631
$\text{TeO}_2\text{aq}(\text{s}) + 4\text{H}^+ + 4\text{e}^- \rightarrow \text{Te}(\text{s}) + 2\text{H}_2\text{O}$	+0.604
$\text{H}_2\text{TeO}_3 + 4\text{H}^+ + 4\text{e}^- \rightarrow \text{Te}(\text{s}) + 3\text{H}_2\text{O}$	+0.589
$\text{Te}_4^{4+} + 4\text{e}^- \rightarrow \text{Te}(\text{s})$	+0.584, +0.568, +0.556
$\text{HTeO}_4^- + \text{H}^+ + 2\text{e}^- \rightarrow \text{TeO}_3^{2-} + \text{H}_2\text{O}$	+0.584
$\text{TeCl}_6^{2-} + 4\text{e}^- \rightarrow \text{Te}(\text{s}) + 6\text{Cl}^-$	+0.55, +0.630
$\text{HTeO}^{2+} + 3\text{H}^+ + 4\text{e}^- \rightarrow \text{Te}(\text{s}) + 2\text{H}_2\text{O}$	+0.551
$\text{TeO}_2(\text{s}) + 4\text{H}^+ + 4\text{e}^- \rightarrow \text{Te}(\text{s}) + 2\text{H}_2\text{O}$	+0.521
$2\text{TeO}_3^{2-} + 12\text{H}^+ + 10\text{e}^- \rightarrow \text{Te}_2^{2-} + 6\text{H}_2\text{O}$	+0.493
$2\text{HTeO}_3^- + 10\text{H}^+ + 10\text{e}^- \rightarrow \text{Te}_2^{2-} + 6\text{H}_2\text{O}$	+0.402
$\text{Te}^{2+} + 2\text{e}^- \rightarrow \text{Te}(\text{s})$	+0.40
$2\text{Te}^{4+} + 10\text{e}^- \rightarrow \text{Te}_2^{2-}$	+0.286
$2\text{HTeO}^{2+} + 6\text{H}^+ + 10\text{e}^- \rightarrow \text{Te}_2^{2-} + 4\text{H}_2\text{O}$	+0.273
$\text{Te}^{4+} + 2\text{H}^+ + 6\text{e}^- \rightarrow \text{H}_2\text{Te}$	+0.132
$\text{HTeO}_2^+ + 5\text{H}^+ + 6\text{e}^- \rightarrow \text{H}_2\text{Te} + 2\text{H}_2\text{O}$	+0.121
$2\text{Te}(\text{s}) + 2\text{H}^+ + 2\text{e}^- \rightarrow \text{H}_2\text{Te}_2$	-0.365
$\text{Te}(\text{OH})_6^{2-} + 4\text{e}^- \rightarrow \text{Te}(\text{s}) + 6\text{OH}^-$	-0.412
$\text{Te}_2^{2-} + 4\text{H}^+ + 2\text{e}^- \rightarrow 2\text{H}_2\text{Te}(\text{g})$	-0.595
$\text{Te}_2^{2-} + 4\text{H}^+ + 2\text{e}^- \rightarrow 2\text{H}_2\text{Te}$	-0.638
$\text{Te}(\text{s}) + 2\text{H}^+ + 2\text{e}^- \rightarrow \text{H}_2\text{Te}(\text{g})$	-0.717
$\text{Te}(\text{s}) + 2\text{H}^+ + 2\text{e}^- \rightarrow \text{H}_2\text{Te}$	-0.739, -0.50
$\text{Te}_2^{2-} + 2\text{H}^+ + 2\text{e}^- \rightarrow 2\text{HTe}^-$	-0.795
$2\text{Te}(\text{s}) + 2\text{e}^- \rightarrow \text{Te}_2^{2-}$	-0.840, -0.790, -0.74
$\text{Te}_2\text{S} + 2\text{e}^- \rightarrow 2\text{Te}(\text{s}) + \text{S}^{2-}$	-0.90
$2\text{Te}(\text{s}) + 2\text{e}^- \rightarrow \text{Te}_2^{2-}$	-0.913, -1.14
$3\text{Te}_2 + 8\text{e}^- \rightarrow 2\text{Te}_2^{2-} + 2\text{Te}^{2-}$	-0.92
$\text{Te}_2^{2-} + 2\text{e}^- \rightarrow 2\text{Te}^{2-}$	-1.445

The potential window in which elemental Te is stable is again much wider than S, it too spans the range of pH values, except for strongly alkaline solutions where the TeO_3^{2-} and Te_2^{2-} species dominate. In reductive acidic environments, it is readily reduced to H_2Te , whereas in the alkali environment the Te_2^{2-} ion forms. This is slightly different to S and Se where the hydrogen chalcogenide was favoured overall in reductive environments. As

for oxidation, there are many different H and O containing species, but the prominent ones are the tellurate and telluric acid species.

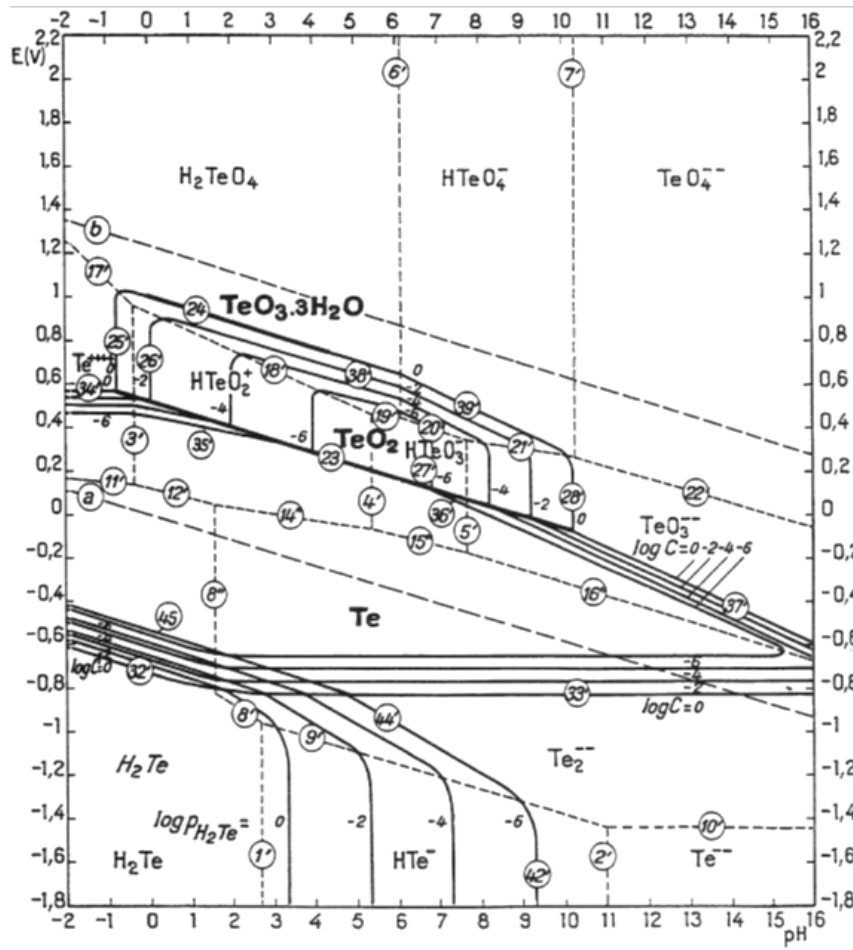


Figure 1.3: The Pourbaix diagram for the tellurium-water system.⁵

The information presented in these Pourbaix diagrams only considers the behaviour of these elements in aqueous systems, and not the chloride rich DES environments in this project. However, they can still provide an insight into the range of species that could potentially form in the DES systems, along with an indication of their electrochemical stability ranges. The high chloride environment exhibited in these DESs (Ethaline ~ 4.5 M) will likely have the effect of limiting the amount of H₂O ligands available and cause the speciation to be controlled by the Cl⁻ ions. At the time of writing, Pourbaix diagrams

do not exist in IL or DES systems, however the uncertainty of the effect of the Cl environment would make an interesting study.

The electrochemistry of these compounds and elements is important because it will provide the basis for identifying viable dissolution and recovery techniques. The electrochemistry of some of the common sulphide minerals (e.g. CuFeS_2 and PbS) has been extensively studied in aqueous media.²⁰⁻²⁴ Whereas, for others such as CuS and Cu_2S there is significantly less literature surrounding their electrochemical analysis. A key issue when investigating the electrochemistry of minerals is the type of working electrode to use. Quite often in earlier research, a solid electrode made directly from the mineral is used.^{23,24} This method has shown to have difficulties in terms of reproducibility. It is dependent on the level of surface polishing that can be achieved, as well as the effect of different crystal faces, the thickness of the mineral section and the presence of any inclusions and impurities. Further research suggests the use of carbon paste electrodes as a better alternative; whereby powdered graphite or paraffin wax is added to the powdered mineral and subsequently pressed into a solid matrix. Carbon paste electrodes provide the extra advantage that there is an even distribution of mineral grain orientations and particle size, along with lower electrode resistance.²⁴ This information along with developments in the techniques are discussed in depth in Chapter 3.

The electrochemistry of tellurides and selenides is reported in the literature to a lesser extent compared to other more common metals. However, the literature is growing continually, specifically due to the possible applications of different metal chalcogenide compounds.²⁵⁻²⁷ There appears to be a focus on the electrochemical studies of CdTe due to its application as Quantum dots^{28,29} and its established use in thin film photovoltaics.³⁰ There is also a pocket of research on the electrochemistry of organoselenides and organotellurides due to their anti-microbial and anti-inflammatory properties.³¹ Literature surrounding the electrochemistry of any of these materials concentrates on processes in aqueous systems, alternative research in Ionic Liquids, or Deep Eutectic Solvents in particular is limited but again, increasing.^{32,33,34} This therefore provides the motivation to lay the fundamental electrochemical groundwork for ultimately developing an electrochemical leaching and recovery process.

1.2.2 Chalcogenide minerals

S most commonly occurs as sulfides (e.g. galena (PbS) or sphalerite (ZnS)) or sulfates such as gypsum ($\text{CaSO}_4 \cdot 2\text{H}_2\text{O}$) and anhydrite (CaSO_4). The sulfides are formed with a wide range of so called chalcophilic metals such as Cu, Pb, Zn, Au, Ag, Cd, Bi and Fe to name a few.⁵ The earliest sulfide crystal structures were established by Bragg in 1913 using X-ray diffraction, these included pyrite (FeS_2) and sphalerite (ZnS).³⁵ Only considering binary sulfides the possible crystal structures are presented in Figure 1.4.

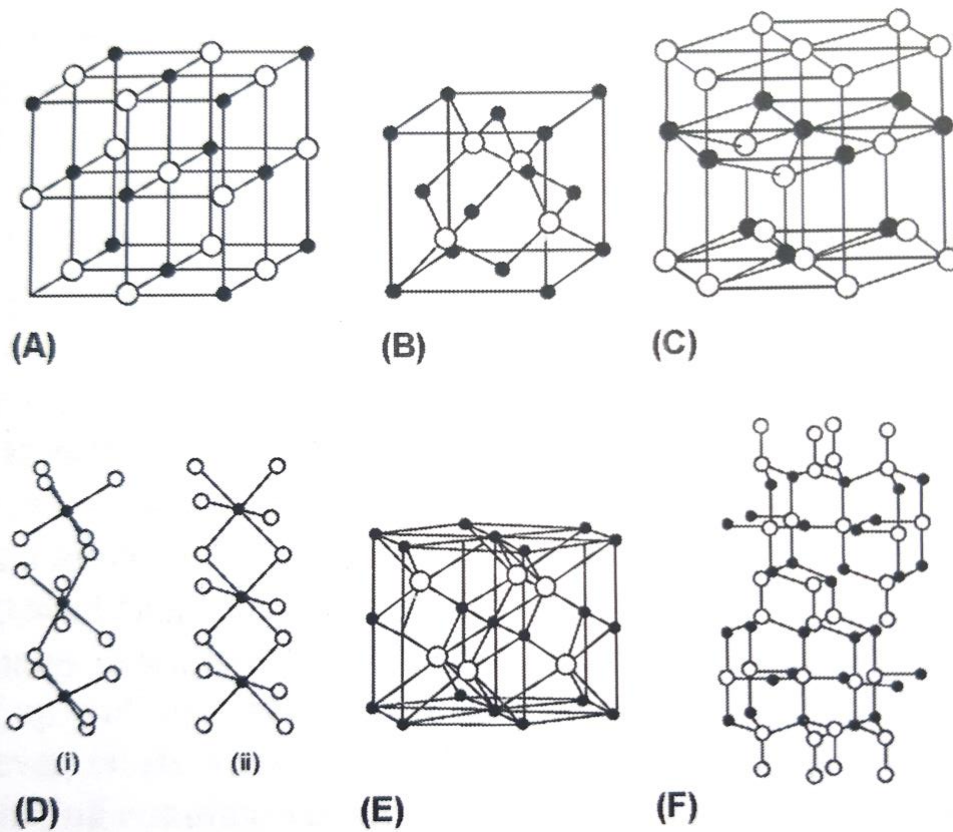


Figure 1.4: Crystal structures of sulfide ores. A: galena (PbS). B: sphalerite (ZnS). C: wurtzite (ZnS) D: i: pyrite (FeS_2) ii: marcasite (FeS_2). E: niccolite (NiAs). F: covellite (CuS).⁵

The structures exhibited in Figure 1.4 only demonstrate a selection of different sulfide ores and clearly only those containing a single metal. Other common multi metallic sulfides include chalcopyrite (CuFeS_2) and arsenopyrite (FeAsS).

Se and Te rarely occur as native elements and instead most typically as selenide and telluride impurities alongside metal sulfides^{5,36} The minerals that exist for selenides and

tellurides are most often isomorphs of the sulfide equivalents. Some examples of common selenides include clausthalite (PbSe), berzelianite (Cu₂Se) and eucairite (CuAgSe). For tellurides, calaverite (AuTe₂), petzite (Ag₃AuTe₂) and nagyagite (Au₂Sb₂Pb₁₀Te₆S₁₅) are among the common examples.^{5,36} These ores are never processed for their Se/Te content due to it not being economically feasible and the ores being too disperse.

1.3 Metallurgy and the environment

All processes have a degree of environmental impact and it is necessary to analyse the energy and material inputs and outputs from each stage to determine whether a new technology is greener than a comparable existing technology. The Life Cycle Assessment (LCA) takes into account every single environmental impact during the entire life cycle of the material or process.³⁷ This so-called “cradle to grave” approach can subsequently be broken down into “cradle to entry gate”, which involves the mining or other extraction methodology. Next is the “entry gate to exit gate” which involves the actual processing and/ or manufacturing of the material to be ready for use and finally the “exit gate to grave” which involves the use of the product followed by either its disposal or more favourably its recycling.³⁷ A typical life cycle system is presented in Figure 1.5.

In the life cycle presented in Figure 1.5, the lines in blue refer to any air or water borne emissions, or any solid residues and the red lines refer to any input of material or energy. During the life cycle of metals, the ores are initially present in the Earth’s crust and they are mined either by open cast or underground mining to acquire the raw materials. From here the processing section of the life cycle system is of most interest for this work. Major metals are most commonly extracted from sulfide, oxide or silicate ores, and as mentioned previously, the processing options can be broadly grouped into pyrometallurgical and hydrometallurgical processes.

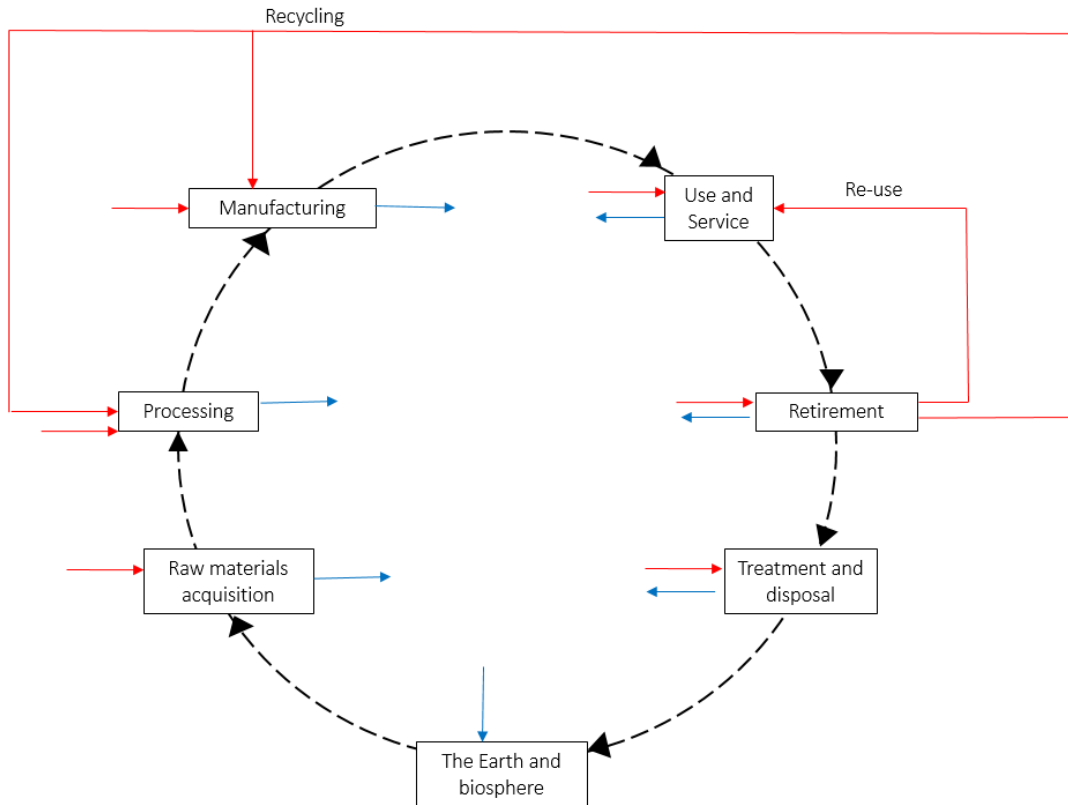


Figure 1.5: A typical life cycle assessment of a generic metal demonstrating the areas that an assessment would concentrate on; blue arrows represent air and water borne emissions and red arrows indicate material or energy input.³⁷

Norgate et al. examined the Life Cycle Assessment of Cu both by hydrometallurgical and pyrometallurgical methods, along with several other metals.³⁷ The different aspects of the early part of the life cycle are analysed and presented in comparison with other common metals. The overall energy requirements for Cu processing both by pyrometallurgy and hydrometallurgy are modest, although the latter is around twice as energy intensive as the former.³⁷ Aside from ore grade, other factors cause an increase in energy requirements, specifically the electricity required in the electrowinning steps and the solid waste generated at the end of the process. The so called solid waste burden (SWB) is included in the LCA as the waste will ultimately require treatment and disposal. One of the worst generators of solid waste in the mining industry is the processing of Ni laterite ores. This is due to them being generally lower grade and containing small amounts of Ni per tonne (~ 1-1.6 wt %).³⁸ However, they are said to contain around 70

% of the worlds Ni and therefore are highly processed. In comparison to the hydrometallurgical processing of Ni laterite ores, the hydrometallurgical processing of Cu ores has the next highest SWB of around 125 kg per kg of Cu produced. Interestingly, the pyrometallurgical processing of Cu generates about half as much solid waste, more likely due to the fact that lower ore grades are not processed pyrometallurgically. The electricity requirements during electrowinning cause an increase in energy requirements for Cu hydrometallurgy over pyrometallurgy. Nevertheless, the energy requirements are low, compared to Al, Ti and Ni processing (between 110 and 360 MJ/kg) but fall roughly in line with the processing of Pb, Zn and steel (between 20 and 50 MJ/kg).³⁷

Lower ore grades directly impact the energy consumption and increase the waste emissions per tonne of metal.^{37,39} For Cu ores, the mineable metal content in 2011 was typically 0.9 % and this was projected to fall to 0.7 % by 2030.⁴⁰ Figure 1.6 shows the impact of declining ore grade on the energy requirements and solid waste that is generated. Norgate showed that the waste emissions and the energy requirements are not affected by the ore grade further downstream after the initial processing. Therefore, it is only necessary to concentrate on the initial processing in terms of comparisons with energy and waste.³⁷

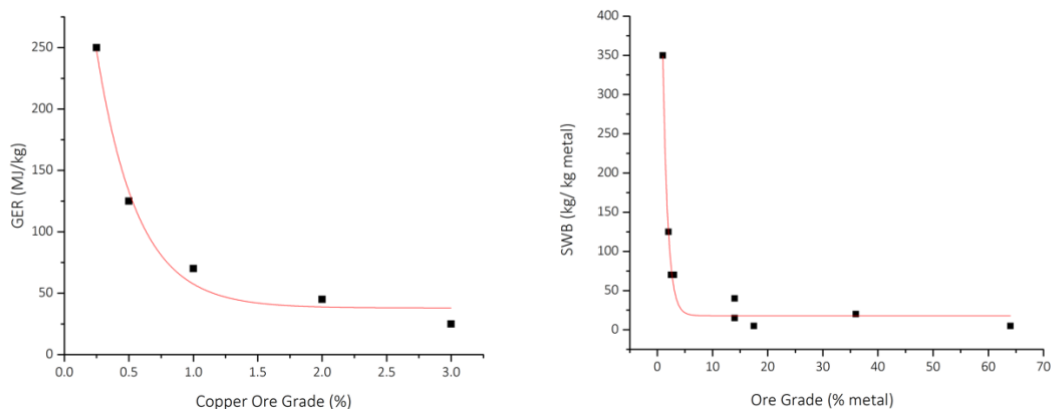


Figure 1.6: An example of how declining ore grade effects the energy requirements and the subsequent waste from a typical copper extraction process.³⁷ [GER (gross energy requirement) and SWB (solid waste burden)]

The grinding and crushing stages of mineral processing (comminution) occur once the ore has been extracted from the ground. This step of the process is one of the most energy intensive steps and it is estimated that around 1 % of the entire world's electricity consumption is used for grinding of metal ores.⁴⁰ This problem will be exacerbated with the decrease in ore quality and availability.

Alternative methods have been proposed for ore pre-treatment. It has been suggested that the use of equipment commonplace in cement plants; a High Pressure Grinding Roll, could have the potential of dramatically reducing the comminution steps of mineral processing. It is even suggested that reductions in energy usage of around 30- 50 % could be possible using these grinding rolls. Another idea is utilising different milling equipment as opposed to the typical ball mill that is most commonly used. A stirred mill for example, could have the potential of reducing energy consumption by 50 %.⁴⁰

On top of altering the comminution steps of the extraction process, the actual metallurgical processing steps can be enhanced to increase their suitability for continually declining ore grades.⁴¹ As for pyrometallurgy, the ore can be smelted as a whole rather than undergoing beneficiation before smelting. Whereas this has clear the advantages of reducing processing steps, a lot of unnecessary energy is applied to the ore in order to extract the desired metals. This technology has not been particularly well reported and instead hydrometallurgical process improvements have appeared more popular. Heap leaching is now commonplace for processing metals such as Au, Cu and Ni from ores that are otherwise uneconomic to process and it has been proposed that a method of in-situ leaching whereby a solvent is used to extract metals directly from the ore veins. This method has the benefit of no waste rock generated because any unwanted materials remain in the ground, with very little surface disturbance.⁴¹

An aspect of life cycle assessment that is often not a big focus is the water consumption, both direct and indirect. Typical LCAs focus on energy usage, emissions and resource depletion whereas there are very few studies that have evaluated the consumption of water in typical mining processes. It is estimated that the direct usage of water when it comes to processing Cu ores is unexpectedly higher for pyrometallurgical processes.

Pyrometallurgy commonly involves a flotation step which requires large amounts of water in order to concentrate the ore. This is discussed in more depth in Chapter 5. Hydrometallurgy on the other hand necessitates large amounts of water 'indirectly', with a significant volume of sulfuric acid consumption. In comparison to a typical pyrometallurgical process, hydrometallurgical processing of a typical grade Cu ore uses 198 m³ of water indirectly where the pyrometallurgy only uses 128 m³ in total, both directly and indirectly to process the same grade ore. The grade of ore is crucial again when considering water usage and a similar trend to both the energy requirements and solid waste emissions is true with water usage.⁴²

The environmental impact of metal processing is one topic of interest, however, metals in theory are infinitely recyclable with no loss of purity. This makes them a very important resource as their source is conversely finite. The problem arises when analysing the LCA of metal recycling or re-processing as it is often subject to a degree of opinion. It is explained in a paper by Haque et al. that there is a lot of complexity surrounding the allocation of environmental burdens and the environmental 'credits' that can be applied to the fact that it is a recycled resource and not extracted from a primary ore.⁴³ On the whole, the application of an LCA enables the comparison of environmental impacts and so-called credits of new technologies against current technologies. This allows an overview of the whole process and can enable an analysis to a theoretical scale up of novel laboratory scale processes.

1.4 Chalcogenide Processing

Metals are most commonly extracted from ores based on oxides, sulfides, carbonates, phosphates and silicates, as well as slags, tailings and slimes from other metal extraction processes. Metal processing can currently be viewed as falling into two main categories, namely pyro- and hydrometallurgy. However, the process of obtaining pure metal from a relatively impure source is much more complex than just applying heat or acid. Park et al. have suggested that metal processing should be split into 3 main categories, with the extraction step being defined by the pyrometallurgical or hydrometallurgical methods.⁴⁴ In this 3-step process, the initial step requires pre-treating the ore prior to processing. This often involves crushing, grinding and separating the ore from large amounts of

gangue material.⁴⁴ The depletion of high-grade ores has made this step particularly important, especially for pyrometallurgical processing. Flotation makes it possible to obtain highly metal rich concentrates from fairly low-grade ores, allowing economical smelting and recovery of the desired metals. This pre-treatment is followed by suitable metal extraction processes and finally the metal is refined in order to make it fit for purpose.⁴⁴

For hydrometallurgy specifically, the metal is often initially dissolved by either a direct chemical digestion or chemical/electrolytic oxidation. The techniques that are ultimately used to recover the metal depend on the desired quality and composition of the original material.⁴⁵ For the most part, the technique that is chosen must be discriminative to the desired metal as well as being highly efficient in purification.¹¹

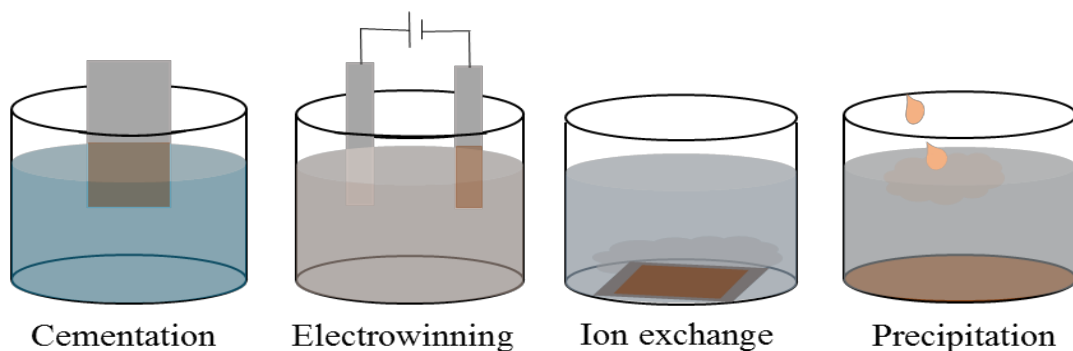


Figure 1.7: Diagrammatic representation of the four different types of metal extraction in hydrometallurgy.

Cementation is a technique that is often carried out for metals that are not considered important enough to be electrowon. One application for cementation is the removal of metals such as Cu from waste water. As a technique it is deemed one of the most economical methods, especially when it comes to the removal of less valuable metals.⁴⁶ Electrowinning involves electrodepositing the desired metal onto another surface. Complexing agents are typically added to the solution to alter the solubility and reduction potential/kinetics of the desired metal. This technique is commonly used for metals such as Au, Ag, Cu and Pb, but rarely used for metals with a low oxidation potential such as Cr, simply because of high energy demands and inefficiency.⁴⁵

Ion exchange, is simply an exchange of ions between electrolytes or between an electrolyte and solid material. For example, polymeric resins are commonly used to exchange metal ions in solution with hydrogen ions in the matrix. To say it is used widely in industry is almost an understatement, it is used in a variety of purification and separation processes from water to nuclear waste treatment as well as in metal recovery.⁴⁵ Metals that have been recovered by ion exchange in hydrometallurgical processing include several rare earth elements, Au, Ag, Cr, Cu, Zn, Ni and Co.⁴⁷

Finally, chemical precipitants can be added to the solution to recover metals as sulphides, hydroxides or carbonates. Often the pH is altered to allow the reaction to occur, for example copper hydroxide precipitates in alkali environments through the addition of hydroxide or ammonia solution.⁴⁸ Some of the steps involved in general metal extraction require the use of huge quantities of strong acids and bases or toxic chemicals, like strongly oxidising cyanide. Therefore, the use and subsequent disposal of these solutions is difficult and often energy intensive.⁴⁹

1.4.1 Selenium and Tellurium Processing

Se and Te are both relatively rare elements and are widely spread throughout the Earth's crust, which comprises of 0.05 ppm and 0.002 ppm for Se and Te respectively. This makes it difficult and not worth mining solely for their extraction. However, demand for these elements has increased in recent years, due to the growing popularity of low CO₂ technologies, such as solar panels, and their use in semiconductor thin films.

Accordingly, Se and Te tend to be obtained as by products from other metal extraction processes such as Cu or Ni. This is also the case for other similarly rare metals such as Cd, In, and Ga.⁵ Se and Te are most commonly extracted from anode slimes that are produced from the electrolytic refining process during copper recovery.⁵⁰ One option for the processing of these slimes involves initial treatment using pyrometallurgy, where the Se and Te is converted to alkali selenite and tellurite. These solutions can be treated with H₂SO₄ in order to remove the Se almost entirely from the Te. Selenous acid remains in solution which can be treated with SO₂ in order to obtain high purity Se. Te on the other hand precipitates as the hydrated dioxide and requires dissolving in H₂SO₄ and HF before

it can be electrowon from the solution. Finally, both elements are electrolytically refined resulting in usable quality metals.⁵ Recovery of Se might seem straightforward with fewer processing steps than Te. However, it is estimated that across a sample of 52 copper refineries that report Se in their anode slimes, only 50 % is able to be successfully extracted, compared to the 70-80 % of Te that is extracted on average.⁵¹ The flow diagram in Figure 1.8 shows a more detailed description of the possible routes of processing the copper anode slimes to recover the Te.⁵² As a direct result of the low Te concentrations found in the slimes, a large number of processing steps are required to concentrate the Te enough for electrowinning to be possible.⁵²

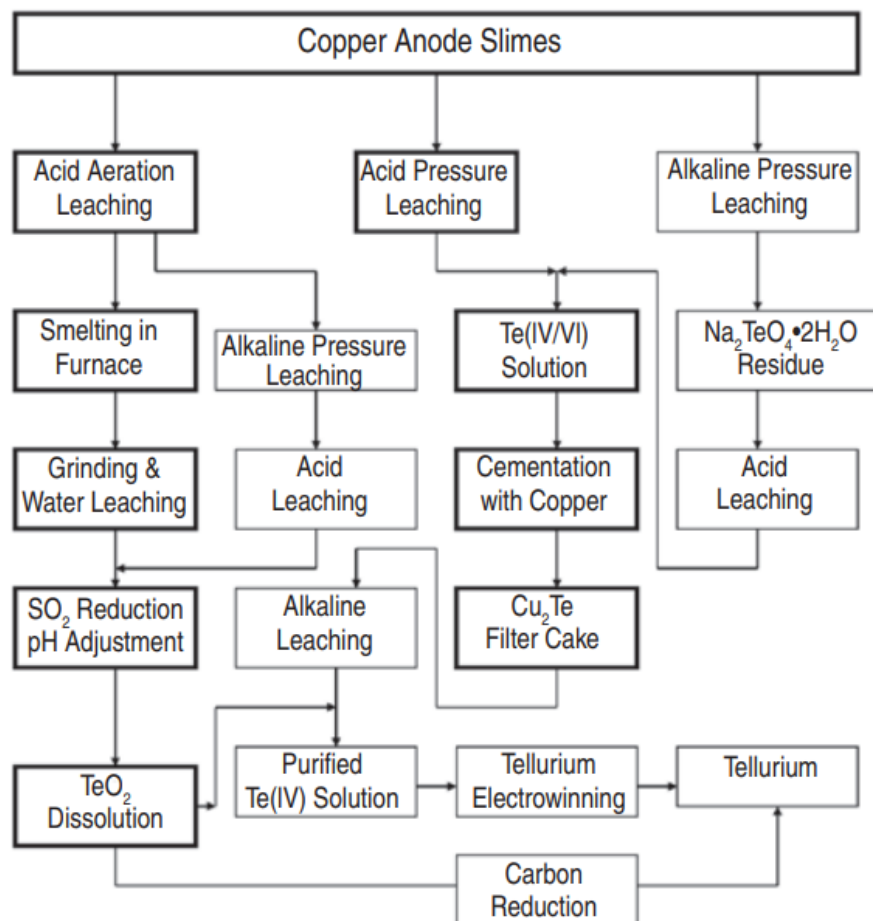


Figure 1.8: A flow chart describing the possible routes of Te extraction from copper anode slimes.⁵²

The U.S Geological Survey estimates quantifying reserves of Se and Te suggest that 90 % of Te is recovered from these Cu anode slimes and therefore the reserves of Te are based on a percentage related to the known Cu reserves.⁵³ As the primary ores of these elements are not processed directly, another option would be to reprocess Te and Se that has already been extracted from the anode slimes. As of 2018, the USGS reported that there was minimal recycling of Te and even less recycling of Se.⁵³ This was justified by the fact that their uses are very dispersive and therefore there is currently little scrap worth reprocessing. A recycling trial using CdTe solar cells was conducted in the USA, however due to the low number of solar cells that had reached the end of their working life, the results were limited.⁵³ In the not so distant future however, the recycling of solar panels is likely to become a major source of Te, as it becomes a more concentrated source, when further solar panels reach their end of life.⁵⁴ CdTe reprocessing from scrap PV films has been investigated by leaching with a sulfuric acid and hydrogen peroxide mixture. Following this, the Cd was recovered by electrowinning and the Te was recovered by precipitation or cementation, whereby TeO₂, TeS and metallic Te were precipitated with NaOH, Na₂S and Zn respectively.⁵⁵ In summary, the current technology surrounding the processing and reprocessing of Se and Te is somewhat limited, requiring new investigations into processes and solvents.

1.5 Solvometallurgy

Solvometallurgy is a non-aqueous analogue of hydrometallurgy and has been defined as “the extraction of metals from ores, residues, production scrap and urban waste using non-aqueous solutions”.⁵⁶ It should, however be noted that non-aqueous does not necessarily mean water-free solvents, but rather solvents with very low water content. Solvometallurgy is still classed as an emerging technique, even though one of the earliest examples of Solvometallurgy was from the 1950’s and was used in the extraction of uranium using non-aqueous mixtures such as acetone-HCl.⁵⁷ However, its Technology Readiness Level, which implies the length of time for execution is low, at only 3-4.⁵⁶ Hence suggesting that any short-term implementation is unlikely.

An overview of the main reasons for using solvometallurgy preferentially over other methods of metal processing is provided in a review by Binnemans et al. One of the

biggest advantages in using solvometallurgical processes instead of hydrometallurgical processes is a reduction in the amount of acid required to leach the metals. This particular advantage is actually two-fold, in that reducing the amount of acid subsequently reduces the amount of water used in the process, which reduces the waste water generated as well as reducing the hydrogen embrittlement of the metals.⁵⁶ The reduction in water use has the additional advantage of simplifying mining in places where water is a limited resource. For example, mines in the Atacama Desert in Chile supply approximately 1/3 of the world's copper but this region has a significantly low annual rainfall.⁵⁸ Accordingly, there is significant competition for precious water resources between agriculture and mining. Another environmental based benefit that coincides with using solvometallurgy is the reduction in energy consumption from the ability to process the minerals at room temperature, as opposed to the extremely high temperatures traditionally used in pyrometallurgy. Ideally, in any metal extraction process, 100 % of the solvent used in leaching would be recovered, and ultimately reused or recycled. However, complete recovery of the solvents is usually impossible due to absorption of solvent onto solid waste material, or evaporative processes.

Hydrometallurgy is generally unselective, leaching unwanted metals alongside the desired metals making processing lower grade ores inefficient. Solvometallurgy also offers the possibility to increase the selectivity for certain metal leaching processes. Selective extraction enables the successful mining of other low-grade ores.⁵⁶ An example of a successful solvometallurgical extraction is the leaching of Cu from Chrysocolla ($\text{CuSiO}_3 \cdot 2\text{H}_2\text{O}$), a Cu silicate ore. The processing of this particular ore with acid is troublesome due to the generation of silica gel. An alternative approach was developed using an extractant containing 5,8-diethyl-7-hydroxy-6-dodecanone oxime dissolved in kerosene with a small amount of aqueous ammonia. It was found that ammonia was able to enter the pores of the highly porous ore and reacted with the Cu^{2+} , subsequently allowing the resulting $[\text{Cu}(\text{NH}_3)_4]^{2+}$ complex to diffuse to the surface and react with the extractant solution. The ammonia is consequently regenerated, almost acting as a catalyst meaning much lower amounts of ammonia are required compared to using an ammoniacal leach solution.⁵⁶

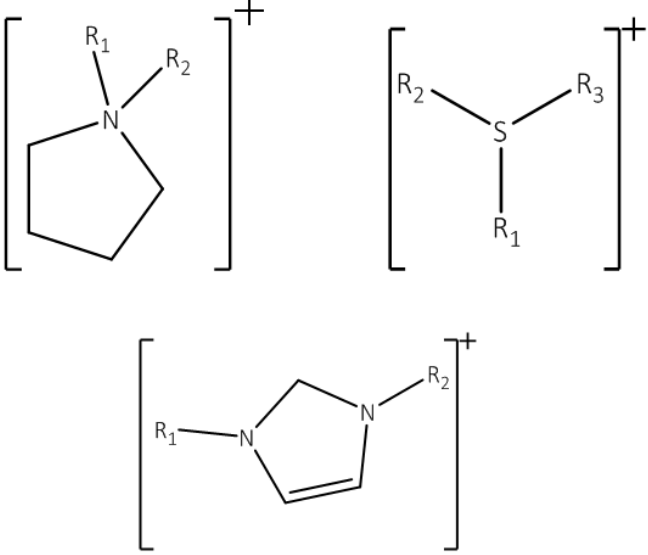
1.6 Ionic Liquids and Deep Eutectic Solvents

Ionic Liquids (ILs) are most commonly defined as salts or mixtures of ions with a melting point below 100 °C.⁵⁹ However, this particular definition, involving a temperature limit is disliked by authors such as Welton, who points out that a salt melting at 90°C has little difference to a salt melting at 110°C.⁶⁰ Instead, the definition of a liquid consisting predominantly of ions is preferred. In general, ILs have very low vapour pressures, are thermally stable and a wide temperature range between the melting and boiling points, similar to that of molten salts. Electrochemically, ILs typically present good conductivity (e.g. 14 mScm⁻¹ for [EMIM][BF₄⁻]), large electrochemical windows (around 4V for imidazolium salts) and suitable transport properties.⁶¹

ILs have large, asymmetrical organic cations which reduce the lattice energy of the salt, allowing it melt at lower temperatures than conventional inorganic salts. Comparing this to typical simple salts such as NaCl and KCl, which have melting points in the region of 800 °C due to their small ion size (high lattice energy).⁶² Historically, the earliest reporting of ILs is often attributed to ethyl ammonium nitrate that was discovered by Walden in 1914. This IL was prepared by the addition of concentrated nitric acid to ethylamine and the subsequent removal of water to leave a salt that remained liquid.⁶³ He determined that the large cation size of this particular salt was affecting the lattice energy and hence causing a decrease in the melting point to around 13 °C. Little was done to further the research into ILs until 1951 when it was found that an ionic mixture of N-ethylpyridinium bromide and AlCl₃ melted at unexpectedly low temperatures.⁶⁴

Since then, it has been reported that around 10¹⁸ ILs are theoretically possible, compared to around 600 known molecular solvents.⁶⁴⁻⁶⁷ This enables the possibility of tuning an IL to a particular process, by judicious selection of both cation and anion.⁶⁸ Some examples of the ions that can be combined to make ILs are presented in Table 1.4. As a result of the large number of combinations that are available, ILs have a wide range of applications, including in metallurgy. For example, Imidazolium based ILs e.g. [C₄mim][HSO₄] have been shown to be a suitable solvent to recover Ag and Au from their ores with iron (III) sulfate and thiourea as oxidant and complexing agent respectively.⁶⁹

Table 1.4: Examples of different anions and cations that together form ionic liquids.

Cations	Anions
	<p>F⁻</p> <p>PF₆⁻</p> <p>BF₄⁻</p> <p>Cl⁻</p> <p>[CF₃CO₂]⁻</p> <p>[N(CN)₂]⁻</p> <p>[CF₃CONCF₃SO₂]⁻</p>

The first reported industrial application that involved the use of ILs was publicised in 2003, the BASIL (Biphasic Acid Scavenging Using Ionic Liquids) enabled a process that produces alkoxyphenylphosphines to increase its space time yield by 80,000.⁷⁰ The process was initiated by BASF in their production of diethoxyphenylphosphine, whereby the HCl generated in the reaction of dichlorophenylphosphine with ethanol needed removing to prevent any further side reactions. The removal of HCl could not be carried out in aqueous solvent extraction and the use of triethylamine as a scavenger proved troublesome. Instead the use of 1-methylimidazole was used as a base to scavenge the acid and ultimately form the IL methylimidazolium chloride, shown in the reaction mechanism below:

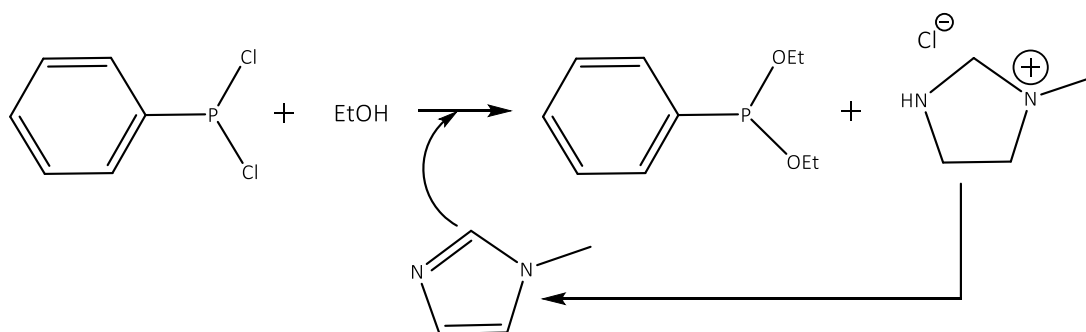


Figure 1.9: Mechanism describing the basis of the BASIL process, whereby methylimidazole is added to the system to scavenge HCl ultimately forming the IL methylimidazolium chloride.⁷¹

Ultimately, the IL can be easily separated from the diethoxyphenylphosphine due to a clear phase separation and is finally deprotonated to regenerate the methylimidazole. Through the development of this process and the fact that the resulting salt is now in a liquid state, the reactor was able to be redesigned and BASF were able to avoid batch reactors and also decrease the size of their reactor significantly. This process is carried out on an industrial scale using several tonnes of ILs, which showed that significant quantities are able to be handled and recycled.⁷¹

ILs have very low, often unmeasurable vapour pressures, this provides numerous advantages and disadvantages. For example, some are not easily purified by distillation like traditional molecular solvents would be. Therefore, it is vital that the starting materials are as clean and free of impurities as possible, before the IL is even generated. From an environmental standpoint however, low vapour pressures are beneficial because the risk of volatile organic compounds (VOCs) is removed.⁷²

Deep Eutectic Solvents (DESs) are produced by mixing quaternary ammonium salts and hydrogen bond donors such as amides, carboxylic acids and glycols.^{73,74} The large non-symmetric salt molecule has low lattice energy, which enables the melting point to be lowered and the solvent to be liquid at room temperature.⁷⁵ Although they do not fit the strict definition of ILs, i.e. only composed of ions, they do share many of the physical characteristics and tend to be discussed as related liquids. Smith *et al.* discusses the properties and applications of these liquids in more detail.⁷⁶ DESs have found different

applications to ILs due to their ease of preparation and generally lower toxicity, which enable their use on a larger scale.⁷⁷⁻⁷⁹

A eutectic is a minimum in the melting point of a two-component phase diagram and is shown schematically in Figure 1.10. It forms due to strong interactions between two components forming non-ideal mixtures and decreasing the lattice energy of the constituents.⁶¹ In DESs such as Ethaline the interactions tend to be hydrogen bonds between the chloride and the hydrogen bond donor (HBD), ethylene glycol. This results in charge delocalisation which ultimately decreases the melting point of the mixture.⁷⁶

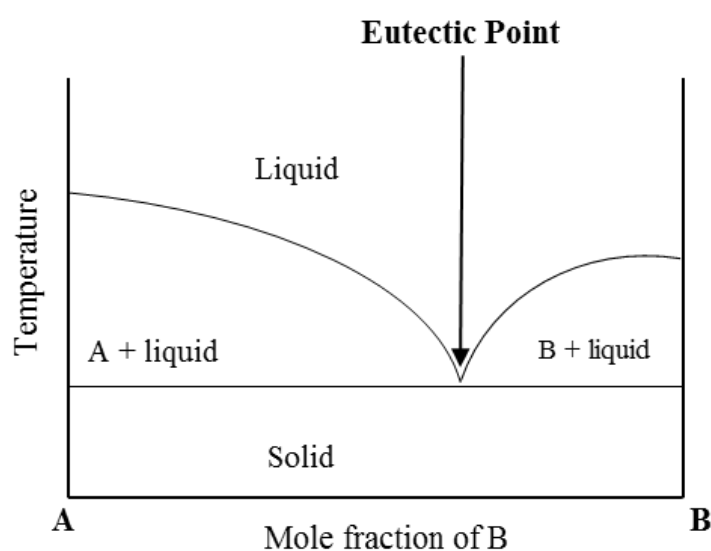


*Figure 1.10: Phase diagram demonstrating the eutectic point of a 2-component system.*⁴⁶

DESs have been divided into 4 categories depending on the two components they are made from and these are listed in Table 1.5. The first DES that was reported in the literature was discovered by Abbott et al. in 2001, it involved the mixing of a quaternary ammonium salt and a metal halide.⁸⁰

Table 1.5: Description of the components that make up the 4 different types of DESs.

Type 1	Quaternary ammonium salt	Metal halide
Type 2	Quaternary ammonium salt	Hydrated metal halide
Type 3	Quaternary ammonium salt	Hydrogen Bond Donor
Type 4	Metal halide (hydrate)	Hydrogen Bond Donor

Since their discovery, DESs have been employed in a number of different applications, including metal processing technologies such as immersion coating^{81,82} of Ag and Au, electrodeposition⁸³⁻⁸⁶ and electropolishing.^{87,88} Within these industries, the traditional methods of using aqueous systems present their own problems. The narrow potential window of water results in gas evolution which ultimately leads to hydrogen embrittlement and a lack of current efficiency. Alongside this, toxic complexing agents (i.e. cyanide) and electrolytes (i.e. hexavalent chromium) are also a problem.^{76,89} The latter is a particular problem for chrome plating industries whereby numerous countries have legislated to limit its use due to its high toxicity. As an alternative, it has been shown that a Type 2 DES of choline chloride and a chrome salt ($\text{CrCl}_3 \cdot 6\text{H}_2\text{O}$) can be prepared and be used to produce a variety of different morphological chrome coatings.⁹⁰

1.6.1 Properties of DESs

In this study, the Type 3 DESs are of most interest, specifically Ethaline, Reline and Oxaline, other common Type 3 DESs include Glyceline and Maline. In all cases, the quaternary ammonium salt remains constant (choline chloride) and the hydrogen bond donor is altered to change the characteristics of the DES, such as viscosity, metal coordination behaviour, acidity, and ability to solubilise metals selectively. The composition of a selection of DESs is presented in Table 1.6, where it can be seen that the choice of HBD has an impact on different physical properties of the DES.

Table 1.6: 5 common type 3 DESs with associated physical properties.^{61,91,92}

DES	HBD	Viscosity /mm ² s ⁻¹	Density /gcm ⁻³	Conductivity /mScm ⁻¹
Ethaline	Ethylene glycol	20	1.12	7.61
Reline	Urea	218	1.24	0.75
Oxaline	Oxalic acid	149	1.20	
Glyceline	Glycerol	118	1.18	1.05
Maline	Malonic acid			0.36

In comparison to water, the viscosities of DESs are significantly higher. Their conductivities cover a wide range of values. In addition to these physical properties, comparisons of speciation and redox potentials between aqueous and DES solvents have been reported.^{12, 93}

The effect of the HBD on pH in these different DESs has also been studied. The activity of the protons in these DESs and subsequently their pH was investigated, revealing that the relative pH of the DES follows the pH of the associated HBD. Of this selection of DESs, Oxaline and Maline have been shown to have the lowest pH at 1.32 and 2.39, respectively, and Reline the highest pH at 8.91. Ethaline and Glyceline which contain glycolic HBDs are considered neutral on this scale.^{92,94}

This project is focused on the electrochemistry of materials in Ethaline specifically. Abbott et al. report the first electrochemical series in DESs whereby an average of the onset potentials for the oxidation and reduction peaks for 17 different redox couples in Ethaline were recorded.¹² This data was compared to the corresponding values in aqueous systems to determine trends on how it would be expected for metals to behave. For example, it is noted that for oxophilic metals in the p-block, DESs tend to destabilise the higher oxidation states compared to the lower oxidation state. Whereas the more chlorophilic elements showed the opposite behaviour of lower oxidation states being destabilised preferentially. The majority of trends in this paper are evidenced by the high chloride environment provided by the DES, suggesting that the metal speciation is

controlled by the anionic component of the liquid, i.e. chloride, resulting in the formation of metal chloride complexes in solution.¹²

The solubility of metal salts is dependent on the salt species as well as the HBD in the DES. Metal oxides present much better solubility in the more acidic DESs (oxaline and maline).⁷⁹ Whereas, metal chlorides have been observed to exhibit high solubility in Ethaline and most DESs.⁹⁵ This has been attributed to the high polarity and ionic nature of these solvents. The speciation of the metals once dissolved are more complex than the speciation in aqueous media due to the differences in Lewis basicity with the anion. Speciation will affect redox potentials, solubilities and electroreduction kinetics and ultimately determine whether dissolution, as well as electrowinning, is possible.

1.6.2 Metal Processing with ILs and DESs

Another branch of solvometallurgy, specifically in IL or DES environments, is referred to as ionometallurgy.¹² Ionometallurgy can be thought of as a way to design processes (e.g. metal stripping and deposition) simply by adjusting the physical and chemical properties of the IL through judicious choice of both cation and anion. An example of where this works more effectively than aqueous solvents is the use of iodine as an oxidising agent to dissolve metal species, instead of using toxic species such as cyanide.^{13,96,97} Iodine has been used as a redox catalyst in Ethaline as it exhibited a high solubility (>200 g/kg) compared to in water (0.29 g/kg), as well as fast electron transfer. The redox potential is high for iodine in Ethaline, between 0.4 and 0.6V, (with Pt disc working electrode vs. Ag/AgCl reference electrode) in comparison to a range of metals ($\text{Cu}^{+0} \sim -0.35 \text{ V}$ and $\text{Zn}^{2+0} \sim -0.85 \text{ V}$).⁹⁷ Therefore it is readily able to oxidatively leach those metals. This has been demonstrated by Abbott et al. with a selection of systems including Cu/Zn, Ga/As and the recovery of Au and Ag from other ores.⁹⁷ One of the major benefits of using ionometallurgy, is the fact that the processes can be carried out in ambient atmospheric conditions. With ambient pressure, temperature and without the need for a dry, inert environment, compared to the extreme temperatures that are used in pyrometallurgical processes.⁹⁸

Metal oxides can typically be processed by pyrometallurgy, they are often insoluble in most molecular solvents, other than strong acids. Type 3 DESs, produced with a

quaternary ammonium salt and a hydrogen bond donor (HBD) have been shown to effectively dissolve a range of metal oxides. The solubility of 17 different metal oxides from across the periodic table from TiO_2 to ZnO in 3 different DESs has been reported and shown that the choice of DES, or more specifically the choice of the HBD, leads to the selective dissolution of certain metals. It was shown that in general the higher solubility was observed for the DESs with the most acidic HBDs. The solubility was also higher with the more ionic oxides (ZnO) and were shown to decrease as they became more covalent.⁷⁹

This successful solubilisation has been utilised in the large-scale extraction of metal oxides from a commercial waste product from the steel manufacturing industry, electric arc furnace (EAF) dust.⁹⁹ EAF dust contains oxides of several metals including Al, Cu, Fe, Mn, Pb and Zn and has been processed by a so-called hybrid DES, a mixture of choline chloride, urea and ethylene glycol. The hybrid DES showed high solubilising ability to the Pb and Zn and was able to selectively dissolve their oxides, while the Fe and Al oxides remained as solids. Initially the high solubility was noticed in the DES Reline, however this liquid has a high viscosity ($218 \text{ mm}^2\text{s}^{-1}$). By adding ethylene glycol to the DES, the high coordinating ability was retained, whilst significantly decreasing the viscosity.

As for ILs, studies have investigated the use of imidazolium based ILs like $[\text{Bmim}][\text{HSO}_4]$ ¹⁰⁰ or $[\text{C}_6\text{mim}][\text{HSO}_4]$ as a leachate for a copper sulfide mineral and it was found that due to its ability to catalyse the transfer of oxygen and accelerate the oxidation of the sulfide it was a better alternative to H_2SO_4 .^{101,102} Although the research into using ILs as mineral leachates has significant potential, there are still several negative aspects that restrict their commercialisation potential. ILs specifically cannot compete with acid/base hydrometallurgical processing as they are prohibitively expensive (e.g. 50 g $[\text{Bmim}][\text{BF}_4^-]$ \sim £100) to produce on a tonne scale and can often be air and moisture sensitive. In addition, losses of solvent due to adsorption onto waste solids will increase any production costs related to replacement of the liquid.

1.6.3 DES Viscosity

The viscosity of DESs is often considered one of their biggest downfalls, however there are processes that have been developed to take advantage of the high viscosity. One

example of this is an application as lubricants⁹¹ for uses in marine industries, and research is also being conducted to incorporate them into the leather processing industry¹⁰³ to replace the fat liquor stage (lubricating and softening the leather by introducing oil) of the treatment. The viscosity of these liquids can be explained by hole theory. This theory assumes that on melting an ionic compound empty spaces (holes) will occur.⁷⁶ In the case of molten salts these holes are a large, allowing easy movement of ions, hence resulting in a lower viscosity. In DESs these holes are smaller and the larger ions generally present in DESs makes their movement into the holes much slower causing them to be more viscous.^{76,104}

A new electrochemical technique, paint casting, also makes use of the viscous character of DESs, whereby a conductive paste is formed with the material that can be applied directly to the surface of a working electrode. It was developed in order to study the electrochemical behaviour of semi-conductors and insulators more easily and has been shown to be an effective technique in the analysis of materials that would otherwise prove difficult to study, such as the mineral galena (PbS).¹⁴

The electrochemistry of several iron sulfide minerals including, pyrite, marcasite, pyrrhotite, arsenopyrite, loellingite along with metal sulfide waste material, jarosite have been investigated in a previous study by Al-Bassam.¹⁰⁵ It was shown through the paint casting method that these typically difficult to study materials could be analysed by cyclic voltammetry. Further to this it was shown that the metals contained within the minerals and the waste material could be leached both through anodic and cathodic dissolution. Jarosite, a waste material from zinc processing, has been shown to contain around 21 different elements with large amounts of Fe, Pb, Zn and S. A method to separate the Pb from the other metals was established using a combination of electrochemical dissolution along with electrochemical reduction and galvanic deposition.¹⁰⁵ This study is very much in its infancy and the potential of extending to other metal sulfides and waste material is currently of great interest.

1.7 Research Objectives

This study aims to investigate the mechanism of dissolution and recovery of chalcogens and chalcogen-containing materials in DESs in order to potentially develop a more environmentally friendly method of extracting and recovering metals.

In the first phase of investigations, a variety of different copper chalcogenides will be investigated, via paint casting, to demonstrate their electrochemical behaviour in Ethaline. The dissolution and subsequent recovery of the copper or chalcogens will be examined and a suitable mechanism elucidated. A variety of sulphides, including copper and iron sulphide, have been studied previously and it is known that they are electrochemically active in Ethaline. However, there are limited studies that present the electrochemistry of selenides and tellurides in DESs.^{34, 106}

The second phase will investigate a wider array of selenides and tellurides, including silver-, cadmium- and zinc-containing systems. From the exhibited electrochemistry, methods will then be investigated with the aim to selectively recover Se and Te from the different compounds. Cadmium sulfide, selenide and telluride are of particular interest due to their applications in increasingly popular low CO₂ technologies such as PV solar cells. This work is essentially laying the foundation that could later be applied to the processing of old solar panels to recover and reuse the elements.

Finally, a method to improve the extraction efficiency of copper from chalcopyrite is explored. Currently, chalcopyrite is the most abundant source of copper worldwide and as discussed previously is under a lot of scrutiny in the literature to provide more environmentally friendly methods that are successful in the extraction of copper. Mixtures of different DESs will be tested in order to obtain a solvent with optimum physical and chemical properties, and improvements to cell design from previous investigations will provide a way to increase the yield of copper.

1.8 References

1. <http://nationalgeographic.org/encyclopedia/ore> (Accessed 05/11/17)
2. Daintith, J., (2008), A Dictionary of Chemistry, 6th Ed., Oxford University Press, Oxford
3. Abbott, A. P., Frisch, G., Hartley, J., Ryder, K. S., (2011) Processing of Metals and Metal Oxides using Ionic Liquids, *Green Chem.*, **13**, 471-481
4. Carrillo-Pedroza, F., Soria-Aguilar, M., Salinas-Rodriguez, E., Martinez-Luevanos, A., Pecina-Trevino, T., Davalos-Sanchez, A., (2012) Recent Researches in Metallurgical Engineering From Extraction to Forming, Chapter 2, InTech.
5. Bouroushian, M., (2010), Electrochemistry of metal chalcogenides, 1st Ed., Springer, Berlin.
6. Deb, S. K., (1996) Thin Film Solar Cells: An Overview, *Renewable Energy*, **8**, 375-379
7. USGS, (2015) Tellurium-The Bright Future of Solar Energy. (<https://pubs.usgs.gov/fs/2014/3077/pdf/fs2014-3077.pdf>)
8. Li, Y., Chandra, A., Gerson, A., (2014) Scanning Photoelectron Microscopy Studies of Freshly Fractured Chalcopyrite Exposed to O₂ and H₂O, *Geochimica et Cosmochimica Acta*, **133**, 372-386
9. Li, Y., Qian, G., Li, J., Gerson, A., (2015) Kinetics and Roles of Solution and Surface Species of Chalcopyrite Dissolution at 650 mV, *Geochimica et Cosmochimica Acta*, **161**, 188-202
10. Baba, A., Ayinla, K., Adekola, F., Ghosh, M., Ayanda, O., Bale, R., Sheik, A., Pradhan, S., (2012) A Review on Novel Techniques for Chalcopyrite Ore Processing, *Int. J. Mining Eng. Min. Proc.* **1**, 1-16
11. Chagnes, A., (2015) Fundamentals in Electrochemistry and Hydrometallurgy, *Lithium Process Chem.*, **1**, 41-80

12. Abbott, A. P., Frisch, G., Gurman, S., Hillman, A., Hartley, J., Holyoak, F., Ryder, K., (2011) Ionometallurgy: Designer Redox Properties for Metal Processing, *Chem. Comm.*, **47**, 10031-10033.
13. Jenkin, G. R. T., Al-Bassam, A. Z. M., Harris, R. C., Abbott, A. P., Smith, D. J., Holwell, D. A., Chapman, R. J., Stanley, C. J., (2016) The Application of Deep Eutectic Solvent Ionic Liquids for Environmentally-Friendly Dissolution and Recovery of Precious Metals, *Minerals Engineering*, **87**, 18-24
14. Abbott, A. P., Bevan, F., Baeuerle, M., Harris, R. C., Jenkin, G. R. T., (2017) Paint Casting: A Facile Method of Studying Mineral Electrochemistry, *Electrochem. Comm.*, **76**, 20-23
15. Abbott, A. P., Al-Bassam, A. Z. M., Goddard, A., Harris, R. C., Jenkin, G. R. T., Nisbet, F. J., Wieland, M., (2017) Dissolution of Pyrite and other Fe-S-As Minerals using Deep Eutectic Solvents, *Green Chem.*, **19**, 2225-2233
16. Kuan, Y. c., Lee, I. H., Chern, J. M., (2010) Heavy Metal Extraction from PCB Wastewater Treatment Sludge by Sulfuric Acid, *J. Haz. Mat.*, **177**, 881-886
17. Watling, H. R., (2013) Chalcopyrite Hydrometallurgy at Atmospheric Pressure: 1. Review of Acidic Sulfate, Sulfate-Chloride and Sulfate-Nitrate Process Options, *Hydromet.*, **140**, 163-180
18. Boulegue, J., (1978) Solubility of Elemental Sulfur in Water at 298 K, *Phosphorus and Sulfur and the Related Elements*, **5**, 127-128
19. Briceno, A., Chander, S., (1990) Oxidation of Hydrosulphide Ions in Gold Part I: A Cyclic Voltammetry Study, *J. App. Electrochem.*, **20**, 506-511
20. Zhao, H., Hu, M., Li, Y., Zhu, S., Qin, W., Qiu, G., Wang, J., (2015) Comparison of Electrochemical Dissolution of Chalcopyrite and Bornite in Acid Culture Medium, *Trans. Nonferrous Metals Soc. China*, **25**, 303-313.
21. Almeida, T., Garda, E., Alves da Silva, H., Matencio, T., Lins, V., (2016) Electrochemical Study of Chalcopyrite Dissolution in Sulfuric, Nitric and Hydrochloric Acid Solutions, *Int. J. Mineral Processing*, **149**, 25-33.

22. Gardner, J., Woods, R., (1979) A Study of the Surface Oxidation of Galena using Cyclic Voltammetry, *J. Electroanal. Chem.*, **100**, 447-459.
23. Cisneros-Gonzalez, I., Oropeza-Guzman, M., Gonzalez, I., (1999) Cyclic Voltammetry Applied to the Characterisation of Galena, *Hydrometallurgy*, **53**, 133-144.
24. Cisneros-Gonzalez, I., Oropeza-Guzman, M., Gonzalez, I., (2000) An Electrochemical Study of Galena Concentrate in Perchlorate Medium at pH 2.0: The Influence of Chloride Ions, *Electro. Acta*, **45**, 2729-2741.
25. Zhang, S. Y., Fang, C. X., Wei, W., Jin, B. K., Tian, Y. P., Shen, Y. H., Yang, J. X., Gao, H. W., (2007) Synthesis and Electrochemical Behaviour of Crystalline Ag₂Se Nanotubes, *J. Phys. Chem. C.*, **111**, 4168-4174
26. Gonzalez- Ibarra, A. A., Nava-Alonso, F., Uribe-Salas, A., (2019) Electrochemical Study of Silver Telluride (Ag₂Te): Anodic and Cathodic Potential Dependent Reactions in Alkaline Cyanide Solutions, *Hydromet.*, **183**, 230-239
27. Kim, S. H., Han, W. K., Lee, J. H., (2010) Electrochemical Characterization of CdSe and CdTe Thin Films using Cyclic Voltammetry, *Current Applied Physics*, **10**, 481-483
28. Hao, N., Jiang, L., Qian, J., Wang, K., (2016) Ultrasensitive Electrochemical Ochratoxi Aptasensor Based on CdTe Quantum Dots Functionalized Graphene/Au Nanocomposites and Magnetic Separation, *Journ. Electro. Anal. Chem.* **781**, 332-338
29. Nedjl, L., Richtera, L., Xhaxhiu, K., et al. (2016) UV Tuning of Cadmium Telluride Quantum Dots Assessed by Spectroscopy and Electrochemistry, *Int. Journ. Electro. Sci.*, **11**, 175-188
30. Wang, J., Li, Q., Mu, Y. N., Zhou, X. M., Yang, L. H., Lv, P., Su, S., Niu, J. S., Fu, W. Y., Yang, H. B., (2015) Effect of Sodium Chloride on the Electrochemistry Activity of Electrodeposited CdTe Films with Various Morphologies, *RSC Adv.*, **5**, 43016-43022

31. Tepecik, A., Altin, Z., Erturan, S., (2008) The Diorganoselenium and Selenides Compounds Electrochemistry, *Journ. Automated Methods and Management in Chemistry*, **2008**, 1-6
32. Hsiu, S. I., Sun, I. W., (2004) Electrodeposition Behaviour of Cadmium Telluride from 1-ethyl-3-methylimidazolium chloride tetrafluoroborate Ionic Liquid, *J. Applied Electrochemistry*, **34**, 1057-1063
33. Catranguiu, A. S., Beregoi, M., Cojocaru, A., Anicai, L., Cotarta, A., Visan, T., (2016) Electrochemical Deposition of Zinc Telluride Thin Films from Ethaline Ionic Liquid, *Chalcogenide Letters*, **13**, 187-199
34. Golgovici, F., Visan, T., (2012) Electrodeposition Behaviour of Cadmium Telluride from Choline Chloride- Urea Ionic Liquids, *Chalcogenide Letters*, **9**, 165-174
35. Vaughan, D. J., Craig, J. R., (1978) Mineral Chemistry of Metal Sulfides, 1st Ed., Cambridge University Press, UK.
36. Bagnall, K. W., (1966) The Chemistry of Selenium, Tellurium and Polonium, 1st Ed., Elsevier, Amsterdam
37. Norgate, T. E., Jahanshahi, S., Rankin, W. J., (2007) Assessing the Environmental Impact of Metal Production Processes, *J. Cleaner Production*, **15**, 838-848
38. Butt, C. R. M., Cluzel, D. (2013) Nickel Laterite Ore Deposits: Weathered Serpentinities, *Elements*, **9**, 123-128.
39. Gandhi, S., Sarkar, B., (2016) Essentials of Mineral Exploration and Evaluation, 1st Ed., Elsevier, Amsterdam
40. Norgate, T., Jahanshahi, S., (2011), Reducing the Greenhouse Gas Footprint of Primary Metal Production: Where Should the Focus Be?, *Minerals Engineering*, **24**, 1563-1570
41. Norgate, T., Jahanshahi, S., (2010) Low Grade Ores- Smelt, Leach or Concentrate, *Minerals Engineering*, **23**, 65-73

42. Northey, S. A., Haque, N., Lovel, R., Cooksey, M. A., (2014) Evaluating the Application of Water Footprint Methods to Primary Metal Production Systems, *Minerals Engineering*, **69**, 65-80
43. Haque, N., Norgate, T., Northey, S., (2014) Life Cycle Greenhouse Gas Footprints of Metal Production with Recycling Scenarios, In *EPD Congress 2014-Held During TMS 2014 143rd Annual Meeting and Exhibition, (The Minerals, Metals and Materials Society)*, 113-120
44. Park, J., Jung, Y., Kusumah, P., Lee, J., Kwon, K., Lee, C., (2014) Application of Ionic Liquids in Hydrometallurgy, *Int. J. Mol. Sci.*, **15**, 15320-15343.
45. Hartley J. (2013) PhD Thesis: University of Leicester, Ionometallurgy: The Processing of Metals Using Ionic Liquids.
46. Al-Saydeh, S. A., El-Naas, M. H., Zaidi, S. J., (2017) Copper Removal from Industrial Wastewater: A Comprehensive Review, *Journ. Ind. And Eng. Chem.*, **56**, 35-44
47. Sole, K. C., Mooiman, M. B., Hardwick, E., (2018) Ion Exchange in Hydrometallurgical Processing: An Overview and Selected Applications, *Separation and Purification Reviews*, **47**, 159-178.
48. Hidmi, I., Edwards, M., (1999) Role of Temperature and pH in $\text{Cu}(\text{OH})_2$ Solubility, *Environ. Sci. Technol.* **33**, 2607-2610
49. Xie, Y., Xie, S., Chen, X., Gui, W., Yang, C., (2015) An Integrated Predictive Model with an On-line Updating Strategy for Iron Precipitation in Zinc Hydrometallurgy, *Hydrometallurgy*, **151**, 62-72.
50. Hoffmann, J. E., (1989) Recovering Selenium and Tellurium from Copper Refinery Slimes, *JOM*, **41**, 33-38.
51. Lu, D., Chang, Y., Yang, H., Xie, F., (2015) Sequential Removal of Selenium and Tellurium from Copper Anode Slime with High Nickel Content, *Trans. Nonferrous Met. Soc. China*, **25**, 1307-1314.

52. Wang, S., (2011) Tellurium, Its Resourcefulness and Recovery, *JOM*, **63**, 90-93
53. U.S. Geological Survey, (2018) Mineral Commodity Summaries 2018, *U.S. Geological Surveys*, 200 p.
54. Lee, C. K., Rhee, K., Sohn, H., (1997) The recovery of Tellurium from Copper Anode Slimes by Hydrometallurgical Processes, *J. Korean Inst. Of Resources Recycling*, **6**, 41-45
55. Fthenakis, V., Duby, P., Wang, W., Graves, C., Belova, A., (2006) Recycling of CdTe Photovoltaic Modules: Recovery of Cadmium and Tellurium, *21st European Photovoltaic Solar Energy Conference, Germany*.
56. Binnemans, K., Jones, P. T., (2017) Solvometallurgy: An Emerging Branch of Extractive Metallurgy, *J. Sustain. Metall.*, **3**, 570-600
57. Kimball, R. B., Ewing, R. A., (1956) Uranium Recovery from Ores with Hydrochloric Acid and Acetone, US Patent 2869980
58. <https://www.bbc.co.uk/news/business-17423097> (Accessed: 05/01/2019)
59. Welton, T., (1999) Room-Temperature Ionic Liquids. Solvents for Synthesis and Catalysis, *Chem. Rev.*, **99**, 2071-2083
60. Welton, T., (2018) Ionic Liquids: A Brief History, *Biophys. Rev.*, **10**, 691-706
61. Endres, F., Abbott, A. P., MacFarlane, D., (2008) Electrodeposition from Ionic Liquids, 1st Ed., Wiley-VCH, UK.
62. Johnson, K., (2007) What's an Ionic Liquid, *The Electrochem. Soc. Inter.* **16**, 38-41
63. Wassercheid, P., Welton, T., (2007) Ionic Liquids in Synthesis, 2nd Ed., Wiley VCH, Germany.
64. Hurley, F. H., Weir, T. P., (1951) The Electrodeposition of Aluminium from Non-Aqueous Solutions at Room Temperature, *J. Electrochem. Soc.*, **98**, 207-212

65. Simka, W., Puszczuk, D., Nawrat, G., (2009) Electrodeposition of Metals from Non-Aqueous Solutions, *Electro. Acta*, **54**, 5307-5319
66. Armand, M., Tarascon, J., (2008) Building Better Batteries, *Nature*, **451**, 652-657
67. Souza, R., Padilha, J., Goncalves, R., Dupont, J., (2003) Room Temperature Dialkylimidazolium Ionic Liquid-based Fuel Cells, *Electrochem. Comm.*, **5**, 728-731
68. Rogers, R. D., Seddon, K. R., (2003) Ionic Liquids- Solvents of the Future?, *Science*, **302**, 792-793
69. Whitehead, J., Zhang, J., Pereira, N., McCluskey, A., Lawrance, G., (2007) Application of 1-alkyl-3-methyl-imidazolium Ionic Liquids in the Oxidative Leaching of Sulphidic Copper, Gold and Silver Ores, *Hydrometallurgy*, **88**, 109-120
70. Andreani, L., Rocha, J. D., (2012) Use of Ionic Liquids in Biodiesel Production: A review, *Brazilian J. Chem. Eng.*, **29**, 1-13
71. Garcia-Verduga, E., Altava, B., Burguete, M. I., Lozano, P., Luis, S. V., (2015) Ionic Liquids and Continuous Flow Processes: A Good Marriage to Design Sustainable Processes, *Green Chem.*, **17**, 2693-2713
72. Benton, M. G., Brazel, C. S., (2002) Effect of Room Temperature Ionic Liquids as Replacements for Volatile Organic Solvents in Free-Radical Polymerization, *ACS Symposium Series*, **818**, 125-133
73. Abbott, A. P., Capper, G., Davies, D. L., Rasheed, R. K., Tambyrajah, V., (2003) Novel Solvent Properties of Choline Chloride/Urea Mixtures, *Chem. Comm.*, **0**, 70-71
74. Abbott, A. P., Boothby, D., Capper, G., Davies, D. L., Rasheed, R. K., (2004) Deep Eutectic Solvents Formed Between Choline Chloride and Carboxylic Acids: Versatile Alternatives to Ionic Liquids, *J. Am. Chem. Soc.*, **126**, 9142-9147

75. Abbott, A. P., Barron, J., Ryder, K., (2013) Electrolytic Deposition of Zn Coatings from Ionic Liquids Based on Choline Chloride, *Int. J. Surf. Eng. Coat.*, **87**, 201-207
76. Smith, E., Abbott, A. P., Ryder, K., (2014) Deep Eutectic Solvents (DES) and Their Applications, *Chem. Rev.*, **114**, 11060-11082.
77. Chemat, F., Anjum, H., Shariff, A., Kumar, P., Murugesan, T., (2016) Thermal and Physical Properties of (Choline Chloride + Urea + L-Arginine) Deep Eutectic Solvents, *J. Mol. Liq.*, **218**, 301-308
78. Rengstl, D., Fischer, V., Kunz, W., (2014) Low-Melting Mixtures Based on Choline Ionic Liquids, *Phys. Chem. Chem. Phys.*, **16**, 22815-22822
79. Abbott, A. P., Capper, G., Davies, D., McKenzie, Obi, S., (2006) Solubility of Metal Oxides in Deep Eutectic Solvents Based on Choline Chloride, *J. Chem. Eng. Data*, **51**, 1280-1282
80. Abbott, A. P., Capper, G., Davies, D., Munro, H., Rasheed, K., Tambyrajah, V., (2001), Preparation of Novel, Moisture-Stable, Lewis-Acidic Ionic Liquids Containing Quarternary Ammonium Salts with Functional Side Chains, *Chem. Comm.*, **19**, 2010-2011
81. Ballantyne, A. D., Forrest, G. C. H., Frisch, G., Hartley, J. M., Ryder, K. S., (2015) Electrochemistry and Speciation of Au⁺ in a Deep Eutectic Solvent: Growth and Morphology of Galvanic Immersion Coatings, *Phys. Chem. Chem. Phys.*, **17**, 30540-30550
82. Abbott, A. P., Nandhra, S., Postlethwaite, S., Smith, E. L., Ryder, K. S., (2007) Electroless Deposition of Metallic Silver from a Choline Chloride-Based Ionic Liquid: A Study using Acoustic Impedance Spectroscopy, SEM and Atomic Force Microscopy, *Phys. Chem. Chem. Phys.*, **9**, 3735-3743
83. Abbott, A. P., Ballantyne, A., Harris, R., Juma, J., Ryder, K., Forrest, G., (2015) A Comparative Study of Nickel Electrodeposition Using Deep Eutectic Solvents and Aqueous Solutions, *Electrochimica Acta*, **176**, 718-726

84. Abbott, A. P., Al-Barzinjy, A. A., Abbott, P. D., Frisch, G., Harris, R. C., Hartley, J., Ryder, K. S., (2014) Speciation, Physical and Electrolytic Properties of Eutectic Mixtures Based on $\text{CrCl}_3 \cdot 6\text{H}_2\text{O}$ and Urea, *Phys. Chem. Chem. Phys.*, **16**, 9047-9055
85. Abbott, A. P., Ttaib, K., Frisch, G., McKenzie, K. J., Ryder, K. S., (2009) Electrodeposition of Copper Composites from Deep Eutectic Solvents Based on Choline Chloride, *Phys. Chem. Chem. Phys.*, **11**, 4269-4277
86. Abbott, A. P., El Ttaib, K., Ryder, K. S., Smith, E. L., (2008) Electrodeposition of Nickel using Eutectic Based Ionic Liquids, *Trans. IMF.*, **86**, 234-240
87. Abbott, A. P., Capper, G., Swain, B. G., Wheeler, D. A., (2005) Electropolishing of Stainless Steel in an Ionic Liquid, *Trans. IMF.*, **83**, 51-53
88. Abbott, A. P., Ryder, K., Konig, U., (2008) Electrofinishing of Metals Using Eutectic Based Ionic Liquids, *Trans. IMF*, **86**, 196-204.
89. Liu, F., Deng, Y., Han, X., Hu, X., Zhong, C., (2016) Electrodeposition of Metals and Alloys from Ionic Liquids, *J. Alloys and Comp.*, **654**, 163-170
90. Ferreira, E. S. C., Pereira, C. M., Silva, A. F. (2013) Electrochemical Studies of Metallic Chromium Electrodeposition from a Cr(III) Bath, *J. Electroanal. Chem.*, **707**, 43-51
91. Abbott, A. P., Ahmed, E., Harris, R., Ryder, K., (2014) Evaluating Water Miscible Deep Eutectic Solvents and Ionic Liquids as Potential Lubricants, *Green Chem*, **16**, 4156-4161
92. Alabdullah, S. S., (2018) PhD Thesis: University of Leicester, pH Measurements in Ionic Liquids.
93. Hartley, J. M., Ip, C. M., Forrest, G. C. H., Singh, K., Gurman, S. J., Ryder, K. S., Abbott, A. P., Frisch, G., (2014) EXAFS study into the Speciation of Metal Salts Dissolved in Ionic Liquids and Deep Eutectic Solvents, *Inorg. Chem.*, **53**, 6280-6288

94. Abbott, A. P., Alabdullah, S. S. M., Al-Murshedi, A. Y. M., Ryder, K. S., (2018) Bronsted Acidity in Deep Eutectic Solvents and Ionic Liquids, *Faraday Discuss.*, **206**, 365-377
96. Abbott, A.P., Frisch, G., Hartley, J., Karim, W. O., Ryder, K. S., (2015) Anodic Dissolution of Metals in Ionic Liquids, *Progress in Nat. Sci.: Materials Int.*, **25**, 595-602
96. Jones, D., Hartley, J., Frisch, G., Purnell, M., Darras, L., (2012) Non-destructive, Safe Removal of Conductive Metal Coatings from Fossils: A New Solution, *Palaeo. Electronica*, **15**, 1-7
97. Abbott, A. P., Harris, R. C., Holyoak, F., Frisch, G., Hartley, J., Jenkin, G. R. T., (2015) Electrocatalytic Recovery of Elements from Complex Mixtures using Deep Eutectic Solvents, *Green Chemistry*, **17**, 2172-2179
98. Abbott, A. P., Frisch, G., (2013) Element Recovery and Sustainability (*Ch 3*), 1st Ed., RSC, U.K.
99. Abbott, A. P., Capper, G., Davies, D. L., Shikotra, P., (2006) Processing Metal Oxides using Ionic Liquids, *Mineral Processing and Extractive Metallurgy*, **115**, 15-18
100. Kuzmina, O., Symianakis, E., Godfrey, D., Albrecht, T., Welton, T., (2017) Ionic Liquids for Metal Extraction from Chalcopyrite: Solid, Liquid and Gas Phase Studies, *Phys. Chem. Chem. Phys.*, **19**, 21556-21564.
101. Aguirre, C. L., Toro, N., Carvajal, N., Watling, H., Aguirre, C., (2016) Leaching of Chalcopyrite (CuFeS₂) with an Imidazolium-Based Ionic Liquid in the Presence of Chloride, *Minerals Engineering*, **99**, 60-66
102. Dong, T., Hua, Y., Zhang, Q., Zhou, D., (2009) Leaching of Chalcopyrite with Bronsted Acidic Ionic Liquid, *Hydrometallurgy*, **99**, 33-38
103. Abbott, A. P., Alaysuy, O., Antunes, A., Douglas, A., Guthrie-Strachan, Wise, W., (2015) Processing of Leather Using Deep Eutectic Solvents, *Sust. Chem. And Eng.*, **3**, 1241-1247

104. Abbott, A. P., Boothby, D., Capper, G., Davies, D., Rasheed, R., (2004) Deep Eutectic Solvents Formed Between Choline Chloride and Carboxylic Acids: Versatile Alternatives to Ionic Liquids, *J. Am. Chem. Soc.*, **126**, 9142-9147.
105. Al-Bassam, A. Z. M. H., (2018) PhD Thesis: The University of Leicester, Mineral Processing using Deep Eutectic Solvents.
106. Golgovici, F., Visan, T., (2011) Cathodic Deposition of Components in PbTe Compounds Using Choline Chloride-Ethylene Glycol Ionic Liquids, *Chalcogenide Letters*, **8**, 487-497.

CHAPTER 2: EXPERIMENTAL & METHODOLOGY

Table of Contents

2.1 Materials	46
2.1.1 <i>Deep Eutectic Solvent preparation</i>	<i>47</i>
2.2 Electrochemical Methods	47
2.2.1 <i>Cyclic Voltammetry.....</i>	<i>49</i>
2.2.2 <i>Chronopotentiometry</i>	<i>52</i>
2.2.3 <i>Chronocoulometry</i>	<i>53</i>
2.3 Bulk dissolution.....	53
2.3.1 <i>UV-Vis</i>	<i>54</i>
2.3.2 <i>ICP-MS.....</i>	<i>55</i>
2.3.3 <i>EXAFS</i>	<i>56</i>
2.4 Recovery.....	57
2.4.1 <i>EDX.....</i>	<i>57</i>
2.4.2 <i>XRD.....</i>	<i>58</i>
2.4.3 <i>Scaled up recovery.....</i>	<i>59</i>
2.5 References.....	61

2.1 Materials

Table 2.1 lists the sources and purities of the chemicals used in this work.

Table 2.1: Sources and purity of the chemicals used in this study.

Chemical	Purity	Source
Choline chloride	99 %	Acros Organic
Ethylene glycol	99 %	Sigma Aldrich
Oxalic acid	98 %	Alfa Aesar
Urea	> 98 %	Sigma Aldrich
Copper (I) sulphide	99.5 %	Alfa Aesar
Copper (II) sulphide	>99 %	Sigma Aldrich
Copper chloride	>99.5 %	Sigma Aldrich
Copper (I) telluride	99.5 %	Alfa Aesar
Copper (I) selenide	99.95 %	Sigma Aldrich
Copper (II) selenide	99.5 %	Alfa Aesar
Sulfur	>99.5 %	Sigma Aldrich
Tellurium	>99.99%	5N+
Selenium	>99.99%	5N+
Cadmium telluride	>99.99%	5N+
Cadmium selenide	>99.99%	5N+
Cadmium sulfide	>99.99%	5N+
Silver telluride	Unknown	Aldrich
Silver selenide	Unknown	Aldrich
Silver sulfide	Unknown	Chem Cruz
Zinc telluride	99.99 %	Alfa Aesar
Zinc selenide	99.99 %	Alfa Aesar
Zinc sulfide	99.99 %	Aldrich
Silver wire	99.99 %	Alfa Aesar
Silver chloride	99.9 %	Sigma Aldrich
Iodine	>99.5 %	Fischer Scientific

Table 2.2: The mineral materials used in this thesis with their location (if known) and any other important information.

Mineral Name	Chemical Formula	Purity (in wt %)	Additional Notes
Chalcocite	Cu ₂ S	88.5	Sample ID: E206
Covellite	CuS	80.3	Sample ID: 20582
Chalcopyrite	CuFeS ₂	80.5	Externally sourced. Originally sourced from Morocco.
Galena	PbS	-	Sample ID: E898
Sphalerite	ZnS	-	Sample ID: E411 and X22

2.1.1 Deep Eutectic Solvent preparation

The most frequently used DES was Ethaline 200, a 2:1 molar ratio of ethylene glycol (62.07 g mol⁻¹) and choline chloride (139.62 g mol⁻¹) mixed together at 50 °C for 2-3 hours in order to form the eutectic solvent. After this time of constant heating and stirring, the solution became clear and homogeneous and was subsequently stored in an oven at 50 °C to prevent recrystallization of the choline chloride. The other solvents used in this study are Oxaline 100 and Reline 200, which are 1:1 and 1:2 molar mixtures of choline chloride with oxalic acid dihydrate and urea, respectively. From here on Ethaline 200, Oxaline 100 and Reline 200 will simply be referred to as Ethaline, Oxaline and Reline respectively. These other solvents are prepared in the same manner as Ethaline; however, Reline takes much longer (~ 5 hours) to form a eutectic, due to both initial components being solid at room temperature. Reline solidifies at cooler room temperatures, therefore it is also stored in the oven at 50 °C to prevent recrystallization.

2.2 Electrochemical Methods

Electrochemistry is often described as the study of charge transfer at an interface, this study is mostly concerned with the interface between a solid electrode and a liquid electrolyte. Electrochemistry often involves the collection of current and voltage data as a function of time upon modification of the electrode conditions.^{1,2} When an external voltage is applied to an electrochemical experiment the system is said to be under

electrolytic control.³ The rate of these reactions can be manipulated by several factors, including the external potential that is applied, the type of electrolyte, electrode material and the species that is being studied. Mass transport can affect the processes that are carried out in an electrolytic process because the electron transfer always occurs at the interface of the electrode with the electrolyte rather than in bulk solution.⁴ Mass transport is limited by the rate of diffusion, convection or migration. Migration is controlled and improved by providing an electrolyte that has good conductive properties and the rate of convection can be increased by stirring. For the case of diffusion, this is described in Fick's first law shown in Equation 2.1.

$$J = -D \frac{\partial[M]}{\partial x} \quad \text{Equation 2.1}$$

Fick's first law describes how species move from an area of high concentration to an area of low concentration, where J is the rate of diffusion, D is the diffusion coefficient, and $\frac{\partial[M]}{\partial x}$ is the concentration gradient of metal species (M) at the electrode surface to the surrounding bulk solution.¹

To conduct the majority of electrochemical experiments, 3 electrodes, an electrolyte solution and a potentiostat are required. A three-electrode cell containing a working electrode, counter electrode and reference electrode is used throughout quantitative electrochemical experiments such as cyclic voltammetry and chronopotentiometry. The working electrode is the interface of interest and it is between the surface of this electrode and the electrolyte that the reactions take place.⁵ The reference electrode provides a constant potential against which any changes in potential at the working electrode can be referenced. Finally, a counter electrode is introduced to prevent any current flowing through the reference electrode.⁵ A diagram showing an example of a three-electrode cell used in the cyclic voltammetry experiments is shown in Figure 2.1.

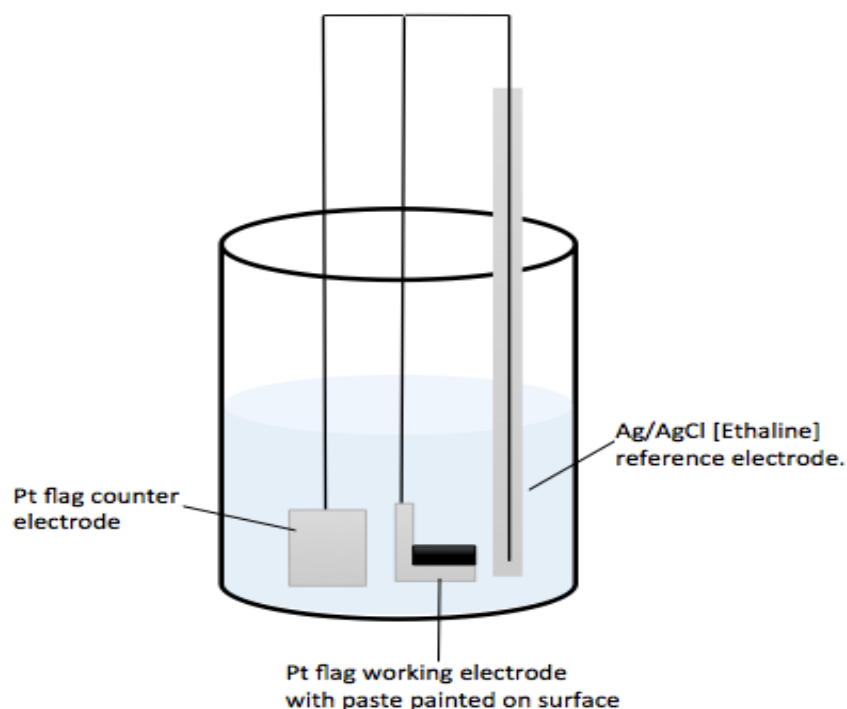


Figure 2.1: Schematic of the three-electrode cell used in the paint casting experiments, using a 1 cm² Pt flag working and counter electrode, with the working electrode bent at a 90 ° angle to allow a suitable surface for the paste to stick to. The reference electrode was generally an Ag/AgCl [0.1 M Ethaline].

2.2.1 Cyclic Voltammetry

Cyclic voltammetry (CV) is a technique employed to investigate the electrochemical reactivity of metals and metal salts in solution. During a CV experiment the potentiostat will record the amount of current that is flowing through the working electrode as a function of the potential. The potential is cycled in a linear manner (Figure 2.2) with respect to time between set limits, and the data is presented as a current vs. potential plot.

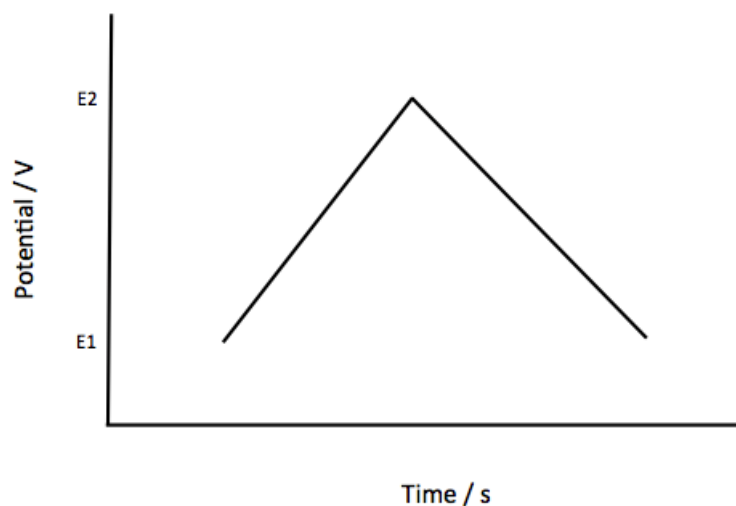


Figure 2.2: Applied potential- time profile used in a typical cyclic voltammogram.³

During the anodic scan the metal species at the electrode surface are oxidised into solution, causing electrons to flow from the metal back to the working electrode which results in a more positive current.⁶ This initial increase in current is due to the system being under kinetic control, once the double layer has built up the reaction at the electrode surface is no longer under kinetic control and is instead dependent on the rate at which the ions can reach the electrode surface, this is observed as a peak and a subsequent decrease in current due to the reaction becoming diffusion controlled. On the reverse scan the opposite occurs, when the potential is able to overcome the activation energy to reduce the metal, the current increases cathodically. Once again, when the double layer has built up the reaction becomes diffusion controlled therefore resulting in a reduction peak in the voltammogram. Each of these peaks reveal the redox reactions that are accessible in the metal being analysed and are unique to each different metal. An example CV for CuCl_2 in Ethaline is shown in Figure 2.3, displaying the $\text{Cu}^{\text{II/I}}$ and $\text{Cu}^{\text{I/0}}$ redox couples.

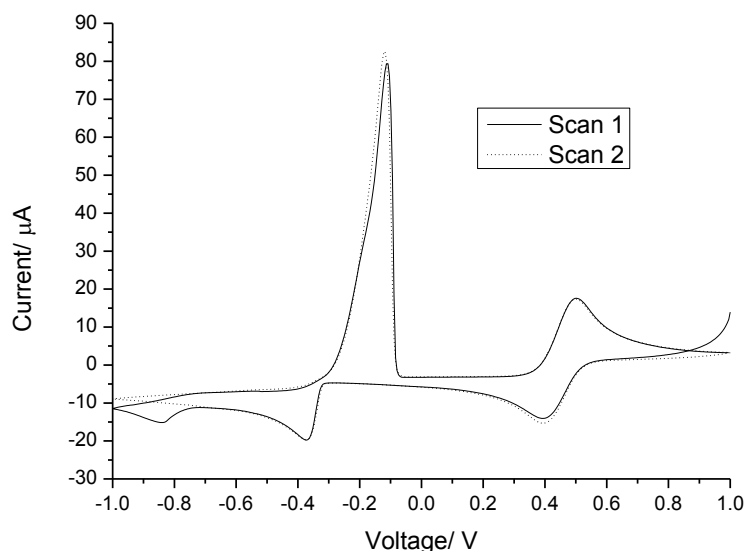


Figure 2.3: The cyclic voltammogram of 100 mM CuCl_2 in Ethaline recorded previously on a 1 mm Pt disc working electrode, Pt flag counter electrode and Ag/AgCl [Ethaline] reference electrode, at a scan rate of 10 mV s^{-1} .¹³

The peaks in this voltammogram signify the voltage at which a reaction occurs on the surface of the electrode; the peaks that appear with a more positive current signify the oxidation reactions that are occurring at the electrode surface, whilst the peaks with negative current are the opposing reduction reactions. It is possible to gain a large amount of information from the voltammograms, as the size and shape of the peaks indicate the type of reaction and the potential at which peaks occur correspond to oxidation and reduction of a species.

The electrode potential is related to the activity of the metal species at the surface of the electrode using the Nernst equation, which is shown in equation 2.2.⁴

$$E = E^0 + \frac{RT}{nF} \ln \frac{[\text{ox}]}{[\text{red}]} \quad \text{Equation 2.2}$$

Where E is the electrode potential, E^0 the standard electrode potential, R is the gas constant, T is temperature, n the number of electrons, F is the Faraday constant and $[\text{ox}]$ and $[\text{red}]$ are the activities of the oxidised and reduced species at the electrode.

In this project, the conventional methods of obtaining cyclic voltammograms are not suitable, for the most part because the minerals are insoluble or only partially soluble.

For this reason, a new method, referred to as 'paint casting', has been developed; the primary benefit of this method is that not only can insoluble minerals be studied, but poorly conducting materials can be investigated as well. The setup that was used in this experiment is shown as a schematic in Figure 2.1 previously.

The paint casting technique involves making a thick paste with finely ground material and Ethaline, painting it onto a platinum flag bent at 90° which is then used as a working electrode. A platinum flag counter electrode and Ag/AgCl [0.1 M in Ethaline] reference electrode were used. This technique will be discussed at great depth in chapter 3, where the quantification of the technique is also examined.⁸

Throughout the cyclic voltammetry experiments, the reference electrode used was an Ag/AgCl electrode. This was made with a 1 mm diameter piece of silver wire immersed in a glass tube filled with 0.1 M AgCl in Ethaline solution. The end of the tube was fritted to allow contact with the electrolyte solution. The Ag/AgCl Ethaline electrode is also used in the CV experiments where the electrolyte is Reline or Oxaline. This results in a liquid junction potential, but these were quantified by Alabdullah and found to be less than 50 mV compared to Ethaline.⁹ An Autolab potentiostat with GPES controlling software was used throughout all of the CV experiments.

2.2.2 Chronopotentiometry

Chronopotentiometry is a technique used to determine the open circuit potential, OCP of an electrochemical reaction. The OCP is simply the experimental potential that is observed when there is no current flowing. It measures the potential of the working electrode relative to the reference electrode when there is no other electrochemical influence on the electrodes. In all of the paint casting experiments the OCP of the paste on the electrode was measured prior to the CV being conducted. Unfortunately in a lot of cases it wasn't possible to obtain an accurate OCP value, most likely as a result of the nature of paint casting and the possibility of chemical reactions being able to occur with the Ethaline. These chronopotentiometry experiments were carried out in the same way as the paint casting cyclic voltammetry experiments using an Autolab potentiostat with GPES software.

2.2.3 Chronocoulometry

Chronocoulometry is an analytical technique that is commonly used to study electrochemical systems. In this technique the charge that is passed following an application of a known voltage is measured as a function of time. The charge can be described using the integrated form of the Cottrell equation shown in equation 2.3

$$Q = \frac{2nFAD^{\frac{1}{2}}[M]}{\frac{1}{2}} t^{\frac{1}{2}} \quad \text{Equation 2.3}$$

Where I is the current that's observed, n the number of electrons, A the area of the electrode, D the diffusion coefficient, $[M]$ is the concentration of metal ions and t is time. This information can be used to determine diffusion coefficients and information about rates of the electrochemical reaction taking place. The experiments were carried out in broadly the same way as the cyclic voltammetry experiments using an Autolab potentiostat with GPES software.

2.3 Bulk dissolution

Figure 2.4 shows the basic set up for the dissolution experiments. This set up is similar to the paint casting method, in that it is a paste of mineral + DES painted onto the surface of an electrode and then suspended in a DES electrolyte. The difference with this experiment is that iridium oxide coated titanium mesh has been used as both the anode and cathode in order to increase the surface area but remain fully inert to any reaction with the mineral. These experiments have been carried out in a 2-electrode cell without a reference electrode.

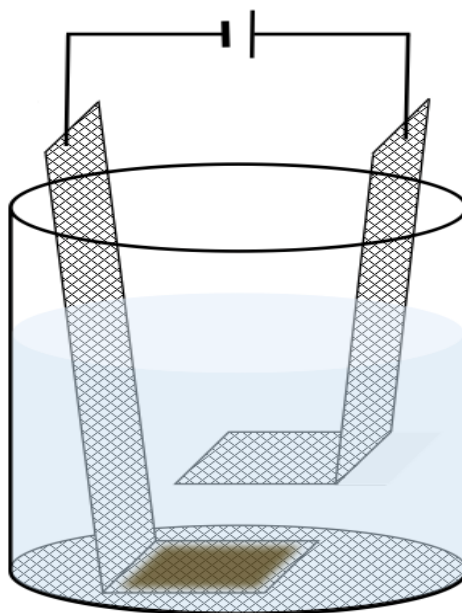


Figure 2.4: Schematic diagram of the bulk dissolution experiment using an IrO_2 coated Ti mesh cathode and anode, with the paste of the material and Ethaline applied to the surface of the anode mesh before being submerged in the Ethaline electrolyte.

2.3.1 UV-Vis

In order to analyse the speciation in each solution after the dissolution experiments, UV-Visible spectroscopy was used. The absorbance of light can be correlated to the concentration of species in solution using the Beer Lambert law shown in Equation 2.4, where A is the absorbance, ϵ the molar absorptivity, l the path length and c the concentration.

$$A = \epsilon / C \quad \text{Equation 2.4}$$

A quartz cell was used throughout with a path length of 10 mm. The focus when using UV-Vis in this work was to determine the speciation of dissolved metals by comparing the data to spectra of known metal composition and concentration. In all cases the samples were used at the concentration obtained from the bulk dissolution experiments. The spectrometers that are used in this work were the Shimadzu 1601 and the Mettler Toledo UV5 Bio.

2.3.2 ICP-MS

ICP-MS could be used to determine the elements present in the solutions after dissolution. In theory ICP-MS can give you accurate abundance measurements of many elements, even when they occur at low concentrations. ICP-MS works by ionising the sample using a plasma source and the ions are detected using mass spectrometry.¹⁰ One of the advantages of this technique is that it can detect very low concentrations of element, e.g. ppm/ppb.⁷ The one downside to this technique for this particular project was that a non-aqueous solvent is used in this project, that may produce an uncalibrated background. To counter this, calibration experiments were run whereby samples of known concentration were diluted very accurately using 2 % nitric acid in order to decrease the viscosity and prevent the Ethaline from corroding the internals of the equipment. In a series of experiments, solutions of known CuCl_2 concentrations in Ethaline were produced. These were first diluted with Ethaline, and subsequently diluted further with trace metal 2 % nitric acid. The calibration curves are shown in Figure 2.5 where each line is representative of a different isotope and detector for Cu (^{63}Cu [STD], ^{65}Cu [STD], ^{63}Cu [KED] and ^{65}Cu [KED])

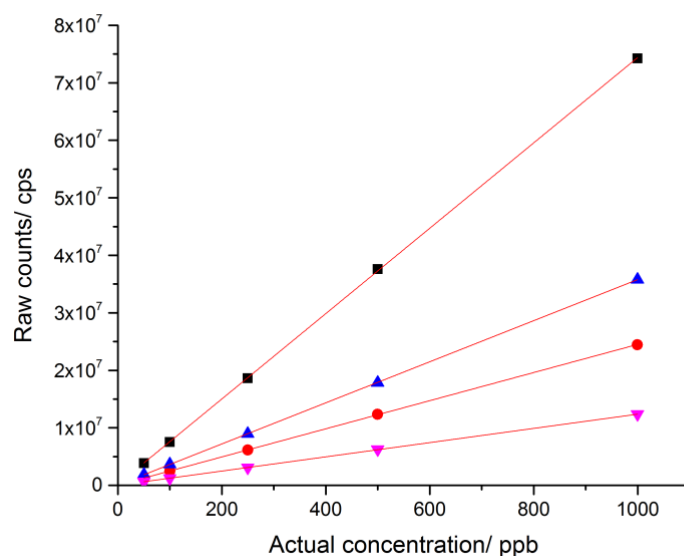


Figure 2.5: ICP calibration plot of actual concentration against the raw counts for copper in Ethaline diluted with 2 % HNO_3 .

The R^2 values from this calibration plot are all calculated to be 1 and therefore better than those in the Ethaline dilution experiments, where the value from the different detectors averaged to be 0.9982. All subsequent ICP-MS experiments were consequently prepared by direct dilution with 2% nitric acid. The same experiment was carried out on solutions of Fe, Co, Zn, Ce and Bi by other students, and their results revealed the same information regarding the direct nitric acid dilution compared to the Ethaline dilution.

2.3.3 EXAFS

EXAFS (extended X-ray absorption fine structure) spectroscopy is a technique used to determine the speciation of a target metal. Monochromatic X-rays are fired at the sample, causing the atoms to become excited. These excited atoms produce and emit a photoelectron wave, causing interference between this emitted wave and the backscattered wave. Properties such as the atomic number of an element, and the distance and coordination number of atoms surrounding the central atom are determined, which ultimately suggests the speciation. The samples used for the EXAFS experiment were obtained from the bulk dissolution experiments. The EXAFS experiments and subsequent data fitting carried out in this study were completed by Jennifer Hartley, and details of how this was carried out are contained in several papers and theses.¹¹⁻¹⁴

After completing the experiment, the data was processed in ATHENA and the data was fitted in EXCURV.¹¹ In order to work out the speciation for each sample, a selection of different parameters needed to be determined, including number and type of scattering atom and their distance from the excited atom. The Debye-Waller factor, a measure of the thermal disorder in the sample, provides an indication of how tightly the scattering atoms are bound to the excited atom. For instance, a long M-Cl bond is likely to have larger thermal disorder than a short M-O bond. The Debye-Waller factor will alter the Fourier transform of the EXAFS causing a broader shrunken signal when the Debye-Waller factor is large. Another parameter that is used in the data fitting stage is the Fermi energy, which allows the effect of atoms causing a phase shift to be taken into account.

2.4 Recovery

The recovery of elements from solution following digestion was carried out in a similar manner to that for digestion. A schematic of the cell is shown in Figure 2.6.

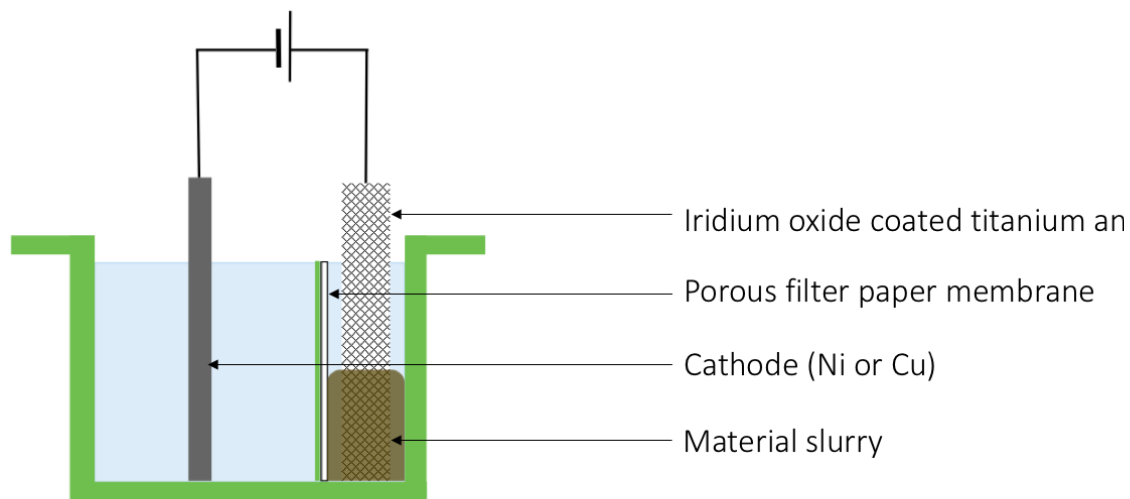


Figure 2.6: Schematic of the small-scale recovery cell.

The cell presented in Figure 2.6 shows a simple design whereby 2 sections of the cell are separated by a piece of filter paper supported by a plastic mesh. A slurry of the mineral/metal salt and DES is packed into the cell on one side of the filter paper divider, with a piece of iridium oxide coated titanium as an anode. On the other side of the filter paper, the cathode (pre-treated Ni or Cu plate) is suspended in the DES electrolyte. The pre-treatment of the cathode simply involved priming the surface by roughening with 100 grit sand paper and subsequently degreasing the surface with acetone. The pre-determined voltage was applied through the electrodes and experiments were typically carried out for either 24 or 48 hours. After the recovery was completed, the plates were rinsed thoroughly with deionised water and dried before storing in individual sample bags. It has been noted that if the DES is not fully rinsed off the electrode, then the surface of the metal degrades once left for several days.

2.4.1 EDX

Scanning Electron Microscopy (SEM) coupled with Energy Dispersive X-ray Analysis (EDX) were techniques used to study the electrodeposited metal coating after the recovery

experiments explained in section 2.4. SEM is primarily used to obtain determine the morphology and structure of the sample. This image is an electron image and it is achieved by monitoring the signals given from the sample when a focused beam of high-energy electrons is scanned over the surface of the material. EDX provides information on the chemical composition of the sample in terms of what elements are present and in what stoichiometry. EDX uses the characteristic X-rays that are emitted by a sample when bombarded by high-energy electrons, and it is possible to achieve a quantitative measure of the elemental composition of the surface of the sample. This technique has also been used in this project to examine minerals prior to them being used in one of the experiments introduced above. It is useful to obtain information about element distribution and concentration in the minerals, and also to determine if there are any other impurities present in the mineral that could affect the electrochemical analysis.

The Zeiss sigma 300 VP EDX was also used to analyse the purity of some of the minerals used in this work. The powdered mineral was set in a resin block and a quick analysis was obtained to determine the most likely minerals/inclusions that were expected in the sample. The scan ran for several hours in order to analyse each individual grain of mineral. This then generated a coloured map containing the identities of each grain, therefore providing a purity value for the different minerals.

2.4.2 XRD

X-ray diffraction (XRD) can provide both quantitative and qualitative information about the atomic and molecular structure of a crystalline material. In this work, XRD was used to analyse both natural and synthetic minerals. XRD was also used to assess the minerals before and after any electrolysis; to see if any crystal faces are more prone to dissolution by electrolysis.

The Bragg equation shown below describes the relationship between the crystal faces and the incident X-rays. X-rays are suitable for the production of diffraction patterns because their wavelength (λ) is typically in a similar order of magnitude to the crystal plane spacing (d).

$$n \lambda = 2d \sin \theta$$

Equation 2.5

Where n is known as the order of reflection and is an integer, λ is the wavelength of the X-rays, d is the characteristic spacing between the crystal planes, and θ is the angle of reflection at which constructive interference occurs. This is shown schematically in Figure 2.7.

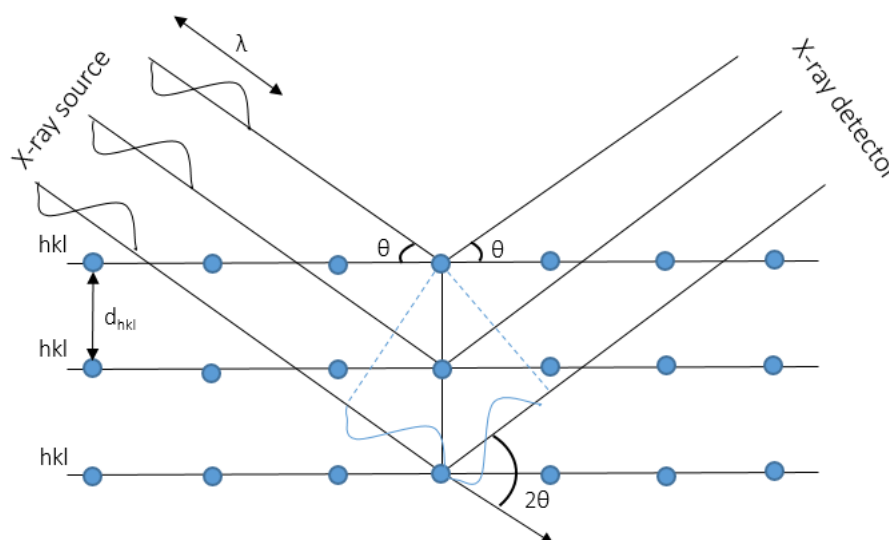


Figure 2.7: Schematic representation of the Bragg equation.¹⁵

X-ray diffraction data was obtained using a Phillips model PW 1730 X-ray generator, with a PW 1716 diffractometer and PW 1050/25 detector. The X-ray tube was a long fine focus Cu anode with Ni $K\alpha$ filtered radiation. Typical operating settings were 40 kV, 30 mA, scanned between 15 and 110° 2θ with a step size of 0.02° 2θ . Angle calibration was carried out using a synthetic Si sintered standard.

2.4.3 Scaled up recovery

The recovery experiment introduced earlier in this chapter was completed for each metal chalcogenide that has been used in this work. All of the experiments were carried out using the cell in Figure 2.6 with 1-2 g of powdered material and 5 ml of Ethaline (or another DES). A further cell was designed in order to increase the amount of material that could be processed in one go, whilst still minimising the solvent use. A schematic of this setup is shown in Figure 2.8; instead of using filter paper as the barrier between solid material and the solvent, a basket covered in nylon mesh was designed and manufactured specifically for this use. The plastic basket contains the IrO₂ coated Ti mesh and ground mineral sample. The cell is suspended in a glass tube containing the cathode

and Ethaline. Again, the resulting Ni plates were analysed by EDAX and SEM to confirm which metals were recovered from solution.

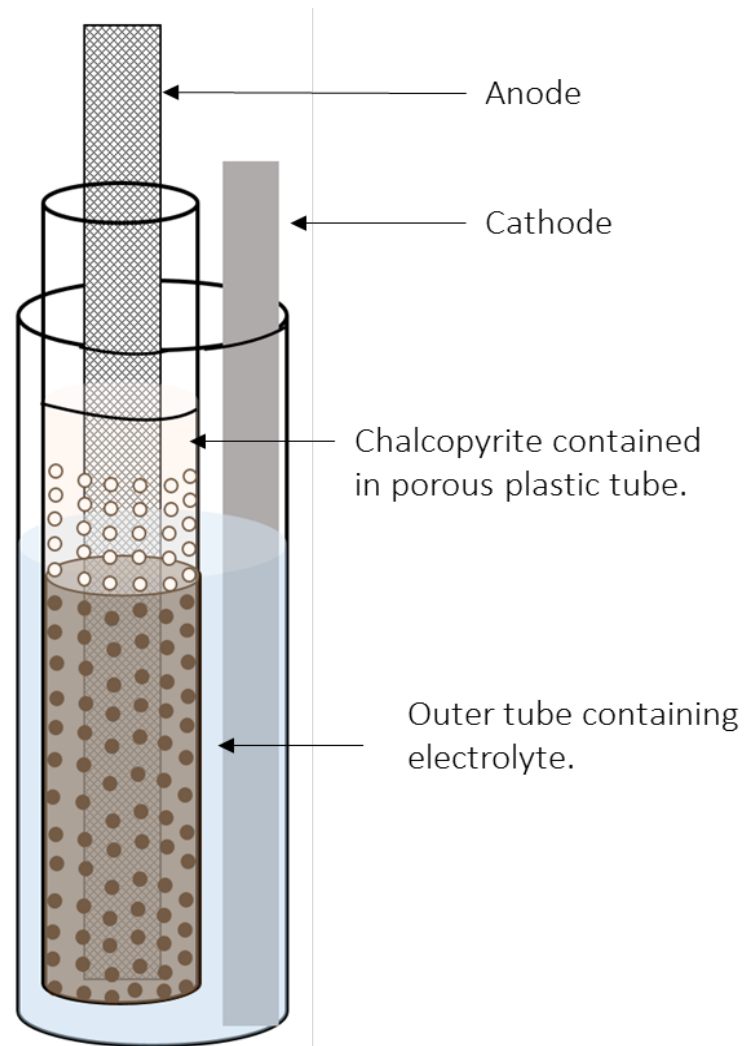


Figure 2.8: Schematic of the scaled-up chalcopyrite recovery. A plastic basket containing the titanium mesh anode, covered with a nylon mesh. Outer tube containing a pre-treated Ni plate submerged in the electrolyte.

2.5 References

1. Daintith, J., (2008), A Dictionary of Chemistry, 6th Ed., Oxford University Press, UK
2. Faulkner, L., (1983) Understanding Electrochemistry: Some Distinctive Concepts, *Journ. Of Chemical Education*, **60**, 262-264
3. Fischer, A. C., (1996) Electrode Dynamics, 1st Ed., Oxford University Press, UK
4. Sawyer, D. T., Sobkowiak, A., Roberts, J. L., (1995) Electrochemistry for Chemists, 2nd Ed., Joh Wiley & Sons, USA.
5. Compton, R. G., Banks, C. E., (2011) Understanding Voltammetry, 2nd Ed., Imperial College Press, UK
6. Rieger, P. H., (1994) Electrochemistry, 2nd Ed., Chapman and Hall Inc., USA
7. Beauchemin, D. ,(2010) Encyclopaedia of Spectroscopy and Spectrometry, 2nd Ed., Elsevier, The Netherlands
8. Abbott, A. P., Bevan, F., Baeuerle, M., Harris, R. C., Jenkin, G. R. T., (2017) Paint Casting: A Facile Method of Studying Mineral Electrochemistry, *Electrochem. Comm.*, **76**, 20-23
9. Alabdullah, S. S., (2018) PhD Thesis: University of Leicester, pH Measurements in Ionic Liquids.
10. Jenner, G. A., Longerich, H. P., Jackson, S. E., Fryer, B. J., (1990) ICP-MS- A Powerful Tool for High Precision Trace-Element Analysis in Earth Science: Evidence from Analysis of Selected U.S.G.S Reference Samples, *Chemical Geology*, **83**, 133-148.
11. Hartley, J. M., Ip, C. M., Forrest, G. C. H., Singh, K., Gurman, S. J., Ryder, K. S., Abbott, A. P., Frisch, G., (2014) EXAFS study into the Speciation of Metal Salts Dissolved in Ionic Liquids and Deep Eutectic Solvents, *Inorg. Chem.*, **53**, 6280-6288
12. Abbott, A. P., Harris, R. C. H., Holyoak, F., Frisch, G., Hartley, J., Jenkin, G. R. T., (2015) Electrocatalytic Recovery of Elements from Complex Mixtures using Deep Eutectic Solvents, *Green Chem.*, **17**, 2172-2179
13. Hartley J. (2013) PhD Thesis: University of Leicester, Ionometallurgy: The Processing of Metals Using Ionic Liquids

14. Abbott, A. P., Azam, M., Frisch, G., Hartley, J., Ryder, K. S., Saleem, S., (2013) Ligand Exchange in Ionic Systems and Its Effect on Silver Nucleation and Growth, *Phys. Chem. Chem. Phys.*, **15**, 17314-17323
15. Dinnebier, R. E., Billimngel, S. J. L., (2008) Powder Diffraction: Theory and Practice, 1st Ed., Royal Society of Chemistry, UK

CHAPTER 3: ELECTROCHEMISTRY OF COPPER CHALCOGENIDES

Table of Contents

3.1 Introduction	64
3.1.1 Metallurgy of copper ores	65
3.1.2 Copper reprocessing.....	69
3.1.3 Aims	70
3.2 Paint casting.....	71
3.2.1 Paint casting sulfur and sulfides	72
3.2.2 Paint casting copper sulfides	77
3.2.3 Quantifying paint casting	79
3.2.4 Effect of water	85
3.3 Electrochemistry of copper sulfide minerals.....	86
3.3.1 Paint casting copper sulfide minerals.....	86
3.4 Electrochemistry of chalcogens and other copper chalcogenides	93
3.4.1 Paint casting copper selenide and telluride compounds.....	96
3.5 Electrochemical studies of copper chalcogenide compounds	98
3.5.1 Chronocoulometry.....	99
3.5.2 UV-Vis Analysis	100
3.5.3 EXAFS.....	104
3.6 Conclusion.....	108
3.7 References	110

3.1 Introduction

This chapter investigates the electrochemistry of copper chalcogenides, specifically CuS, Cu₂S, CuSe, Cu₂Se and Cu₂Te. The oxides are not included in this chapter however comparisons to Cu₂O and CuO are drawn when appropriate.

Copper has a wide variety of uses from electronics to machinery and other transportation applications. A typical home contains around 100 kg of Cu and there is anything up to 20 % Cu in waste electronic equipment.¹ Total Cu production is around 20 million tonnes annually, with mines extracting 10,000 to 250,000 tonnes a day.¹ Cu is one of the most highly recycled metals after Fe, Al and Pb, with nearly half the Cu reaching the market today being recycled from a waste source.^{1,2}

Figure 3.1 shows the usage for copper in the USA in 2017, it is based on 1.27 million tonnes of copper recovered from a variety of mines and other sources.³

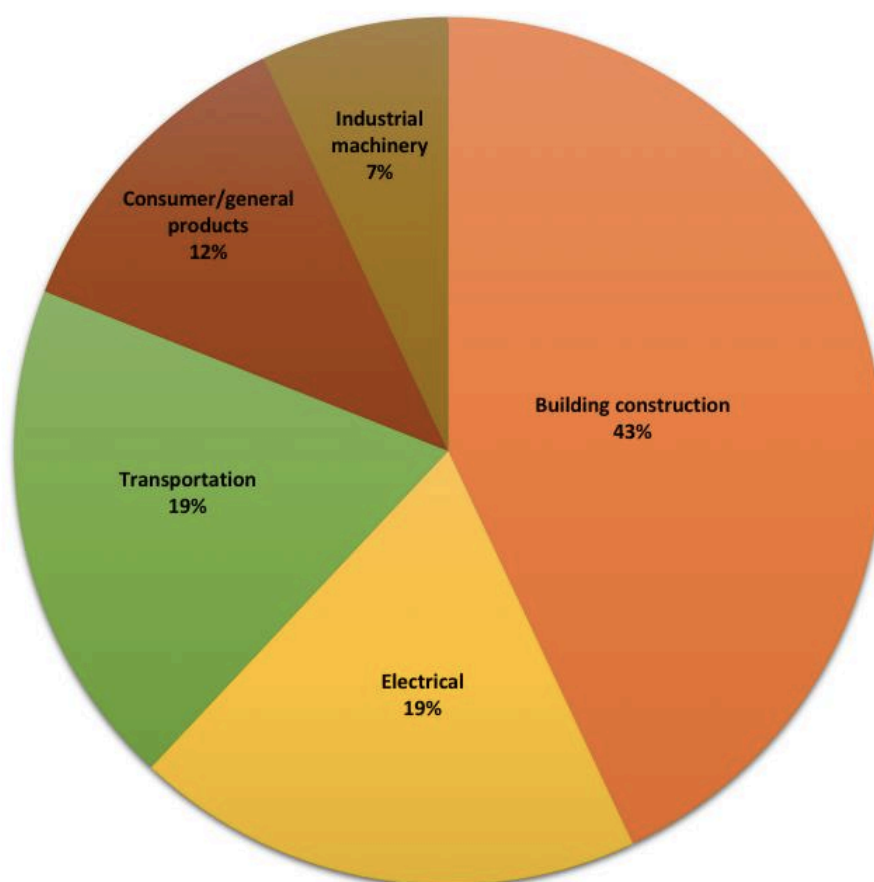


Figure 3.1: Typical uses of Cu in the USA in 2017. ³

Copper is found in a variety of ores including but not limited to: malachite ($\text{Cu}_2\text{CO}_3(\text{OH})_2$), azurite ($\text{Cu}_3(\text{CO}_3)_2(\text{OH})_2$), chrysocolla ($(\text{Cu},\text{Al})_2\text{H}_2\text{Si}_2\text{O}_5(\text{OH})_4\text{nH}_2\text{O}$), bornite (Cu_5FeS_4), chalcocite (Cu_2S) and chalcopyrite (CuFeS_2). The majority of copper is extracted from sulfides and currently the most common commercially processed mineral is chalcopyrite, largely taking over from chalcocite as their deposits have been depleted. For the most part copper is extracted and refined in Chile (5.8Mt p.a.) with Peru (2.4 Mt p.a.), China (1.6 Mt p.a.), Democratic Republic of Congo (1.2 Mt p.a.), USA (1.2 Mt p.a.) and Australia (0.99 Mt p.a.) being the following top 5 countries for production in 2018.^{3,4}

3.1.1 Metallurgy of copper ores

Ores can be processed by one of two overall methods, either pyrometallurgy or hydrometallurgy, the processes of mining and further processing of ores are summarised in the flow chart in Figure 3.2 below. This is a simplified flow chart that shows the overall steps that would be typically involved in processing copper ores to get it from the cradle to the gate, both by pyro- and hydro-metallurgy.

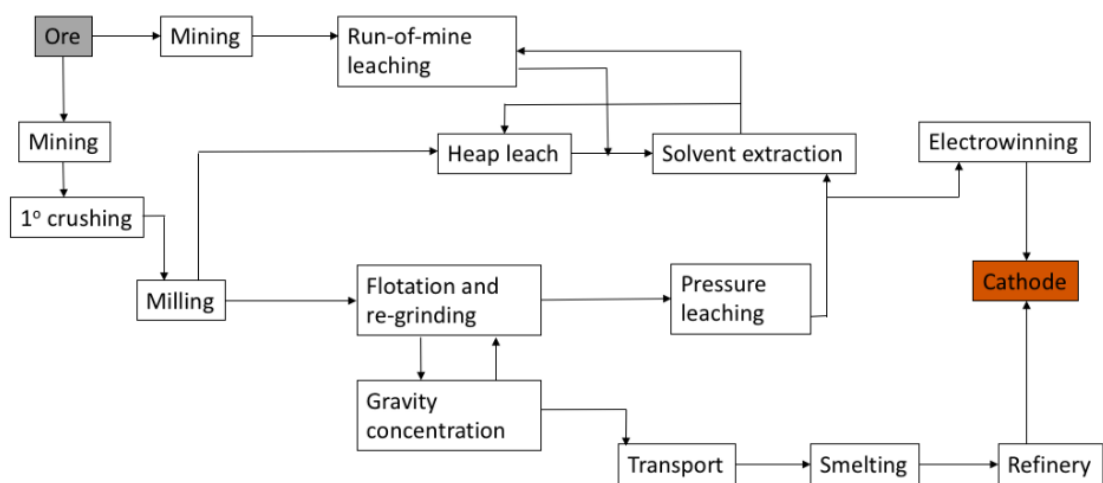


Figure 3.2: Flow chart showing the steps in processing a copper ore by both hydrometallurgy and pyrometallurgy.⁵

The production of Cu uses large amounts of energy, third only after the production of Fe and Al. So, to accompany this flow chart, some overall approximate energy usages are noted for several stages in the process. This information is shown in Table 3.1 and

demonstrates that pyrometallurgy is the most energy intensive processes with mining and milling requiring the most energy after that.

Table 3.1: Approximate energy usage per process for the production of copper. ⁶

Process	Energy/ kJ t ⁻¹
Surface Mining	72,377
Ball Milling	39,037
Overall pyrometallurgy	510,647
Overall hydrometallurgy	1572

Pyrometallurgy is of greater interest in this chapter as it is the more common method for processing the sulfidic ores. It can also be seen from the data in Table 3.1 that the overall steps in pyrometallurgy are far more energy intensive than the hydrometallurgy stages. Pyrometallurgy, using high temperatures to extract metals from ores, is currently responsible for the processing of around 80 % of the world’s copper.⁷ The overall reaction in the process is seemingly simple between molten copper sulfide and air:



Initially the ore must be extracted and concentrated to make it suitable for processing; after the mining and crushing stages the ore is mixed with an oil in order to make it hydrophobic, this is then added to combination of water and a foaming agent. When air is passed through the liquid, bubbles are formed, and the hydrophobic constituents are attracted and cling to the surface of bubbles. This generates a ‘froth’ on the surface which can easily be extracted and subsequently be roasted and smelted. These processes simply involve heating the froth at high temperatures in air to remove sulfur and other metals, such as iron that are associated with the copper ores. The final product from the smelter is referred to as blister copper, named as a result of the bubbles (blisters) of SO₂ produced on the surface, is simply copper metal. The final stage of the pyrometallurgical

processing of copper involves the use of electrochemistry to refine the copper, which utilises very high purity copper as cathodes and the blister copper as anodes. The copper in the anode is purified through the constant oxidation and reduction of the copper from the anode to the cathode at a low potential of 1.3 V.⁸

An issue with this reaction is the large volumes of SO₂ that are produced during the reaction; a tonne of copper produces 2 tonnes of SO₂. To avoid atmospheric SO₂ emissions in the environment numerous SO₂ scrubbing systems have been developed and most of the captured gas is used to produce either sulfuric acid or gypsum (CaSO₄). For each tonne of copper approximately 3 tonnes of sulfuric acid are produced.⁷ This is one reason why sulfuric acid is the one of the most commonly used bulk chemicals.

Ore grades for almost all resources are falling worldwide as the more favourable ores become depleted. Increasingly lower grades are being mined but the increasing world population and the development of technologies such as electronics and electric vehicles has produced an increase in demand for almost all metals. In the 5 years prior to 2017 the usage of copper worldwide has exceeded production demand as shown in Figure 3.3.

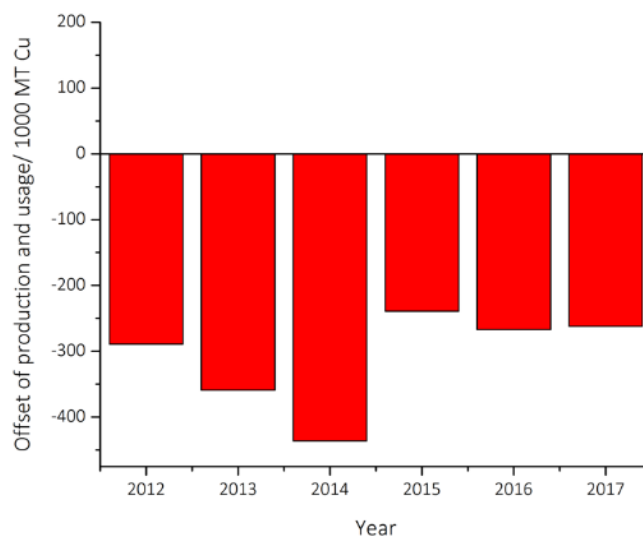


Figure 3.3: The offset of production and usage of copper over a 5 year period.⁹

According to Watling, the last time copper production outweighed demand was in 2009.¹⁰ This drives the requirement for better processes to extract Cu more efficiently

from lower grade ores. Another significant point to note is that many Cu ores are also associated with As, which from an environmental point of view makes pyrometallurgy a largely unsuitable technique in terms of containing and disposing of residues.⁷

Hydrometallurgy is often regarded as a better alternative to pyrometallurgy, due to the avoidance of high energy usage. It is more commonly used in processing oxide ores, however the hydrometallurgical processing for sulfidic copper ores removes the issue with the production of SO₂ as elemental sulfur is largely produced. The use of acidic solutions however, can lead to the generation H₂S gas.

The primary aim of the leaching stages is to solubilise any copper from the ore. Heap leaching involves piling the crushed ore, typically copper oxides, into a heap and spraying a leaching reagent (sulfuric acid) directly onto the heap.

The pregnant leach solution containing CuSO₄ can then undergo solvent extraction, commonly using a phenolic oxime dissolved in kerosene as it has a high affinity for Cu²⁺. The copper is concentrated in the organic phase and therefore separated from any other metal species and impurities. The H₂SO₄ is recovered and recycled. The Cu²⁺ can finally be transferred back to the aqueous phase and consequently be used in the electrowinning step to recover the metal.¹¹

The extraction and purification of copper using sulfuric acid can be written as the following steps.

Table 3.2: Hydrometallurgy of copper oxide ores shown in separate reactions.¹²

$\text{CuO} \rightleftharpoons \text{Cu} + \frac{1}{2} \text{O}_2$	OVERALL
$\text{CuSO}_4 + 2\text{LH}_{(org)} \rightleftharpoons [\text{Cu}(\text{L})_2] + \text{H}_2\text{SO}_4$	Extraction
$[\text{Cu}(\text{L})_2] + \text{H}_2\text{SO}_4 \rightleftharpoons \text{CuSO}_4 + 2\text{LH}_{(org)}$	Stripping
$\text{CuSO}_4 + \text{H}_2\text{O} \rightleftharpoons \text{H}_2\text{SO}_4 + \frac{1}{2} \text{O}_2 + \text{Cu}$	Electrolysis
$\text{CuO} + \text{H}_2\text{SO}_4 \rightleftharpoons \text{CuSO}_4 + \text{H}_2\text{O}$	Leaching

It can be seen from the overall reaction shown in Table 3.2 that hydrometallurgy could be considered a fairly environmentally benign process whereby overall only Cu and O₂ are produced and the H₂SO₄ can undergo recycling back into the process.

The biggest problem with hydrometallurgy as discussed in Chapter 1, is the requirements for large amounts of water. This is a particular problem in Chile, where a large amount of copper is mined. The mines are generally located in the Atacama Desert where water is not an abundant resource. The other problem associated with water is the treatment of it particularly when lower grade ores are processed generating a lot more unwanted material.

3.1.2 Copper reprocessing

Another important source of copper to consider is waste streams that can be reprocessed, it is estimated that >95 % of mined ore material is disposed in the form of mine tailings.¹³ These tailings are highly reactive and often contain large quantities of metals such as iron, copper, zinc and nickel. They have also been known to contain precious metals such as gold and silver as well as toxic elements like arsenic, cadmium and lead.^{13,14} Mine tailings present challenges, both economically and environmentally. For instance, it is necessary to store them somewhere and their constant exposure to air and water leads to the oxidation and subsequent acidification of sulfides in the tailings.¹³

It is often the case, as improvements have been made to processing technologies, that historical mine tailings have very high concentrations of metals. In some cases, the concentration of metals in historical tailings is higher than primary ores that are currently mined.¹³ This point, along with the fact that the material tend to be easier to process, makes reprocessing mine tailings a more attractive option to processing low grade ores.¹³ It is also suggested that reprocessing these mine tailings along with recycling metals currently in use, could stabilise the price of metals worldwide by increasing their availability.¹⁴

Several studies have been conducted on extracting and processing copper from mine tailings. Bioleaching was found to be a highly effective technique at relatively low temperatures (45 °C). However, chalcopyrite, along with other complex copper sulfide ores remain immune to bioleaching and still present the same problems as when they

are mined as a primary ore.^{13,15} Flotation of the tailings has also been investigated; it has been particularly useful for oxidised tailings and can successfully extract copper.¹⁴ One study in particular found that the addition of an ultrasound treatment complements and increases the efficiency of the extraction process.¹⁶ It is noted by Videla et al. however, that the marginal increase in copper extraction may not outweigh the economic cost of applying ultrasound to the tailings.¹⁶

Along with reprocessing copper mining waste, a large amount of copper is contained in post-consumer materials or waste from generating copper goods. The latter is often referred to in the literature as 'new scrap' and it is relatively easy to sort and subsequently economical to recycle^{17,18} Old scrap on the other hand is the copper obtained from products at the end of their life, most commonly wiring, and tends to be much more expensive to recycle. It is estimated that around half of the copper products that are on the market today is made with recycled scrap metal.¹⁸ The most difficult aspect of recycling wiring is the fact that it tends to be covered in plastic/rubber insulation, which somehow needs to be separated and ideally recovered. Using the specific gravity of copper/ insulation has been successful in solving this problem; a large amount of copper is now recovered using this method.¹⁸

3.1.3 Aims

The aim of this chapter is to study the electrochemistry of copper chalcogenides using a new process called paint casting. The hypothesis is that since most copper chalcogenide compounds have relatively good conductivities it should be possible to study their dissolution using electrochemistry. The higher viscosity of DESs hypothetically enable them to be mixed with minerals to form a conducting paste.

The main objectives from this chapter are:

1. To quantify the electrochemical technique of paint casting and understand the mechanism by which copper minerals dissolve in DESs.
2. To understand the speciation of copper and the chalcogens after they have been electrochemically dissolved in Ethaline.
3. To achieve electrochemical separation of copper and associated chalcogen (S/Se/Te).

3.2 Paint casting

The electrochemical properties of minerals are often quite difficult to study as it is necessary to maintain an electrical contact with the electrode. Unlike more typical electrochemical investigations, whereby a metal salt can be dissolved into solution and used as an electrolyte, mineral analysis is more complex as they are often insoluble.¹⁹ In this chapter, a technique for carrying out simple CV's referred to as paint casting, will be developed. A review by Grygar et al. investigates different methods of electrochemically analysing solid samples including minerals and other similar insoluble (or barely soluble) materials.²⁰ It is suggested that there are a number of requirements that must be met in order to develop a suitable technique to electrochemically analyse solid materials. The particles must have good contact with the electrode, they must also maintain contact with the electrolyte. The method itself needs to remain simple and reliable and be suitable for a large variety of different materials.²⁰

The electrochemistry of solid materials such as minerals, can be studied by a selection of different methods, the first simply being a single crystal electrode, or "compact crystal electrode".²⁰ This method works by attaching an individual crystal of the material to an electrode via a conductive resin or epoxy, this has the benefit of being fairly simple to do, with little work involved in making the electrode. The downsides to this method however, are that low resolution voltammograms are common. This is because minerals, for the most part, tend to be poorly conducting resulting in Ohmic resistance, leading to broad peaks in the voltammograms. Grygar et al. states that this style of electrode is only suitable for materials with high conductivity, and the desire to study more poorly conducting materials revealed the major downsides to this method.²⁰ A further problem with this method is that using a single crystal, only exposes one face of that crystal for electrochemical analysis. Previous work carried out by Al-Bassam observed that different crystal faces of the same mineral produce different CVs.²¹ This will not give a representative indication of how a bulk mineral will behave electrochemically. This compact crystal method has been trialled previously for the mineral galena.²² It has been shown to be a viable method when it comes to more conducting minerals like galena, the problem arises when other, poorly conducting, mineral deposits such as pyrite, are not able to be investigated this way.

Another method that is often employed involves taking a finely powdered mineral and mixing it with a conductive medium, such as graphite. These powders are then mixed further with an inert oil and subsequently pressed into an electrode. These electrodes are often referred to as composite electrodes. Although they allow access to all the different crystal faces of the minerals, they have a variety of practical limitations, primarily the time it takes to prepare. The degradation of CPEE's is also relatively fast. The different materials that are used to induce conductivity as well as the binder material, can both effect the performance of the electrode over time and not necessarily give representative results.²³

The concept used in this study is to mix a relatively viscous DESs with the mineral to create a paste which is nevertheless relatively conductive. This can be applied to the face of an electrode, in a process called paint casting. This enables voltammetry of a powder to be rapidly studied.

3.2.1 Paint casting sulfur and sulfides

To demonstrate the paint casting method, galena (PbS), the primary ore mined for lead, was initially used as a test mineral. Figure 3.4 shows the paste formed when grinding galena and Ethaline (63 mg and 106 mg respectively) and the electrode configuration used for paint casting. One advantage of this approach is that the fluidity of the paste can be controlled using the viscosity of the DES or via the loading of the mineral.

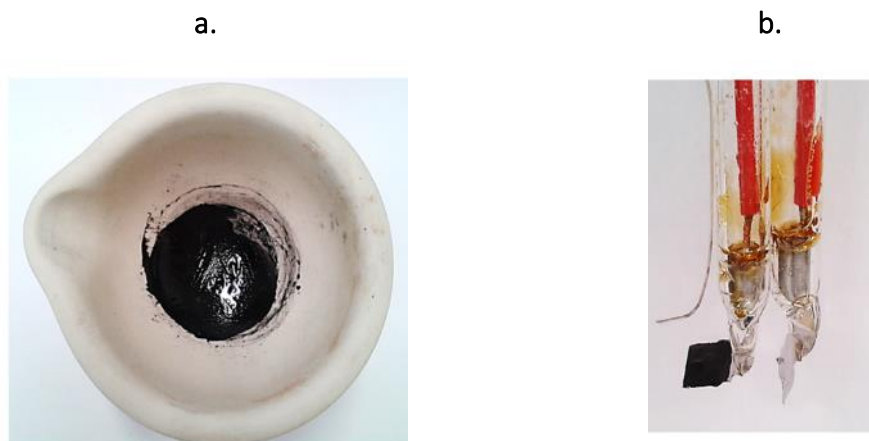


Figure 3.4: **a.** The paste of 63 mg galena and 106 mg of Ethaline, **b.** The paste painted onto the surface of a Pt flag working electrode with a Pt flag counter electrode and a Ag wire reference electrode for demonstration purposes.

Figure 3.5a shows a voltammogram of galena painted on to a Pt electrode shown in Figure 3.4. When the electrode was immersed in the electrolyte (in this case also Ethaline) the mineral remained adhered to the electrode surface during and after immersion. Three anodic peaks can be seen (A1 to A3) and two cathodic peaks (C1 and C2). Starting with the potential at 0.0 V and scanning in a negative direction the peak C2 does not appear and C1 is small. C1 and C2 only become pronounced once the anodic sweep has gone beyond A3. It is proposed that A3 is due to the oxidation of PbS and C2 is due to the reduction of a species formed in this process.¹⁹ A3 must also release a lead species as the electrodeposition of lead can be assigned to C1 while A1 is the subsequent stripping of Pb.¹⁹ The process was also attempted by making a paste of the mineral in Ethaline and immersing it in aqueous sodium chloride solution. There were 2 problems with this approach, firstly the paste did not fully remain adhered to the electrode and the cyclic voltammogram was less well resolved as the aqueous solution did not wet the mineral well.

Figure 3.5b shows a cyclic voltammogram of lead chloride powder made into a paste with approximately the same particle size and mass loading as that for galena. It can be seen that two anodic processes (A4 and A5) and one cathodic process (C3) occur at approximately the same potentials as A1 and A2 on the anodic sweep and C1 on the cathodic sweep. The shapes of these peaks are characteristic of metal dissolution and

deposition. Recent work by Liao et al. studied the electrochemistry of PbSO_4 and PbO which are both soluble in Ethaline and the same shaped voltammograms were observed with peaks at the same potentials.²⁴ The peak at C3 was attributed to lead deposition, A4 is bulk lead dissolution and A5 is the dissolution of a Pb-Pt alloy. The peak at C2 is not observed for PbSO_4 and PbO so can therefore be ascribed to the S species in galena.

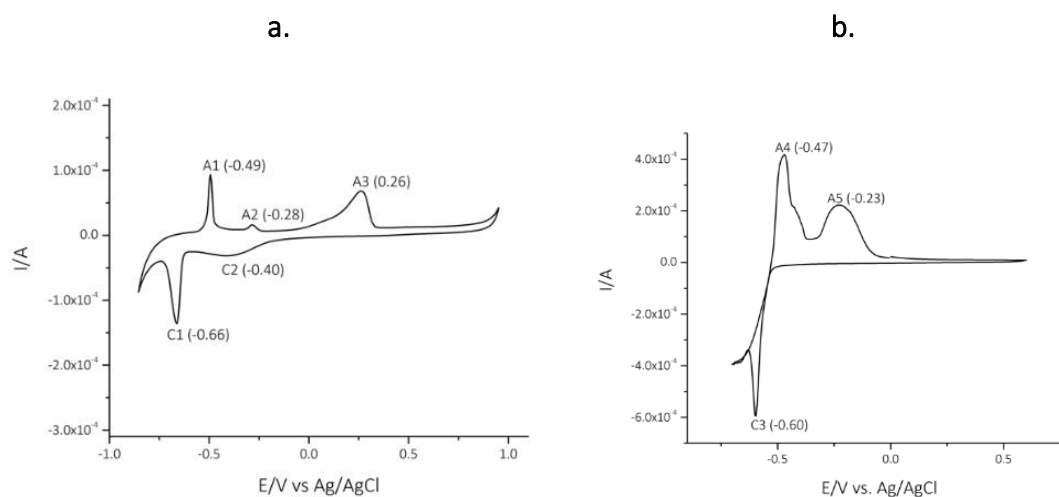


Figure 3.5: *a. Cyclic voltammogram of 10 mg of galena paste b. Cyclic voltammogram of lead chloride. Both voltammograms were conducted in Ethaline, with a 1 cm² Pt flag working & counter electrode and Ag/AgCl [0.1 M in Ethaline] reference electrode, at a scan rate of 5 mVs⁻¹.*

Voltammetry also shows no evidence of passivation and observing the surface under a 3D optical microscope, clear bulk dissolution of the surface can be observed. Gardner and Woods studied the redox chemistry of a single crystal sample of galena in aqueous solutions as a function of pH. It was found that in acidic HClO_4 solutions anodic oxidation led to a soluble Pb species with a layer of amorphous sulfur forming on the electrode which restructures to become porous and enable further surface dissolution.²⁵ In basic solutions (pH 6.8 to 11) the principal product was lead oxide with some thiosulfate and sulfur. The voltammograms exhibit one anodic and one cathodic response both of which are irreversible in acidic solutions. The cathodic response becomes partially reversible in basic solutions.

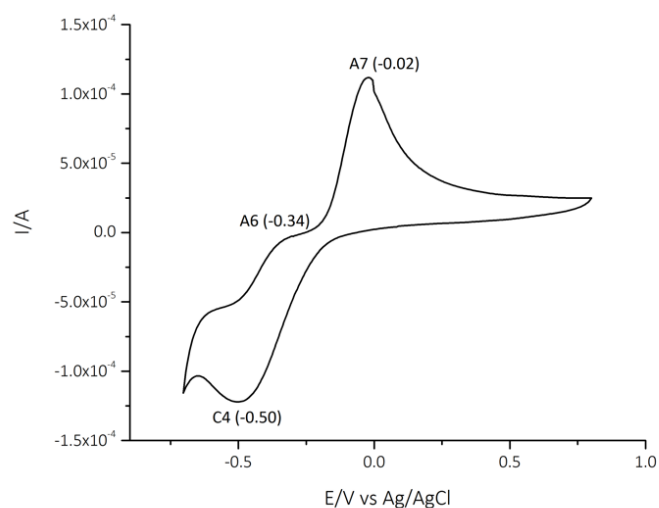


Figure 3.6: Cyclic voltammogram of sulfur paste, conducted in Ethaline, with a 1 cm² Pt flag working & counter electrode and Ag/AgCl [0.1 M in Ethaline] reference electrode, at a scan rate of 5 mVs⁻¹.

Figure 3.6 shows that the technique can also be used for more electrically resistive materials such as S. In this case yellow S was used with Ethaline. This voltammogram shows one main anodic process, A7, and one cathodic process C4 with a shoulder A6 in the anodic sweep.

The cyclic voltammetry of a solution saturated with sulfur has also been reported by Manan *et al.*²⁶ who used glassy carbon, Au and Pt electrodes to study sulfur electrochemistry but using an IL, 1-butyl-3-methyl-imidazolium dicyanamide as the electrolyte. They saw a similar response to that shown in Figure 3.6 although the cathodic signal was clearly separated into two signals on Au and GC whereas the two peaks overlapped more on Pt.

They assigned the cathodic processes to:



and proved this by synthesising Na₂S₆ and Na₂S₄ and comparing the optical properties of their solutions with that produced from the reduction of S₈. It is proposed that C4 is an amalgamation of Equations 3.2 and 3.3 and A6 and A7 are the re-oxidation processes.

The charge on the anodic and cathodic sweeps are very similar ($Q_+ = 5.1 (\pm 0.1) \times 10^{-3}$ and $Q_- = 6.2 (\pm 0.1) \times 10^{-3}$ C). The lack of redox signals in Figure 3.5a corresponding to the potentials shown in Figure 3.6 for sulfur oxidation and reduction seem to suggest that A3 is not the process in Equation 3.4.



which was proposed by Cisneros-Gonzalez et al.²⁷ in aqueous solutions i.e. elemental sulfur is not produced by the galena oxidation process.

The voltammetry of galena was also studied in aqueous solutions at pH 2 using a carbon paste electrode by Cisneros-Gonzalez et al.²⁸ Scanning the potential in a positive direction first resulted in a large, irreversible oxidation process at + 0.6V vs SCE which could be due to the oxidation of sulfide to sulfur followed by the formation of sulfate at higher anodic over-potentials. On the cathodic sweep a smaller, reversible redox process was observed at -0.5 V which was ascribed to Pb deposition and stripping, presumably released by the first oxidation process. The authors also showed the effect on the voltammetry from the addition of chloride ions to the solution and it was found that the anodic process became more resolved and its shape and potential became similar to that seen in Figure 3.5a.²² The difference in oxidation potential between A1 and A3 is the same as that reported with aqueous 1.0 mol dm⁻³ sodium chloride. Comparison of the redox potentials is difficult due to the different reference electrodes, but the relative positions of the peaks are similar. The anodic peak A2 is missing from both of the aqueous studies as they did not use Pt as a current collector, and therefore did not form an alloy. The aqueous study did, however observe a quasi-passivation of the electrode due to the precipitation of insoluble PbCl₂ which does not appear to occur in Ethaline. It is proposed that the oxidation of galena in a high chloride environment leads to a soluble Pb species with a S ligand. The same behaviour has been observed for a variety of Fe minerals including pyrite and marcasite.²⁹

To determine whether metallic Pb could be recovered from galena paste in Ethaline a bulk electrolysis experiment was carried out as described in section 2.3. Bulk electrolysis was carried out for 5 hours at a constant potential of 1.5 V which led to solubilisation of

some of the material. Following electrolysis the Ni sheet cathode was rinsed with water and found to be coated with a grey layer as shown in Figure 3.7. Analysis with EDX showed it was metallic lead with negligible sulfur or chloride.



Figure 3.7: Photograph of the Ni cathode surface after electrolysis of PbS in Ethaline for 5 hours at a constant 1.5 V.

3.2.2 Paint casting copper sulfides

For galena the redox chemistry of lead is limited to the $\text{Pb}^{\text{II}/0}$ couple as the $\text{Pb}^{\text{IV}/\text{II}}$ couple occurs outside the potential window of the DES. In this section two copper sulfide compounds are studied, Cu_2S and CuS respectively. These are more complex than lead since both the $\text{Cu}^{\text{II}/\text{I}}$ and $\text{Cu}^{\text{I}/0}$ couple will also be active. In this section the electrochemistry of Cu_2S and CuS will be compared to determine whether the oxidation of the metal or the sulfide is responsible for mineral dissolution.

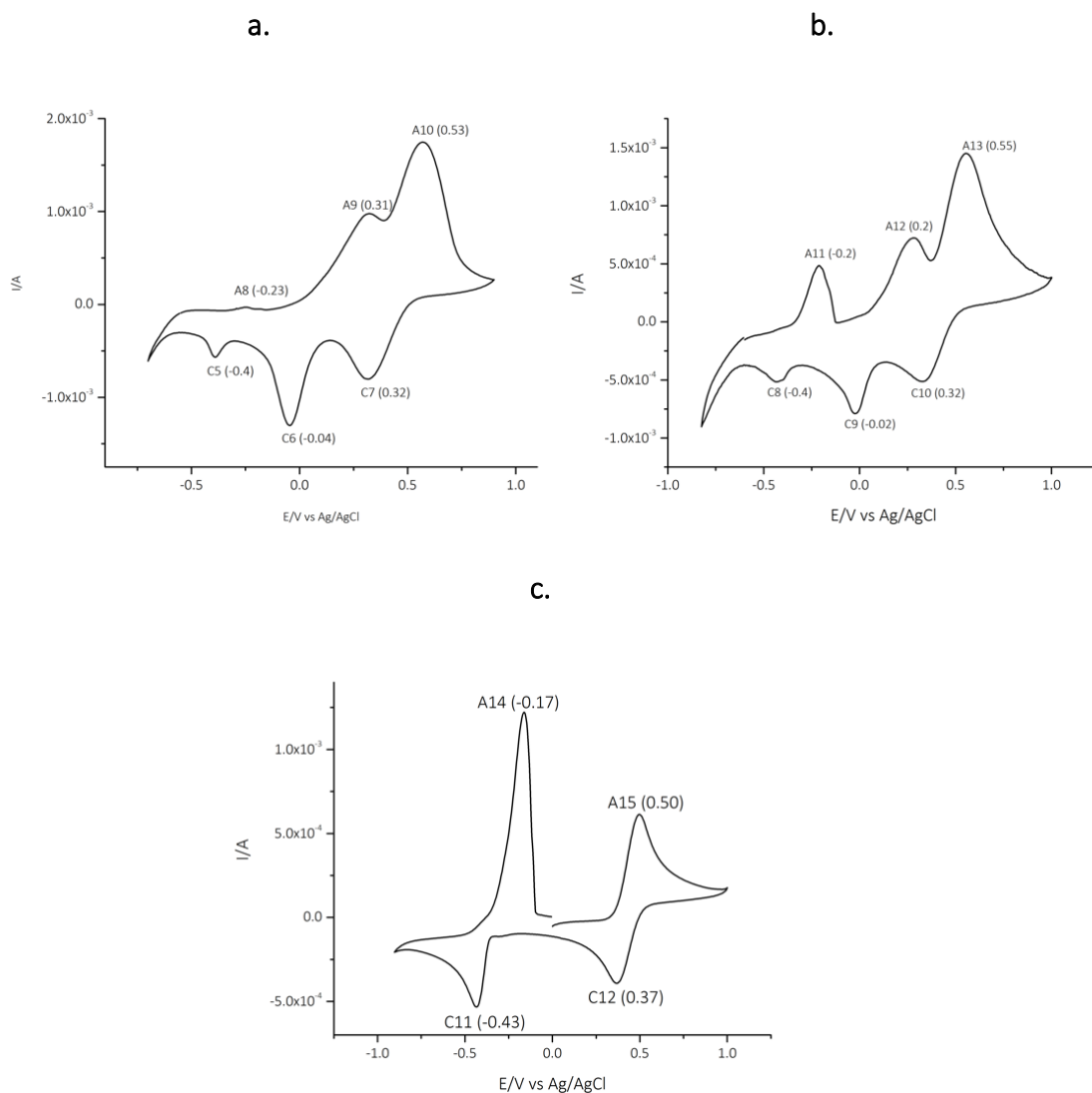


Figure 3.8: Paint casting CVs of 2mg **a.** CuS **b.** Cu_2S and **c.** CuCl_2 powders. All voltammograms were conducted in Ethaline, with a 1 cm^2 Pt flag working & counter electrode and Ag/AgCl [0.1 M in Ethaline] reference electrode, at a scan rate of 5 mVs^{-1} .

Figure 3.8c shows the paint cast voltammogram for CuCl_2 which is nearly identical to a solution of CuCl_2 in Ethaline CV^{30,31} (also shown previously in Figure 2.3) showing that this method produces results that can be directly compared to solution electrochemistry. Figure 3.8 a and b show the electrochemistry of Cu_2S and CuS . The redox couples labelled A8/C5 and A10/C7 for CuS (and the equivalent: A11/C8 and A13/C10 for Cu_2S) can be deduced to be due to the $\text{Cu}^{\text{I}}/\text{Cu}^0$ and $\text{Cu}^{\text{II}}/\text{Cu}^{\text{I}}$ respectively. The peaks A9 and A12 can

therefore be concluded to be due to the oxidation of the sulfide ion (Figure 3.6 a). This is analogous with both galena and pyrite from a previous study.^{21,29}

3.2.3 Quantifying paint casting

In the following section the mass of CuS that is applied to the surface of the electrode is altered to determine if the electrochemical responses are quantitative to the amount of material on the electrode. Figure 3.9a shows the cyclic voltammograms for masses of paste samples ranging from 0.4 to 2 mg. It can be seen that that charge is related to the loading of the mineral, suggesting that this could be a possible basis for a mineral assay. Figure 3.9b shows that there is a relationship between the mass and the anodic charge of the voltammogram showing that electrochemistry can be used as an approximate assay for mineral content for CuS providing the sample to be studied is homogeneous. The results from a similar experiment are shown in Figure 3.9c using galena instead, the masses used were much higher ranging from 10.3mg to 78.3 mg but the trend was similarly linear.

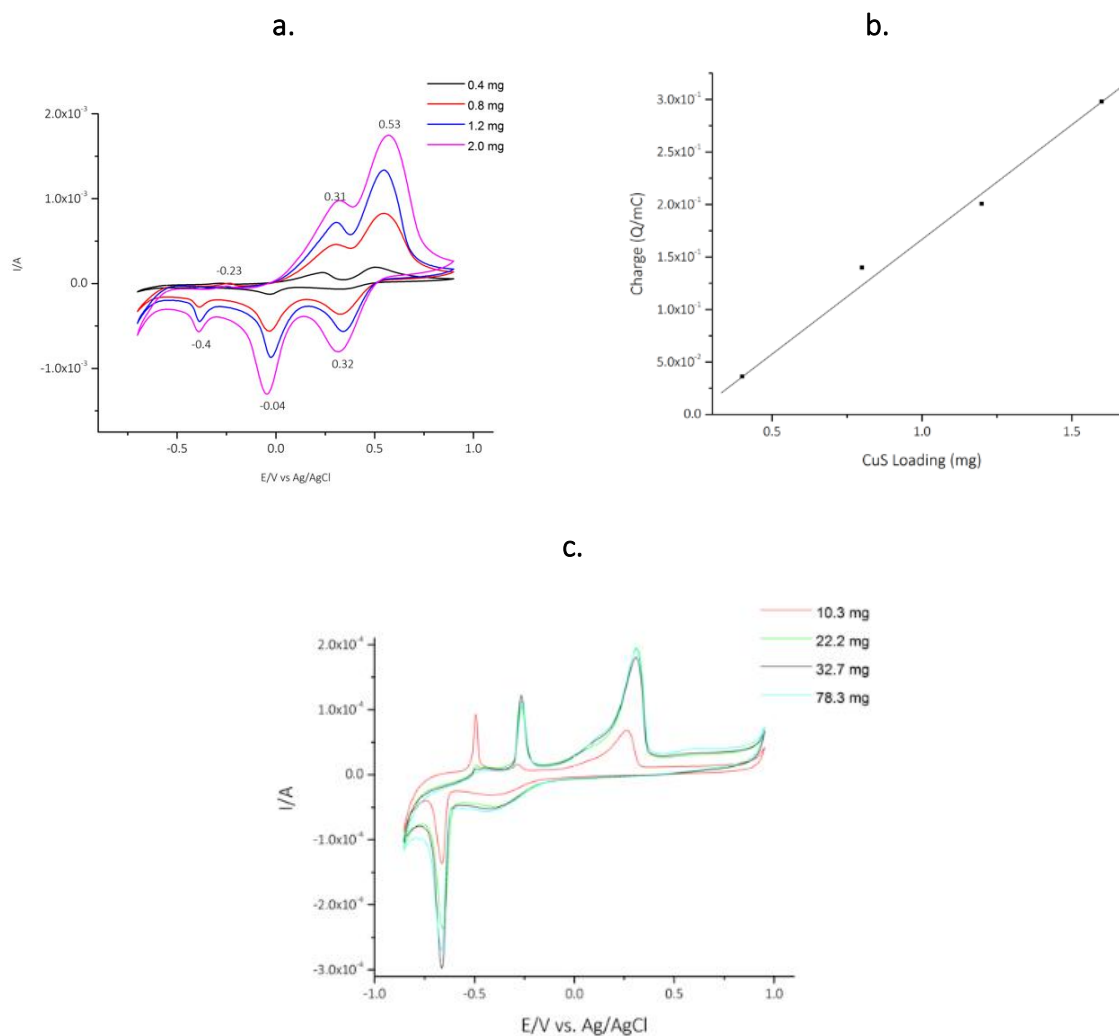


Figure 3.9: **a.** Overlaid paint casting CV's of different masses of CuS,. **b.** The CuS mass loading from the CV's plotted against the overall charge of the CVs respectively. **c.** Similar experiment using differing masses of galena instead. All voltammograms were conducted in Ethaline, with a 1 cm² Pt flag working & counter electrode and Ag/AgCl [0.1 M in Ethaline] reference electrode, at a scan rate of 5 mVs⁻¹.

Clearly resolved voltammograms are, however only obtained over a relatively narrow material loading which depends upon the conductivity of the material. Increasing the loading of CuS on the electrode to 4 mg led to a loss of peak definition as shown in Figure 3.10a. The cause of this is probably due to an increase in the Ohmic resistance caused by the resistance of the material and the difficulty of species to flow to the interface between the electrode and the paste.

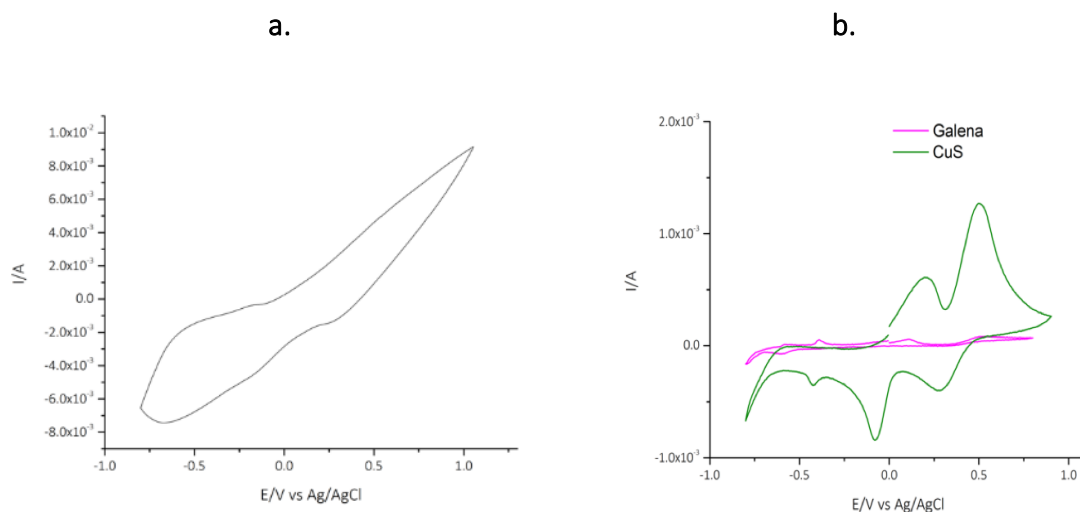


Figure 3.10: *a.* An example of a CuS cyclic voltammogram, with 4 mg of paste applied to the surface of the working electrode. *b.* overlaid paint cast CVs of 2 mg galena and 2 mg CuS to show the difference in charge. Both voltammograms were conducted in Ethaline, with a 1 cm² Pt flag working & counter electrode and Ag/AgCl [0.1 M in Ethaline] reference electrode, at a scan rate of 5 mVs⁻¹.

An important observation to make is that differences in conductivity between different minerals/ materials causes the charge for each CV to also differ. This is shown with an example using the mineral galena (PbS) and CuS powder in Figure 3.10b, the mass used of both materials was 2 mg but the cyclic voltammograms are significantly different. Aside from the conductivity of the mineral, the amount of non-conducting gangue material and the particle size of the mineral will also have an effect. For this reason, it is difficult to be specific about the optimum mass of mineral needed to conduct a paint casting CV, but it is in the region of 0.5 to 5 mg cm⁻².

Figure 3.11, shows the effect of scan number on the cyclic voltammetry of CuS . The CV was started at 0 V where negligible Faradaic current flowed and as it was scanned in the anodic direction where an oxidation peak (A 17) due to the Cu^{II/I} couple is observed. The anodic peak A16 is only seen on the second and subsequent scans showing that it either comes from the re-oxidation of the sulfur containing species or from a species released into solution following the Cu^I oxidation. This suggests that the initial dissolution of the Cu ultimately liberates the S species enabling its dissolution. There also appears to be a small shoulder on peak C13 on the first scan that disappears on subsequent scans. All the

peaks are shown to increase in current over the course of the 3 scans suggesting that these are solution-based processes.

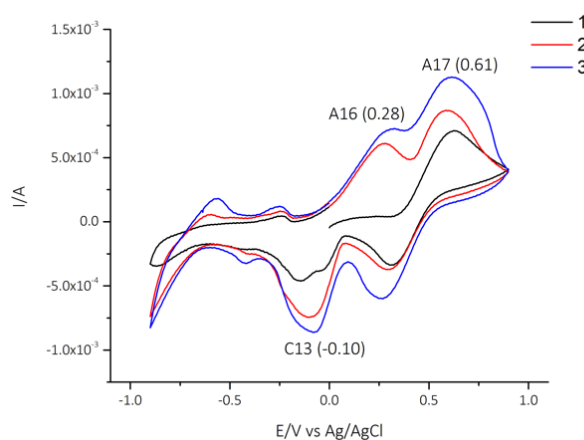


Figure 3.11: First 3 scans of CuS paint casting cyclic voltammogram conducted in Ethaline, with a 1 cm^2 Pt flag working & counter electrode and Ag/AgCl [0.1 M in Ethaline] reference electrode, at a scan rate of 5 mVs^{-1} .

To study the effect of mineral purity a sample of CuS was diluted with different quantities of alumina, an inert and non-conducting diluent. Figure 3.12a shows the CVs for different CuS: alumina ratios (with the overall mass of CuS + alumina remaining at 2 mg). As expected the addition of more alumina causes the charge for the CuS oxidation to decrease. Figure 3.12 b shows that the charge is proportional to the CuS loading. Decreasing ore grades that are increasingly the necessary option for metal extraction results in lower yield for an equivalent energy input as discussed previously.¹⁰ This experiment, could therefore be used to mimic the behaviour of a low-grade ore with alumina acting as an inert gangue material.

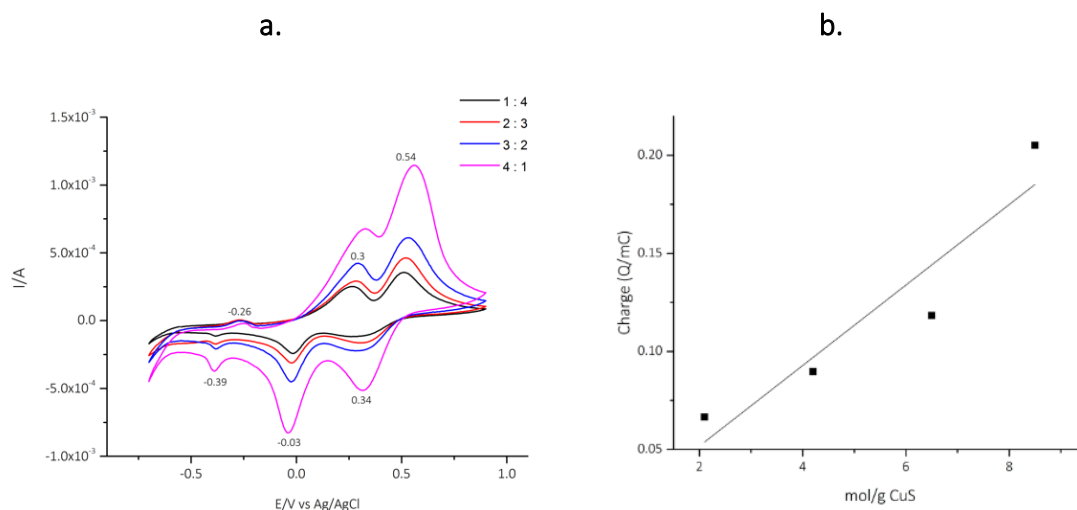


Figure 3.12: a. Overlaid paint casting CV's of different ratios of CuS: alumina powder. **b.** The mol/g CuS in each paste plotted against the overall charge of the respective CV's. All voltammograms were conducted in Ethaline, with a 1 cm² Pt flag working & counter electrode and Ag/AgCl [0.1 M in Ethaline] reference electrode, at a scan rate of 5 mVs⁻¹.

The analytical response was also studied as a function of potential scan rate and temperature to optimise the conditions. Figure 3.13a shows the effect of scan rate for 2 mg of CuS powder in Ethaline at sweep rates of 5, 10, 20, 50 and 100 mVs⁻¹. It demonstrates that the resolution decreases and the peaks get wider as the scan rate increases. This is because the mineral is relatively resistive and adds an iR artefact to the voltammogram. The best resolution is obtained at slow scan rates so in the subsequent scans in this thesis all the voltammograms are measured at 5 mVs⁻¹.

As for the temperature experiments, it is clear from Figure 3.13c that an increase in temperature from 20 °C to 80 °C results in a peak height increase, in particular for the Cu^{II/I} oxidation peak. At the same time there is also a decrease in peak resolution to the point where the oxidation peak related to the sulfide species is completely unresolved at 80°C. The Nernst equation tells us that temperature has an effect on the electrochemical potentials of the cell.³² At the same time, the viscosity of Ethaline is largely affected by the change in temperature as well, this results in an increase in mass transport which can have the effect of increasing the rate of the electrochemical reaction, resulting in a

change of peak shape and height. It is therefore determined that for conducting electrochemical analysis on unknown minerals, room temperature appears to be the best, and oftentimes easiest condition. Notably, an elevated temperature will not have a detrimental effect.

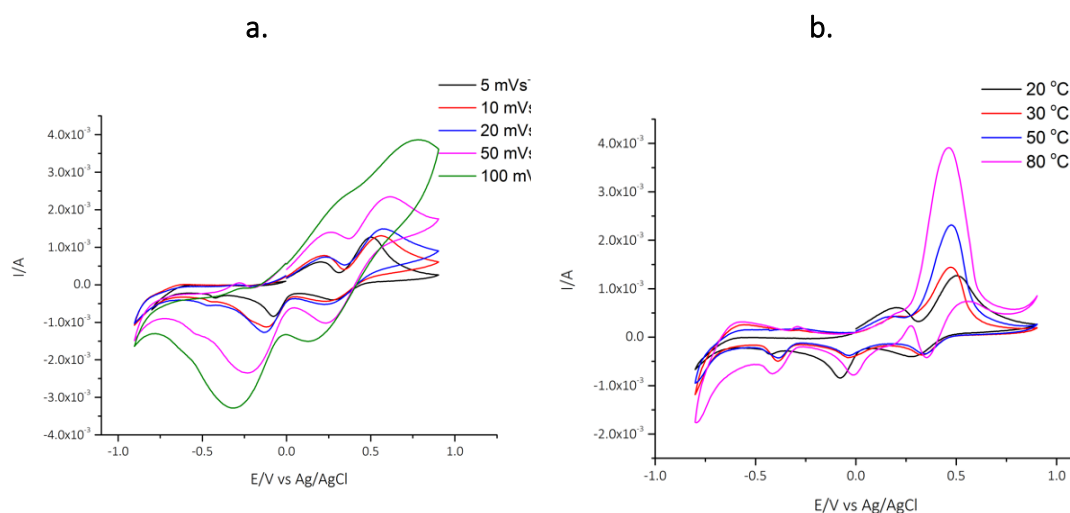


Figure 3.13: a. Overlaid paint cast CV's, all with 2 mg of CuS with varied scan rates. **b.** Paint cast CVs of CuS with varied temperatures all conducted at 5 mVs⁻¹. All voltammograms were conducted in Ethaline, with a 1 cm² Pt flag working & counter electrode and Ag/AgCl [0.1 M in Ethaline] reference electrode.

Ordinarily, in traditional CV analysis the Randles Sevcik equation (3.5), can be used to determine the diffusion coefficients of an electroactive species.³³

$$i = 269000n^{\frac{3}{2}}AD^{\frac{1}{2}}Cv^{1/2} \quad \text{Equation 3.5}$$

Where i is the peak current, n is the number of moles involved in the oxidation or reduction reaction, A is the electrode area, D the diffusion coefficient, C is the concentration of the solution and v is the scan rate. This is only strictly valid for a diffusion-controlled reaction, however numerous studies have applied it to dissolution processes. Palin studied the voltammetry of CuCl₂ in Ethaline and found a value of 7.51 x 10⁻⁸ cm²s⁻¹ for the Cu^{I/0} redox couple.³⁰ It was determined that the equation couldn't be applied conclusively in the case of paint casting due to the fact that the material is applied

to the surface of the electrode and therefore the diffusion coefficient as well as concentration doesn't directly apply.

3.2.4 Effect of water

The processing of minerals in strictly anhydrous conditions is not practical and so the effect of water on the voltammogram was investigated. The effect of water on DESs has been studied^{31,34} and it has been shown that water can significantly improve mass transport while not significantly affecting speciation. Al-Murshedi³¹ used NMR to measure self-diffusion coefficients for components of the DES with different amounts of water. It was concluded that the mixtures were not homogeneous and there were clear signs of water dominant and ion dominant phases. Dynamic light scattering was used to show that these dispersed phases were c.a. 100 to 300 nm.³¹ It was also shown that when DESs were dispersed in water this two-phase behaviour still exists. It was found that there was no significant change in the potential window when different amounts of water were added (up to 40 wt%) suggesting that the double layer structure must be dominated by the choline. This was later confirmed using AFM to study interfacial structures. Al-Murshedi showed that the speciation of CuCl_2 in Ethaline water mixtures changed with varying amounts of water. It was also shown that water had a significant effect on the morphology of the copper deposited from electrorecovery in Ethaline water mixtures.³¹

Figure 3.14 shows the voltammograms for 2 mg of CuS paint cast on a Pt electrode with varied amounts of water in Ethaline. The addition of 20 wt % water causes a small increase in the peak currents and a slight shift in the peak potentials of all the couples primarily due to a decrease in solution resistance and an increase in mass transport. The addition of 30 wt% water caused a decrease in the oxidation current and the signal for the sulfide oxidation to merge with that for copper oxidation. As discussed earlier, the same paint casting experiments were carried out in 3 mol dm^{-3} NaCl solutions but due to the nature of water being non-viscous, the mineral was unable to adhere to the electrode and instead was washed off the electrode surface. This shows that paint casting is unique to viscous, conducting pastes but the addition of small amounts of water to Ethaline are not detrimental and occasionally is beneficial to the electrochemical process.

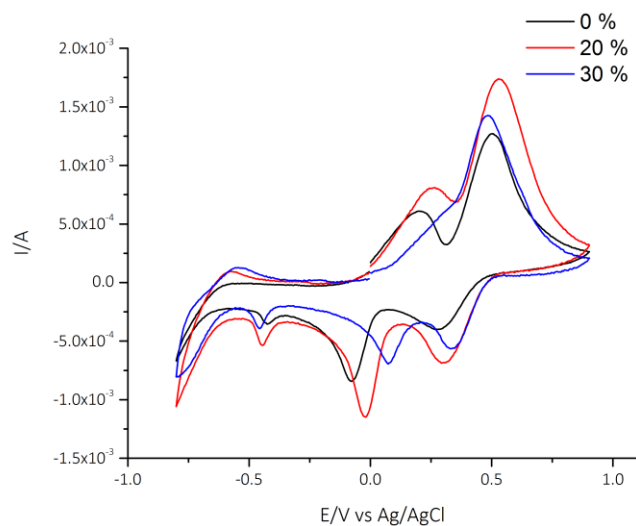


Figure 3.14: Overlaid paint cast CV's, all with 2 mg of CuS with varied amounts water in Ethaline. All voltammograms were conducted in Ethaline with varying amounts of water. Each voltammogram used a 1 cm² Pt flag working & counter electrode and Ag/AgCl [0.1 M in Ethaline] reference electrode, at a scan rate of 5 mVs⁻¹.

3.3 Electrochemistry of copper sulfide minerals

3.3.1 Paint casting copper sulfide minerals

Covellite and chalcocite are both copper containing sulfides, CuS and Cu₂S respectively. They are the simplest of the copper sulfides, not having the complication of containing other metals. Chalcocite used to be one of the major sources for copper extraction before most of the deposits were largely depleted. It contains 80 % by weight of copper and is easily separated from the sulfur. Chalcocite is a fairly soft, lead grey coloured mineral, measuring between 2.5 and 3 on the Mohs hardness scale.³⁵ To put this into perspective, talc is measured at 1 and diamond at 1600 on the same scale.³⁶ Chalcocite is occasionally found as a primary mineral however more commonly as a secondary mineral that forms as a result in changes in other minerals.³⁵ Chalcocite is described as being a pseudomorph, whereby a mineral replaces another but the crystal shape of the original mineral remains intact. Chalcocite is able to form a pseudomorph of bornite, covellite and chalcopyrite among others.³⁷

Covellite is also known as a secondary mineral and is rarely found, if ever, as a primary mineral. It is not worth mining covellite for its copper content, as quite often it will be found as thin layers on top of other minerals.³⁵ As with some other minerals, the assignment of expected oxidation states is often deceptive and incorrect. It would be expected that the oxidation states of copper and sulfur in covellite were +2 and -2 respectively, however, there is a lot of confusion in the literature as to what the correct oxidation states of both elements should be. $[(\text{Cu}^{\text{I}})_3(\text{S}_2^{2-})(\text{S}^-)]$, $[(\text{Cu}^{\text{I}})_3(\text{S}_2^-)(\text{S}^{2-})]$ and $[(\text{Cu}^{\text{III/IV}})_3(\text{S}_2^{2-})(\text{S}^{2-})]$ are all propositions from the literature however, it is generally agreed that these suggestions do not fully describe the oxidation state situation.³⁸ It is however safe to assume that covellite is not as simple as it may seem and therefore the oxidation state of the copper in the solid (or once dissolved) cannot be just assumed to be 2+. Covellite is a highly iridescent blue mineral with an interesting crystal structure, which is often referred to as being “layered”, whereby individual layers of CuS_3 form in planes; one on top of each other.³⁹ The sulfur atoms in these layers are subsequently attached to 2 tetrahedral CuS_4 molecules extending either side of the structure. For the case of chalcocite the structure alters depending on the temperature, both structures however are based on a hexagonal close packed structure of the sulfur atoms, regardless of the temperature. When the temperature is lower than 103.5 °C, a monoclinic superstructure is observed with the copper atoms in triangular configurations within the sulfur structure. Above 103.5 °C the structure is more disordered, and the copper atoms can be in one of either triangular or tetrahedral arrangement within the hexagonal structure.³⁹

The analysis of the covellite and chalcocite samples used in the following electrochemical analysis is shown in Figure 3.15. The SEM image in 3.15a clearly shows the characteristic layered structure of the covellite that was described previously. As mentioned earlier in this section, several oxidation states of copper and sulfur have been suggested for covellite, including but not limited to $[(\text{Cu}^{\text{I}})_3(\text{S}_2^{2-})(\text{S}^-)]$, $[(\text{Cu}^{\text{I}})_3(\text{S}_2^-)(\text{S}^{2-})]$ and $[(\text{Cu}^{\text{III/IV}})_3(\text{S}_2^{2-})(\text{S}^{2-})]$.³⁸

To ensure the synthetic CuS was not just simply $\text{Cu}^{\text{II}}\text{S}^{2-}$ and therefore not comparable to the natural mineral, XRD was carried out and the result shown in Figure 3.15 c. The patterns correspond to those for pure CuS . The same analysis has been done on

chalcocite and synthetic Cu_2S shown in Figure 3.15 d, again the reflects are comparable to each other confirming that any investigation carried out on the pure materials is also crystallographically comparable to the mineral material.

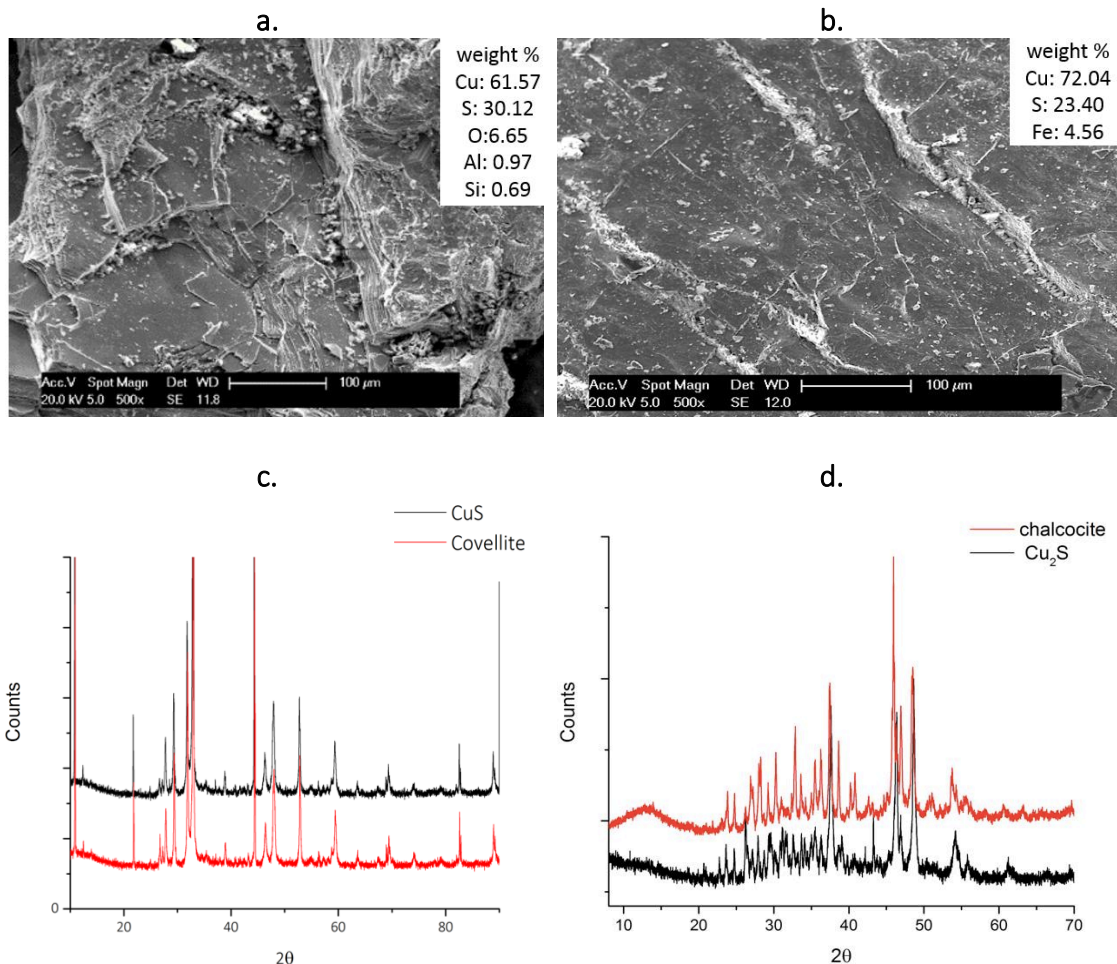


Figure 3.15: SEM images of **a.** powdered covellite sample & **b.** chalcocite sample, both on carbon stubs. XRD pattern comparison for **c.** powdered CuS natural mineral & synthetic material and **d.** powdered Cu_2S natural mineral and synthetic material.

Analysis of the minerals using back-scattered electrons can be seen in Figures 3.16 and 3.17 where it is clear, the majority of the samples are one main phase. Chalcocite (Figure 3.16) makes up 88 wt % of the sample (Table 3.3) with the remainder being mainly covellite. There are only trace amounts of magnetite and chalcopyrite which accounts for the presence of Fe in the EDX data from Figure 3.15.

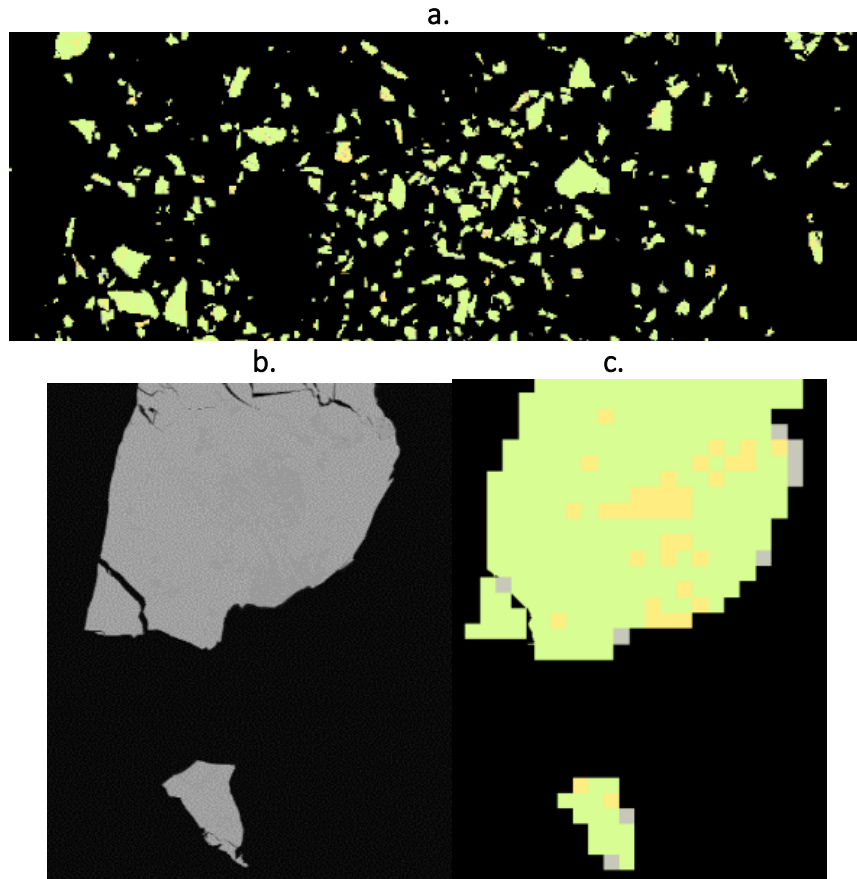


Figure 3.16: *a. Section of the overall coloured chalcocite mineral map. b. back scattered electron image from a small section. c. Corresponding mineral map image to the back scattered electron image.*

Table 3.3: *Table describing the composition and occurrence of minerals in the electron image from Figure 3.16 a.*

	Average composition	Weight %	Number
Chalcocite (green)	Cu 82.02; S 17.68; Fe 0.3;	88.49	1744
Chalcopyrite (beige)	Cu 48.36; S 27.29; Fe 24.35;	0.01	5
Quartz (blue)	Si 53.1; O 46.9;	(0.006)	4
Galena (mauve)	Pb 100;	0.02	5
Covellite (yellow)	Cu 65.27; S 24.65; Fe 10.09;	11.47	1438
Magnetite (red)	Fe 56.82; O 43.18;	(0.003)	1

There is a wide variety of grain sizes in this sample, however the largest grains are generally the chalcocite and the impurities tend to make up the smaller grains. For example the average grain size for chalcocite is $110 \pm 103 \mu\text{m}$ whereas for all the other

mineral impurities the largest grain size is found for covellite at $40 \pm 37 \mu\text{m}$. (Error in both cases demonstrates the wide range of grain sizes).

The EDX analysis for the sample of covellite in Figure 3.15 suggests the presence of more mineral impurities than was observed for chalcocite. This is also supported in the following data where the mineral map appears to have larger areas of colours other than the bulk yellow (covellite).

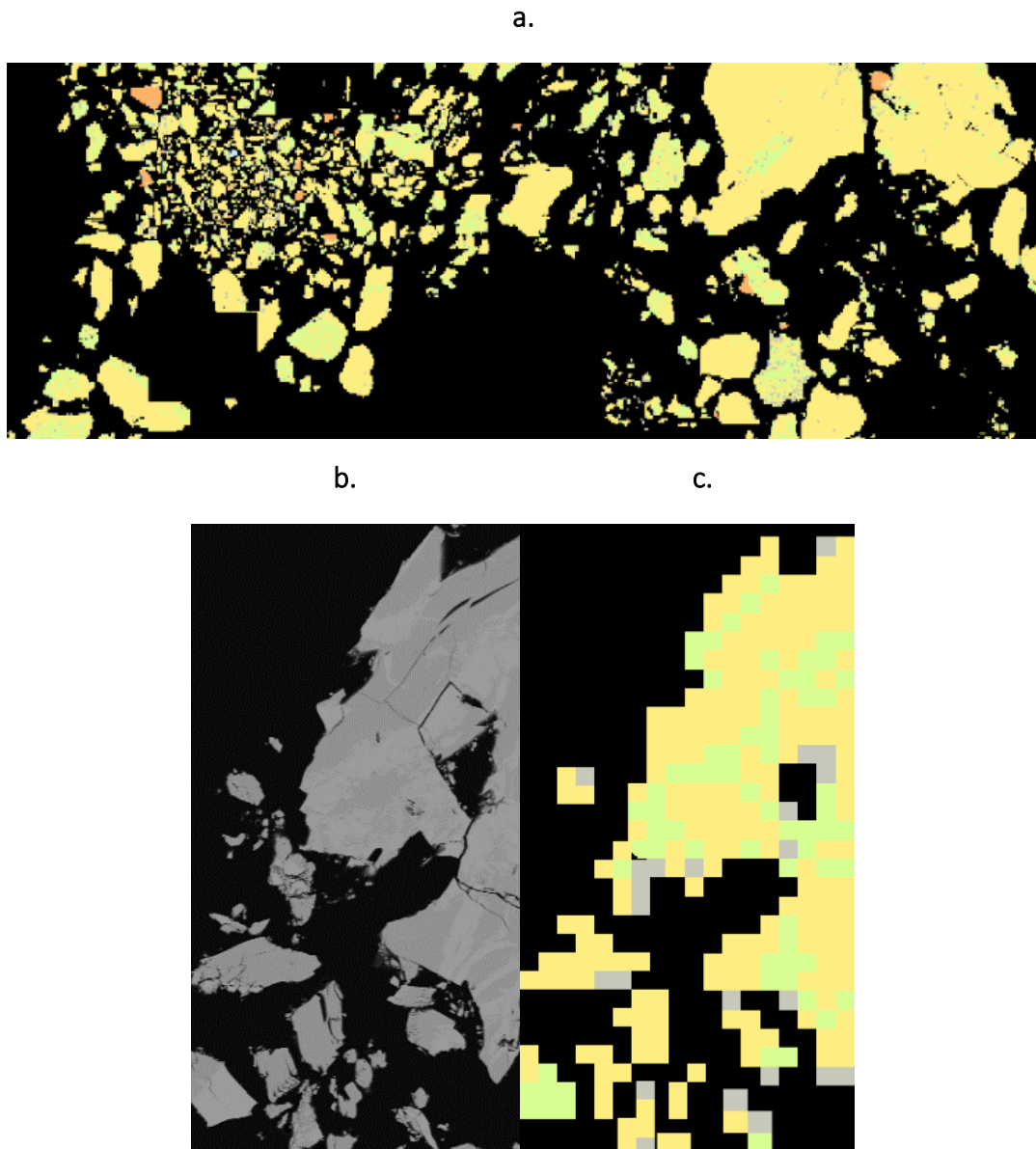


Figure 3.17: *a. Section of the overall coloured covellite mineral map. b. back scattered electron image from a small section. c. Corresponding mineral map image to the back scattered electron image.*

In this sample of covellite, it can still be seen that the majority of the sample is covellite (signified by the yellow coloured particles). The average composition of covellite in this sample is 69.65:30.29:0.06 (Cu:S:Fe), compared to 66.46 : 33.54 (Cu:S) for a standard sample of covellite. The main impurity in this sample is chalcocite as well as a small amount pyrite. There are also trace amounts of several other minerals all shown in Table 3.4, the clinopyroxene, quartz and barite accounts for some of the oxygen present in the EDX data, however the rest could be a result of water. This analysis shows that both mineral samples contain traces of both Cu sulfides which is not surprising, but it also shows that they are largely free from other metal ions which may interfere with the electrochemical signals. The main associations in this particular sample are between covellite and chalcocite, it is shown in the zoomed image in Figure 3.17.c that there are chalcocite inclusions in the covellite, which is to be expected. It is shown that the backscatter electron image (b.) can detect these inclusions from the varying grey scale, which matches the mineral map (c.).

Table 3.4: Table describing the composition and occurrence of minerals in the electron image from Figure 3.16. a.

	Average composition	Weight %	Count
Covellite (yellow)	Cu 69.65; S 30.29; Fe 0.06;	80.3	5163
Galena (mauve)	Pb 99.75; S 0.25;	0.04	29
Clinopyroxene (purple)	O 53.91; Fe 26.19; Ca 13.74; Al 6.17;	(0.003)	4
Chalcopyrite (beige)	Cu 37.93; S 35.94; Fe 26.13;	0.10	109
Pyrite (dark orange)	S 52.98; Fe 46.61; Cu 0.28; Ti 0.13;	1.32	234
Chalcocite (green)	Cu 79.89; S 20.06; Fe 0.05;	18.2	4046
Quartz (blue)	Si 53.83; O 45.03; S 0.8; Al 0.33;	0.04	49
Barite (pink)	Ba 74.98; S 13.46; O 11.56;	(0.002)	2

The electrochemistry of selected minerals has been studied and reviewed by Niu et al.⁴⁰ This has concentrated on sulfide minerals due largely to their higher conductivity than oxides. Several electrochemical techniques have been used including cyclic voltammetry, chronopotentiometry, coulometry and impedance spectroscopy. Most studies have used either solid single crystals or paste electrodes. Despite the importance of redox

chemistry in mineral dissolution relatively few electrochemical studies of minerals have been published due to the complexity of sample preparation.⁴⁰

Figure 3.18 shows the CV's of 2 copper sulfide minerals. Both CVs have peaks at the same potentials as the pure materials shown in Figure 3.8 but the relative peak heights are different. All-natural minerals are clearly impure but redox properties highlight the presence of Cu and S based materials.³⁹

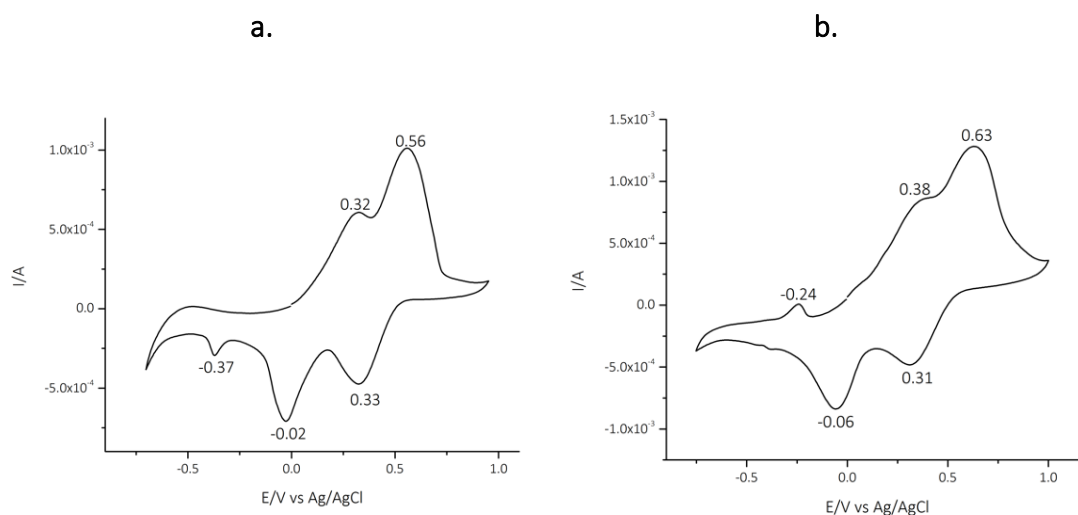


Figure 3.18: The paint casted cyclic voltammograms of **a.** covellite and **b.** chalcocite both carried out in Ethaline with a 1 cm² Pt flag working and counter electrode and a Ag/AgCl [0.1 M Ethaline] reference electrode at a scan rate of 5 mVs⁻¹

The first point to note is that the peak heights corresponding to Cu^I and S²⁻ oxidation for the two minerals are relatively similar to those for the pure materials. The peaks are less well defined, but this is to be expected given the purity shown in Table 3.3. It does confirm that impure minerals can be studied in a similar manner to pure materials. The peak for chalcocite oxidation at -0.24 V is less well defined in the mineral than it is in the pure material. This is however, only the reoxidation of copper deposited on the cathodic sweep and could be due to the poorer conductivity of the mineral compared to the pure sulfide.

3.4 Electrochemistry of chalcogens and other copper chalcogenides

The electrochemistry of sulfur and sulfides has been studied in far greater detail than the corresponding selenium and tellurium containing compounds due mainly to their respective abundances and applications. As described in the introduction, the aim of the NERC TeaSe (Tellurium and Selenium) project was to identify and extract selenium and tellurium from both primary and secondary sources. Figure 3.19 shows the voltammograms of the individual chalcogen (Se and Te) powders applied as paint cast films on a Pt electrode. Figure 3.19 also shows the corresponding Pourbaix diagrams for the elements in aqueous solutions (See chapter 1 for thermodynamic analysis). Pourbaix diagrams show the thermodynamically stable phase of a metal as a function of potential and pH. They are extensively used to predict passive phases in the corrosion of metals in different environments. They are also used in mineralogy to aid mineral dissolution by predicting soluble phases. There are numerous issues with Pourbaix diagrams including the lack of kinetic information and the inability to predict whether films are porous or occur away from the metal surface. They also do not account for local H changes which are particularly important for corrosion studies.

Additionally, the Pourbaix diagrams presented here are based on aqueous solutions and therefore do not account for the chloride species in Ethaline. Beverskog et al. used the example of Cu in aqueous chloride environments for their study on the effect of a high chloride environment on metal Pourbaix diagrams. They found that the molality of chlorine in the solution determined which species predominated. For example, a typical Cu Pourbaix diagram is dominated by Cu, its oxide and hydroxide species. Reductive environments (below 0V) allow elemental Cu to dominate whereas in the oxidative environment at more acidic pH Cu^{II} governs with CuO/Cu₂O and hydroxide species overruling at neutral and alkali pH's respectively. This remains somewhat similar at low (0.2 molal) chlorine concentrations, however a window of CuCl₂ is available in acidic oxidative environments. As the chloride molality increases to 1.5 the chloride species completely dominates, whereby in reductive environments below pH11 the CuCl₃²⁻ species is available. These diagrams are also dependent on the concentration of Cu in solution and therefore there ends up with a sort of sliding scale of species accessible.⁴¹ This is vital to consider when analysing the following Pourbaix diagrams.⁴²

For the Se electrochemistry, it is likely that peak C15 is due to the reduction of Se^0 to H_2Se , from analogy with the aqueous Pourbaix diagram in Figure 3.19c. This is supported by the presence of the characteristic smell of H_2Se during the experiment, it is also supported in the literature by a couple of studies conducted on the electrochemistry of Se and selenide studies.^{43,44} Firstly a paper by Bougouma et al. investigating the electrochemical behaviour of selenium in Reline, a DES containing choline chloride and urea. They showed a reduction peak at -0.7 V that they attributed to the reduction from Se^0 to Se^{2-} .⁴³ This study also reported another reduction peak, or collection of peaks that they suggested was due to the reduction from Se^{IV} to Se^0 that occurred at -0.3 V, as well as an oxidation peak at 0.5 V. The nature of their voltammograms, being conducted on a gold electrode in a solution of SeO_2 might go some way to explain why the results differ from those obtained by the paint casting in Ethaline voltammogram presented in Figure 3.19a.⁴³ The lack of peaks at c.a. 0.5 V suggests that SeO_2 is not formed in Ethaline, even though the Pourbaix diagram would suggest that the oxidation of Se^0 is attainable at relatively low potentials. A review on Se electrochemistry by Saji et al. contains a small amount of information on selenium electrochemistry in ILs and DESs, it confirms that selenium behaves very differently in these electrolytes compared to their aqueous counterparts.⁴⁴

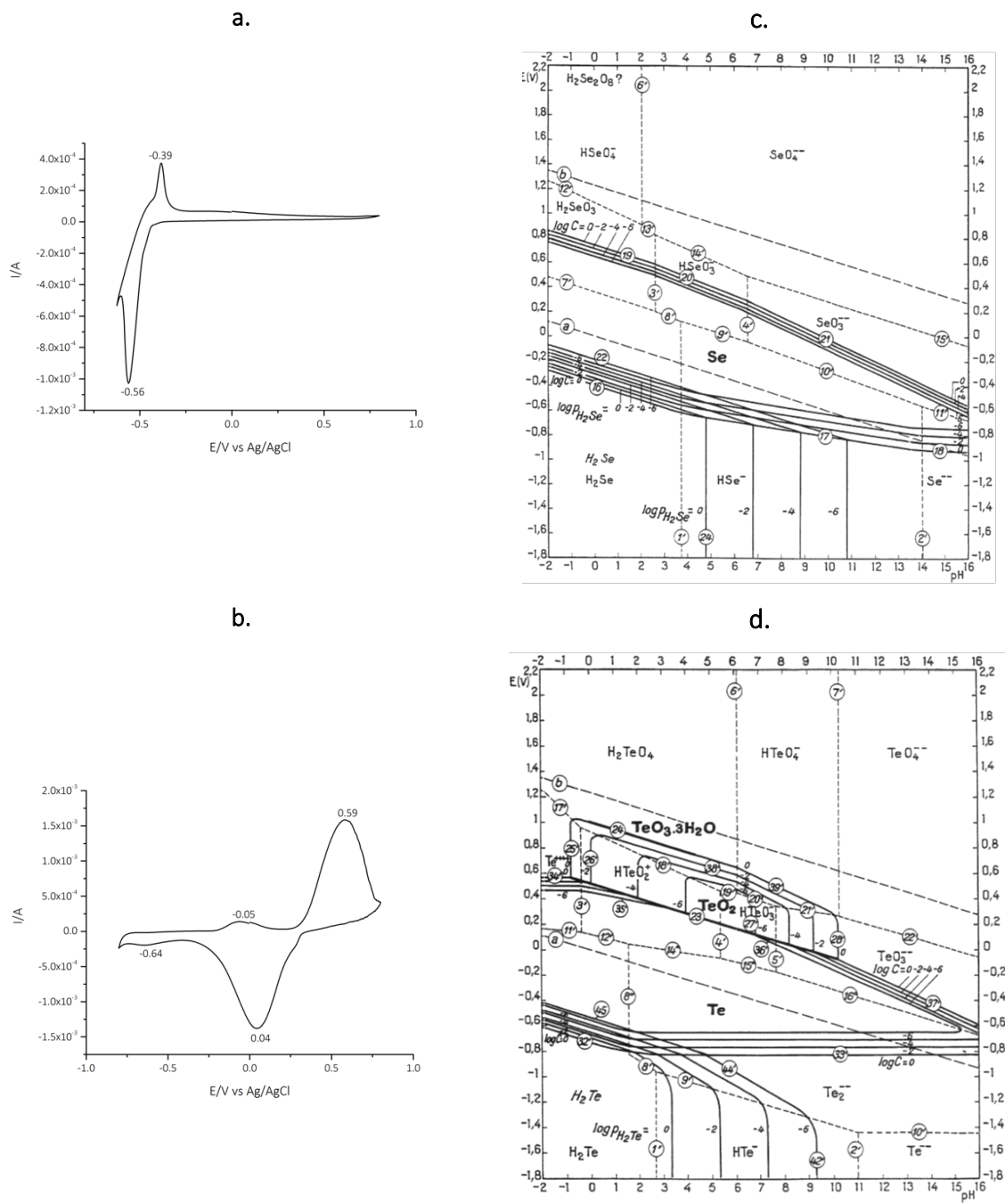


Figure 3.19: a.& b. Paint casting cyclic voltammograms for Se and Te, both conducted in Ethaline with a 1 cm² Pt flag working and counter electrode and Ag/AgCl [0.1 M Ethaline] at 5 mVs⁻¹ c.& d. Pourbaix diagrams for Se and Te in water.⁴⁵

As for the Te, there is less literature on its electrochemistry, especially in ILs and DESs. With the pH of Ethaline at approximately 6 it could be suggested that the oxidation of Te yields either TeO₂ or HTeO₃⁻, however, as Te has more metallic characteristics it could just as well form a chlorometallate complex such as TeCl₄²⁻. The only precedent for this

is the study of the electrochemistry of tellurium in methylene chloride where a variety of chloride species were produced.⁴⁶

3.4.1 Paint casting copper selenide and telluride compounds

The electrochemistry of other copper chalcogenides, in particular CuSe, Cu₂Se and Cu₂Te have also been studied and their CV's are shown in Figure 3.20. These voltammograms have not been widely reported in the literature, but the method of paint casting made studying the electrochemistry of these materials accessible and easily repeatable. All 3 voltammograms show the clear combination of Cu and either Se or Te peaks respectively. The first thing to note from these CV's is the very apparent differences between the CuSe and Cu₂Se, unlike the Cu sulfide CV's that are for the most part very similar. In all cases there is evidence of the Cu^{I/I} couple although with slightly shifted potentials. In the Cu₂Te voltammogram the Cu^{I/I} oxidation peak (A26) is almost a shoulder for another peak (A27) which is likely to be the Te oxidation peak at 0.59 V shown previously in Figure 3.19b. In the CuSe CV in Figure 3.18a there is the unmistakable redox couple (A18/C14) that is present in the Se CV from Figure 3.19a. It was mentioned in the previous section that it is likely due to the redox reactions between Se and H₂Se, determined both from the Pourbaix diagram and the presence of a characteristic H₂Se smell. In the CuSe CV there is also does not appear to be a Cu^{I/0} couple unless this is being swamped by the Se redox. In contrast to this, both the Cu₂Se and Cu₂Te exhibit the Cu^{I/0} couple: A21/C17 and A24/C20 respectively. All 3 voltammograms shown in Figure 3.20 exhibit a similar peak to that seen in the copper sulfides which was assigned to some sort of sulfur species. Interestingly these peaks are not present in the Cu oxide and also, they are not present in the CuCl₂ paint casting CV shown previously in Figure 3.8c therefore are not an artefact of analysing Cu compounds with this technique. Interestingly, the couples A19/C15 and A22/C18 from the Cu selenide voltammograms occur at very similar potentials to the sulfide couples A10/C7 and A13/C10 in Figure 3.8. Whereas the peaks in the Cu₂Te (A25/C21) are shifted to more cathodic potentials by around 15 mV. The Pourbaix diagrams do not show evidence of polymeric anions for Se and Te and so it is assumed that these peaks are due to the oxidation to a selenium or tellurium chloride containing species.

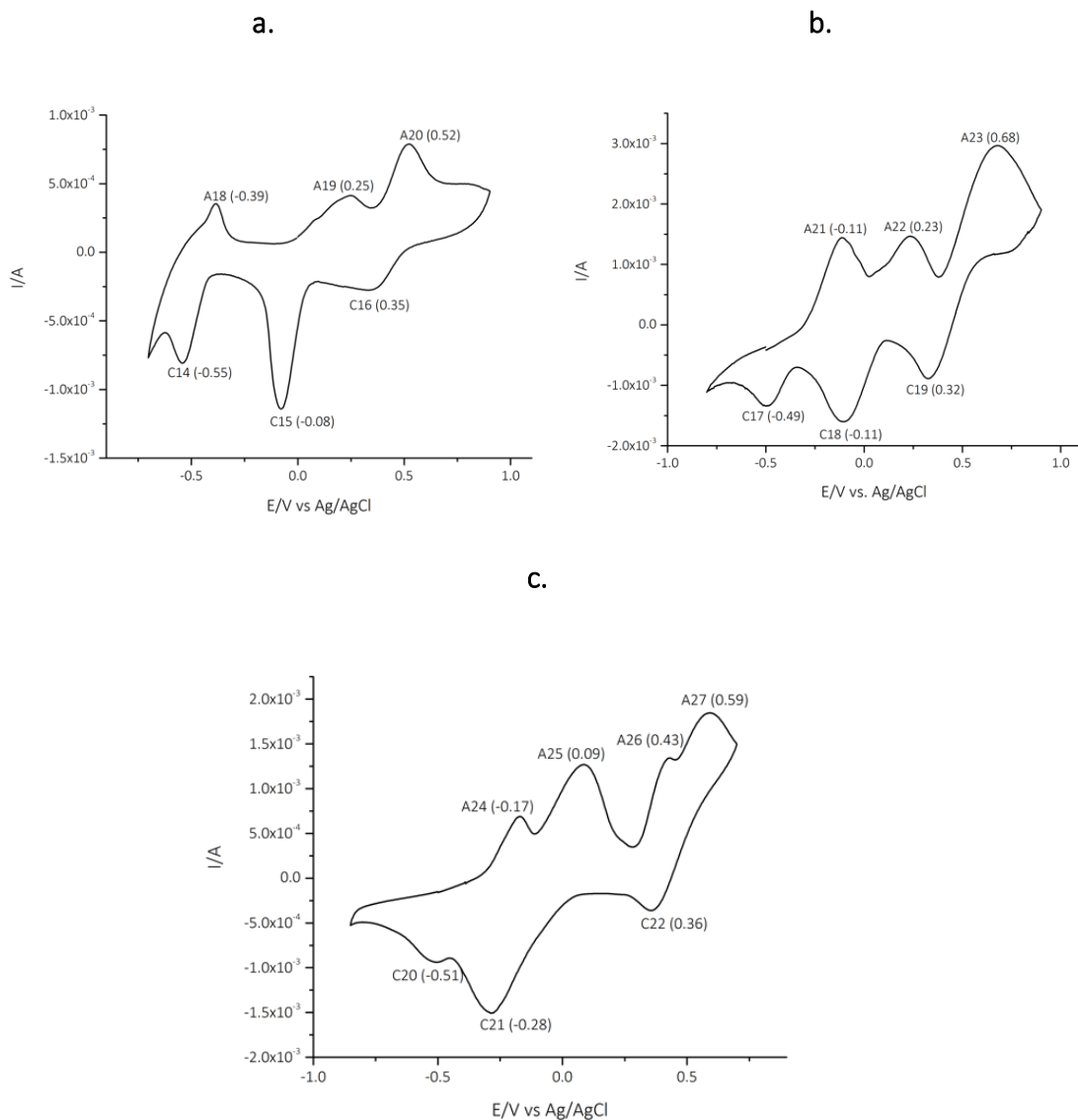


Figure 3.20: The paint casting cyclic voltammograms of **a.** CuSe **b.** Cu₂Se **c.** Cu₂Te. All voltammograms were conducted in Ethaline with a 1 cm² Pt flag working & counter electrode and Ag/AgCl [0.1 M in Ethaline] reference electrode, at a scan rate of 5 mVs⁻¹.

Golgovici et al. investigated the electrodeposition of copper telluride films on a platinum substrate in Ethaline and presented CV's of solutions containing CuCl and TeO₂.⁴⁷ The CV's that are shown in this work do not represent what is shown in the paint casting experiments with Cu₂Te powder. Although not directly studying the same processes, it is interesting to note in this work that there does not appear to be any obvious peaks related to the tellurium electrochemistry, like there is in the CV presented in Figure 3.20.

For the copper selenides, again, the direct electrochemical analysis of these compounds is similarly scarce. Copper selenides are important in applications such as CIGS (copper, indium, gallium, diselenide) solar panels, and a large portion of the literature surrounds this application and investigations into the deposition of copper selenide as an intermediate.⁴⁸⁻⁵¹ The Pourbaix diagram of copper selenide indicates that there is a clear redox process that occurs, regardless of the pH, at around -0.75 V to -1 V. The copper selenide is reduced to Cu^0 and HSe, or H_2Se in acidic conditions, this could explain what is happening to the selenium at these lower potentials as it is possible to assign the reduction to Cu^0 quite easily.⁴⁸

3.5 Electrochemical studies of copper chalcogenide compounds

While the studies above give an indication of the electron transfer processes occurring during oxidation and reduction they do not provide an insight into the bulk dissolution process and the factors affecting the rate of dissolution. In this section bulk electrolysis experiments were carried out and combined with spectroscopic investigations on the resulting solutions to understand the factors affecting the dissolution rate and the species formed in solution. This uses pure, synthetic chalcogenides. The hypothesis is that all of the materials act as semiconductors and it is the ease of electron injection or extraction that will affect the rate of oxidation. If this is the case, then the dissolution rate should be related to the band gap or conductivity of the bulk material.

The band gap of a material describes the energy difference between the conduction band and the valence band and this controls whether a compound is a conductor, semiconductor or insulator. For conducting materials the two bands overlap and the band gap would be 0, whereas for insulators there is a very large gap between the valence and conduction, enough of a gap to prevent the electrons moving between the two.⁵² For semiconductors the bands are close enough to each other to allow electrons to transfer between them, the electrons move from the valence band which is essentially acting as the HOMO (highest occupied molecular orbital) to the conduction band or LUMO (lowest unoccupied molecular orbital), due to the small energy gap. The excited electron is able to move freely around the conduction band and hence act as a conductor, the hole that is left behind in the valence band can then be filled by other

electrons in the same band. Applying a voltage to a semiconductor would have the effect of exciting these valence band electrons and hence generating a current, which would consequently lead to the oxidation and dissolution of the semiconductor. A material with a small band gap should be more conducting and easier to oxidise.²¹

3.5.1 Chronocoulometry

To test this a series of chronocoulometry experiment were carried out on different copper chalcogenides. This approach was used by Al-Bassam²¹ who studied the dissolution rate of four Fe-S mineral and found a rough correlation between the charges passed and band gap for the mineral. 40 mg of material was pasted onto the surface of a platinum flag electrode and a potential of 1.2 V was applied to the electrode for 1800 s. The charge passed was then plotted vs the band gap of the compound and presented in Figure 3.21a.

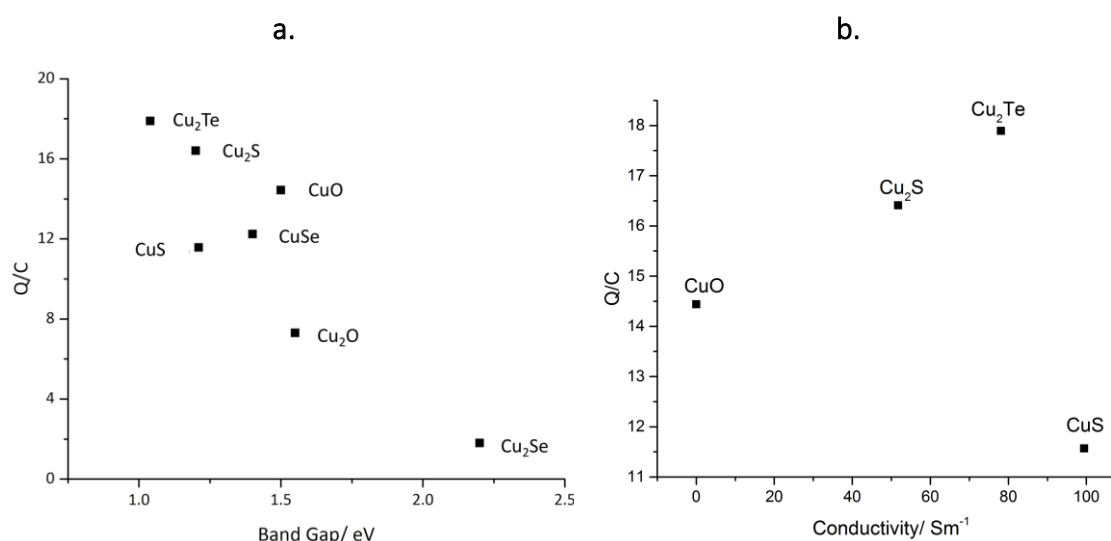


Figure 3.21: *a. Band gap and b. electrical conductivity (measured using a 4 point conductivity probe on a pressed disk of the powdered material) both plotted against the charge resulting from chronocoulometry experiments, with a constant potential of 1.2 V applied in a paint casting style experiment in Ethaline for 1800 s. (1 cm² Pt flag working and counter electrode and Ag/AgCl [0.1 M Ethaline]).*

The results in Figure 3.21a conform to the theoretically expected results whereby as the band gap increases and the material is more electrically insulating, the rate of dissolution decreases. This could also be described as an effect of the *iR* drop across the material.

The results explain why the dissolution of Cu_2Te is relatively fast whereas that for the closely related Cu_2Se is much slower. The band gap is a useful concept but can be practically difficult to determine as it depends on the form of the material. A more practical solution would be to measure the conductivity of the sample, but this is very difficult for a powdered sample as the connectivity of the particles will limit the conductivity. To circumvent this the semiconductor powder was pressed into a disc in the same way that a salt would be made into a plate for an infra-red experiment. The discs were then used to measure the electrical conductivity using a 4-point conductivity probe. A selection of the powders did not form discs that remained whole or there was not substantial material to make a disc, therefore Figure 3.21b is not complete with all data.

The data that is present shows that the electrical conductivity correlates well with the electrochemical dissolution rate of materials with CuO , Cu_2S and Cu_2Te . This is a novel discovery of this project and provides a simple method by which the dissolution rates of materials could be predicted. It also widely supports the correlation observed with the band gap, and therefore can be used in conjunction for materials with an unknown band gap.

3.5.2 UV-Vis Analysis

The results from the voltammetry and chronocoulometry experiments indicate the electrochemical behaviour of the individual minerals and provides an insight into the voltages that allow oxidation and reduction of the different elements to occur. To determine whether metallic copper can be recovered from the various copper compounds, bulk dissolution and electrolysis experiments were carried out, as described in sections 2.2 and 2.3 respectively. The anodic dissolution of the pastes led to the solubilisation of some of the material, this is shown in Figure 3.22. The colours of the solutions indicate a presence of copper ions and after electrolysis the occurrence of copper metal on the nickel plates is confirmed by EDX.

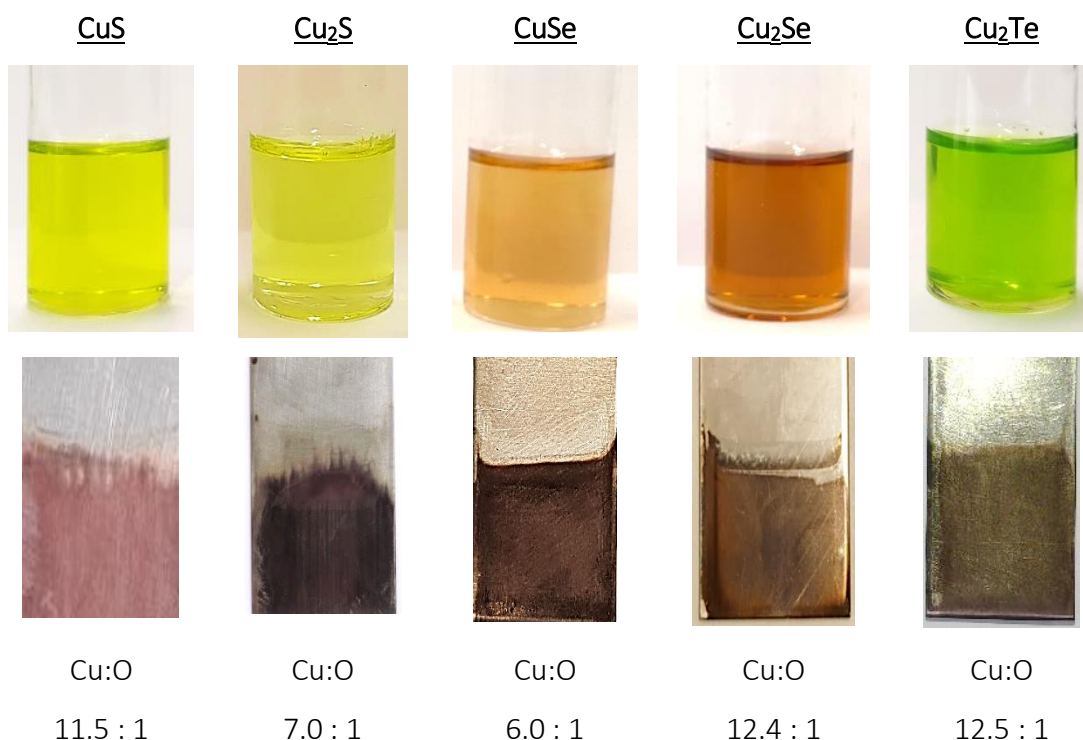


Figure 3.22: The electrochemical dissolution solutions of CuS, Cu₂S, CuSe, Cu₂Se and Cu₂Te, the corresponding plates and EDAX results from their electro-recovery and the ratio of Cu:O obtained from the EDAX data.

The solutions shown above all show typical colours you might expect from a copper containing compound. It is interesting to note the similarities in the CuS and Cu₂S solution colours and intensities. In these electrochemical dissolutions they both exhibit similar yellow solutions, without either solution turning green. Both the selenide solutions have a brown/orange tinge which suggests the selenium is having an effect on what you would expect to be a similar yellow colour to the sulfides. Finally, the telluride exhibits a very strongly coloured green solution that is relatively opaque. On repetition of these experiments, the results were fairly constant in terms of the colour and intensity that was obtained, however, occasionally the Cu₂Te would result in a definite blue colour, which is likely due to the presence of water in the Ethaline. It is important to point out here that regardless of the colour that was obtained in any of the dissolution experiments, the recovery always resulted in copper being achieved with some signal for oxygen.

The solutions shown in Figure 3.22 were analysed by UV-Vis to determine speciation of the elements in solution. Figure 3.23a shows the UV-Vis of electrochemically dissolved CuS, Cu₂S and chemically dissolved CuCl₂, all in Ethaline. All 3 spectra are identical confirming that they are forming the same species in solution. These particular peaks are reported by Al-Murshedi as being CuCl₄⁻ in Ethaline likely formed due to the high chloride environment in Ethaline.³¹ This is confirmed as well by some EXAFS experiments that were conducted on these samples revealing CuCl₄²⁻ speciation with Cu-Cl bond lengths of 2.25 Å. It is also interesting to point out that regardless of whether the copper is in the 2+ or 1+ oxidation state in the compound does not affect this peak. So for CuS and Cu₂S the peak occurs in the same place, this would be expected simply from looking at the images of the solutions in Figure 3.22. The sulfur/ sulfide or any related species is clearly not altering the Cu aspect of the UV-Vis, however, on addition of BaCl_{2(aq)} to the solutions a precipitate is formed. Thus signalling the presence of SO₄²⁻ in solution as well.

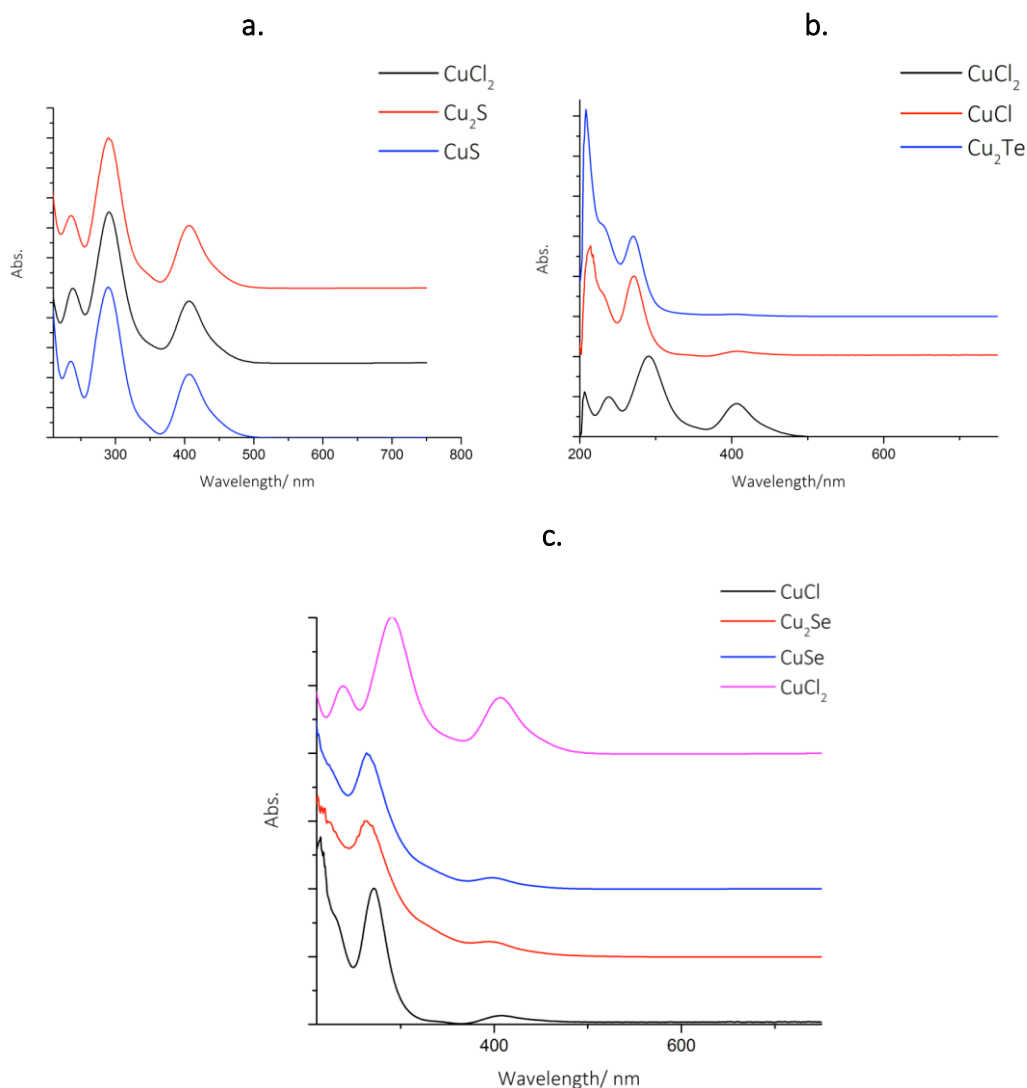


Figure 3.23: Overlaid UV-Vis (offset for clarity) from the different copper chalcogenide solutions after the electrochemical dissolution (constant 1.5 V for 24 hours in Ethaline, using an IrO₂ coated Ti anode and cathode), solutions pictured in Figure 3.22.

In the case of the Cu₂Te and Cu₂Se/CuSe solutions the peak around 400 nm has all but disappeared or is very small. This is more characteristic in the CuCl in Ethaline UV-Vis shown in Figure 3.23b and c. The Cu₂Te solution has an almost identical UV-Vis to CuCl and it is shown in Figure 3.21b the extent of the shift from the peaks obtained from the CuCl₂ solution. It is suggested that the cause of the green solution shown in Figure 3.22 is due to a mixture of yellow CuCl₄ and blue Cu(H₂O)₆. During the dilution of this solution for the purposes of UV-Vis the green colour disappears, leaving a yellow solution reminiscent of the CuS/Cu₂S solutions, meaning that there is no peak around 800 nm

that would be expected from blue Cu complexes. Data from HPLC coupled with ICP-MS suggested that both tellurate and tellurite are present in the solution. The same was true when the selenide solutions were analysed in that they contained a combination of selenite and selenate in solution. Interestingly, there was no suggestion of chloride species which is what might have been expected. The results for both Cu_2Te and Cu_2Se dissolution are shown in Figure 3.24a and b respectively.

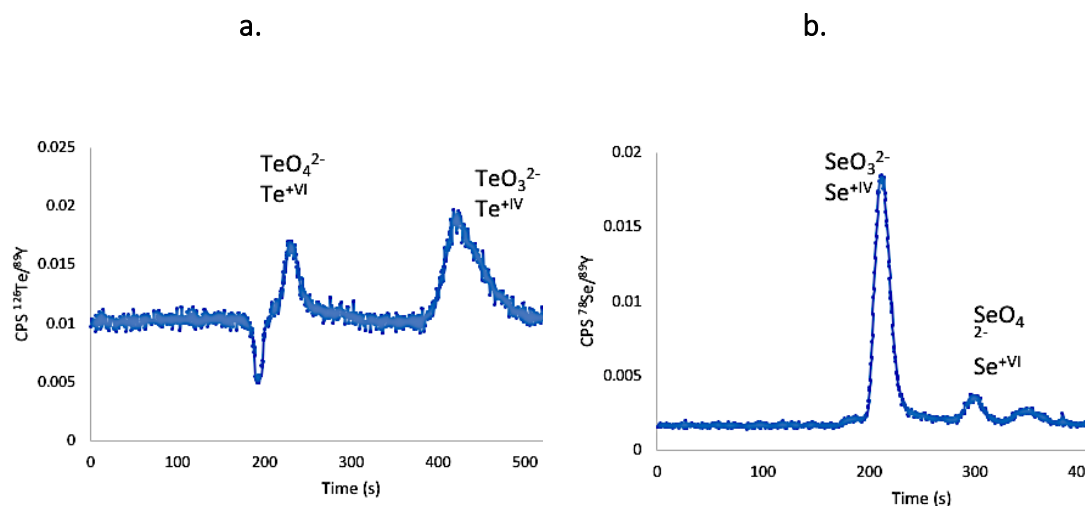


Figure 3.24: The HPLC-MS plots for **a.** Cu_2Te and **b.** Cu_2Se both electrochemically dissolved in Ethaline for 24 hours at 1.5 V, using an IrO_2 coated Ti anode and cathode. Solutions pictured in Figure 3.22

The UV-Vis for the Cu_2Se and CuSe solutions is neither like CuCl_2 nor like CuCl as shown in Figure 3.23c, it shares most similarities with CuCl however the predominant peak at around 300 nm is shifted to a lower wavelength. A preliminary EXAFS experiment was also conducted on some of these samples and the fitting for the selenide solutions suggests a mixture of CuCl_2^- and CuCl_3^{2-} which could account for this shift.

3.5.3 EXAFS

UV-Vis has proven to be a useful technique in determining certain aspects of speciation; however, it cannot be used alone to identify metal coordination when unknown ligands are involved. Therefore, EXAFS was used in conjunction with UV-Vis experiments to determine the speciation of Cu ions in the solutions in Figure 3.25. From X-ray absorption near edge spectroscopy (XANES), it is possible to obtain an indication of which oxidation

states are present. Once speciation is known for the samples, UV-vis spectra can then be used as a fingerprinting technique to identify speciation in others. The UV-Vis of the Cu sulfide solutions suggests that CuCl_4^{2-} is the species present in solution. It is confirmed in the EXAFS data fit which is indicated from the single peak in the Fourier transform (Figure 3.25b) that an individual coordinated species was present for both Cu_2S and CuS . The spectra fit the tetrachloride species with Cu-Cl bond lengths of around 2.25 Å. The XANES regions are also comparable for both the Cu sulfides as well as the CuCl_2 again confirming the presence of Cu^{II} ions in solution. EXAFS is unable to easily distinguish between Cl and S coordination to the Cu ions and because there is a possibility of a sulfur ligand being present in solution. In this case, the UV-Vis can be used to match the fingerprints of CuCl_2 and $\text{CuS}/\text{Cu}_2\text{S}$ to confirm it is CuCl_4 .

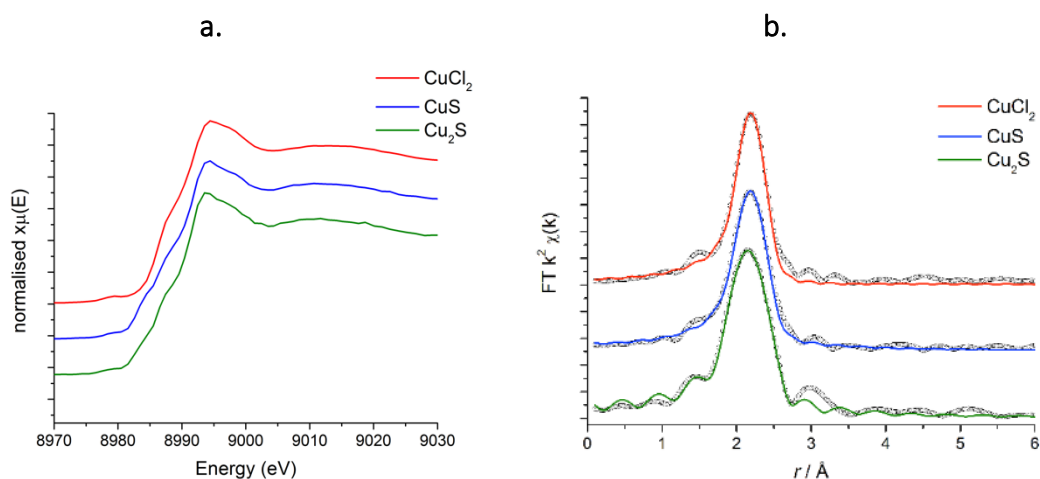


Figure 3.25: *a.* XANES and *b.* Fourier transforms (right) of solutions of CuCl_2 (red), CuS (blue) and Cu_2S (green) in Ethaline, CuS and Cu_2S are both electrochemically dissolved in Ethaline for 24 hours at 1.5 V, with IrO_2 coated Ti electrodes, whereas CuCl_2 plots were obtained from chemical dissolution. Data are circles, fits are lines.

The solutions from both Cu selenide dissolutions are unusual. They appear to exhibit a brown/orange colour in Figure 3.22; however after they were shipped to the EXAFS experiment and left for two weeks, it was reported that the solutions turned very pale yellow. Both solutions were incredibly dilute ($< 2.5\text{mM}$) and in the case of CuSe too dilute to measure with EXAFS. However, due to the CuSe and Cu_2Se UV-Vis spectra being identical, it can be assumed that the EXAFS are likely to be the same. The Cu_2Se solution

was also dilute, and only one scan was conducted; therefore the result is very noisy, and there is a much higher degree of error with the results. Data fitting indicated coordination of 3.2(2) Cl, at bond lengths of 2.19(1) Å. These values are similar to those of CuCl in Ethaline, suggesting that the Cu^I initially present in the material is not oxidised during the electrodisolution process, counter to what is observed for Cu₂S. XANES data also agreed with the proposed Cu^I oxidation state.

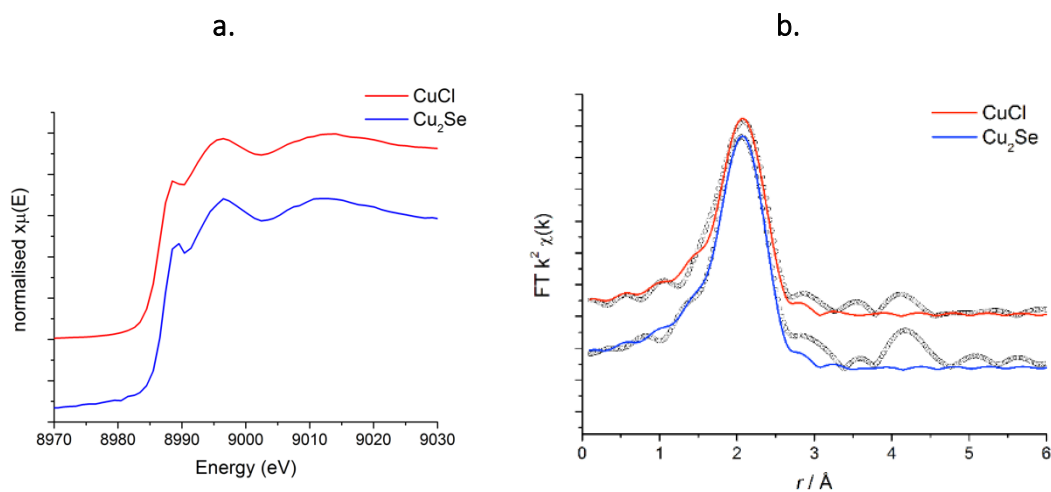


Figure 3.26: **a.** XANES and **b.** Fourier transforms of solutions of CuCl (red) and Cu₂Se (blue) in Ethaline. Cu₂Se was electrochemically dissolved in Ethaline for 24 hours at 1.5 V, with IrO₂ coated Ti electrodes, whereas CuCl plots were obtained from chemical dissolution.. CuData are circles, fits are lines.

As for the Cu₂Te solution, there was also a change of colour between the sample preparation and arrival of the sample at the synchrotron. The green colour shown in Figure 3.22 changed to blue suggesting a slow ligand exchange between Cl⁻ and H₂O. In this case, the EXAFS data indicated that the Cu ions coordinated to lighter atoms than Cl⁻ such as O⁻. This could potentially be from H₂O from atmospheric moisture, OH⁻ from electrolysis of water in the Ethaline or another oxygen ligand from the decomposition of the Ethaline. An O-donor fitted in this case with 3.9 Cu-O paths with lengths 1.948 Å. Earlier it was mentioned that tellurate and tellurite species were also present in solution. Therefore, there is a possibility that the O from these species has coordinated with the Cu while remaining associated with the Te. It is not possible to say that TeO₃ has

coordinated in whole to the Cu because an extra peak would have to be present in the Fourier Transform.

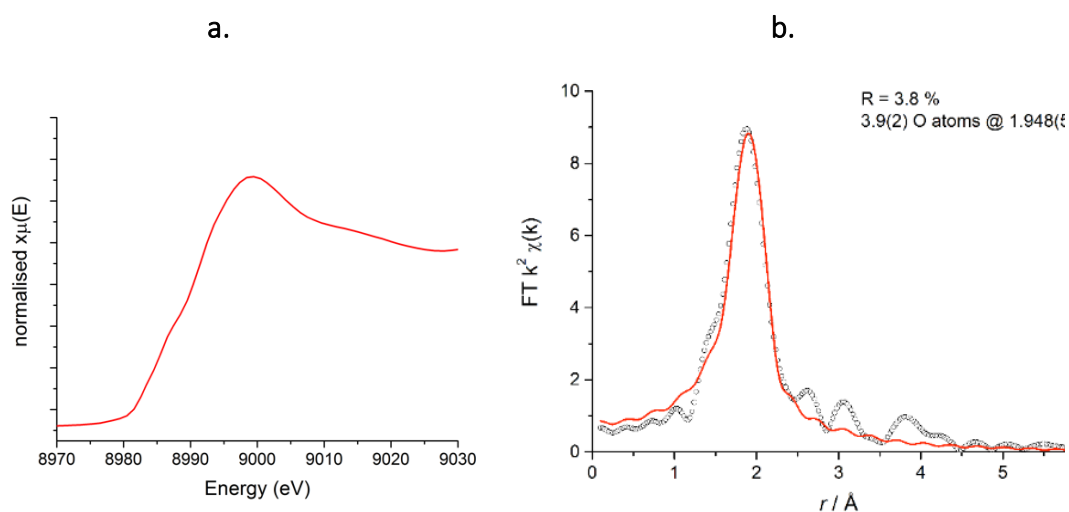


Figure 3.27: *a.* XANES and *b.* Fourier transforms (right) of solution of Cu_2Te electrochemically dissolved in Ethaline at 1.5 V for 24 hours using IrO_2 coated Ti electrodes.. Data are circles, fits are lines.

Table 3.5: EXAFS fit parameters for solutions of copper salts in Ethaline and electrochemical dissolution of copper chalcogenides (1.5 V, 24 hours) in Ethaline.

Solute	Coordinating atom/group	Number of atoms, N	Distance from Cu, $r/\text{Å}$	Debye-Waller factor, a (Å^2)	Fit index, $R1/\%$
CuCl_2 *	Cl	3.7(2)	2.252(5)	0.008(1)	4.48 %
CuCl *	Cl	2.4(2)	2.190(9)	0.016(3)	8.08 %
CuS	Cl	4.4(2)	2.248(4)	0.012(1)	2.74 %
Cu_2S	Cl	4.3(4)	2.239(7)	0.010(2)	5.87 %
Cu_2Se [§]	Cl	3.2(3)	2.19(1)	0.020(4)	9.60 %
Cu_2Te	O	3.9(2)	1.948(5)	0.008(1)	3.77 %

* Data already presented in reference ⁵³

[§] Data from a single scan

Returning to the bulk electrolysis reactions, a single cell as described in section 2.4 was used to recover metal ions on a nickel plate. In all cases shown in Figure 3.22, nearly pure Cu was obtained in every case. The reason for the varying colours in each plate is just due to the crystallite type and size, generally the small crystals lead to much shinier and brighter copper deposits. As well as this, it can be seen visually that the darker coloured plates generally contain a small amount of O as well, which is also likely to affect the colour. As an aside, it has been shown by Al-Murshedi that it is possible to improve copper deposits by increasing the water content in the Ethaline.³¹ However in the case of these experiments it is only necessary to recover metals as pure as possible with the lowest space time yield possible to improve on the efficiency of any current processes. The difficulty then comes when the mineral that is being electrolysed is more complex, for example in the case of chalcopyrite (CuFeS_2). The presence of another metal, in this case iron, makes it more difficult to obtain pure copper quickly and easily, this has also been investigated and the results are presented in chapter 5.

3.6 Conclusion

In this section, an efficient, effective and reliable novel technique for studying mineral electrochemistry was introduced. Paint casting provides a method with simple sample preparation that can be applied to a wide variety of materials including natural minerals. The premise behind the development of this technique was not to replace current analytical processes. Instead it is to work in combination with other techniques as an initial analysis on unknown samples to obtain very basic information on the mineral, before continuing with more laborious and generally more expensive techniques such as XRD, XRF and EDAX.

In this chapter, paint casting has been characterised and shown to be semi-quantitative, enabling the determination of levels of electrolyse-able material in a mineral sample. The quantification of paint casting has been achieved by altering the mass of material that is applied to the electrode surface and measuring the corresponding charge of the CV and also by adding varying proportions of alumina to the powdered mineral. The limits of the technique have also been tested and it was determined that for each sample, there is an optimum and maximum amount of material that can be applied to the electrode surface.

Further analysis of paint casting involved altering the temperature, scan rate and addition of water and evaluating their effect, this showed that the voltammetric response was what would be expected for a Faradaic process. It was determined in these experiments that in order to obtain comparable results relatively slow scan rates were required (c.a. 5 mVs^{-1}), the absence of water conducted at room temperature gave the optimal results but the addition of up to 10 wt% water and slightly elevated temperatures were not overly detrimental to the process.

The other 2 main aims of this chapter were to understand the speciation in Ethaline of the chalcogens after they have been electrochemically dissolved in Ethaline along with achieving electrochemical separation of the copper and associated chalcogen (S/Se/Te). The electrochemistry of a variety of compounds was studied using this paint casting method; S, Se and Te powder that have been either difficult to study in the past or just not really attempted all provided good CV's with clear reduction and oxidation peaks. The electrochemistry of the Cu chalcogenides was studied namely, CuS, Cu₂S, CuSe, Cu₂Se and Cu₂Te. The voltammograms for all of these compounds was presented in this chapter and again showed clear oxidation and reduction peaks that were combinations of copper peaks and chalcogen peaks. It was shown that the redox properties are being controlled by the chalcogenide and demonstrated when it comes to dissolving the compounds electrochemically, and they all produce different coloured solutions. UV-Vis and EXAFS analysis revealed that the different chalcogenides resulted in different Cu speciation in the Ethaline, and the speciation was not controlled by the oxidation state of the Cu in the compound. It was also shown in this chapter that it is possible to obtain reasonably pure Cu by the electrooxidation followed by electrowinning from any of the Cu compounds investigated in this work.

3.7 References

1. Schlesinger, M. E., Kind, M. J., Sole, K. C., Davenport, W. G., (2011) *Extractive Metallurgy of Copper*, 5th Ed., Elsevier, Netherlands.
2. US Geological Survey, (2016) *Minerals Yearbook: Recycling Metals*. (Available: <https://www.usgs.gov/centers/nmic/recycling-statistics-and-information>) (Accessed: 17/09/18)
3. US Geological Survey, (2018) *Mineral Commodity Summary* (Available: <https://www.usgs.gov/centers/nmic/copper-statistics-and-information>) (Accessed: 17/09/18)
4. Da Silva, O., (2019) *Top Copper Production by Country*, *Copper Investing News*, (Available: <https://investingnews.com/daily/resource-investing/base-metals-investing/copper-investing/copper-production-country/>) (Accessed 13/06/2019)
5. Marsden, J.O., (2008), *Energy Efficiency and Copper Hydrometallurgy*, **PowerPoint**, (Available: https://www.researchgate.net/publication/265156153_Energy_Efficiency_Copper_Hydrometallurgy) (Accessed: 18-09-18)
6. U.S. Department of Energy (2002) Chapter 5: Copper, Energy and Environmental Profile of the U.S. Mining Industry. (Available: <https://www.energy.gov/eere/amo/downloads/itp-mining-energy-and-environmental-profile-us-mining-industry-december-2002>) (Accessed: 28/07/19)
7. Habashi, F., (2007) *Copper Metallurgy at the Crossroads*, *J. Mining and Metallurgy*, **43**, 1-19
8. <https://copperalliance.org.uk/knowledge-base/education/education-resources/copper-mining-extraction-sulfide-ores/> (Accessed: 18-09-18)
9. <https://www.icsg.org/index.php/component/jdownloads/finish/165/871>
10. Watling, H. R., (2013) *Chalcopyrite Hydrometallurgy at Atmospheric Pressure: 1. Review of Acidic Sulfate, Sulfate-Chloride and Sulfate-Nitrate Process Options*, *Hydromet.*, **140**, 163-180

11. Smellie, I. A., Forgan, R. S., Brodie, C., Gavine, J. S., Harris, L., Houston, D., Hoyland, A. D., McCaughan, R. P., Miller, A. J., Wilson, L., Woodhall, F. M., (2016) Solvent Extraction of Copper: An Extractive Metallurgy Exercise for Undergraduate Teaching Laboratories, *J. Chem. Educ.*, **93**, 362-367
12. Wilson, A. M., Bailey, P. J., Tasker, P. A., Turkington, J. R., Grant, R. A., Love, J. B., (2014) Solvent Extraction: The Coordination Chemistry Behind Extractive Metallurgy, *Chem. Soc. Rev.*, **43**, 123-134.
13. Falagan, C., Grail, B. M., Johnson, D. B., (2017) New Approaches for Extracting and Recovering Metals from Mine Tailings, *Minerals Engineering*, **106**, 71-78
14. Lutandula, M. S., Maloba, B., (2013) Recovery of Cobalt and Copper Through Reprocessing of Tailings from Flotation of Oxidised Ores, *J. Environ. Chem. Eng.*, **1**, 1085-1090
15. Kondrat'eva, T. F., Pivovarova, T. A., Bulaev, A. G., Melamud, V. S., Muravyov, M. I., Usoltsev, A. V., Vasil'ev, E. A., (2012) Percolation Bioleaching of Copper and Zinc and Gold Recovery from Flotation Tailings of the Sulfide Complex Ores of the Ural Region, Russia, *Hydromet.*, **111-112**, 82-86
16. Videla, A. R., Morales, R., Saint-Jea, T., Gaete, L., Vargas, Y., Miller, J. D., (2016) Ultrasound Treatment on Tailings to Enhance Copper Flotation Recover, *Minerals Engineering*, **99**, 89-95
17. Gomez, F., Guzman, J. I., Tilton, J. E., (2007) Copper Recycling and Scrap Availability, *Resources Policy*, **32**, 183-190
18. Schlesinger, M.E., King, M. J., Sole, K. C., Davenport, W. G., (2011), Collection and Processing of Recycled Copper, *Extractive Metallurgy of Copper*, 5th Ed., 373-387
19. Abbott, A. P., Bevan, F., Baeuerle, M., Harris, R. C., Jenkin, G. R. T., (2017) Paint Casting: A Facile Method of Studying Mineral Electrochemistry, *Electrochem. Comm.*, **76**, 20-23
20. Grygar, T., Marken, F., Schroder, U., Scholz, F., (2002) Electrochemical Analysis of Solids. A Review, *Collect. Czech. Chem. Comm.*, **27**, 163-208
21. Al-Bassam, A. Z. M. H., (2018) PhD Thesis: University of Leicester, Mineral Processing Using Deep Eutectic Solvents.

22. Doyle, F. M., Kelsall, G. H., Woods, R., (2006) Electrochemistry in Mineral and Metal Processing, *The Electrochemical Society*, **2**.
23. Nunez, M., (2005) Progress in Electrochemistry Research, 1st Ed., Nova Science Publishers, USA.
24. Liao, Y. S., Chen, P. Y., Sun, I. W., (2016) Electrochemical Study and Recovery of Pb using 1:2 Choline Chloride/ Urea Deep Eutectic Solvent: A Variety of Pb Species PbSO₄, PbO₂, and PbO Exhibits the Analogous Thermodynamic Behaviour, *Electrochim. Acta.*, **214**, 265-275.
25. Gardner, J. R., Woods, R., (1979) A Study of the Surface Oxidation of Galena using Cyclic Voltammetry, *J. Electroanal. Chem.*, **100**, 447-459.
26. Manan, N. S. A. Aldous, L., Alias, Y., Murray, P., Yellowless, L. J., Laguna, M. C., Hardacre, C., (2011) Electrochemistry of Sulfur and Polysulfides in Ionic Liquids, *J. Phys. Chem. B*. **115**, 13873-13879.
27. Cisneros-González, I., Oropeza-Guzmán, M. T., González, I., (1999) Cyclic Voltammetry Applied to the Characterisation of Galena, *Hydromet.* **53**, 133-144.
28. Cisneros-González, I., Oropeza-Guzmán, M. T., González, I., (2000) An Electrochemical Study of Galena Concentrate in Perchlorate Medium at pH 2.0: The Influence of Chloride Ions, *Electrochim. Acta.*, **45**, 2729-2741.
29. Abbott, A. P., Al-Bassam, A. Z. M., Goddard, A., Harris, R. C., Jenkin, G. T. J., Nisbet, F., Wieland, M., (2017) Dissolution of Pyrite and Other Fe-S-As Minerals using Deep Eutectic Solvents, *Green Chem.*, **19**, 2225-2233
30. Palin, E., (2019) PhD Thesis: University of Leicester, An In-situ Study of Buried Metal Interfaces using Electrochemical and Neutron Scattering Techniques.
31. Al-Murshedi, A. Y. M., (2018) PhD Thesis: Deep Eutectic Solvent- Water Mixtures, University of Leicester
32. Rieger, P. H., (1994) Electrochemistry, 2nd Ed., Chapman and Hall, USA.
33. Sawyer, D. T., Sobkowiak, A., Roberts Jr., J. L., (1995) Electrochemistry for Chemists, 2nd Ed., Wiley and Sons Inc., Canada.
34. Azaga, R. M. M., (2018) PhD Thesis: University of Leicester, Surfactant Aggregation in DESs.

35. Anthony, J. W., Bideaux, R. A., Bladh, K. W., Nichols, M. C., Handbook of Mineralogy, Mineralogical Society of America, Chantilly, Available: <http://www.handbookofmineralogy.org> (Accessed: 30-08-18)
36. <https://geology.com/minerals/mohs-hardness-scale.shtml> (Accessed: 04-09-18)
37. <http://mineral.galleries.com/minerals/sulfides> (Accessed: 30-08-18)
38. Conejeros, S., Moreira, I. P. R., Canadell, E., (2014) Nature of Holes, Oxidation States and Hypervalency in Covellite (CuS), *Inorg. Chem.* **53**, 12402-12406
39. Vaughan, D. J., Craig, J. R., (1978) Mineral Chemistry of Metal Sulfides, 1st Ed., Cambridge University Press, UK.
40. Niu, Y., Sun, F., Xu, Y., Cong, Z., Wang, E., (2014) Applications of Electrochemical Techniques in Mineral Analysis, *Talanta*, **127**, 211-218
41. Beverskog, B., Pettersson, S. O., (2002) Pourbaix Diagrams for Copper in 5M Chloride Solution, *SKI Report*, **2**, 1-31.
42. Golgovici, F., Visan, T., (2012) Electrochemical Deposition of BiTe Films from Choline Chloride-Malonic Acid Mixture as Ionic Liquid, *Chalcogenide Lett*, **9**, 427-434.
43. Bougouma, M., Elewyck, A. V., Steichen, M., Buess-Herman, C., Doneux, T., (2013) Selenium Electrochemistry in Choline Chloride-Urea Deep Eutectic Electrolyte, *J. Solid State Electrochem.*, **17**, 527-536
44. Saji, V., Lee, C-W., (2013) Selenium Electrochemistry, *RSC Advances*, **3**, 10058-10077
45. Bouroushian, M., (2010) Electrochemistry of Metal Chalcogenides, 1st Ed. Springer, Switzerland
46. Liftman, Y., Albeck, M., Goldschmidt, J.M. E., Yarnitsky, C., (1984) The Electrochemistry of Tellurium in Methylene Chloride, *Electrochim. Acta*, **29**, 1673-1678.
47. Golgovici, F., Catrangiu, A.S., Stoian, A. B., Anicai, L., Visan, T., (2016) Preparation of Copper Telluride Films by Co-Reduction of Cu(I) and Te(IV) Ions in Choline Chloride: Ethylene Glycol Ionic Liquid, *J. Electronic Materials*, **45**, 3629-3639.
48. Carbonelle, P., Lamberts, L., (1992) Electrochemical Study of the Copper-Selenium System using Carbon Paste Electrode, *Electrochimica Acta.*, **37**, 1321-1325

49. Valderrama, R. C., Sebastian, P. J., Miranda-Hernandez, M., Enriquez, J. P., Gamboa, S. A., (2004) Studies on the Electrochemical Stability of CIGS in H₂SO₄, *J. Photochemistry and Photobiology A: Chemistry*, **168**, 75-80
50. Gustafsson, A. M. K., Bjorefors, F., Steenari, B. M., Ekberg, C., (2015) Investigation of an Electrochemical Method for Separation of Copper, Indium and Gallium from Pretreated CIGS Solar Cell Waste Materials, *The Scientific World Journal*, **2015**, 1-11
51. Chang, T. W., Su, Y. H., Lee, W. H., (2014) Improvement on Conversion Efficiency of CIGS Thin Film Solar Cell Using Electrochemical Depleting, *J. Electrochem. Soc.*, **161**, 167-172
52. Yu, P., Cardona, M., (2010) Fundamentals of Semiconductors, 4th Ed., Springer, Switserland.
53. Hartley, J. M., Ip, C. M., Forrest, G. C. H., Singh, K., Gurman, S. J., Ryder, K. S., Abbott, A. P., Frisch, G., (2014) EXAFS Study into the Speciation of Metal Salts Dissolved in Ionic Liquids and Deep Eutectic Solvents, *Inorg. Chem.*, **53**, 6280-6288

CHAPTER 4: ELECTROCHEMISTRY OF TRANSITION METAL CHALCOGENIDES

Table of Contents

4.1 Introduction	116
4.1.2 <i>Transition metal chalcogenides</i>	116
4.1.3 <i>Naturally occurring transition metal chalcogenides</i>	117
4.1.4 <i>Uses of transition metal chalcogenides</i>	119
4.1.5 <i>Aims</i>	122
4.2 Paint casting.....	123
4.2.1 <i>Zinc chalcogenides</i>	124
4.2.2 <i>Silver chalcogenides</i>	131
4.2.3 <i>Cadmium chalcogenides</i>	134
4.2.4 <i>Electrochemical rate comparison</i>	137
4.3 Speciation in solution	139
4.3.1 <i>Electrochemical dissolution</i>	139
4.3.2 <i>Rate of dissolution</i>	141
4.3.3 <i>Chalcogen speciation analysis</i>	143
4.3.4 <i>Recovery/ extraction</i>	148
4.4 Conclusions	149
4.5 References	151

4.1 Introduction

4.1.1 Chalcogens and chalcogenides

The chalcogens, S, Se and Te and their corresponding chalcogenide complexes all differ significantly from O and the oxide compounds. The chalcogens are much larger and heavier than O and they all exhibit much lower electronegativities, meaning their bonds with transition metals are mostly covalent. This covalency occurs as a result of the strong mixing of *s* - and *p* - block chalcogen valence orbitals and *s* and *p* outer orbitals of the transition metal.

A wide variety of different structures and stoichiometries are found with the compounds of the chalcogenides and there are structures present with some chalcogens that are simply not possible with others. This is most notable with compounds containing Te, as it has greater metallic character than the other chalcogenides, with larger and more diffuse orbitals, resulting in different behaviour to compounds containing S, for example. As is generally the case in inorganic chemistry, the size of each atom, the degree of metallic character of the chalcogen, and the available valence electrons all affect the structure of the compound.¹

4.1.2 Transition metal chalcogenides

Most transition metals react with chalcogens to form dichalcogenides. Generally, metals residing in groups 4-7 of the periodic table (other than Mn) form so-called “layered structures” of MX_2 type compounds.¹ These layered structures consist of sheets of X-M-X layers sandwiched on top of each other, separated by repulsive van der Waals forces between the chalcogen atoms. This layered structure makes up about 60 % of MX_2 compounds, with the non-layered structure only being present for metals in group 8 and above in the periodic table. Instead these compounds are composed of infinite 3D networks of metal atoms and X_2 units. Structures like pyrite and marcasite are included in this description.

The layered structures can show a wide range of characteristic electrical properties, ranging all the way from completely insulating compounds, such as HfS_2 , through to fully

metallic compounds like VSe_2 , with semiconductors (MoS_2) and semi metals (WTe_2) in between.¹ They also provide varying chemical, and more importantly, enhanced electrical properties to other more traditional bulk semi-conductors, mainly as a result of their layered structure.^{2,3} This variety of structures and properties also leads to their use in a variety of applications, which are discussed further in section 4.1.4.

4.1.3 Naturally occurring transition metal chalcogenides

Of the transition metal chalcogenides discussed in this chapter, there are several that exist as natural minerals as well. These include acanthite (Ag_2S), naumannite (Ag_2Se), hessite (Ag_2Te), sphalerite (ZnS), stilleite ($ZnSe$), hawleyite/greenockite (CdS) and cadmoselite ($CdSe$). Among these, there is a wide range of different abundancies, where some are the major source of their metal (e.g. sphalerite) and others are relatively rare (e.g. hawleyite).⁴

Ag_2S can exist in two forms, the most common of which is acanthite. Acanthite has a monoclinic structure containing linear chains of S-Ag-S-Ag which hold half of the Ag atoms. The other half bind the chains together and are in a distorted tetrahedral arrangement. Acanthite occurs in relatively low temperature hydrothermal sulfide veins.⁴ At higher temperatures (above 173 °C) argentite can form; this is generally not present in natural material due to its high temperature formation. It has a cubic structure where the S atoms are in a body centred cubic lattice with the Ag atoms distributed throughout.⁵ As for tellurides and selenides of Ag, naumannite (Ag_2Se) is an orthorhombic structure that is found in sulfur-deficient hydrothermal veins and is often associated with other selenide minerals.⁴ Hessite (Ag_2Te) is a lead-grey monoclinic telluride that often occurs in medium to low temperature hydrothermal veins. It is also found occasionally in some massive pyrite deposits, but in significantly small quantities.

As for the Zn minerals, sphalerite (ZnS) is the most important Zn ore, which the majority of Zn metal is extracted from.⁶ It has a cubic structure and exhibits a wide variety of different colours, from colourless to dark brown/grey as well as yellow, red and green. Completely pure sphalerite, which is incredibly rare and almost never found naturally is entirely colourless. The colour is dependent on the levels of Fe that are also present in

sphalerite, whereby low Fe levels result in a yellow colour and higher Fe sphalerites can exhibit an opaque black colour. Sphalerite occurs under a wide temperature range hydrothermal conditions in a variety of sedimentary deposits. Another Zn chalcogenide mineral that can also be found naturally is ZnSe, it is also in the sphalerite mineral group, in the sense of it being in that structural family and is often found intermixed with other selenides.

Finally, the cadmium chalcogenide compounds that are investigated in this chapter have naturally occurring mineral equivalents, such as cadmoselite (CdSe) and greenockite and hawleyite (CdS). The latter two are dimorphs of each other, both occurring as coatings on sphalerite. Greenockite has a hexagonal structure and exhibits many varying shades of yellow or orange and occasionally deep red, however hawleyite is cubic and has a bright yellow colour. Cadmoselite occurs in sedimentary strata under relatively alkaline secondary conditions, it is black/grey mineral with a hexagonal structure.⁴

Of all the minerals mentioned in this section, sphalerite is the one that is found at high enough abundancies to warrant processing and extracting the zinc. Sphalerite is most commonly processed by smelting in order to oxidise the ZnS via Equation 4.1.



The ZnO can then be pyrometallurgically treated further in order to obtain molten Zn. It is also possible to extract Zn through electrolysis from ZnO however this is less common compared to the pyrometallurgy processes. Acenthite can also be processed along with other common Ag containing ores in order to obtain Ag. Ag can be obtained either by pyrometallurgy or hydrometallurgy but can also be extracted during the electrorefining stages of Cu recovery. Cd is most commonly extracted as a by-product of processing Zn/Fe/Cu ores as pure Cd containing ores are rare.⁵

This chapter is focussed on the initial electrochemical analysis of different transition metal chalcogenides in Ethaline and what controls their dissolution rate. Synthetic compounds of the above minerals are generally used instead of natural material. This

ensures a known, high purity with consistent particle size, enabling a clear identification of redox peaks, without the complication of impurities or other materials.

4.1.4 Uses of transition metal chalcogenides

Transition metal chalcogenides have shown a rise in popularity in recent years due to their interesting properties that can be applied to uses in photovoltaic (PV) devices, including photo absorber layers, buffer materials and anodes. Due to their key properties, most notably their suitably small band gaps, it is estimated that around 15,000 different transition metal chalcogenide semiconductors could be suitable for PV devices in some shape or form. The main advantage of using transition metal chalcogenide based photovoltaic cells over more traditional solar cell materials such as organic photovoltaics or Pb perovskites is the enhanced chemical stability. Both are highly sensitive to oxygen, causing bleaching of the organic photovoltaics and destabilising the perovskites.² CdTe solar cells⁷ are slowly becoming a key competitor, although the market is still very much dominated by silicon-based cells, it is estimated that CdTe now accounts for around 7 %. It has been suggested that the use of CdTe can provide the lowest cost per watt whilst providing the shortest energy pay-back time. On top of this, they are shown to have the lowest impact in terms of a carbon footprint during their production. There is still the downside however, of them only achieving a maximum 22 % efficiency in the lab, compared to the industry accepted minimum of 30 %. The most current design of a CdTe solar cell is shown schematically in Figure 4.1.²

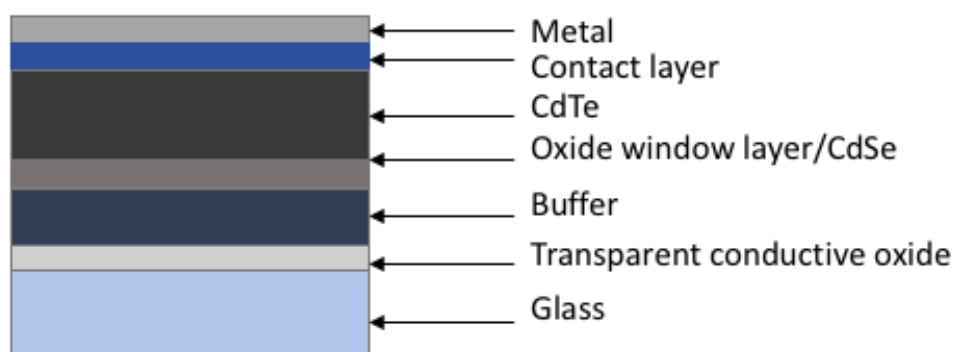


Figure 4.1: A schematic of a 'state of the art' CdTe solar cell currently being investigated.

The relatively thin (1-8 μm) CdTe layer is quite often deposited by close space sublimation, but it can also be deposited electrochemically, by sputtering or by thermal evaporation. These techniques require some source of both Cd and Te in order to deposit these thin films.

The window layer, shown in Figure 4.1 is more traditionally a layer of CdS however, this has been shown to cause problems with respect to a loss in performance of optical absorption at particular wave lengths ($< 520 \text{ nm}$).² Making the CdS layer as thin as possible has previously been trialled and now it is suggested that the addition of CdSe in conjunction or instead of the CdS. The CdSe will maintain a suitable band gap while still enabling a structure that can intermix with CdTe, which is not possible with other potential window materials like ZnO or SnO_2 .²

Ultimately, the interest in these solar cells, is from a perspective of recovering the elements from the panels at the end of their life. It is hoped that this study will show the viability of recycling the solar panels by an electrochemical leaching technique to recover the elements in quantities and purities high enough to reuse in new solar panels.

The Zn chalcogenides have also been considered for their potential in photoelectrochemical applications, however to a much lower degree compared to the Cd chalcogenides. This is mainly as a result of their bigger band gaps. They are however used in other applications for example ZnS is industrially important phosphor used in TV and X-ray fluorescent screens. ZnS fluoresces in a variety of colours after stimulation by cathode rays, X-rays and radioactivity. The colours can be extended by replacing Zn with Cd and/or S with Se. The colours can be activated by doping with other metals, e.g doping with Ag gives a blue luminescence and with Cu to give green. ZnSe is also used with ZnS as a phosphor and is commonly used in the manufacturing of blue light photoelectronic diodes.¹

The Ag chalcogenides present the most metallic properties of all the compounds in this chapter and this is indicated by the very small band gap shown in Table 4.1. Interestingly,

there are few current applications that make use of any of the Ag chalcogenides other than the sulfide being used as a photosensitizer in photography.

The potential uses and applications of transition metal chalcogenides all rely on the specific properties that are provided by these compounds. For example, band gaps are an important parameter when it comes to considering the suitability of transition metal chalcogenide semiconductors for electronic applications. The basic concept of band gaps and the effect they have on the dissolution behaviour of minerals and other powdered materials has already been discussed in Chapter 3. However, the band gap structure can actually be explained by a slightly more complex mechanism, involving a direct or indirect band gap. These are demonstrated in Figure 4.2

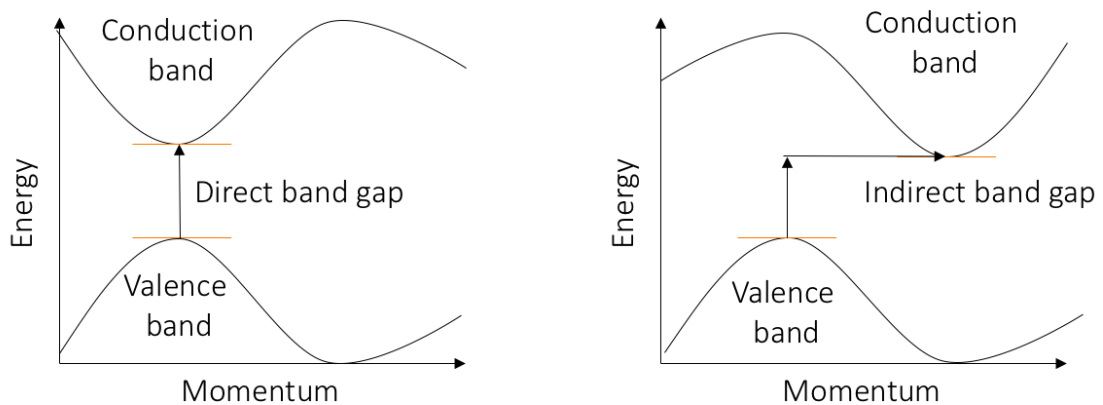


Figure 4.2: Energy vs. momentum plots demonstrating the difference between direct and indirect band gaps of semiconductors.⁸

CdTe, as well as GaAs and CuInSe₂, are examples of so-called “direct” semiconductors exhibiting the direct band gap structure, whereby the energy maximum and energy minimum in the valence and conductance band respectively have the same momentum. In an indirect band gap example (e.g. GaP), the energy maximum and minimum do not have the same momentum. This results in a situation whereby a photon cannot simply move directly from the valence band to the conductance band and instead needs to alter its momentum through the absorption of a phonon. The transition metal chalcogenides studied in this chapter generally have relatively low band gaps and are shown in Table 4.1. They are all the direct band gap unless stated otherwise.

Table 4.1: The band gaps (eV) for the 9 different transition metal chalcogenides studied in this chapter.

compound	Band gap/eV	compound	Band gap/eV	compound	Band gap/eV
CdS	2.42 ⁹	Ag ₂ S	1.0 ¹¹	ZnS	3.7 ¹³
CdSe	1.74 ¹	Ag ₂ Se	0.27 ¹	ZnSe	2.7 ¹⁴
CdTe	1.45 ¹⁰	Ag ₂ Te	0.2 ¹²	ZnTe	2.25 ¹⁵

The band gaps are typically smaller for the other chalcogenides compared to the oxides, and it can be seen from looking at the values in Table 4.1 that band gap decreases from the sulfide to telluride for each compound, due to a decrease in the electronegative character of the chalcogenide, and the metallic properties increase.¹⁶

4.1.5 Aims

This chapter will build upon the work conducted on the Cu chalcogenides in Chapter 3 and aims to determine what controls the dissolution of the different chalcogenide materials. The objective is to establish whether the electrochemical dissolution is dependent on the band gap, and hence the conductivity of the material. It is proposed that this could provide the groundwork for future investigations into the extraction of metals and Te/Se from these materials.

The main objectives for this chapter are:

1. To further examine the extent of the paint casting techniques, especially when it comes to analysing non-conductive or minimally conducting materials.
2. To understand the speciation of the transition metals and chalcogens after they have been electrochemically dissolved in Ethaline.
3. To determine what controls the rate of dissolution of the different transition metal chalcogenides.

4.2 Paint casting

This section will examine the electrochemistry of a selection of transition metal chalcogenides, specifically the sulfides, selenides and tellurides of Zn, Cd and Ag. These 3 metals are being considered due to their location in the periodic table with respect to Cu and the interest in making comparisons between them and the Cu chalcogenides that were discussed in Chapter 3. The other interesting comparison with these metals is that they have one stable oxidation state, so it is the chalcogenide which is mainly oxidatively active.

In the literature, the electrochemistry of all these different transition metal chalcogenides has been extensively studied.¹⁷⁻²³ The research is most commonly conducted in aqueous solutions for purposes such as electrodeposition of compounds for an easier, more cost-effective method of producing thin films compared to techniques such as chemical vapour deposition.¹⁷ The major benefits of using electrodeposition are that it can be done at room temperature as well as it being an easy method to produce an even layer across an uneven surface.¹⁷ There were a few studies conducted in ILs/DESSs that provide some interesting insight, most interesting were 2 studies looking at the electrochemistry of CdTe and ZnTe in choline chloride based DESSs, Reline and Ethaline respectively.^{10,15} The purpose of both these papers was to investigate the ability of electrodepositing CdTe/ZnTe as thin layers for use in solar cells. The benefits of using a DES over an aqueous solvent were three-fold: to improve low current efficiency from H₂ evolution, to reduce corrosion effects and to ideally prevent the deposition of elemental Te amongst the CdTe layer.^{10,15}

The following results are also discussed with respect to the Pourbaix diagrams for the compounds of interest. It must be noted that these diagrams are constructed from data in aqueous systems, as at the time of writing, diagrams in ILs or DESSs do not exist. The effect of chloride must be taken into account when using the diagrams, as it is known that the presence of a high chloride environment (4.5 M in Ethaline) will have some the effect of limiting the H₂O competing ligands and the speciation is highly likely to be

controlled by either the Cl from the anion or the glycol group from the hydrogen bond donor.

4.2.1 Zinc chalcogenides

This section begins by looking at Zn as it lies directly next to Cu in the periodic table and therefore has the same valence shell (Cu: $3d^{10} 4s^1$ and Zn: $3d^{10} 4s^2$). The compounds that form between the chalcogens and Zn generally involve the Zn having a +2 oxidation state in comparison to the Cu chalcogenides, where both 2+ and 1+ oxidation states are exhibited.

To begin with it is important to note that Zn oxidation and reduction lies outside the electrochemical window allowed for the particular electrode/electrolyte set up in the paint casting experiment. To demonstrate this the paint casting of $ZnCl_2$ is shown in Figure 4.3a and a solution of $ZnCl_2$ in Ethaline from the literature is shown in Figure 4.3b. Both voltammograms are in conducted in Ethaline on Pt electrodes however the solution CV is against a Ag wire reference electrode which shifts the potential more positive.

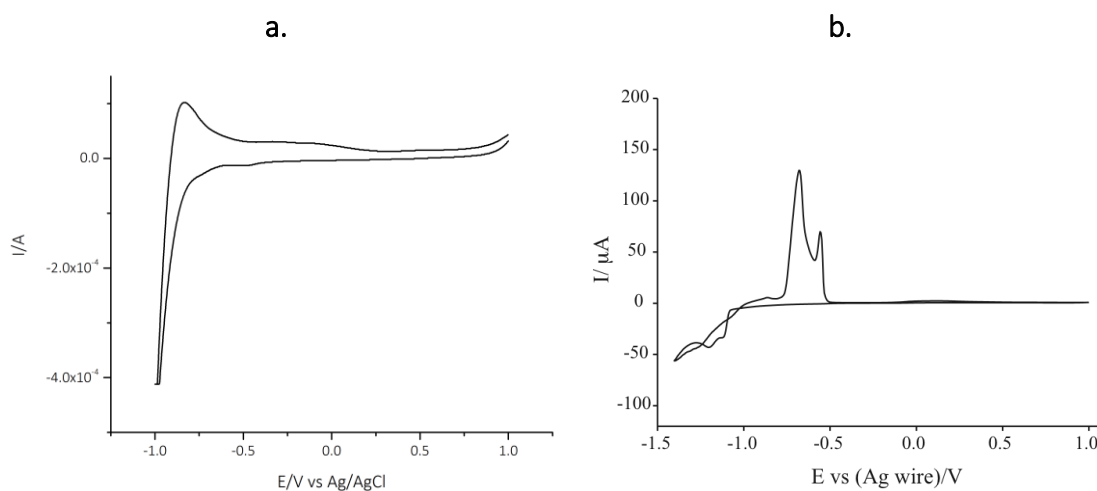


Figure 4.3: **a.** Paint cast cyclic voltammogram of $ZnCl_2$ in Ethaline using a 1 cm^2 Pt flag working and counter electrodes and an Ag/AgCl [0.1 M in Ethaline] reference electrode, scanned at 5 mVs^{-1} and **b.** Cyclic voltammogram of 0.3 M $ZnCl_2$ in Ethaline reported in the literature on a 0.5 mm Pt electrode and Ag wire reference.²⁴

The Pourbaix diagrams for the Zn chalcogenides are shown in Figure 4.4 and in general are similar across the 3 target chalcogenides (S, Se, and Te). In all 3 diagrams it can be seen that the metal with a 0 oxidation state dominates in the reductive region across the entire pH range, below -0.8 V for the sulfide and selenide, but at much lower voltages for the telluride (< -1.4 V). For the selenide and telluride there is a small region between 0 V and 0.6 V in more acidic environments where the chalcogen is dominant. As for the sulfide, this section, although still present in very acidic, slightly oxidising environments, is a very small window. The sulfate, tellurate and selenate and other oxygen rich chalcogen species dominate in the remaining oxidative part of the diagram. The Pourbaix diagrams are from 2 separate sources in the literature and although the ZnSe is the only one that demonstrates the presence of the H₂Se/HSe, it is likely the general similarities between all the diagrams that in the most reductive environments (< -1.0 V) there will also likely be H₂S and H₂Te gas produced in both the ZnS and ZnTe respectively.

Figure 4.4 also shows the corresponding paint casting CV's conducted on each Zn chalcogenide powder. The peaks are labelled A for anodic and C for cathodic as well as having the peak potentials in brackets for each peak. ZnS demonstrates a highly resistive CV with a low current which is due to the more insulating nature of the material.¹³ This is also supported in the band gap data in Table 4.1, it shows ZnS has the highest band gap of all the chalcogenides being studied (3.7 eV), therefore indicating it having a worse ability to conduct electrons. It is interesting, regardless of the low conductivity and larger band gap, that paint casting has still been possible and there are still peaks that are present.

A blank Ethaline CV, without the limits of the window included can exhibit peaks and therefore these peaks are not necessarily worth assigning. This result could almost provide a window of paint casting possibility and indicates that results of materials with a larger band gap may not be as reliable. It is shown by the CV results in Figure 4.4 that as the band gap decreases from ZnS-ZnSe-ZnTe the CV's become more resolved with less resistance. That reliability with achieving a better, more resolved CV increases with a decreasing band gap as shown to an extent with the CV's presented in Figures 4.4 a, b & c.

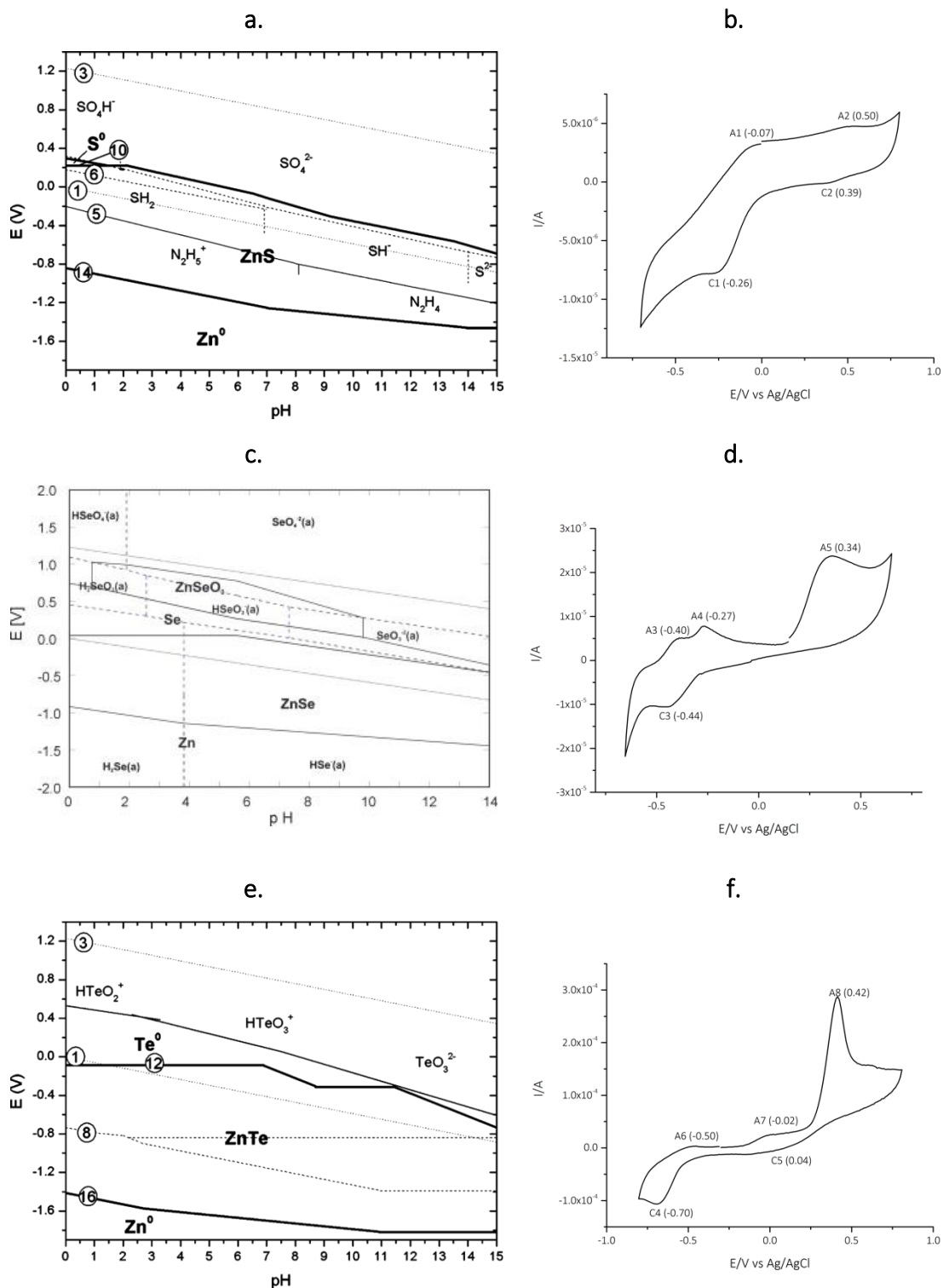


Figure 4.4: Pourbaix diagrams of **a.** ZnS^{25} **c.** ZnSe^{26} and **e.** ZnTe^{25} and paint casting CV's of **b.** ZnS powder, **d.** ZnSe powder **f.** ZnTe powder. All voltammograms conducted in Ethaline using a 1 cm^2 Pt flag working and counter electrodes and an Ag/AgCl [0.1 M in Ethaline] reference electrode, scanned at 5 mVs^{-1}

For ZnSe the CV is much less resistive compared to the ZnS (both shown in Figure 4.4) but still has a low current. This is mirrored in a decreased band gap from 3.7 eV to 2.7 eV. Of note was the strong and distinctive smell of H₂Se that is produced with using this powder, specifically during the CV. This was not the same for any of the other selenide CV's from the remainder of this chapter or from Chapter 3. The electrochemistry of ZnCl₂ has been investigated previously in Ethaline to reveal a very clear oxidation peak (split into two peaks at low scan rates) at around -0.4 V.²⁷ It is discussed in the paper that the occurrence of 2 stripping peaks suggests the presence of 2 separate Zn phases dissolving. This is possibly the cause of the oxidation peak A3 however this may also be as a result of the Se. Comparing the elemental Se paint cast CV shown in Figure 3.19 it can be seen that there is 1 strong redox couple at -0.39/ -0.56 V that could also relate to the A3/C3 in Figure 4.4. The oxidation peak A5 at 0.34 V does not correlate to the elemental Se or the ZnCl₂ results presented previously. This suggests that it could be the result of oxidising ZnSe to its constituent parts. This peak is also present in a study by Colletti et al. whereby a CV of a solution of ZnSO₄ using a Se electrode is carried out. The peak is not assigned in this paper however it is most likely to be due to the re-oxidation of after the Zn has deposited on the Se electrode surface.¹⁷

ZnTe exhibits a very strong oxidation peak (A8) which corresponds to the Te peak shown previously in Figure 3.19. This large peak is a characteristic peak that runs through all of the different telluride compounds examined in this chapter. The electrochemistry of ZnTe in Ethaline has been previously studied by Catrangiu et al., who used ZnCl₂ and TeO₂ dissolved in Ethaline to electrodeposit a thin layer of ZnTe.¹⁵ During their electrochemical analysis, a sharp oxidation peak was observed at around 0.6 V.¹⁵ This has been attributed to the stripping of a Te monolayer from the surface of the Pt electrode that was deposited in a reduction peak around -0.5 V which is also present in the CV in Figure 4.4 (C4). This is also supported by the fact that during the 1st scan, the characteristic Te peak (A8) was not observed and only occurred on subsequent scans.

A study investigating the possibility of electrodepositing thin films of ZnS, ZnSe and ZnTe analysed the CV's of all 3 compounds in aqueous solvents against an Ag/AgCl reference

electrode.¹⁷ A similar pattern in the appearance of the CV's was observed in this study to the voltammograms in Figure 4.4. The CV for ZnTe presented much clearer more resolved peaks compared to the ZnS which although did not show the same resistive character as the one presented in this chapter did show much less resolution in the peaks.¹⁷

The most common naturally occurring mineral of ZnS is sphalerite which is also one of the most common sulfide minerals. It is the most important ore of Zn, accounting for the majority of its extraction.⁶ Sphalerite is quite often found with large amounts of Fe impurities that contributes largely to the colours exhibited by the mineral. In the following work, 2 separate samples of sphalerite were examined, one labelled X22 was known to contain Fe called dark sphalerite. The other, labelled E411 was described as being an Fe-free sample, or light sphalerite. The EDX of the samples confirmed this with X22 showing an average analysis of Zn: 42.6, S: 54.6, Fe: 1.7 and Cu: 1.5 at %. The Fe free sample E411 showed Zn: 45.2 and S: 54.8. The XRD of each sample compared with the synthetic material used above is shown in Figure 4.5. The XRD pattern of sphalerite has been reported in the literature^{28,29} and supports the results obtained in the following patterns. The X22 sample has an extra reflect that does not appear in either of the other samples in Figure 4.5 or in the literature and is likely due to the effect of the additional Fe or Cu in the sample.

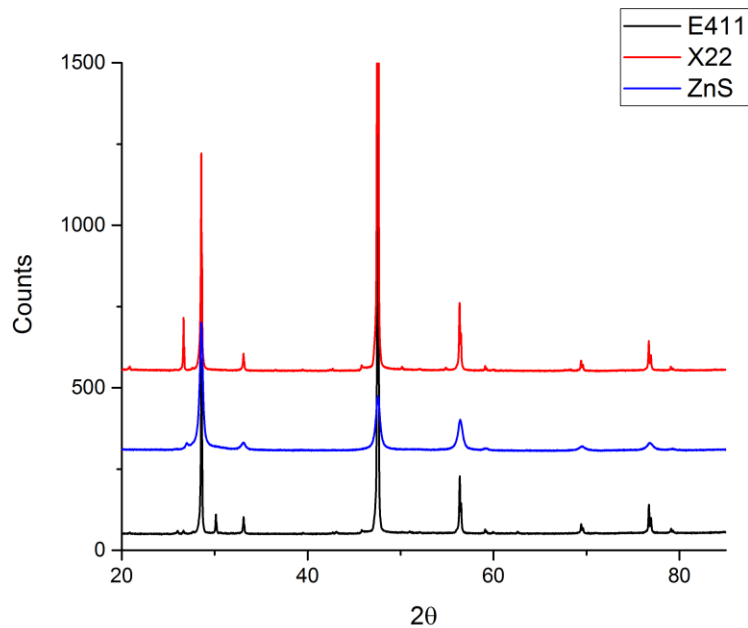


Figure 4.5: Powder XRD plots of the 2 natural sphalerite samples (E411 and X22) and synthetic ZnS.

The electrochemical behaviour of these samples was also analysed by the paint casting method and the results are shown in Figure 4.6. It can be seen how significantly these two samples differ, just with the small quantity of Fe and Cu present in the X22 sample, completely altering the redox couples and general shape of the CV. The CV for the Fe-free sample (Figure 4.6 b) is most similar to the pure ZnS, whereas the X22 sample (Figure 4.6 a) looks more similar to the CV of a Cu sulfide shown in Chapter 3, or the Fe sulfide presented by Al-Bassam.^{30,31} The peaks in Figure 4.6 a can be attributed to the same peaks as in a pyrite/chalcopyrite or other Cu sulfide material, whereby the redox couple A10/C8 is the oxidation and reduction of the metal species, this is either Cu or Fe as shown by Equation 4.2 and 4.3 or even an overlap of both redox couples.



The oxidation A9 and reduction C7 is likely linked to the sulfide species as before. Finally the small shoulder of reduction C6 is either associated with a Cu reduction or it is potentially linked to the ZnS, as it also appears as a similar peak in both the synthetic sample and the other natural sample in Figure 4.6b just at slightly shifted potentials.

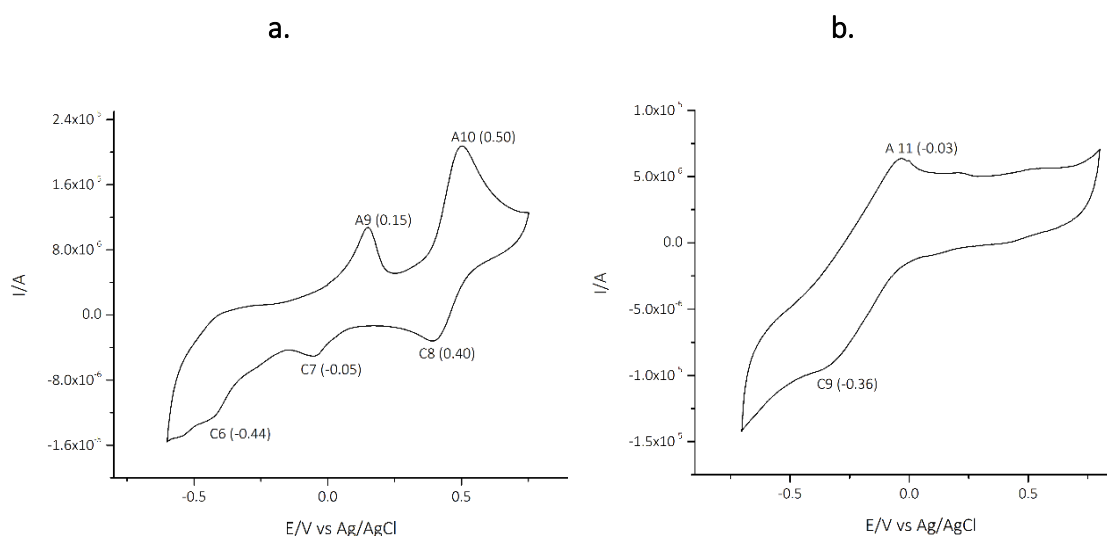
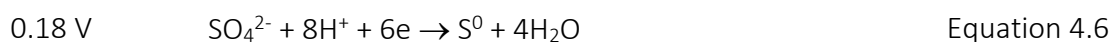


Figure 4.6: Paint casting cyclic voltammograms of sphalerite mineral (ZnS) **a.**X22 and **b.**E411. Both voltammograms were conducted in Ethaline using a 1 cm² Pt flag working and counter electrodes and an Ag/AgCl [0.1 M in Ethaline] reference electrode, scanned at 5 mVs⁻¹.

The electrochemistry of sphalerite has been studied previously.³² Due to its low conductivity, the method involved using carbon paste electrodes, with the addition of 30 % graphite in order to allow the material to conduct. It was suggested in the paper that the inclusion of graphite was acting as a galvanic couple enabling the easier oxidation and reduction of the sample. The authors present a CV of this sample in varying concentrations of H₂SO₄, and it is made up of 2 oxidation peaks at 0.02 V and 0.12 V and 2 reduction peaks at 0.18 V and -0.10 V.³² They have ascribed these peaks to the following equations:



Interestingly, in this paper the sample of sphalerite had a reasonably high quantity of Fe (8.08 %) as well as small amounts of other metal impurities (Pb and Cd).³² As shown

previously in Figure 4.6, the inclusion of even very small amounts of Fe and Cu make a large difference to the CV. Whereas, in the case of this paper there was no consideration of the effect of those additional metals when assigning the peaks. When comparing the results in Figure 4.6 to the paper, it is likely that the peak A11 is the oxidation of ZnS via the reaction shown Equation 4.4. Overall, the method described by Srinivasan is slightly more laborious but altogether necessary when working in an aqueous media.³² Paint casting can be shown to have comparable results with a quicker and easier method and without the requirements of adding a conductive material to the mineral, however, it does require the use of a viscous conductive solvent.

4.2.2 Silver chalcogenides

The Ag chalcogenides share chemical similarities to the corresponding Cu chalcogenides. The sulfide, selenide and telluride compounds of Ag are most common when Ag is in the +1 oxidation state, which is also common for Cu compounds. For these compounds, the Pourbaix diagrams were less well reported and it was not possible at the time of writing to find an Ag_2S and Ag_2Te diagram. The Ag_2Se Pourbaix diagram is presented in Figure 4.7. It appears to be very similar to the ZnSe diagram in the sense that the Ag_2Se compound is stable in the middle portion of the diagram between 1.0 V and -0.4 V across the majority of the pH range. The oxidative environment is dominated by elemental Ag as well as Ag_2O and a variety of oxidised Se ions including SeO_4^{2-} , SeO_3^{2-} and H_2SeO_3 . Similarly again to the ZnSe Pourbaix diagram, the reductive section of the diagram for Ag_2Se is dominated by H_2Se in an acidic environment ($< \text{pH } 4$) and HSe^- across the remaining pH range. Due to the similarities shown by previous Pourbaix diagrams for the Zn (Figure 4.4) and Cu (Chapter 3) chalcogenides, it is likely that the Ag chalcogenides will show a similar pattern, this is also supported in the close similarities of the CV's more so than the Zn CV's from previously.

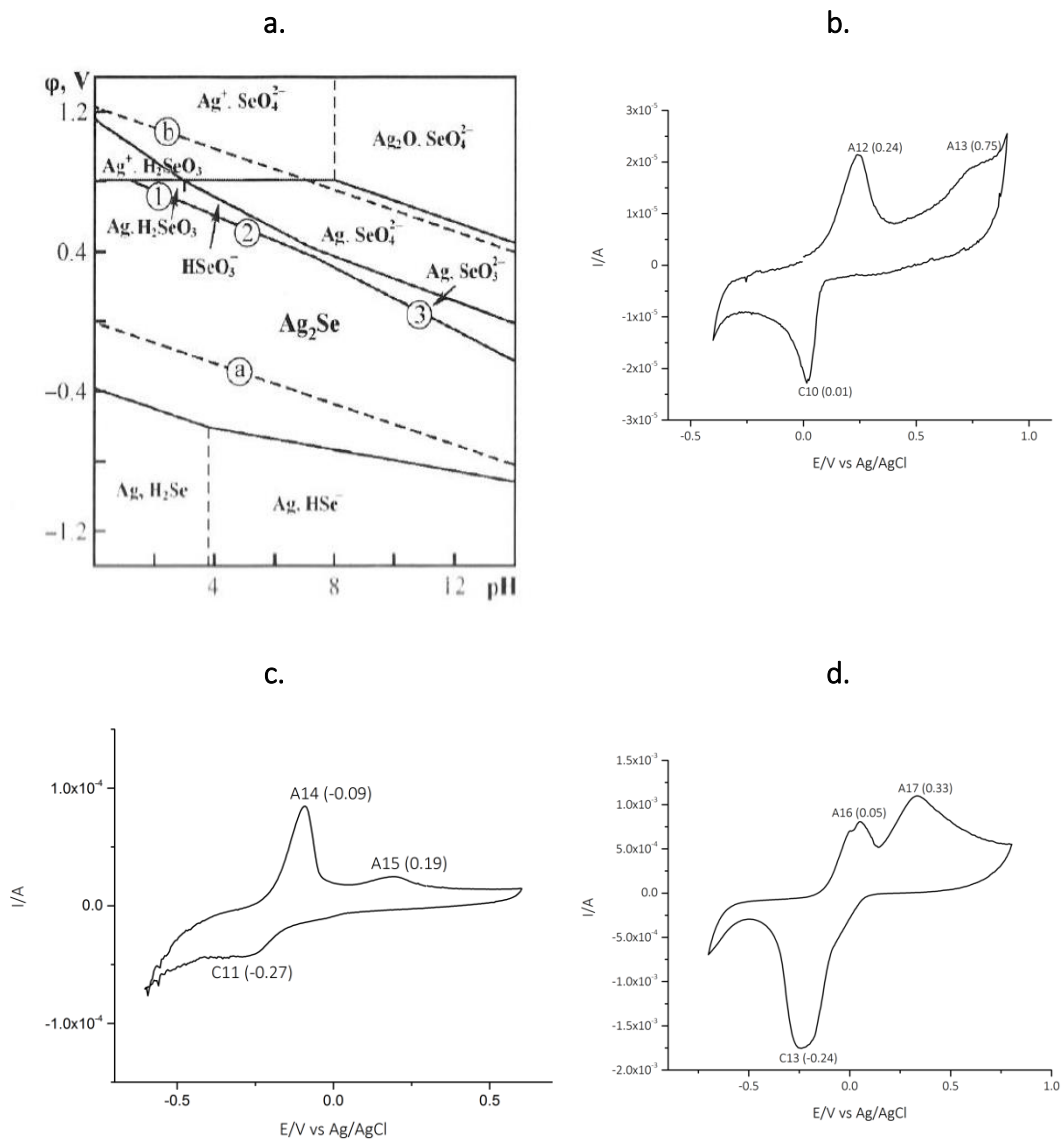


Figure 4.7: a. Pourbaix diagram of Ag_2Se , paint casting CV's of b. Ag_2Se powder, c. Ag_2Se powder d. Ag_2Te powder. All voltammograms were conducted in Ethaline using a 1 cm^2 Pt flag working and counter electrodes and an Ag/AgCl [0.1 M in Ethaline] reference electrode, scanned at 5 mVs^{-1}

In the case of the Ag chalcogenide CV's also shown in Figure 4.7, they are similar in some ways to the Cu chalcogenide CV's in Chapter 3. In each case the metal redox couple or couples are distinctive and present in each CV, in this case it is the $\text{Ag}^{I/0}$ that is clearly present in all 3 CV's shown in Figure 4.7. This is supported by the AgCl paint casted CV in Figure 4.8 a, which presents one very clear redox couple A18/ C14 that has also been shown in previous studies to be related to the $\text{Ag}^{I/0}$ in an Ethaline electrolyte.^{33,34} Comparing this paint casting CV with a solution-based CV presents a difference in peak

shape, with the peaks from paint casting being much broader. This is not the same scenario as with the CuCl_2 CV presented in Chapter 3, where the overall CV looked similar regardless of whether it was paint casted or a solution. This is likely to be due to the fact that the CuCl_2 dissolves almost instantly on contact with Ethaline and therefore it is more similar to conducting a solution CV rather than it actually electrochemically oxidising and reducing the solid material on the electrode. Importantly though, the CV's are still presenting the same peaks just different overall shapes.

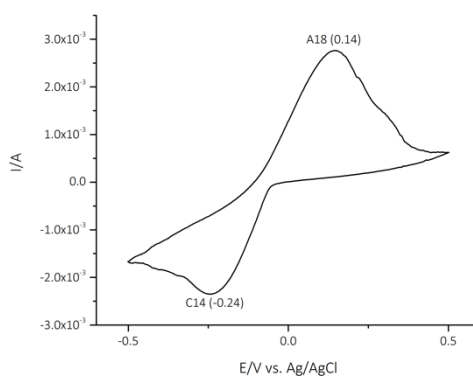


Figure 4.8: Paint casting CV of AgCl in Ethaline using a 1 cm^2 Pt flag working and counter electrodes and an Ag/AgCl [0.1 M in Ethaline] reference electrode, scanned at 5 mVs^{-1} .

In the case of Ag_2Se , this $\text{Ag}^{\text{I}/0}$ couple appears to have been shifted from between 0.1 V from the AgCl CV and +0.2 V from both the Ag_2Te and Ag_2S CV's. The signal for Ag reduction could come from the silver released during the oxidation of the telluride, a slight solubility of silver telluride in Ethaline or the direct electroreduction of silver telluride from the solid state. The direct electroreduction from the solid has previously been demonstrated for Cu from copper oxide.³⁵ Repeating the CVs in Figure 4.7 but scanning in a negative direction first resulted in the reduction peak attributed to $\text{Ag}^+ \rightarrow \text{Ag}^0$ which shows that direct Ag reduction is possible in this system.

These CV's differ from the Zn chalcogenides mainly because there are no clear Zn redox couples. This is likely due to the fact that in Ethaline, Zn deposition has been shown to occur at around -1.3 V ²⁷ and in the current system such a negative potential was not achievable due to solvent degradation. The characteristic Te stripping peak mentioned previously for the ZnTe CV is again present in the Ag_2Te CV (A17), at potential 0.33 V. For

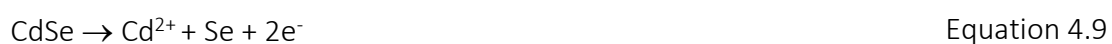
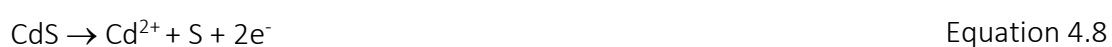
both Ag_2S and Ag_2Se the major couple is related to the redox couple $\text{Ag}^{I/0}$ with only a small couple A15/C12 for Ag_2S and an oxidation peak A13 for Ag_2Se . A similar peak at a slightly higher potential has been attributed to the $\text{Se}^{IV/0}$ couple in an investigation of the electrochemical behaviour of Ag_2Se nanotubes,¹⁸ so by inference A15/C12 could be similarly assigned. As for the small redox couple present in the Ag_2S CV, a similar peak has been previously ascribed to the formation and subsequent reduction of an Ag_2O film on the surface of the electrode.³⁶ However, Ag_2O has been shown previously to be soluble in Ethaline forming an $[\text{AgCl}_2]^-$ complex in solution,^{37,38} this explains why the couple is so small in the CV shown in Figure 4.7c as the Ag_2O is able to dissolve as it is formed.

The Ag_2S CV is very different to the ZnS voltammogram from Figure 4.4a and also the CdS CV in the next section, mainly in that the redox couples are better resolved, and the CV shows a smaller Ohmic distortion. This matches the trend in band gap and conductivity of the compounds and therefore the results follow the anticipated trends.

4.2.3 Cadmium chalcogenides

The final transition metal of interest in this chapter is Cd. The electron configuration of Cd is $[\text{Kr}]4d^{10} 5s^2$, which provides an interesting final comparison to Zn, as Ag was to Cu. The compounds that form with the chalcogens are again the same as with Zn whereby the metal is in the 2+ oxidation state. The Pourbaix diagrams for CdS , CdSe and CdTe are presented in Figure 4.8 and although at first glance the CdTe looks slightly more complex, they are largely the same as the previous Ag and Zn ones. The Cd-chalcogen complex dominates the same central window as the other compounds previously, with the oxidised metal species and an oxide species of the chalcogen appearing in the oxidative region of the diagram. As with the Zn diagrams from section 4.2.1 these diagrams were from different sources in the literature, with the CdTe and CdSe showing that the $\text{H}_2\text{chalcogen}$ is dominant in the reductive environments across the entire pH range. The diagram for CdS does not present a voltage at a low enough value (< -1.0 V) to demonstrate the presence of H_2S . It is likely however, knowing the behaviour similarities of the different metal chalcogenides, that H_2S would dominate this region in the same way H_2Se and H_2Te do in their respective Pourbaix diagrams.

The CV's conducted on the powdered Cd chalcogenide materials are also shown in Figure 4.9 and they are similar to the Zn chalcogenide CV's from Figure 4.4. The CdS is similarly resistive to the ZnS with a couple of small peaks, however the main feature of this CV is the larger oxidation peak A19 is possibly the oxidation of Cd from CdS, the other possibility that was considered was an affect from the Ag/AgCl electrode, therefore it was repeated with an Ag wire and the peak was still present. Equation 4.8 below was presented by Bouroushian et al. and was suggested to occur at around 0.008 V in aqueous solutions.¹



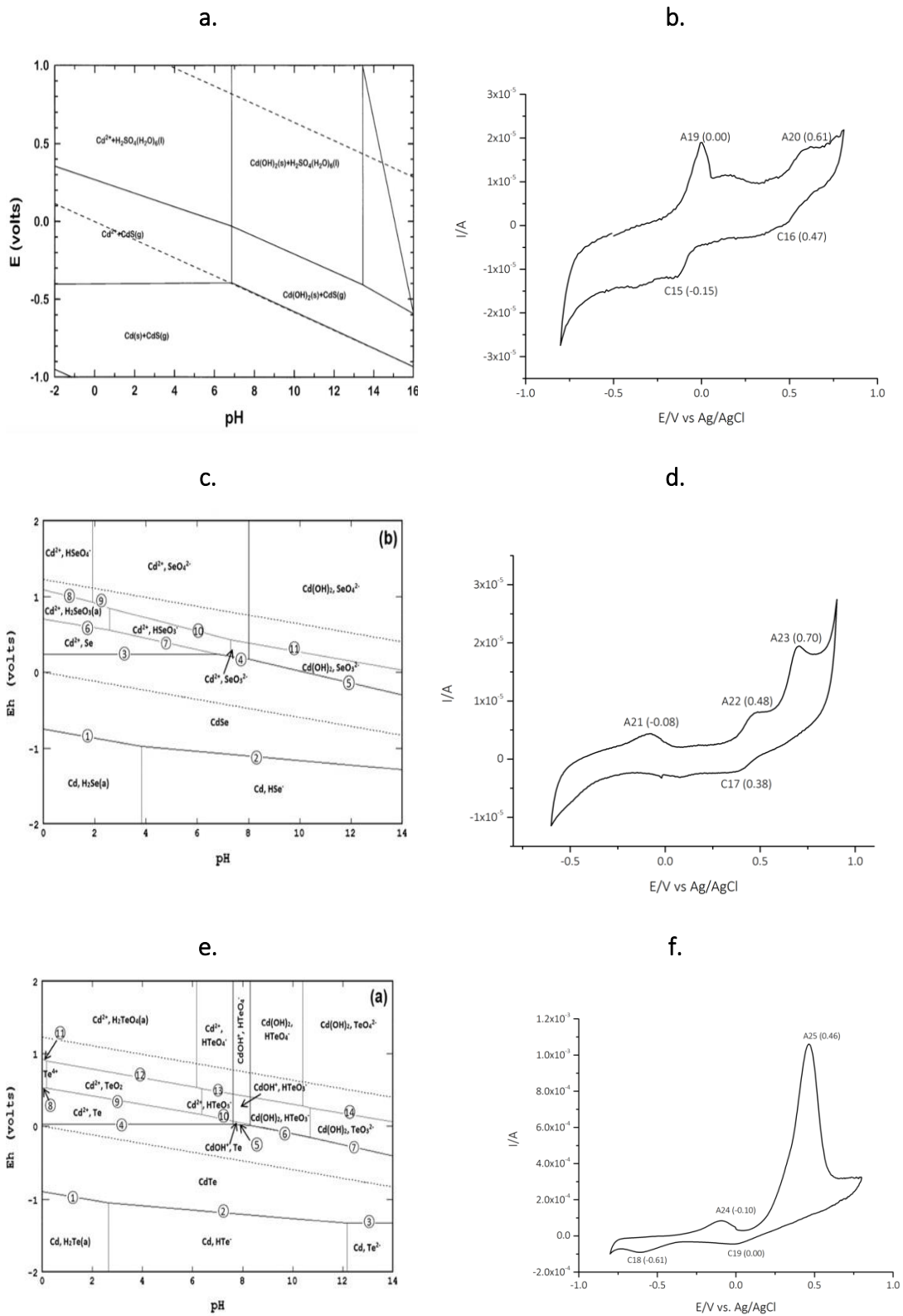


Figure 4.9: Pourbaix diagrams of **a.** CdS^{39} **c.** CdSe^1 and **d.** CdTe^1 and paint casting CV's of **a.** CdS powder, **b.** CdSe powder **c.** CdTe powder. All voltammograms were conducted in Ethaline using a 1 cm^2 Pt flag working and counter electrodes and an Ag/AgCl [0.1 M in Ethaline] reference electrode, scanned at 5 mVs^{-1} .

The CV of CdSe shown in Figure 4.9 exhibits a similar oxidation peak A23 related to the $\text{Se}^0 \rightarrow \text{Se}^{4+} + 4\text{e}^-$.⁴⁰ It also shows a couple of other oxidation peaks (A21 and A22) the first one of which at -0.12 V is likely to be a similar oxidation as was observed in the CdS CV via Equation 4.9. In general, the CV is slightly resistive, however not to the same extent as the CdS or ZnS CV's.

The CdTe CV is very similar to the ZnTe CV with the strong Te peak (A25) present again caused by the dissolution of the Te layer that forms on the Pt electrode after the reduction peak (C18) as discussed previously in section 4.2.2. The peak A25 was not observed in the first scan and instead only occurred after the deposition peak, confirming this theory. Interestingly, the electrochemistry of CdTe has been previously studied in a DES, Reline, specifically¹⁰ Through the use of this solvent and a Pt quasi-reference, a very large potential window was achievable. During this study Golgovici et al. conducted a CV of 100 mM CdCl₂ in Reline.¹⁰ In this CV a clear redox couple was present at -0.9 V/ -1.05 V which was ascribed to the oxidation and subsequent reduction of the Cd^{II} ions in solution to Cd⁰. This was confirmed through the presence of a Cd deposit forming on the Pt electrode during the reduction peak.¹⁰ In comparison to the data in the present study it is likely that A24 is the oxidation from this redox couple and the shift is possibly due to the different reference electrode. Also, clearly the results in Figure 4.9 do not present such a low potential due to the limits of the window in Ethaline and therefore it is possible that the redox of Cd is simply not available within the window of Ethaline in this experiment. The voltage could not be scanned any further beyond -0.8 V due to the edge of the electrochemical window and solvent decomposition being observed.

4.2.4 Electrochemical rate comparison

A good measure of the rate a material will ultimately be electrochemically dissolved, is by measuring the charge passed during one scan of a voltammogram. In order to determine if the charge bears any relation to the conductivity, the band gap and the charge are plotted below. In Chapter 3, the difference between the band gap and the measured conductivity were discussed. It was suggested that measuring the conductivity of a pellet of pressed powder was a better alternative to the band gap measurement due

to the challenges presented in determining the band gap of a powdered material. From that data it was seen that there were difficulties making the pellets and measuring a conclusive conductivity value. As well, the trend obtained from plotting the charge vs. the band gap was more representative of what would be expected, following a near linear trend of decreasing charge to increasing band gap. Therefore in the following results the band gap is used as a representation of conductivity, again simply due to the difficulties in obtaining accurate conductivity data.

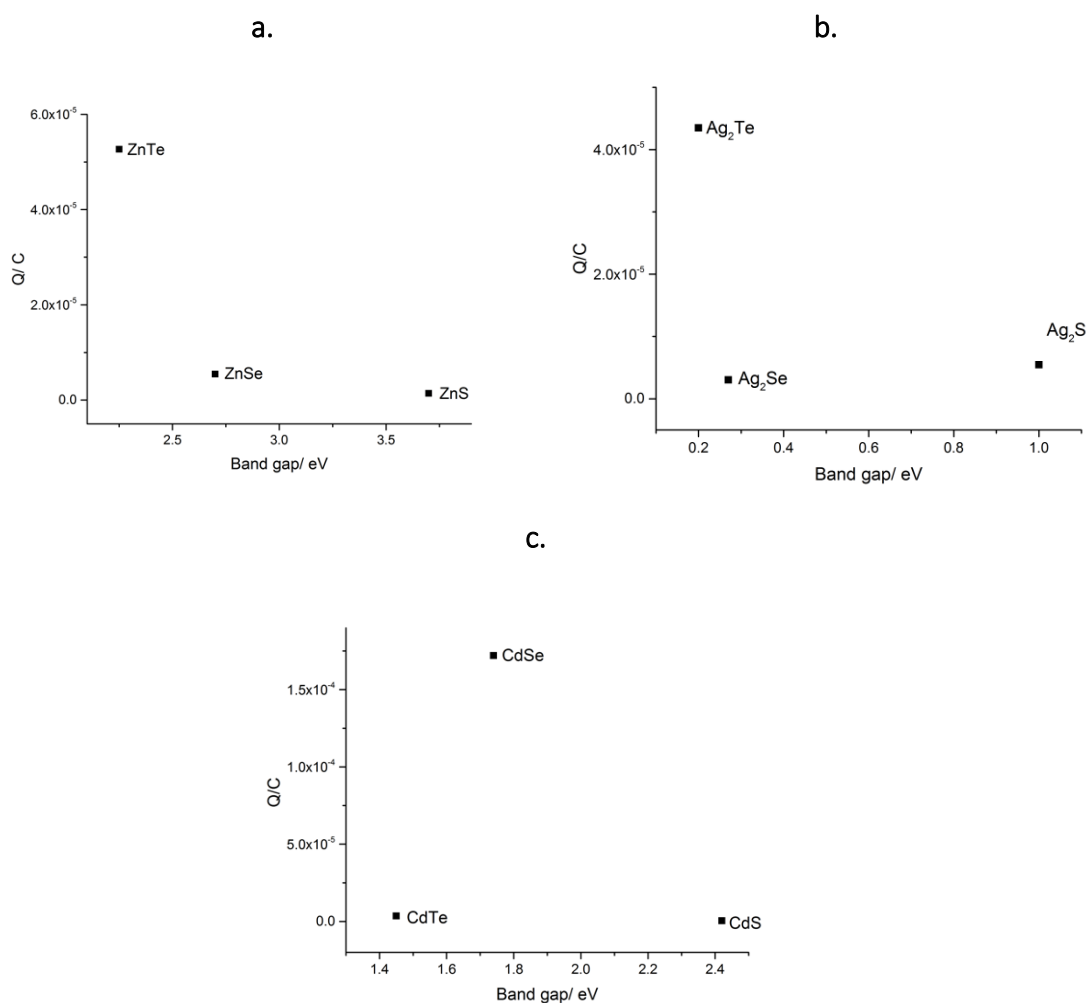


Figure 4.10: Band gap vs overall charge passed during the CV's shown in the previous Figures for **a.** ZnS, ZnSe and ZnTe **b.** Ag₂S, Ag₂Se and Ag₂Te and **c.** CdS, CdSe and CdTe. All paint casting voltammograms were conducted in Ethaline using a 1 cm² Pt flag working and counter electrodes and an Ag/AgCl [0.1 M in Ethaline] reference electrode, scanned at 5 mVs⁻¹

The results presented in Figure 4.10 show the overall charge passed in the voltammograms in Figures 4.4, 4.7 and 4.9 against the band gaps presented in the introduction to this chapter. The Zn and Ag chalcogenides follow the expected trend whereby as the band gap increases from the telluride to selenide to sulfide the charge passed on the voltammogram decreases. This is again showing how band gap is directly related to the conductivity and therefore will directly affect the rate at which the material can be electrochemically dissolved. Interestingly, the results from the Cd data are not expected, where the charge passed on the telluride CV is significantly lower than that for the selenide CV and is more in line with the sulfide. This is possibly due to the nature of the paint casting technique in the accuracy of loading the mass onto the surface and is why the technique can only really be described as semi-quantitative.

4.3 Speciation in solution

4.3.1 Electrochemical dissolution

The recovery of elements from spent solar cells is important for creating closed loop economy in rare elements such as selenium and tellurium. In this section selenide and telluride of cadmium, silver and zinc are studied to see the speciation of the chalcogenide. The main objective for this section is to try and determine what controls the dissolution of different chalcogenide compounds.

The bulk dissolution experiments were carried out in the same method as the Cu chalcogenides in Chapter 3. The results for the 6 compounds used are presented in Figure 4.11. In contrast to the results obtained in Chapter 3, where all the solutions were strongly coloured, the results for Zn, Cd and Ag all presented colourless solutions, showing as expected they have a fully filled d-shell and empty 4s shell. It also shows that whatever form the Se and Te is in, it does not contain a chromophore.

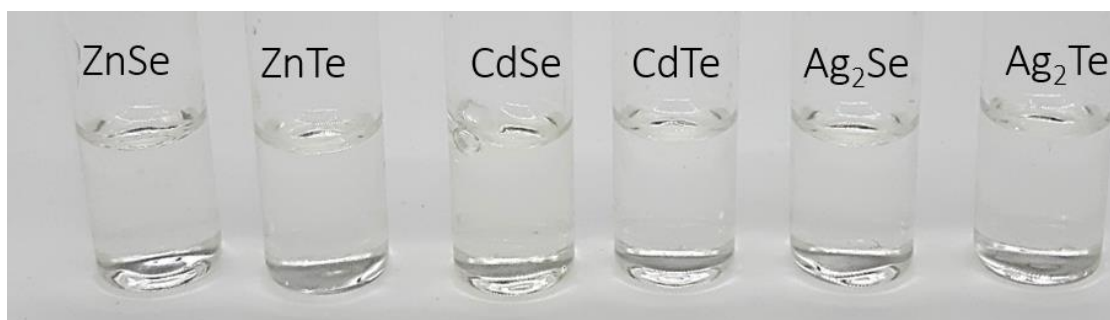


Figure 4.11: The solutions achieved from the electrochemical dissolution of each transition metal chalcogenide at 1.5 V for 24 hours in Ethaline using IrO₂ coated Ti mesh electrodes.

ICP-MS and UV-Vis were conducted on all the solutions and in all cases the ICP-MS indicated that both the metal and chalcogen were present in solution. The results for this are presented in Table 4.2.

Table 4.2: The concentration (ppm) of metal (either Zn, Cd or Ag) and the chalcogen (Se or Te) in each solution obtained during the electrochemical dissolution of the metal chalcogenides at 1.5 V for 24 hours in Ethaline, solution images in Figure 4.10.

	ZnSe	ZnTe	CdSe	CdTe	Ag ₂ Se	Ag ₂ Te
Metal / ppm	404.8	519.26	196.2	2730.6	77.7	162.9
Chalcogen / ppm	37.0	286.0	2.72	307.7	6.7	1429.5

In general the dissolution ability of the metal and chalcogen appears higher for the tellurides than for the corresponding selenides. The dissolution of the selenium compounds is significantly lower compared to the corresponding telluride. This is in agreement with the voltammetry in Figure 4.4, 4.7 and 4.9 where the anodic current is at least an order of magnitude larger for the telluride than the corresponding selenide. It is likely that this difference between the selenides and tellurides is due to the conductivity of the material as it would be expected that the more conductive a material is the easier it is able to be dissolved electrochemically. Table 4.2 shows a significant disparity between the metal and chalcogenide concentrations. This could be because a solid Se containing species is formed on one of the electrodes or more likely that a gaseous product is formed. The production of H₂Se could clearly be smelt during the electrolysis of ZnSe. This is likely to account for the lower Se concentrations but not for

the lower concentrations of metal in these solutions. While H_2Se is a toxic product it is also easy to separate from the DES and could potentially be scrubbed and recovered.

4.3.2 Rate of dissolution

During the electrochemical dissolution of each chalcogenide a sample was retrieved after 1, 2, 4, 6, and 24 hours. The samples were then analysed by ICP-MS in order to ascertain any dissolution rate data related to the metal and associated chalcogen. In general the Te and the metal dissolved more from the tellurides than the equivalent in the selenides. This is likely to be linked to the conductivity of the solids, given that the tellurides have been shown in all cases to exhibit a more metallic character, shown previously with their specifically small band gaps (Table 4.1). Interestingly, each sample appears to dissolve differently, at different rates over different time periods. The results for the concentration of metal (b and d) in each of the selenides and tellurides as well as the concentration of the chalcogens (a and c) are presented in Figure 4.12.

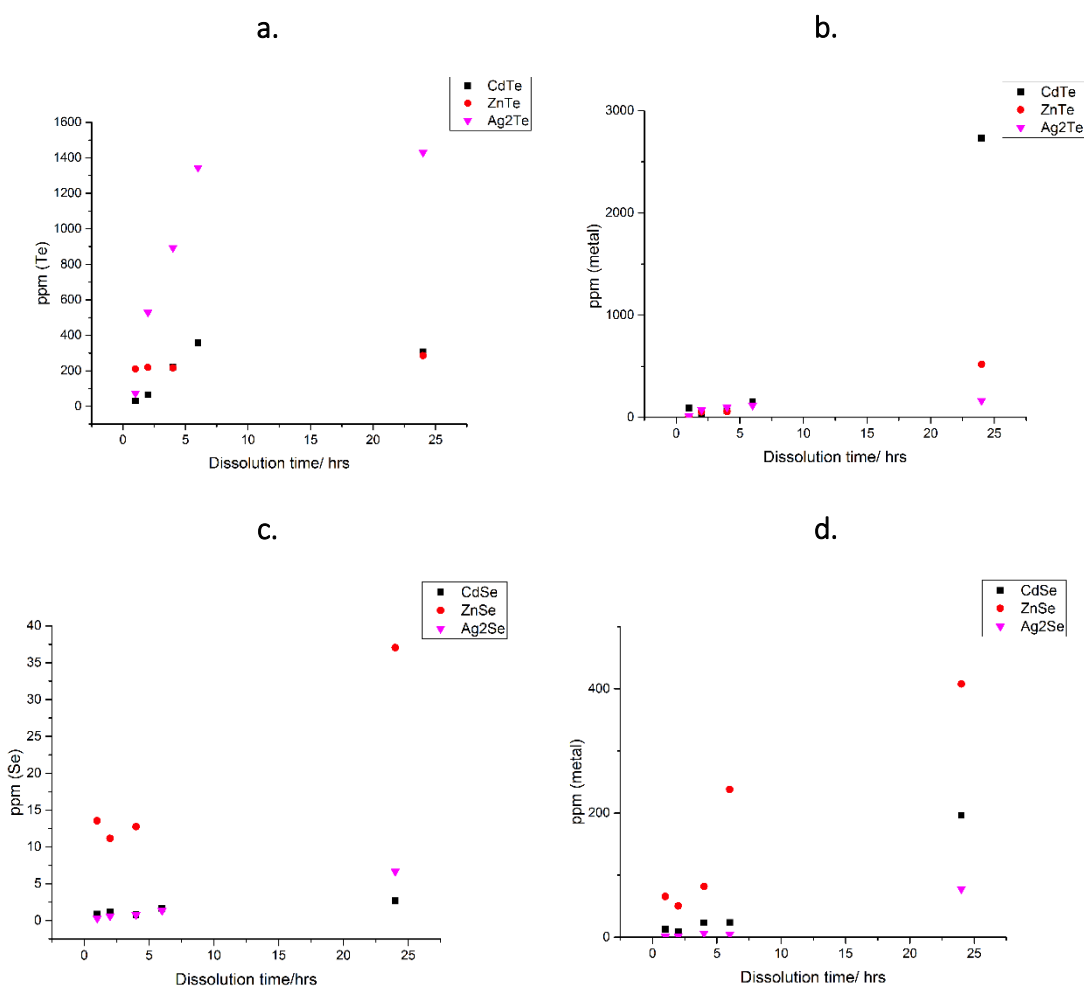


Figure 4.12: The concentration of **a.** Te in the telluride solutions, **b.** metal in the telluride solutions, **c.** Se in the selenide solutions and **d.** metal in the selenide solutions, plotted against the time in hours. Each material was electrolysed at 1.5 V for 24 hours in Ethaline.

From the results shown in Figure 4.12, it is interesting to note the differences in how the different chalcogens and metals have dissolved from the 6 different metal chalcogenides. For Te it appears that $Cd > Zn > Ag$ whereas for Se it appears that $Zn > Cd > Ag$. This is at odds with the band gaps in Table 4.1 where $Ag < Cd < Zn$ so Ag should be the easiest to dissolve and this is borne out in the voltammetric data. The results in Figure 4.12 show only the concentrations of metals in solution and ignore that during the bulk electrolysis metals are also deposited on the cathode in the bulk electrolysis cell. Naturally it should be easier to deposit silver on the cathode than cadmium and zinc. The low silver concentration in solution in Figures 4.12b and d reflect the increased efficiency by which the metal is removed from solution onto the cathode. The high Te

concentration for Ag_2Te electrolysis shows the higher solubility for the Te species compared with the formation of H_2Se which is lost from solution. It can be seen that ICP-MS is not necessarily a suitable method for following dissolution rates as it does not account for solid and gaseous reaction products.

4.3.3 Chalcogen speciation analysis

The UV-Vis results from the solutions in Figure 4.11 are shown in Figure 4.13. They demonstrate that there are no peak similarities when it comes to comparing the selenides to each other and the tellurides to each other. There are however similarities with certain metals. For example the Ag_2Te and Ag_2Se UV-Vis results shown by the blue lines in Figure 4.13b and c, show a very strong absorbance peak at around 250 nm which is present for both solutions. This corresponds to an Ag peak also presented by Trinh et al. of an AgCl suspension.⁴¹ It has been shown in a previous EXAFS study dissolving several different Ag salts (Ag_2O , AgNO_3 , AgAc and AgCl) in Ethaline, that the speciation of the Ag in solution was always $[\text{AgCl}_2]$.⁴² As for the Zn and Cd UV-Vis spectra shown by the red and black lines respectively in Figure 4.13b and c they show a couple of absorbance peaks but nothing that correlates to a chalcogen species that has been observed. A UV-Vis conducted on different Te containing compounds is shown in Figure 4.13a, and it is shown that TeCl_4 dissolved in Ethaline gave 2 very strong peaks at 249 nm and 288 nm. The same is not true for SeCl_4 in Ethaline which did not show any distinct peaks, only a very broad shoulder at around 230 nm. Overall, the main conclusion here is that the use of UV-Vis is not necessarily a suitable technique to determine speciation in these particular solutions due to the low concentrations shown in Table 4.2 and the low extinction coefficients of most Te and Se containing species.

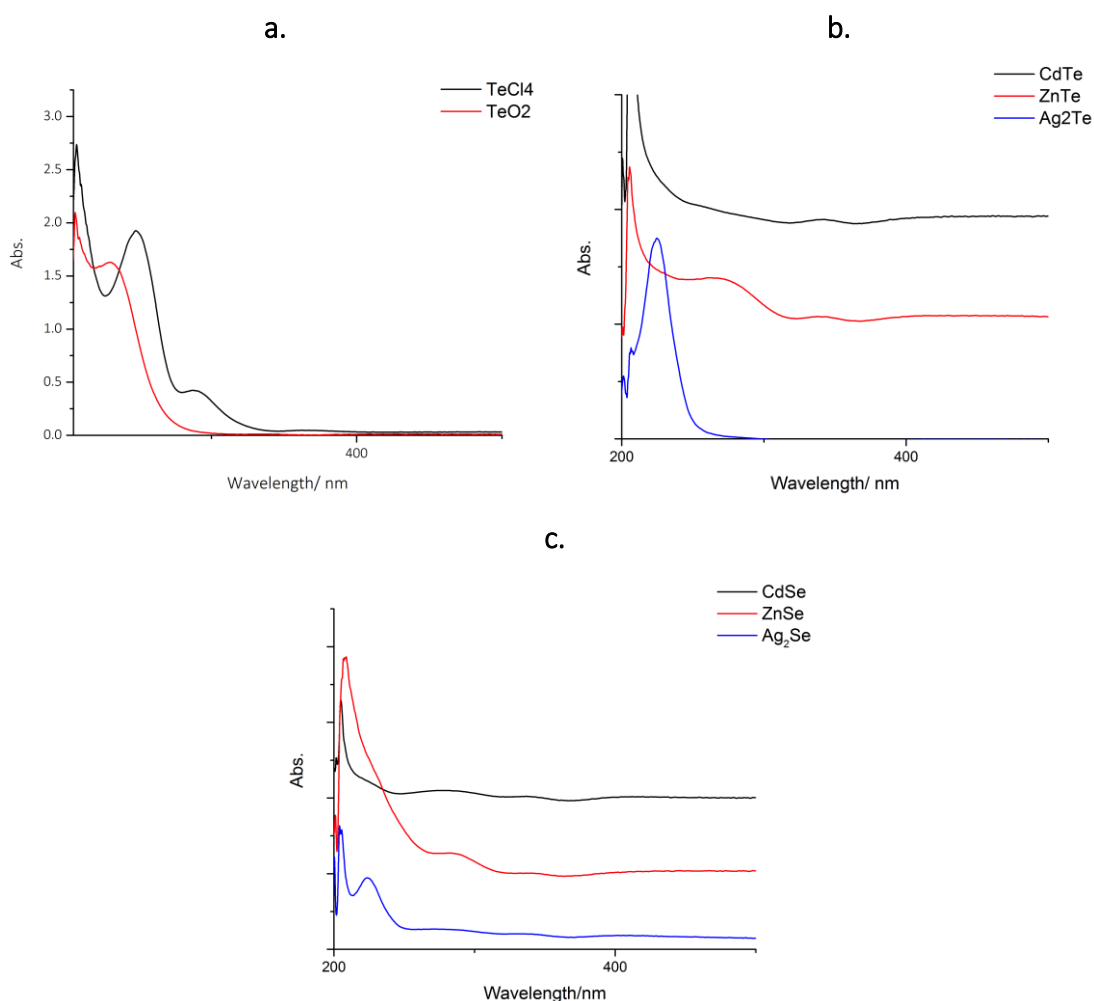


Figure 4.13: The UV-Vis results for **a.** TeCl_4 and TeO_2 dissolved in Ethaline **b.** Telluride solutions from Figure 4.11 and **c.** Selenide solutions from Figure 4.11. (constant 1.5 V for 24 hours in Ethaline)

The solutions from Figure 4.11 were also sent off and analysed by HPLC coupled with ICP-MS. The calibration was carried out with known concentrations of sodium selenate (SeO_4^{2-}), sodium selenite (SeO_3^{2-}), sodium tellurate (TeO_4^{2-}) and sodium tellurite (TeO_3^{2-}) solutions and the results are shown in Figure 4.14. This clearly shows that the metal tellurides and selenides clearly form complexes with O rather than the Cl, either from trace amounts of water or a reaction with the hydrogen bond donor (ethylene glycol). A similar situation is observed with As which is also a semi metal and is observed to form complexes more favourably with O-donor ligands than Cl ligands.⁴³ The lack of a chromophore means that Se and Te do not form polyatomic anions as is observed with sulfur.

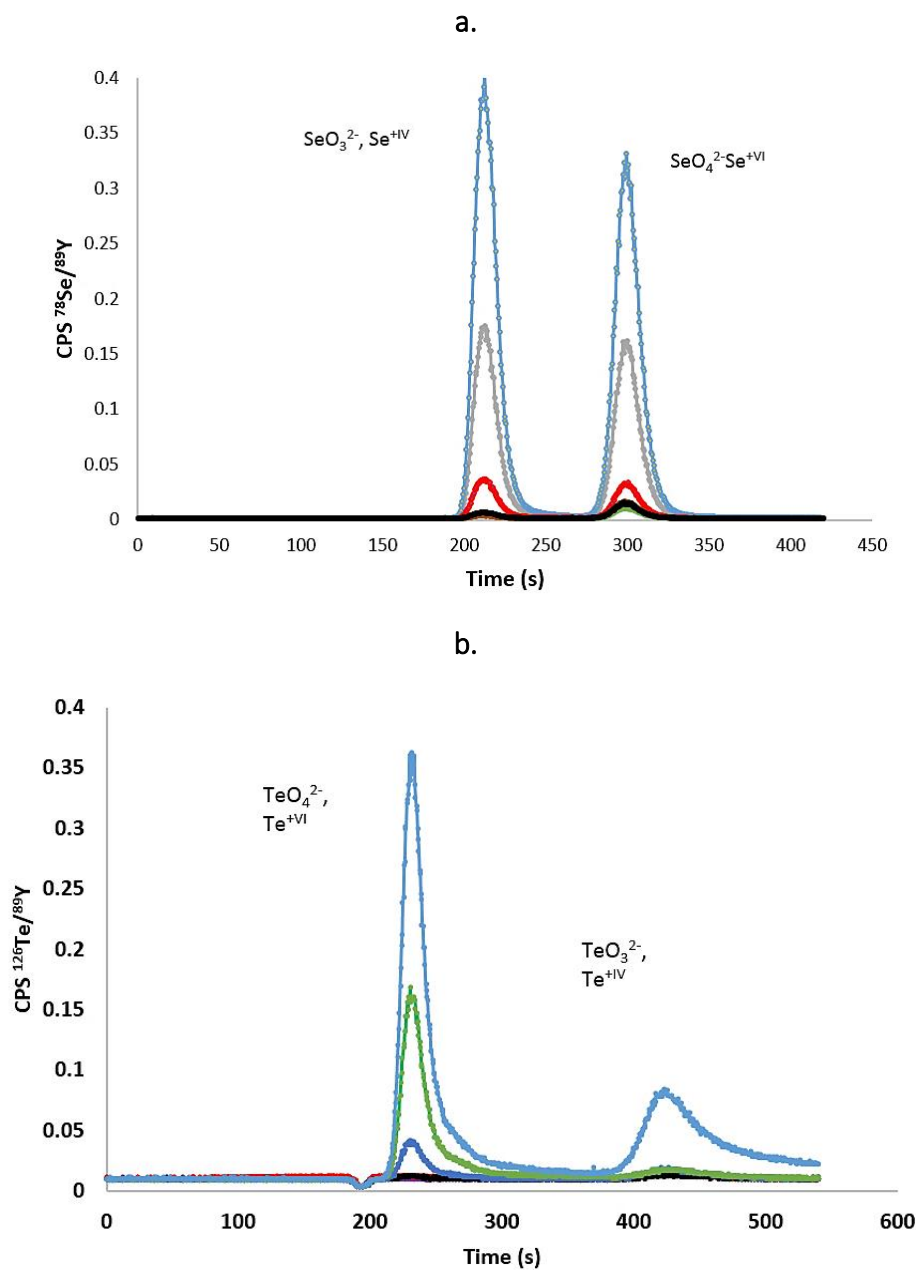


Figure 4.14: Results from the standard solution of **a.** sodium selenate and selenite and **b.** sodium tellurate and tellurite. (Different lines are the results from varying concentrations, between 0.05 ppb to 100 ppb. Concentration correlates to the peak heights in both cases).

When the different solutions were tested it revealed that they all contained in varying intensities either the selenate and selenite or the tellurate and tellurite. The results from the successful experiments are shown in Figure 4.15. Results for CdSe and ZnTe are missing due to inconclusive results, which in the case of CdSe is likely to be due to the very low concentration of Se species in solution.

From the Pourbaix diagram in Figure 4.7a it can be seen that Ag^+ and SeO_4^{2-} are stable at very positive overpotentials and so SeO_3^{2-} is likely to form. By inference with the DESs it should be concluded that this is why the signal for SeO_3^{2-} is bigger than that for SeO_4^{2-} in Figure 4.15a. Although the Pourbaix diagram for Ag_2Te is not available it must be concluded that TeO_4^{2-} is less oxidising and therefore more stable in Ethaline as the signal for TeO_4^{2-} is bigger than that for TeO_3^{2-} in Figure 4.15c. Figure 4.4c shows that for ZnSe in aqueous solutions Se is only stable over a limited potential range as is SeO_3^{2-} so it is understandable that the signal for SeO_4^{2-} is larger than SeO_3^{2-} in Figure 4.15.

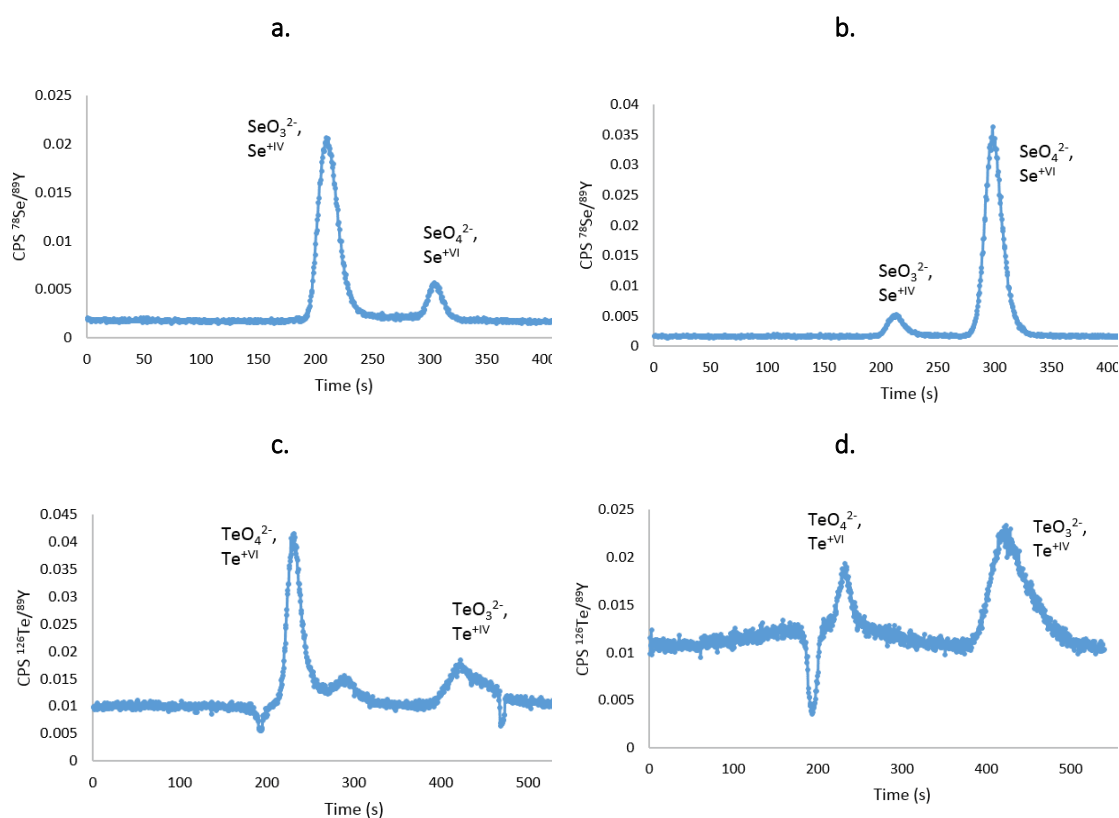


Figure 4.15: The HPLC-ICP-MS data recovered measuring the speciation of Se in **a.** Ag_2Se , **b.** ZnSe and the speciation of Te in **c.** Ag_2Te and **d.** CdTe . Solutions obtained from the electrochemical dissolution in Ethaline for 24 hours at 1.5 V.

In aqueous solutions there are numerous spot tests which can be carried out to detect Se and Te species in solution.⁴⁴ Clearly many of these rely on these rely on H^+/OH^- chemistry and are not directly transferrable to DESs. As a starting point, the spot tests that are used for aqueous solutions in determining the presence of tellurates and tellurites and selenates and selenites are trialled with the Ethaline solutions. These included hydrazine, thiourea, hydriodic acid, $FeSO_4$ (with phosphoric acid) and $BaCl_2$.

Several of these tests were unsuccessful and did not provide any precipitate. The thiourea test resulted in a faint black/red precipitate in all the selenide solutions. However this precipitate was too small to photograph and an attempt to scale up and generate more precipitate was unsuccessful, which is unsurprising considering the low concentrations exhibited by the ICP-MS results. The $BaCl_2$ test did give a small white precipitate with the CdSe and ZnSe solutions, however again it was so small and not possible to photograph it successfully. Finally, the $FeSO_4$ test was successful in scenarios containing either Se or Te. The pictures presented in Figure 4.16 show the results from the $FeSO_4$ test on both the Ag and Zn solutions. Clearly these are not 'spot tests' and are instead scaled up versions where equal parts $FeSO_4$, phosphoric acid and test solution were mixed together in an attempt to extract as much precipitate as possible in order to analyse it.

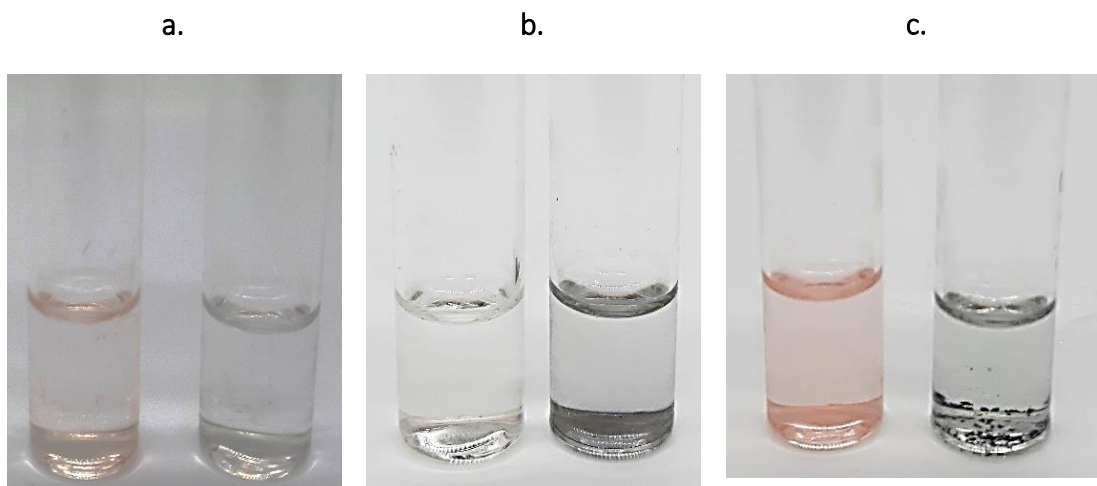


Figure 4.16: The results from the FeSO_4 'spot tests' for the **a.** CdSe/CdTe **b.** $\text{Ag}_2\text{Se}/\text{Ag}_2\text{Te}$ and **c.** ZnSe/ZnTe solutions. Solutions originally obtained by electrochemical dissolution at 1.5 V for 24 hours in Ethaline.

After filtering the black precipitate and examining with EDX it was revealed that the precipitate is Te, therefore confirming the presence of a Te species in solution. As for the detection of Se in the solutions, it is very likely to be concentration that is limiting both the Cd and Ag selenide solutions, as the concentration of Se species in these solutions is low, 2.72 ppm and 6.68 ppm respectively compared to the 37.04 ppm for the Zn solution.

4.3.4 Recovery/ extraction

As shown above, anodic dissolution of the selenides and tellurides leads to a metallic deposit on the cathode of the electrolysis cell. The images of any cathodes that were obtained from successful experiments are presented in Figure 4.17. For the electrolysis of Ag_2Te using a copper cathode the only metal detected by EDX was silver and there was no signal for Te. For CdTe both Cd and Te were detected but in an atomic ratio of 16:1 showing a purification. The presence of tellurium in the deposit can be attributed to the more similar reduction potentials of the two elements.



Figure 4.17: Shows the resultant cathodes (Cu left, Ni right) of the recovery experiments conducted on the transition metal chalcogenides for 24 hours at a constant 1.5 V in Ethaline.

This work needs a lot more optimization in order to separate the components completely, in an ideal scenario, the chalcogen or metal would be deposited on an electrode and the other left in solution, either to be precipitated or extracted at a different potential. In the next chapter, the mineral chalcopyrite is investigated and the effect of changing the composition of the DES is also examined. This could also be a possibility when investigating the metal chalcogenides and that a change in DES properties could enable a purer or more efficient extraction.

4.4 Conclusions

This chapter has shown that metal chalcogenides where the metal only exists in one oxidation state, can be dissolved using paint casting. The main aims for this chapter were to determine what controls the rate of dissolution during electrochemical dissolution of the different transition metal chalcogenides and to understand the speciation of the metals and more importantly the chalcogens after they have been electrochemically dissolved in Ethaline.

In the first section of this chapter it was shown that the electrochemistry of a selection of metal chalcogenides were caused by the conductivities of the compound. The conductivity affects the quality of the voltammogram and the resolution of the peaks but it was also possible to study more resistive materials such as ZnS. It was shown that the

voltammetric peaks can be correlated to the aqueous Pourbaix diagrams for the compounds and this gives some idea about speciation which is relatively similar to what would be observed in aqueous solutions.

The rate of dissolution during the electrochemical dissolution of a selection of compounds was investigated. It was found that the rate of dissolution differed significantly. ICP-MS was used but the amount of metal and chalcogenide in solution did not follow the charge passed on the voltammetric signal. It was shown that the voltammetric charge correlates with the band gap of the semi-conductor but not with the amount of metal in solution following bulk electrolysis. This discrepancy is because during bulk electrolysis the metal in solution is extracted onto the cathode and the more positive the reduction potential the faster it is deposited. ICP analysis also fails to capture gaseous products such as H_2Se .

One major question answered in this chapter was the speciation of Se and Te when it was oxidised in the paint casting experiments. The HPLC-ICP-MS revealed that the most likely species are tellurate/tellurite and selenite/selenite respectively. The metals are most likely to form the chloride salts in solution. This shows that the electrochemistry of Se and Te is similar in DESs to that observed in aqueous solutions.

4.5 References

1. Bouroushian, M., (2010) *Electrochemistry of Metal Chalcogenides*, 1st Ed. Springer-Verlag Berlin Heidelberg
2. Matthews, P. D., McNaughter, P. D., Lewis, D. J., O'Brien, P., (2017) Shining a Light on Transition Metal Chalcogenides for Sustainable Photovoltaics, *Chem. Sci.*, **8**, 4177-4187
3. Tedstone, A. A., Lewis, D. J., O'Brien, P., (2016) Synthesis, Properties and Applications of Transition Metal-Doped Layered Transition Metal Dichalcogenides, *Chem. Mater.*, **28**, 1965-1974.
4. Anthony, J. W., Bideaux, R. A., Bladh, K. W., Nichols, M. C., *Handbook of Mineralogy*, Mineralogical Society of America, USA. <http://www.handbookofmineralogy.org> (accessed 13/05/2019)
5. Vaughan, D. J., (1978) *Mineral Chemistry of Metal Sulfides*, 1st Ed., Cambridge University Press, Cambridge UK.
6. Wei, C., Huang, Z., Yan, Z., Hu, Y., Ye, L., (2018) Trace Element Contents in Sphalerite from Nayongzhi Zn-Pb Deposit, Northwestern Guizhou, China: Insights into Incorporation Mechanisms, Metallogenic Temperature and Ore Genesis, *Minerals*, **8**, 490-495
7. Letcher, T. M., Fthenakis, V. M., (2018) *A Comprehensive Guide to Solar Energy Systems*, 1st Ed., Elsevier, The Netherlands.
8. Kim, B. S., Kyung, W. S., Seo, J. J., Kwon, J. Y., Denlinger, J. D., Kim, C., Park, S. R., (2017) Possible Electric Field Induced Indirect to Direct Band Gap Transition in MoSe₂, *Scientific Reports*, **7**, 1-6.
9. Boakye, F., Nusenu, D., (1997) The Energy Band Gap of Cadmium Sulphide, *Solid State Communications*, **102**, 323-326
10. Golgovici, F., Visan, T., (2012) Electrodeposition Behaviour of Cadmium Telluride from Choline Chloride- Urea Ionic Liquids, *Chalcogenide Letters*, **9**, 165-174
11. Gordienko, A. B., Zhuravlev, Y. N., Fedorov, D. G., (2006) Band Structure and Chemical Bonding in Silver Sulphide, *Russian Physics Journal*, **49**, 893-894

12. Pei, Y., Heinz, N. A., Snyder, G. J., (2011) Alloying to Increase the Band Gap for Improving Thermoelectric Properties of Ag₂Te, *J. Materials Chemistry*, **45**, 18256-18260
13. Pearce, C. I., Pattrick, R. A. D., Vaughan, D. J., (2006) Electrical and Magnetic Properties of Sulfides, *Reviews in Mineralogy and Geochemistry*, **61**, 127-180
14. Guha, S., (2001) *Encyclopedia of Materials: Science and Technology*, 2nd Ed., Elsevier, Netherlands
15. Catrangiu, A. S., Beregoi, M., Cojocar, A., Anicai, L., Cotarta, A., Visan, T., (2016) Electrochemical Deposition of Zinc Telluride Thin Films from Ethaline Ionic Liquid, *Chalcogenide Letters*, **13**, 187-199
16. Jellinek, F., (1988) Transition Metal Chalcogenides. Relationship Between Chemical Composition, Crystal Structure and Physical Properties, *Reactivity of Solids*, **5**, 323-339.
17. Colletti, L. P., Thomas, S., Wilmer, E. M., Stickney, J. L., (1996) Thin Layer Electrochemical Studies of ZnS, ZnSe and ZnTe Formation by Electrochemical Atomic Layer Epitaxy (ECALE) *Technical Report*
18. Zhang, S. Y., Fang, C. X., Wei, W., Jin, B. K., Tian, Y. P., Shen, Y. H., Yang, J. X., Gao, H. W., (2007) Synthesis and Electrochemical Behaviour of Crystalline Ag₂Se Nanotubes, *J. Phys. Chem. C.*, **111**, 4168-4174
19. Gonzalez- Ibarra, A. A., Nava-Alonso, F., Uribe-Salas, A., (2019) Electrochemical Study of Silver Telluride (Ag₂Te): Anodic and Cathodic Potential Dependent Reactions in Alkaline Cyanide Solutions, *Hydromet.*, **183**, 230-239
20. Kim, S. H., Han, W. K., Lee, J. H., (2010) Electrochemical Characterization of CdSe and CdTe Thin Films using Cyclic Voltammetry, *Current Applied Physics*, **10**, 481-483
21. Tang, C., Wei, X., An, Q., Jiexin, Z., (2018) ZnSe Microspheres/Multi-Walled Carbon Nanotubes Composites as High-Rate and Long-Life Anodes for Sodium Ion Batteries, *Appl. Mater. Interfaces*, **10**, 19626-19632.
22. Hsiu, S. I., Sun, I. W., (2004) Electrodeposition Behaviour of Cadmium Telluride from 1-ethyl-3-methylimidazolium chloride tetrafluoroborate Ionic Liquid, *J. Applied Electrochemistry*, **34**, 1057-1063

23. Aparicio-Razo, M., (1983) PhD Thesis: Portland State University , A Mechanistic Study of the Electrochemical Formation of CdS CdSe Semiconducting Films.
24. Abbott, A. P., Barron J. C., Frisch, G., Ryder, K. S., Silva, A. F., (2011) The Effect of Additives on Zinc Electrodeposition from Deep Eutectic Solvents, *Electrochim. Acta*, **56**, 5272-5279.
25. Chaparro, A. M., (2005) Thermodynamic Analysis of the Deposition of Zinc Oxide and Chalcogenides from Aqueous Solutions, *Chem. Mater.*, **17**, 4118-4124.
26. Kowalik, R., Zabinski, P., Fitzner, K., (2008) Electrodeposition of ZnSe, *Electrochim. Acta*, **53**, 6184-6190
27. Abbott, A. P., Barron, J. C., Ryder, K. S., (2009) Electrolytic Deposition of Zn Coatings from Ionic Liquid Based on Choline Chloride, *Trans. IMF.*, **87**, 201-207.
28. Zhang, Y., Lv, J., Wang, H., Wen, S., Pang, J., (2018) Formation of Zinc Sulfide Species During Roasting of ZnO with Pyrite and its Contribution on Flotation, *Scientific Reports*, **8**, 1-10
29. Li, Y., Zhang, L., Kisslinger, K., Wu, Y., Green Phosphorescence of Zn Sulfide Optical Ceramics, *Optical Materials Express*, **4**, 1140-1150.
30. Al-Bassam, A. Z. M. H., (2018) PhD Thesis: University of Leicester, Mineral Processing Using Deep Eutectic Solvents.
31. Abbott, A. P., Al-Bassam, A. Z. M., Goddard, A., Harris, R. C., Jenkin, G. R. T., Nisbett, F., Weiland, M., (2017) Dissolution of Pyrite and other Fe-S-As Minerals using Deep Eutectic Solvents, *Green Chem.*, **19**, 2225-2233
32. Srinivasan, G. N., Iyer, S. V., (2000) Cyclic Voltammetric Studies on Sphalerite Electrodes, *Bulletin of Electrochemistry*, **16**, 5-9
33. Azam, M., (2011) PhD Thesis: The University of Leicester, The Electrochemistry of Ag in Deep Eutectic Solvents.
34. Palin, E., (2019) PhD Thesis: University of Leicester, An in-situ Study of Buried Metal Interfaces using Electrochemical and Neutron Scattering Techniques.
35. Zhang, Q., Wang, R., Chen, K., Hua, Y., (2014) Electrolysis of Solid Copper Oxide to Copper in Choline-EG Eutectic Melt, *Electrochim. Acta*, **121**, 78-82.

36. Bayesov, A., Tuleshova, E., Tukibayeva, A., Aibolova, G., Baineys, F., (2015) Electrochemical Behaviour of Silver Electrode in Sulphuric Acidic Solution During Anodic Polarization, *Oriental Journal of Chemistry*, **31**, 1867-1872
37. Abbott, A. P., Azam, M., Frisch, G., Hartley, J., Ryder, K. S., Saleem, S., (2013) Ligand Exchange in Ionic Systems and its Effect on Silver Nucleation and Growth, *Phys. Chem. Chem. Phys.*, **15**, 17314-17323.
38. Hartley, J. M., Ip, C. M., Forrest, G. C. H., Singh, K., Gurman, S. J., Ryder, K. S., Abbott, A. P., Frisch, G., (2014) EXAFS Study into the Speciation of Metal Salts Dissolved in Ionic Liquids and Deep Eutectic Solvents, *Inorg. Chem.*, **53**, 6280-6288
39. Savadogo, O., (1998) Chemically and Electrochemically Deposited Thin Films for Solar Energy Materials, *Sol. Energy Mater. Sol. Cells*, **52**, 361-388
40. Saji, V. S., Lee, C. W., (2013) Selenium Electrochemistry, *RSC Adv.*, **3**, 10058-10077.
41. Trinh, N. D., Nguyen, T. T. B., Nguyen, T. H., (2015) Preparation and Characterization of Silver Chloride Nanoparticles as an Antibacterial Agent, *Adv. Nat. Sci. Nanosci. Nanotechnol.*, **6**, 1-6.
42. Hartley, J. M., (2013) PhD Thesis: University of Leicester, Ionometallurgy: The Processing of Metals Using Ionic Liquids.
43. Personal communication with Hartley, J. M., University of Leicester, (2019)
44. Feigl, F., Anger, V., (1982) Spot Tests in Inorganic Analysis, 6th Ed., Elsevier, The Netherlands

CHAPTER 5: ELECTROCHEMICAL PROCESSING OF CHALCOPYRITE

Table of Contents

5.1 Introduction.....	156
5.1.1 <i>Chalcopyrite</i>	156
5.1.2 <i>Current chalcopyrite processing methods.....</i>	157
5.1.3 <i>Challenges and improvements in chalcopyrite processing</i>	158
5.1.4 <i>Aims.....</i>	161
5.2 Analysis of chalcopyrite.....	162
5.2.1 <i>Chalcopyrite sample analysis</i>	162
5.2.2 <i>Paint casting chalcopyrite</i>	165
5.3 Cell design	173
5.4 Hybrid DESS	181
5.4.1 <i>Reline and Oxaline.....</i>	182
5.5 Analysing the experiment design	186
5.5.1 <i>Green metrics</i>	186
5.5.2 <i>Cell design problems/improvements.....</i>	188
5.6 Conclusions.....	191
5.7 References.....	193

5.1 Introduction

5.1.1 Chalcopyrite

As discussed in Chapter 3, the majority of Cu (70-80 %) is currently extracted from chalcopyrite (CuFeS_2),¹ Geologically, chalcopyrite was mostly deposited along with massive porphyry rock sediments, with some of the largest deposits being in the Atacama Desert, Chile, although Cu deposits are found widely distributed throughout the world as shown in Figure 5.1.

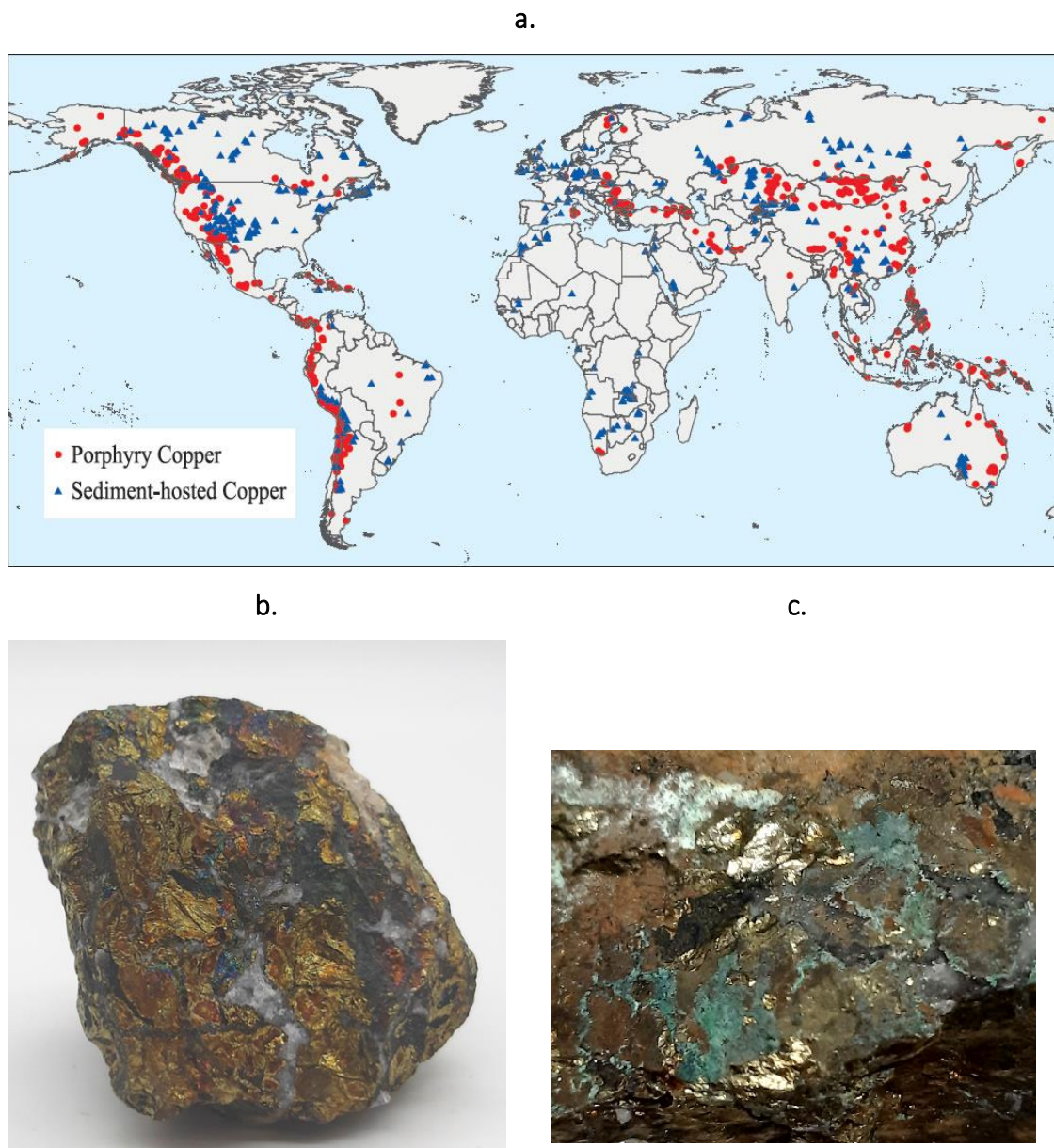


Figure 5.1: a. A world map showing the main locations of copper deposits.² b. A sample of chalcopyrite. c. Green chalky deposit on the sample of chalcopyrite.

Chalcopyrite is described as a covalent copper sulfide with a brassy yellow metallic lustre that weathers to a chalky green/grey colour. Crystallographically, a unit cell of chalcopyrite contains 4 Cu, 4 Fe and 8 S atoms.³ Whereby each S is coordinated by a tetrahedral arrangement of 2 Fe and 2 Cu and each metal is subsequently coordinated by a tetrahedron of S atoms.³ There is a degree of uncertainty in the oxidation states of the atoms in chalcopyrite, however, it is mostly agreed to be $\text{Cu}^{\text{I}}\text{Fe}^{\text{III}}(\text{S}^{2-})_2$ as opposed to $\text{Cu}^{\text{II}}\text{Fe}^{\text{II}}(\text{S}^{2-})_2$ which has also been suggested.^{4,5} When chalcopyrite is crushed it exhibits poor cleavage, resulting in a smooth (conchoidal) surface as opposed to fracturing in defined cleavage planes.³ This means that a selection of surface orientations are present with different species on the surface. On a freshly fractured surface of chalcopyrite there have been 3 different S species reported, S^{2-} , S_2^{2-} and a low coordination S_n^{2-} . It is suggested that the S_2^{2-} species is a result of surface reconstruction along with redox processes which ultimately leads to a pyrite like surface layer.³

5.1.2 Current chalcopyrite processing methods

The majority of chalcopyrite is processed by pyrometallurgy as it does not readily dissolve in aqueous solutions, due to its refractive nature. The proportion of Cu present in chalcopyrite is too small to directly smelt due to the large gangue fraction. Therefore, the ore is usually concentrated by froth flotation.¹ This technique was touched upon in section 3.1 and works by selectively attaching the high concentration Cu minerals with bubbles of air passing through the mixture. A common reagent to use in the separation of chalcopyrite from unwanted oxide minerals is xanthate, which contains a polar sulfur group on one end and a long hydrocarbon tail on the other.⁶ The polar group will preferentially attach to the sulfide mineral allowing it to be made selectively hydrophobic.¹ Chalcopyrite is quite often found associated with pyrite (FeS_2) and galena (PbS) and the separation of these minerals is slightly more complex. The presence of OH^- ions in solution can be altered by pH adjustment to preferentially float certain minerals. The OH^- will compete with the xanthate, binding to pyrite and galena more favourably than chalcopyrite. In an acidic solution all minerals will float, whereas as the pH is increased only the chalcopyrite and galena will float. Eventually, if the pH is high enough (7.5- 10.5) only the chalcopyrite is able to float.¹ The overall flotation process is demonstrated in Figure 5.2.

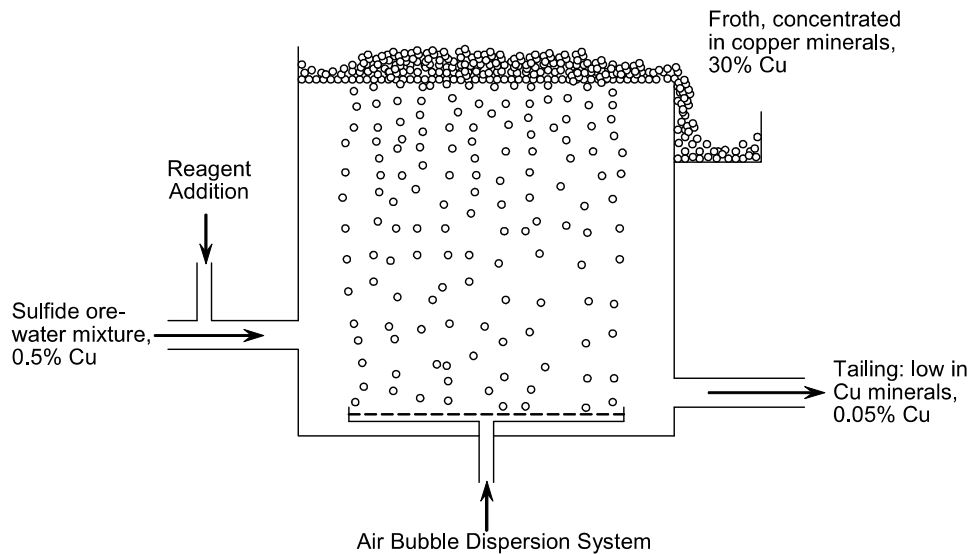


Figure 5.2: Typical setup of froth flotation for chalcopyrite concentration.¹

From here the concentrated chalcopyrite is able to be smelted, proceeding by equation 5.1.¹



The SO₂ gas generated in each smelting stage is collected and used to make H₂SO₄. The removal of Fe is important as more Fe means more slag.¹ Cu₂O which is also generated by the smelting of Cu sulfide minerals is readily dissolved in the slag, which decreases the Cu recovery efficiency. It is therefore important to reduce the overall amount of slag and optimise Cu recovery. The matte formed in equation 5.1 contains between 40-75 % Cu which is then converted to obtain molten metallic Cu. In this stage of the process the Fe and S present in the matte are oxidised by oxygen rich air, generating the blister copper necessary for electrorefining and finally electrowinning.¹

5.1.3 Challenges and improvements in chalcopyrite processing

The issues surrounding decreasing ore grade were also discussed in section 3.1, however Cu ore availability is increasingly dominated by lower grade chalcopyrite ores. This is a significant problem for minerals that are typically processed via pyrometallurgy, i.e. chalcopyrite, as it is not economically viable to smelt gangue material and unwanted

minerals. Clearly, if the ore grade is lower, a greater degree of concentration will be required.

Hydrometallurgical processing is much better suited to lower grade, more complex ores, simply because of the energy wastage and production of slag and pollutant SO_x gases from pyrometallurgical processing.⁷ However, the direct leaching of chalcopyrite is often kinetically very slow due to slow surface reactions, commonly attributed to a passivation layer forming on the surface of the mineral^{8,9} These have been suggested to be due to a complex film formed from sulfides, polysulfides and elemental sulfur, the partial oxidation of chalcopyrite leading to a Cu rich layer or some sort of Fe hydroxide mineral.¹⁰ Various studies¹⁰⁻¹³ have investigated methods to improve the slow surface reactions and therefore the leaching rate of chalcopyrite. Firstly, galvanic interactions with FeS₂ were utilised to increase electrochemical leaching by a factor of 4.6.¹² The pyrite was shown to cause the normally thick sulfur/sulfide coatings to remain porous and therefore not passivate the surface. A change in temperature, agitation, and chalcopyrite particle size, have all been shown to have an effect on the leaching rate.^{10,13} Interestingly, an increase in stirring or agitation has not always shown an increase in dissolution. It is suggested that this is a result of decreasing the contact between the oxidants in solution and the chalcopyrite surface for long enough to allow oxidation to occur. Changing the particle size of the chalcopyrite allows a greater surface area to be accessible by the lixiviant, therefore increasing the overall rate of leaching. Increasing the temperature has been shown to increase the rate of dissolution as well.¹¹ An increase from 70°C to 90°C resulted in a leaching increase from 28 % to 70 % in a 1.5 M H₂SO₄ solution.¹⁴ This increased dissolution rate suggests that the chemical reaction is the limiting factor in the leaching mechanism, hence an increase in dissolution with respect to higher temperatures.

Leaching of chalcopyrite in ILs has also been investigated in a growing number of cases.¹³⁻¹⁸ Whitehead et al. presented a highly efficient method of Cu extraction from a sample of chalcopyrite using the IL Bmim(HSO₄).¹⁵ They were able to achieve 85 % efficiency when it came to the extraction of Cu which was supported by further studies by Dong et al. who utilised the same IL and achieved 88 % Cu extraction efficiency.¹⁴ Higher

extraction efficiencies have been achieved with ILs when they have been used almost as an additive in an aqueous or acidic solvent. Hu et al. presented a 93.8 % efficiency in the extraction of Cu in an aqueous solution of 10 % [Hmim]HSO₄ with 25 % H₂O₂ added as an oxidant.¹⁸ Carlesi et al. presented a similar scenario and determined that the IL was acting like a catalyst in conjunction with the sulfuric acid used in their system.¹⁶ They proposed that this was a result of the IL allowing continuous acid leaching of the surface chalcopyrite by reducing any hydrophobic resistance between the acid and the solid surface.¹⁶ The IL leaching of chalcopyrite has been described complex and the nature of the anion has a significant effect on the dissolution behaviour.¹³ The cationic component has been shown to have much less of an effect than the anion. In a selection of ILs based on [Bmim]⁺ with varying anions, [HSO₄]⁻, [NO₃]⁻, [N(CN)₂]⁻ and [OAc], the leaching rate was highest with [HSO₄]⁻, and slowest with [OAc]⁻. Interestingly, the [N(CN)₂]⁻, [NO₃]⁻ and [OAc]⁻ anions are all more basic than [HSO₄]⁻, however the leaching rate was not correlated to pH. Interestingly, in ILs, it has been found that the formation of CS₂ gas during leaching led to a decrease in the sulfide passivation layer therefore increasing the rate of leaching.¹³

The process by which chalcopyrite leaches, including the formation of a passivation layer, is often described kinetically using the “shrinking core model”.¹⁹ This model, shown schematically in Figure 5.3, describes the addition of reaction material (sulfide/polysulfide) on the surface of each chalcopyrite grain, causing the core (the chalcopyrite) to ‘shrink’. As more passivation occurs on the surface the core shrinks even more, making it increasingly harder to leach the chalcopyrite.

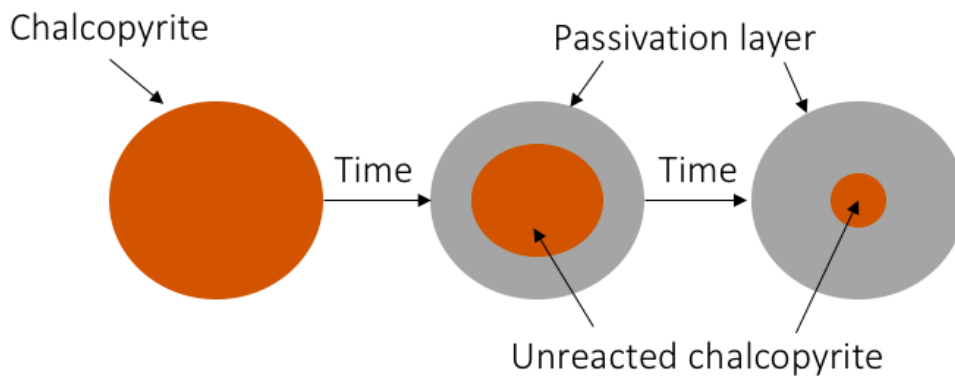


Figure 5.3: A schematic of the shrinking core model of mineral dissolution, demonstrating the kinetics of chalcopyrite dissolution and the formation of the passivation layer.¹⁹

5.1.4 Aims

The aim of this chapter is to electrochemically analyse chalcopyrite in Ethaline to determine its suitability for dissolution and extraction. The main aim is to see how minerals with two redox active metals behave and whether it is possible to separate metals with significantly different redox potentials.

The main objectives from this Chapter are:

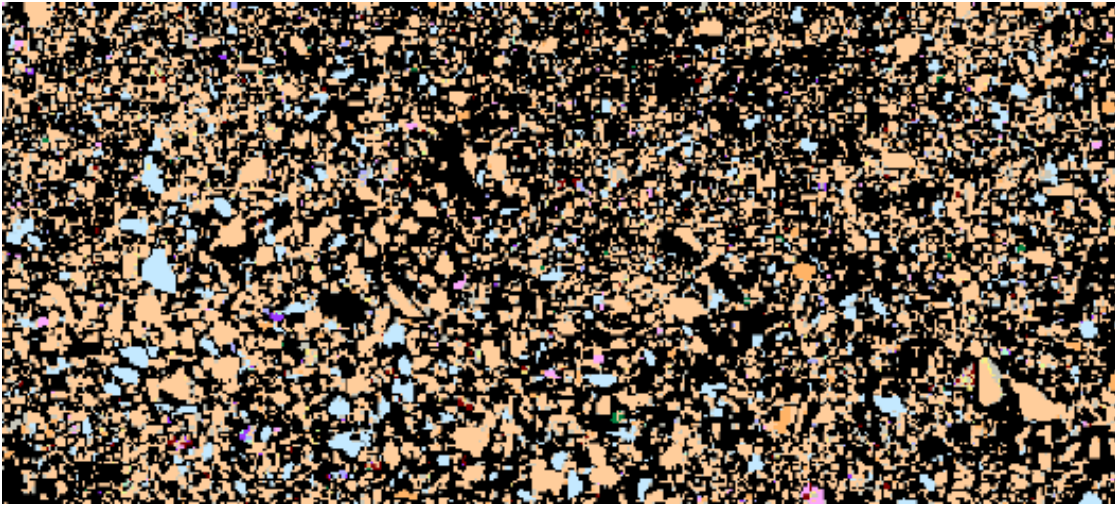
1. To investigate the electrochemical properties of multi-metal minerals using paint casting voltammetry.
2. To utilise the paint casting method to leach and ultimately recover the Cu from the chalcopyrite, in the same way that it was recovered from the Cu sulfides in Chapter 3.
3. To optimise a cell design that was previously developed for the extraction of metals from a mining waste, in order to develop a more efficient method of Cu extraction.

5.2 Analysis of chalcopyrite

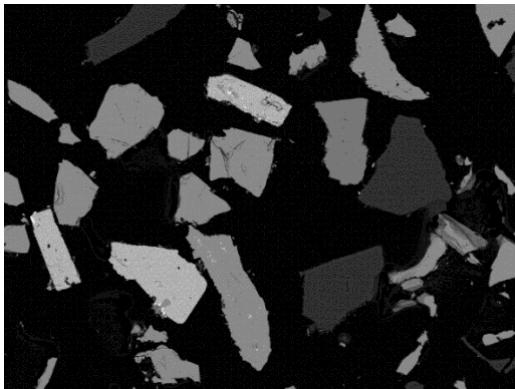
5.2.1 Chalcopyrite sample analysis

The majority of the chalcopyrite used in these investigations was obtained from a mine in Morocco and presented in large pieces of between 4 cm³ and 8 cm³. Generally, the chalcopyrite would be described as massive, with some very sharp crystal faces visible with no host rock present. The chalcopyrite itself has the typical appearance of a dark golden lustre with some small areas of iridescent blue/purple (possibly from some acid weathering). There appears to be some minor secondary weathering effects of the chalcopyrite, as demonstrated by the green chalky-looking deposits on a few areas of the chalcopyrite (see Figure 5.1b). From visual observations, the other major minerals associated in this sample of chalcopyrite are quartz and a very small amount of bladed calcite. The quartz appears to post-date the chalcopyrite from the textural relationships shown in several areas of the sample and is present in both distinct veins and vugs. Generally, the quartz in the veins is anhedral and the vugs are very much euhedral. The sample of chalcopyrite was analysed by EDAX to determine the purity of the sample and any other minerals or materials that are present in the sample that could ultimately affect its electrochemical behaviour.

a.



b.



c.



Figure 5.4: a. Section of the overall coloured chalcopyrite mineral map. b. back scattered electron image from a small section. c. Corresponding mineral map image to the back scattered electron image. (beige = chalcopyrite)

Table 5.1: Table describing the composition and occurrence of minerals in the electron image from Figure 5.4a.

Mineral (colour)	Average composition	Wt %	Number
Chalcopyrite (beige)	Cu 34.62; S 33.3; Fe 32.09;	80.54	26341
Quartz (blue)	Si 59.48; O 40.33; S 0.18; Al 0.01; K 0;	10.7	5315
Pyrite (orange)	S 49.71; Fe 49.67; Cu 0.53; Ti 0.09;	3.89	4464
Galena (mauve)	Pb 92.83; S 7.17;	1.34	780
Magnetite (red)	Fe 68.75; O 28.07; Mn 2.2; S 0.97;	1.17	1046
Barite (pink)	Ba 69.3; S 16.77; O 13.94;	1.04	629
Covellite (yellow)	Cu 66.25; S 26.63; Fe 7.12;	0.76	1515
Sphalerite (dark green)	Zn 64.81; S 33.28; Fe 1.91;	0.20	213
Clinopyroxene (purple)	O 47.27; Fe 25.84; Ca 21.3; Mg 3.98; Si 1.55; Al 0.06;	0.15	358
Chalcocite (green)	Cu 77.03; S 19.22; Fe 3.75;	0.13	290
Gypsum (turquoise)	O 45.11; Ca 32.13; S 22.76;	0.08	169

It can be seen that there are more impurities in this sample compared to the samples of chalcocite and covellite used in Chapter 3. The average composition of the chalcopyrite in this sample is 34.62: 33.3: 32.09 for Cu: S: Fe, which is similar to the standard ratio of elements in a typical chalcopyrite mineral (34.63: 34.94: 30.43). The sample is predominantly made up of chalcopyrite (80.5 wt. %) with the most common impurities being quartz and pyrite with a few other sulfides and oxides as shown in Table 5.1. In the case of this sample the association data cannot be used as easily as with the covellite and chalcocite data from earlier, as each individual particle in the resin is too close to other particles, giving misrepresentative associations. However, it is possible to see just by looking at the coloured mineral map data that the particles are generally separated into individual minerals with minimal inclusions, especially when it comes to the chalcopyrite. The same is true for the back scattered electron image shown in Figure 5.4 b, it is possible when compared to the coloured diagram indicating the different mineral areas that the varying grey scale also indicates those separate mineral phases.

5.2.2 Paint casting chalcopyrite

The Pourbaix diagram and consequently the electrochemistry of chalcopyrite is significantly more complex than any of the diagrams presented so far. The addition of another metal (Fe) means that species are present for each metal and their separate oxidation states, the oxides of each metal, the sulfur containing species of each metal, and the mixed metal sulfide species, causing the inherent complexity of the diagram.

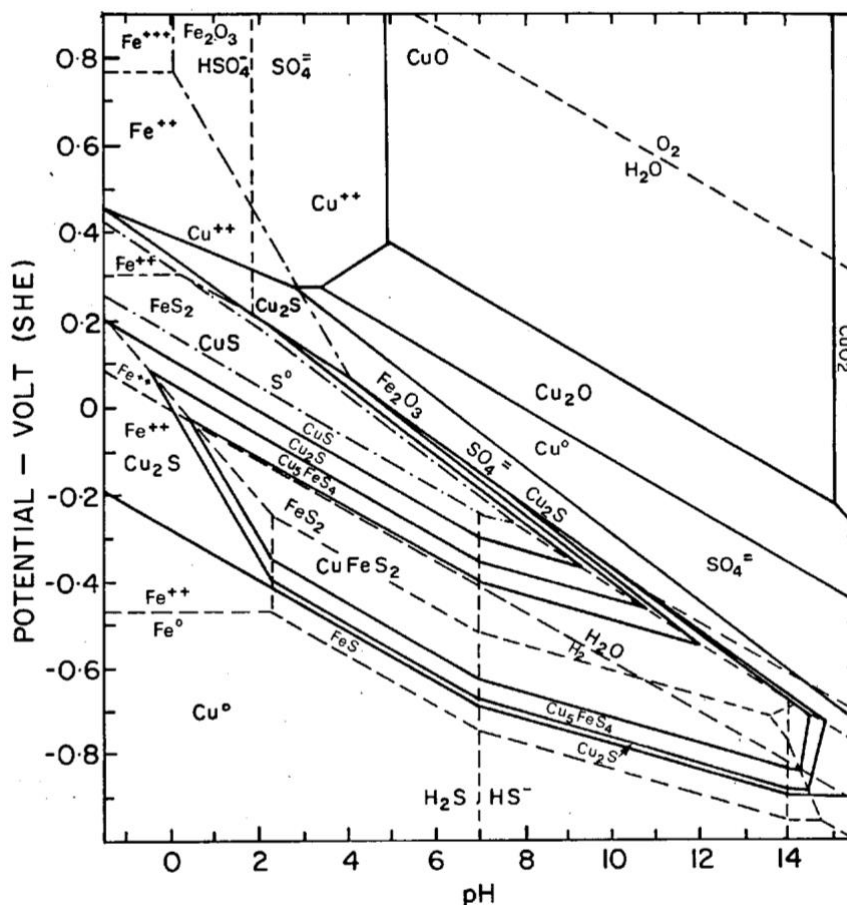


Figure 5.5: Pourbaix diagram for a $\text{CuFeS}_2\text{-H}_2\text{O}$ system.²⁰

From the Pourbaix diagram in Figure 5.5, Cu reactions dominate the oxidative environment, specifically above 0.4 V, whereas the Fe redox reactions are more prominent in the reductive environment. Fe^{II} species are already present at much more cathodic potentials (-0.45 V) but only in a more acidic environment (< pH 2), which is important as it is likely to affect the leaching of Cu. It can be seen that the conditions required for Cu oxidation in order to leach and successfully extract the metal are a reasonably oxidative potential (above 0.4 V) and an acidic pH (around 5 or lower). It can

also be seen that during the leaching of Cu from chalcopyrite, several other Cu oxide and sulfide intermediate species are accessible. As with the previous Pourbaix diagrams presented in both Chapter 3 and 4, the discussion of a chloride environment is the same as here. It has already been shown through the addition of another metal into the system that the complexity increases, and a similar scenario is true for when there is a high chloride environment. This introduces the likely occurrence of chloride species for both Cu and Fe metals in solution.

The paint casting voltammogram of crushed chalcopyrite mineral is shown in Figure 5.6a. It exhibits 3 cathodic peaks and 2 anodic peaks, similar to that obtained with covellite in Chapter 3. It does not mirror the inherent complexity exhibited in the Pourbaix diagram. Interestingly, despite the mineral containing Fe as well as Cu, there are no additional peaks present compared to the CuS CV. From the position of both the Cu^{II/I} and Fe^{III/II} couples reported previously in Ethaline, they could be expected to overlap at the same potential and therefore appear as 1 peak.

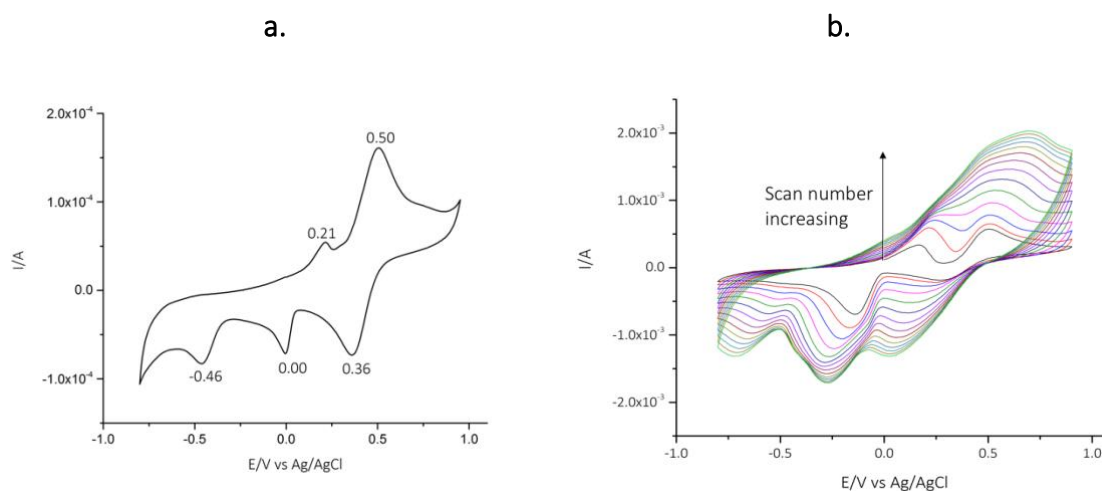


Figure 5.6: The paint casting cyclic voltammograms of **a.** chalcopyrite powder and **b.** chalcopyrite powder cycled 15 times, increasing scan number from black line (inside) to green line (outside). All voltammograms were conducted in Ethaline using a 1 cm² Pt flag working and counter electrodes and an Ag/AgCl [0.1 M in Ethaline] reference electrode, scanned at 5 mVs⁻¹

The paint casting of pyrite (FeS₂) has also been reported in the literature,²¹ interestingly, in this study 2 separate results were obtained for a paint cast CV of natural pyrite.²¹ One

result indicated 2 oxidation peaks and 3 reduction peaks, very similar to that obtained in Figure 5.6a. The other result, also reported in the same paper indicated 4 distinct reduction peaks and 3 oxidation peaks. It is likely that this is due to the presence of impurities or other minerals, similarly in the results shown in Figure 5.6 these peaks could potentially be a result of pyrite (or other mineral) impurities in the sample. However, it is proposed that the peaks in the voltammogram in Figure 5.6 can be assigned in the same way as the CuS CV from section 3.2. Whereby the Cu^{II/I} redox couple is present at 0.3/0.45 V and the couple at -0.3/0.16 can be ascribed to the same sulfide/sulfur redox as before. This is also supported by the analysis in the pyrite paper where it was suggested that the reduction peak at ~ -0.45 was as a result of a sulfur/sulfide species similar to Manan.²² For the CV in Figure 5.6a it is also proposed that any peaks related to Fe species are being hidden by the Cu redox couple, possibly providing an explanation of why it looks similar to the previous pyrite CV. Interestingly, in both CV's in Figure 5.6 the Cu^{I/0} oxidation peak that is in the CuS/Cu₂S from Chapter 3 and CuCl₂ from Chapter 2 is not present. Chalcopyrite electrochemistry has previously been investigated and it is suggested that the overall process is made up of oxidation of chalcopyrite via Equation 5.2²³ coupled with the subsequent reduction of those species.

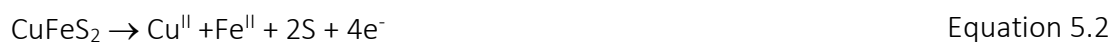


Figure 5.6b also shows the result of several repeats of the chalcopyrite voltammogram; interestingly the anodic peaks merge to form one larger peak after scan 4. This could signal the mechanism of how the chalcopyrite is dissolving anodically. In the literature, the formation of a passivation layer on the surface of the chalcopyrite is observed. This CV suggests that this is not the case in Ethaline as you would expect the current to decrease with increasing scan number. In comparison to 30 scans of a CuS CV, the 2 oxidation peaks at around 0.15 V and 0.50 V remain clearly resolved and do not merge together like in Figure 5.6.

5.2.2 Electrochemical dissolution and recovery

The electrochemical dissolution of chalcopyrite was carried out using bulk electrolysis with 2 iridium coated Ti mesh electrodes, as described in section 2.4, and the pale-yellow solution obtained is shown in Figure 5.7. This has a similar colour, to that obtained from the electrolysis of CuS and Cu₂S Chapter 3. Al-Bassam conducted a similar dissolution on pyrite, this formed a yellow/brown coloured solution which was attributed to Fe^{III} in solution and developed a precipitate after being left in air for 3 days, which was ascribed to the formation of an oxide or hydroxide of Fe.²⁴ No precipitate developed in the solution in Figure 5.4, which remained the same colour for several weeks after. The solution was analysed by UV-Vis, CV and EXAFS, and the results are presented in Figure 5.7 a & b and Figure 5.9 respectively.

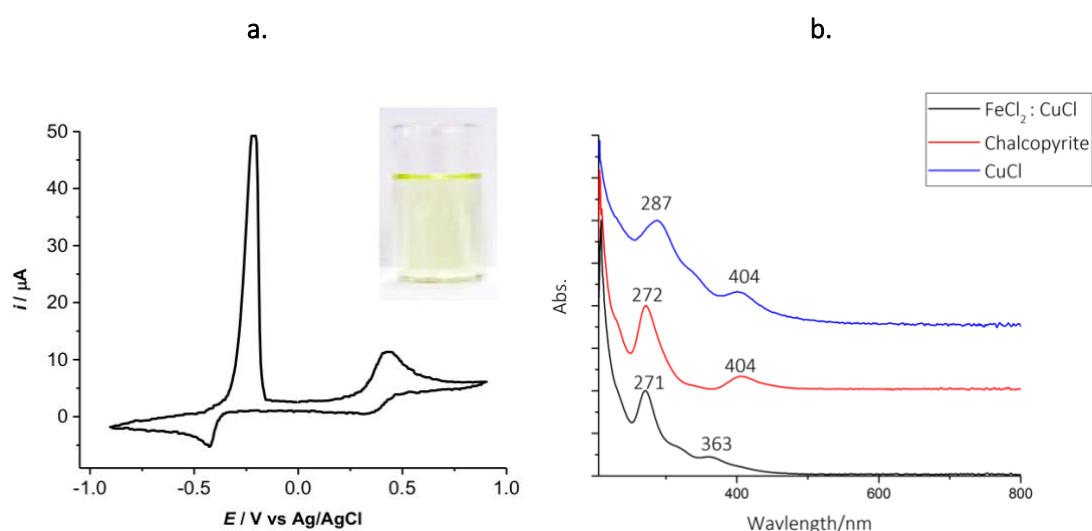


Figure 5.7: **a.** CV from the solution obtained in the bulk dissolution (1.5 V for 24 hours) of chalcopyrite (inset: picture of solution) conducted on 1 mm Pt disk electrode and Ag/AgCl [0.1 M in Ethaline] and **b.** UV-VIS (offset for clarity) of the same solution, overlaid with a solution of CuCl and a 1:1 molar ratio solution of CuCl:FeCl₂.

The CV in Figure 5.7a supports the absence of Fe species in the solution, as it appears to be almost identical to the CV of a solution of CuCl₂ in Ethaline (shown in section 2.2). As with the previous paint casting CVs there is a possibility that the Fe^{III/II} redox couple is being masked by the Cu^{II/I} couple. To test the effect that the presence of Fe^{II} or Fe^{III}

complexes may have on a Cu solution, 4 different solutions were made each containing 1:1 molar ratios of CuCl:FeCl₂, CuCl:FeCl₃, CuCl₂:FeCl₂ and CuCl₂:FeCl₃ (Figure 5.8). It is shown that the addition of FeCl₃ specifically changes the UV-Vis and extra peaks around 300 nm are present. The spectrum of CuCl:FeCl₂ matched the closest, indicating that any Fe species present is probably in the 2+ oxidation state. The presence of Fe^{II} in solution as opposed to the more likely Fe^{III} that would be expected to be liberated during the electro-dissolution, could possibly be explained by a reduction of the Fe^{III} at the cathode or be the sulfur/sulfide species in solution during the course of the experiment.

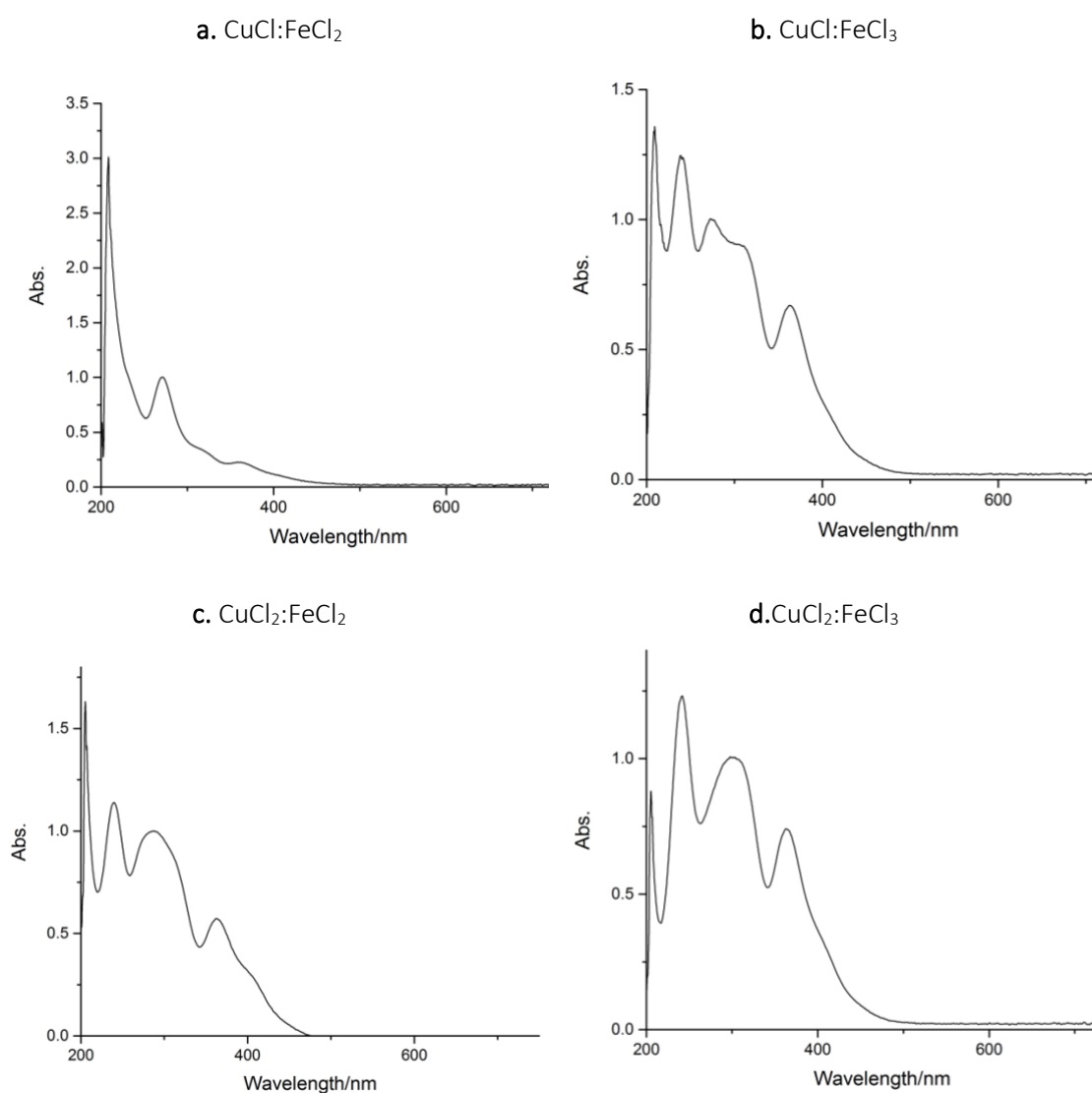


Figure 5.8: UV-Vis spectra of solutions of Ethaline with 1:1 molar mixtures of CuCl, CuCl₂, FeCl₂ and FeCl₃.

The UV-Vis in Figure 5.7b is shown overlaid with a solution of CuCl: FeCl₂ (also in Figure 5.8a) and a solution of CuCl only. The chalcopyrite shows 2 absorbance maxima (272 and 404 nm), the peak at 272 nm is also present in the CuCl: FeCl₂ UV-Vis whereas in the CuCl plot, this peak is shifted by 15 nm. The opposite is true for the peak at 404 nm which is also present in the CuCl plot but is shifted in the solution containing CuCl: FeCl₂ by 41 nm. Figures 5.8b and c are clearly similar and this is due to Fe^{III} oxidising Cu^I to produce Fe^{II} and Cu^{II}.

The suspected Cu species in solution is supported by the results from XANES and EXAFS data, whereby the presence of Cu(I) species similar to that shown for the Cu₂Se data was exhibited (see section 3.5). As with the Cu₂Se data, only a single scan was performed, and the solution was very dilute. This gave a much noisier spectra, however a data fit suggested a coordination of $3.0 \pm 0.4 \times \text{Cl}$, with a path length of $2.21 \pm 0.01 \text{ \AA}$ to the Cu, as shown by the parameters in Table 5.2. There was a large degree of error in this measurement, however the support from the UV-Vis means that it can still be assumed with a reasonable degree of confidence.

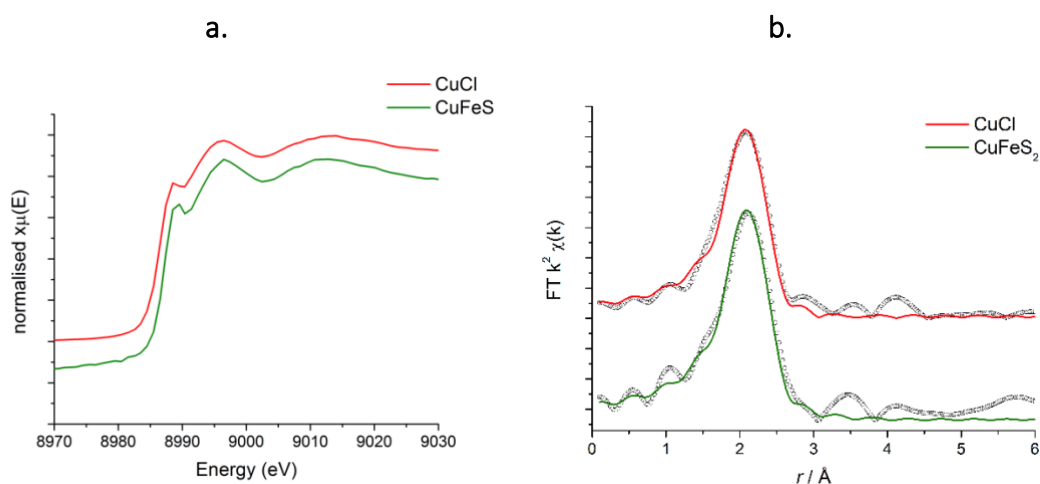


Figure 5.9: *a.* XANES and *b.* Fourier transforms of solutions of CuCl (red) and CuFeS₂ (green) in Ethaline. CuFeS₂ solution obtained from electrochemical dissolution at 1.5 V for 24 hours with IrO₂ coated Ti mesh electrodes. Data are circles, fits are lines.

Table 5.2: The data fit parameters for the results shown in Figure 5.7.

Solute	Coordinating atom/group	Number atoms, <i>N</i>	Distance from Cu, <i>r</i> /Å	Debye-Waller factor, <i>a</i> (Å ²)	Fit index, <i>R1</i> /%
CuCl ₂ *	Cl	3.7 (2)	2.252 (5)	0.008 (1)	4.48 %
CuCl *	Cl	2.4 (2)	2.190 (9)	0.016 (3)	8.08 %
CuFeS ₂	Cl	3.0 (4)	2.21 (1)	0.019 (5)	15.21 %

* from reference²⁵

The Fe concentration in this solution was too low to be able to obtain data with a good signal-to-noise ratio, therefore it is not possible to confirm the speciation or oxidation state of iron in solution via EXAFS. Nevertheless, it has been shown previously that iron chloride salts form either [FeCl₄]²⁻ or [FeCl₄]⁻, depending on the Fe oxidation state.²⁵ Normal dissolution and electro-dissolution seem to have no obvious effect on the speciation and coordinating ligand for copper in Ethaline, it is proposed that any soluble Fe species formed during electro-dissolution are also likely to be the chloride species. Also, no Cu-Fe paths were observed in any of the Cu-edge data, therefore it is unlikely that mixed-metal species are present in solution.

Near-edge measurements supported the observations from the UV-Vis that the oxidation state of the electro-dissolved Cu changed based on the chalcogen species or the presence of any other metals (Fe) in the material. It is suggested that the change in Cu oxidation state of this particular case with chalcopyrite could be explained via electrode potentials. In Ethaline, the formal electrode potentials for the Cu^{II/I} and Fe^{III/II} couples are +0.349 V and +0.293 V respectively (vs. a [Fe(CN)₆]^{3-/4-} internal standard). It is therefore possible that any Fe^{II} formed during the electrolysis is ultimately reducing Cu^{II} to Cu^I. There is no Fe present in either the CuS or Cu₂S systems reported in Chapter 3, hence the copper species retain the higher oxidation state rather than being reduced to Cu^I in solution.

Finally, following the same process as in Chapter 3, a bulk electrolysis recovery experiment was done in an attempt to recover the Cu. In Chapter 3, it was shown that regardless of what chalcogen was coordinated with the Cu, it was always possible to

obtain pure Cu on a Ni cathode after this experiment. In the case of pyrite from the previous work by Al-Bassam,²¹ a similar experiment was carried out, showing that after electrolysis Fe had been recovered along with significant amounts of S, O and C. It was determined that no elemental Fe was deposited (due to lack of magnetism) and instead it was a mixture of Fe oxides, sulfides and potentially glycolates. The deposit shown in Figure 5.10, achieved by applying a constant 1.5 V for 24 hours, was mostly Cu with a small amount of Fe sulfide, which is likely to have been trapped on the surface during the electrodeposition of Cu.

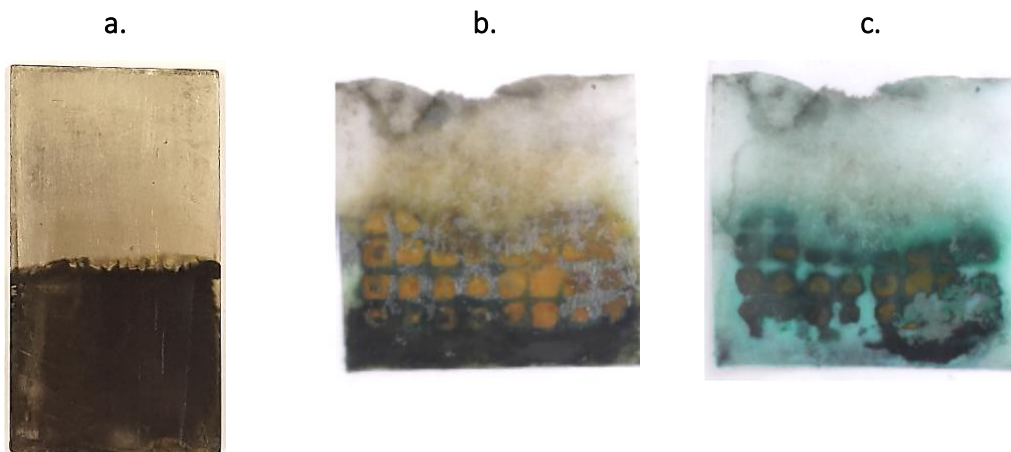


Figure 5.10: a. Ni cathode after the chalcopyrite bulk electrolysis experiment (1.5 V for 24 hours in Ethaline). Filter paper membrane from the bulk electrolysis of CuFeS_2 immediately after the experiment and 1 week after.

An issue that occurred during all bulk electrolysis experiments was the build-up of material on the filter paper membrane, as shown in Figure 5.10 b & c. It was determined in the study by Al-Bassam that the membrane was adding resistance to the cell which was ultimately causing the current to drop and the dissolved metal species in solution to plateau.²⁴ Once the metal has been electrochemically dissolved in one side of the cell, it must diffuse through the membrane to reach the other side containing the cathode. Once the membrane is saturated with the metal species, the diffusion gradient is reduced therefore leading to slower diffusion and hence reduced recovery rate. This phenomenon has also been demonstrated by Hartley, using a filter paper membrane in the recovery of Cu from a Cu-In-Ga alloy.²⁶ The Cu was reduced by the sugars in the membrane and resulted in crystals of Cu forming on the surface, again affecting the rate of the process.

5.3 Cell design

In a previous investigation the recovery of Pb, Fe and Zn from a mining waste (jarosite) was trialled using the same cell from the previous section. In both experiments, the filter paper membrane became saturated, decreasing the rate the diffusion and hence prohibiting the recovery. Therefore, a new cell type was designed to improve the rate of recovery, as well as the space time yield. The cell, (Figure 5.11) was a scaled-up design (~500 g of mineral), whilst also reducing the necessary ratio of material: solvent from about 1:14 to 1:1.7.

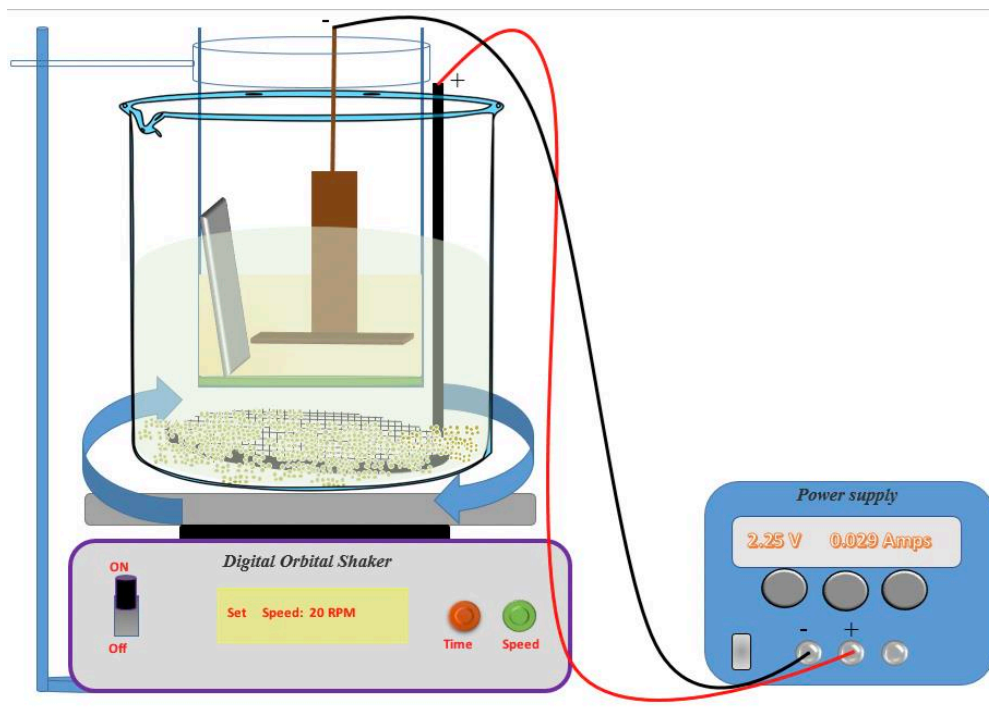


Figure 5.11: The cell used in a previous investigation by Al-Bassam in the recovery of Pb, Fe and Zn from a sample of jarosite using a copper cathode in the top cell with a zinc sheet for cementation and an IrO₂ coated titanium anode in the bottom section for dissolution.²⁴

One main improvement with Al-Bassam's cell over the cell with filter paper separators, aside from the reduction in the solvent necessary is the constant movement of the cell. This enables the material being processed to be continually agitated allowing it all to come into contact with the anode to be oxidised. Instead of using a filter paper membrane to separate the anodic and cathodic areas of the cell, a porous glass

bottomed beaker was used as the cathodic compartment. The glass frit had 2 μm pores, with the idea being to decrease the resistance by reducing material precipitating on the surface. This was partly successful, but by the end of the experiment a large amount of material precipitated had within the glass frit. Due to the smaller amounts of chalcopyrite material available, this particular cell was deemed unnecessarily large (5L). However, in order to improve on this cell further it was necessary to further reduce the precipitation in the separation membrane.

5.3.2 Nylon membrane

To prevent precipitation of metal species, a membrane with a large surface area and larger pore sizes was employed. A piece of thin nylon fabric with pore dimensions $\sim 40 - 60 \mu\text{m}$ was stretched over a plastic tube with large (5 mm) holes. An issue with this approach is that particles smaller than 100 μm were able to pass through the nylon membrane, and therefore it is necessary to use a range of particle sizes that will be suitable for this experiment (1000 – 100 μm).

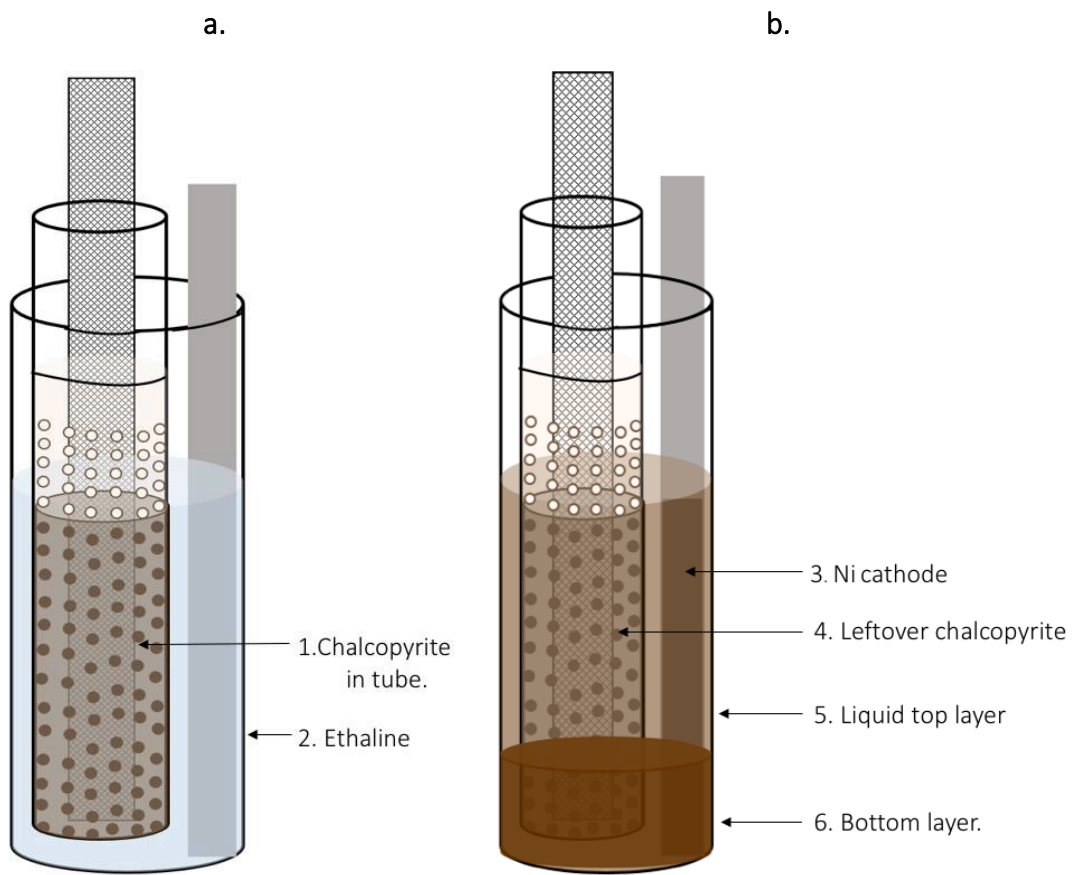


Figure 5.12: *a.* A schematic of the cell design before, showing glass tube containing Ethaline, Ni cathode and porous plastic tube that contains the chalcopyrite powder and IrO₂ coated Ti mesh anode. *b.* after the experiment for the recovery of copper from bulk chalcopyrite.

Figure 5.12 shows a schematic diagram of the cell design and shows the phase behaviour before and after electrolysis. The ratio of mineral: solvent was 1:2.3. The Ni cathode was replaced every 24 hours for 5 days without replacing the Ethaline or the sample of chalcopyrite. Following the 5-day experiment, the cell appeared as shown in Figure 5.12b. The Ethaline appeared a pale brown colour and a dark brown 'sludge' had formed in the bottom of the cell. The descriptions and masses for each aspect of the cells in Figure 5.12 are shown in Table 5.3.

Table 5.3: Descriptions and masses from labels in Figure 5.9

Number	Mass	Description
1	45 g	Powdered chalcopyrite (1000 – 100 μm).
2	102 g	Ethaline
3	0.34 g	Overall material on 5 Ni cathodes
4	55.6 g	Left over chalcopyrite paste with Ethaline
5	27 g	Brown liquid top layer
6	2.1 g	Brown sludge bottom layer (after wash and dry)

All experiments discussed in this chapter were carried out at room temperature, and this particular experiment proceeded by applying a constant current of 5 mA for 24 hours to the sample. The Ni cathodes were replaced every 24 hours and washed with distilled water and dried before being weighed and photographed. At the start of each 24 hour experiment the measured voltage was around 1.8 V which increased to around 2.5 V through the course of the experiment.

Using such a low current was necessary to prevent degradation of the liquid, however this also means that the possible mass of Cu that can be extracted from the chalcopyrite is low. The charge passed over the course of the experiment is 2160 C (at a constant 0.005 A over 43,200 s). If 100 % efficiency is assumed, then the amount of Cu that could be extracted is 0.7 g over the course of the entire experiment (or 0.14 g per Ni cathode). The actual results obtained in the experiment reveal a lower mass than this, whereby the overall mass across the 5 Ni cathodes at the end of 120 hours was 0.34 g (of all material not just Cu). Interestingly, as each plate was replaced, the mass of material extracted remained stable, (i.e. plate 1 weighed 0.05g and plate 5 weighed 0.07g) suggesting that a passivation effect, over the course of the experiment was not causing a decrease in extraction ability over time.

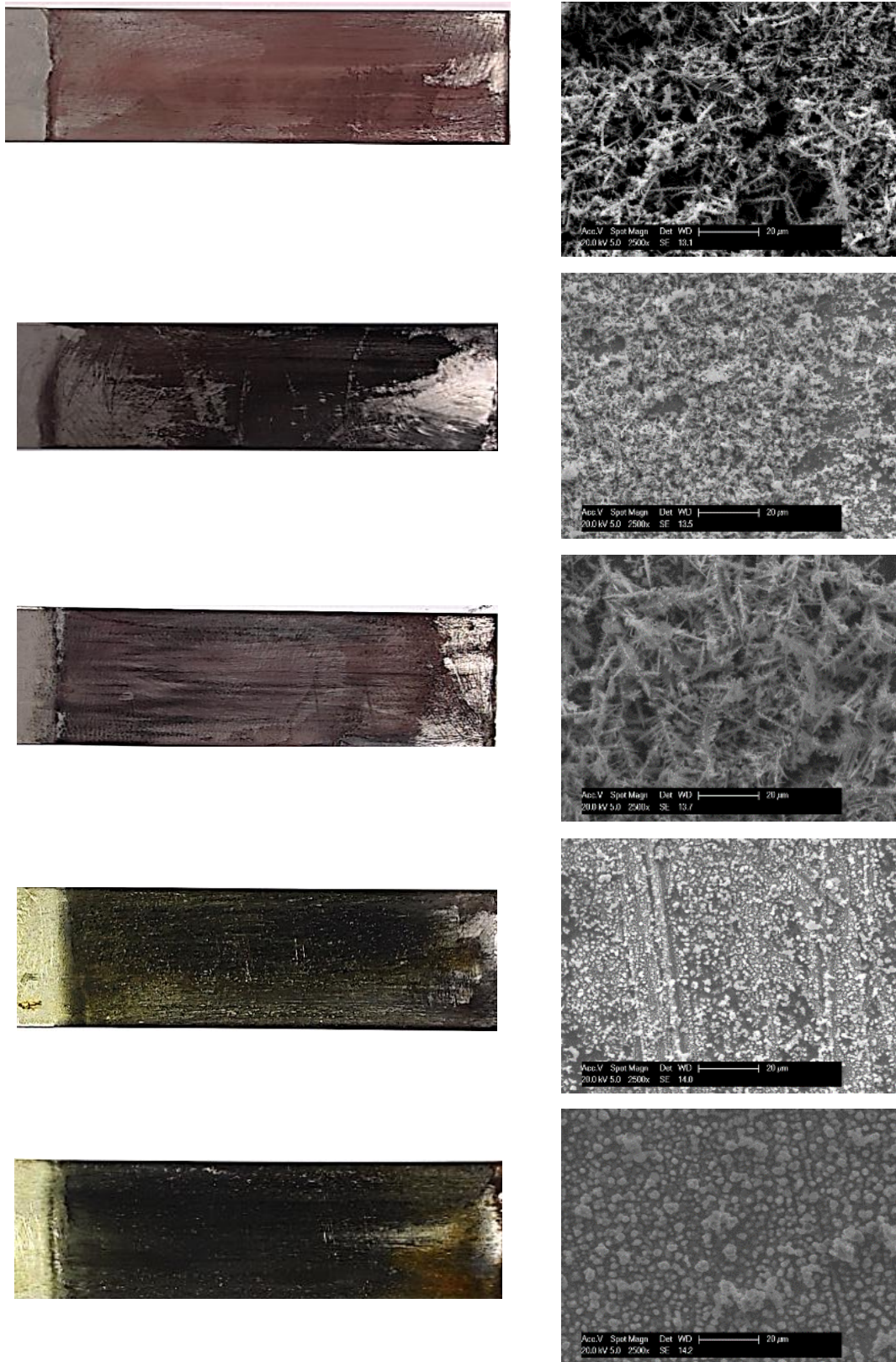


Figure 5.13: 5 consecutive Ni cathodes after their subsequent 24 hour experiments at 5 mA in Ethaline and their corresponding SEM images from the experiment in Figure 5.9.

The Ni cathodes shown in Figure 5.13 were then examined by EDX to determine the elements that had been recovered. The initial plate, was significantly more copper coloured than the subsequent plates and only showed Cu in the elemental analysis. Cathodes 2-5 showed a successive decrease in the Cu content and an increase in the atomic % of Fe. There is a concomitant increase in the sulfur content. It is proposed that this is due to the Fe becoming liberated on electrochemical dissolution of Cu from the chalcopyrite. The liquid in the cathodic compartment became progressively darker in colour and it was clear that this was not a homogeneous solution but rather a colloidal dispersion, most probably from an iron-based material. Figure 5.13b shows a typical dendritic crystalline structure expected for copper deposition from a DES.²⁷ However, as the Fe content increases the deposit becomes less crystalline and more amorphous. There are clear differences in the phase behaviour in Figure 5.13f where both amorphous and crystalline materials can be seen, probably showing an iron sulfur deposit 'trapped' in a copper matrix. This is suggested from the colour of the solution, as over the course of the experiment, the electrolyte in the cell went from a pale-yellow indicative of Cu-chloride species, to a dark brown solution, suggesting the presence of Fe. When the solution was filtered however, the solution remained yellow in colour but with a dark brown precipitate, indicating that it is only the copper that remains soluble.

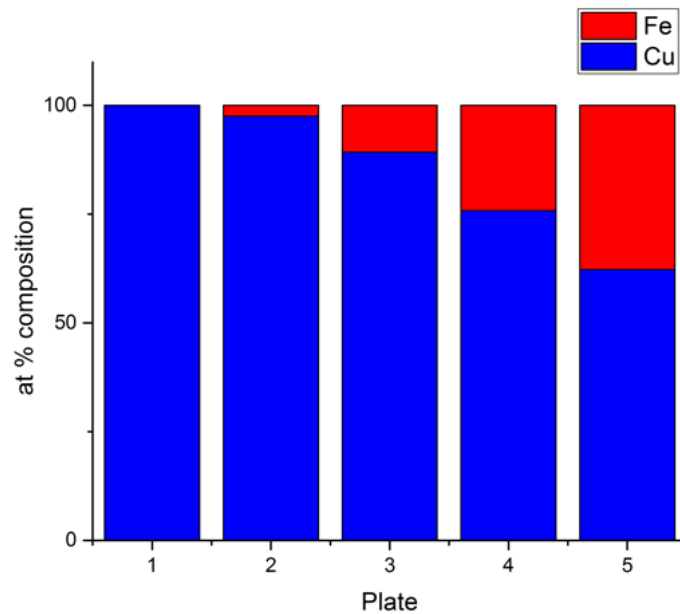


Figure 5.14: Demonstrating the ratio of Fe:Cu in the deposits obtained on 5 consecutive Ni cathodes (each 24 hours at 5 mA in Ethaline) from the experiment in Figure 5.9.

The leftover liquid obtained in the cathodic compartment was filtered and analysed by UV-Vis and CV and the results are shown in Figure 5.15.

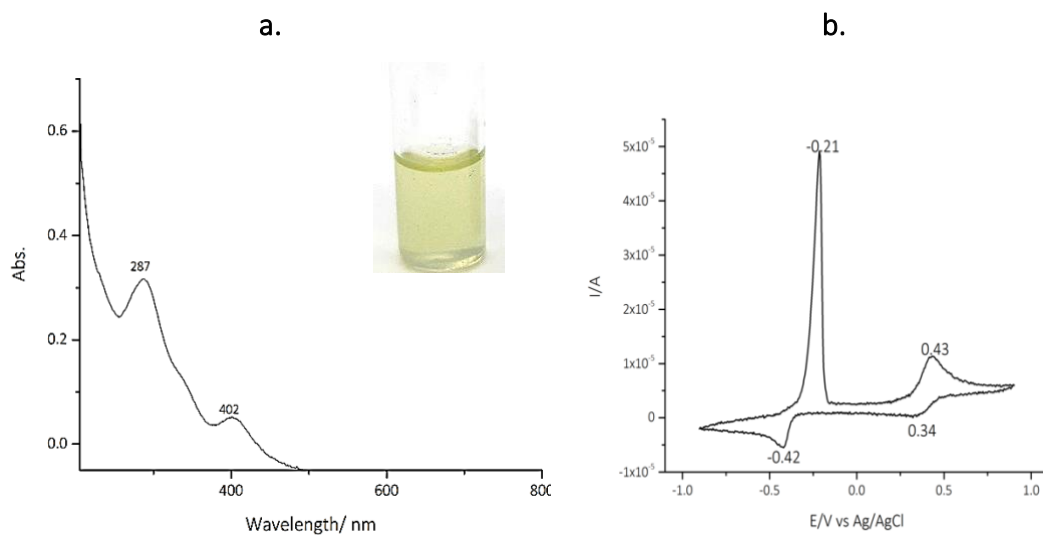


Figure 5.15: a. The UV-Vis of the solution from the liquid top layer (marked as 5 in Figure 5.9) b. The CV from the same solution conducted with a 1 mm Pt disk working electrode, Pt flag counter and Ag/AgCl [0.1 M in Ethaline] reference electrode.

These results indicate a presence of Cu in the solution, and the CV is similar to that of CuCl_2 in Ethaline. There does not appear to be appreciable amounts of Fe in solution. The iron is therefore probably in the suspended colloidal phase. The fate of the sulfur is unknown but analysis of the Pourbaix diagram for sulfur would predict the formation of sulfate. This is indeed one of the fates of sulfur electrolysed from minerals such as pyrite in aqueous solutions. The Ethaline from the cathodic compartment was also tested with $\text{BaCl}_{2(\text{aq})}$ which subsequently turned cloudy indicating the presence of sulfate in solution. This shows that at least some of the sulfur is oxidised to sulfate during the electrolysis of chalcopryrite in Ethaline.

EDX and XRD of the leftover chalcopryrite at the end of the experiment (label 4 in Figure 5.12), revealed, as expected, that some full chalcopryrite grains were left over with no change in mineralogy. This indicates that full grains of chalcopryrite, or at least surface chalcopryrite, had been dissolved, as opposed to Cu being liberated from the mineral and leaving and Fe sulfide complex behind. XRD cannot conclusively prove this, however, since the signal at $2\theta = 29$ is the same for pyrite (111) and chalcopryrite (112), although none of the other characteristic pyrite reflects are observed.

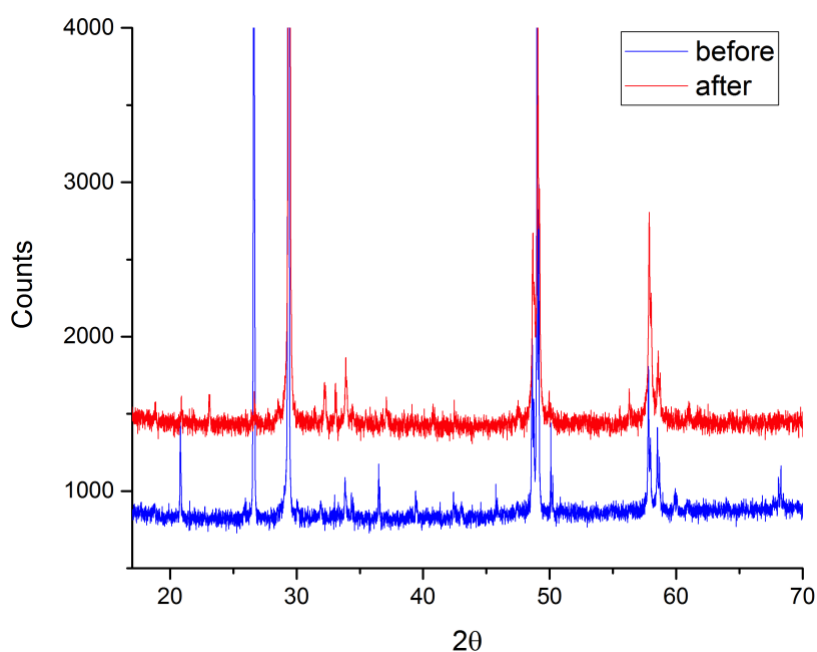


Figure 5.16: XRD patterns of the chalcopryrite before (blue) and after (red) the extraction experiment, indicated by the labels 1 & 4 in Table 5.3.

The 'sludge' layer was filtered, washed with D.I. water and dried in air before being analysed by EDX and XRD. The XRD results revealed that it was a completely amorphous unidentifiable material, that could not be matched to other patterns. The EDX results indicated a mix of Cu, Fe, S and O with 10.5, 17.1, 36.2 and 36.2 at % respectively. This mixed material clearly suggests that the dissolution process liberates Cu, Fe and S in roughly stoichiometric quantities, but the sludge is deficient of copper (collected on the cathode) and some sulfur (in the form of sulfate) in solution. The S:O ratio shows that the sulfur cannot all be in the form of sulfate. The lack of carbon would suggest that the iron is not present as a glycolate, however, the C was removed from the EDAX results due to the use of carbon conductive stubs. It is possible that the Fe is forming a glycolate as was observed from the anodic dissolution of iron during electropolishing.^{28,29}

5.4 Hybrid DESs

Hybrid DESs are simply mixtures of the different DES components in varying molar ratios. The use of hybrid DESs (usually in the form of mixed HBDs) opens up the potential to tune the properties of the lixiviant. Metals and metal salts have been shown to exhibit varying solubilities in different DESs, and it could reasonably be expected that hybrid DESs could be used in targeted metal dissolution and recovery processes.^{30,31} An example of this was in a study of metal extraction from EAF dust. An electric arc furnace (EAF) is commonplace in steel production and is used in the re-melting of steel scrap. It is necessary to pass around 450-500 kWh tonne⁻¹ through scrap steel to generate molten steel. In this process a large amount of dust (~15-20 kg) is produced with considerable metal content (Pb, Zn and Cd). Reline had previously been shown to be a suitable solvent in selectively extracting Zn and Pb from the dust. However, Reline has a high viscosity (~800 cP)³² making it difficult to work with. In order to reduce the viscosity and make pumping and filtering the solution easier, different amounts of ethylene glycol were added. A molar ratio of 1 choline chloride: 1.5 ethylene glycol: 0.5 urea resulted in the viscosity dropping to 56 cP. The main aim of using this particular hybrid DES was to maximise the solubility potential while minimising the viscosity of the solution.³²

In this chalcopyrite investigation the use of Ethaline alone showed a gradual increase in the amount of Fe extracted along with the Cu. To avoid this, small amounts (20 wt %) of

a more acidic (Oxaline 100) or a more basic (Reline 200) DES were added to Ethaline to investigate their effect on Cu recovery. It was proposed that altering the HBD could alter the speciation and complex stability of the Fe complexes, in turn altering the reduction properties of the Fe without affecting the Cu.

5.4.1 Reline and Oxaline

Reline 200, a 1:2 molar mixture of choline chloride and urea and has been shown to be one of the more basic DESs (pH ~ 8.9),³³ whereas Oxaline 100, a 1:1 mixture of choline chloride and oxalic acid, is a fairly acidic DES (pH~1.32).³³ The solubilities of metal salts are likely to depend on the relative proportions of ligands in the liquid. A previous study by Abbott et al.³¹ investigated the solubility of different metal oxides in a variety of solvents, including 3 DESs. For CuO and Cu₂O, the solubilities in Ethaline and Reline over 48 hours were similar, 394 ppm (Ethaline) and 219 ppm (Reline) for Cu₂O and 4.6 ppm (Ethaline) and 4.8 ppm (Reline) for CuO. In the more acidic DESs, Maline (1:1 malonic acid: choline chloride), these copper oxides showed a considerably higher solubility, with 18337 ppm and 14008 ppm for Cu₂O and CuO respectively. This is more comparable to more conventional aqueous acid leaching solutions. This claim of acidity enhancing the rate of solubility of metal salts is supported by Alabdullah³³ investigated the solubility of metal oxides in different DESs. It was again found that Maline and Oxaline both showed higher solubilising ability than both Reline and Ethaline and correlated the solubility of metal oxides to the pH of the liquid.

One issue with both Oxaline and Reline are their higher viscosities (261 cP (40°C) and 800 cP (25°C))^{32,34} in comparison to Ethaline (36 cP (25°C))³⁵, resulting in slower mass transport in these solvents. For this reason, it was decided to use a hybrid DES containing 20 wt % of Reline or Oxaline in Ethaline. By only using 20 wt% of each solvent in conjunction with Ethaline, the pHs of these liquids will be slightly different to those quoted above. However, it is assumed that the presence of different ligands will provide an influence on the leaching rate of the Cu/Fe. To ensure no H₂S was produced in the experiment with 20 wt % Oxaline a dampened strip of lead acetate paper was suspended above the experiment and no blackening was observed.

The conditions used in each of these experiments are the same as was described for the Ethaline only experiment. A constant current of 5 mA was applied to the cell for 24 hours for each cathode. The resulting potential was similar to the previous experiment and was not altered by the addition of another DES. The results for the 5 consecutive Ni cathodes used in each experiment are shown in Figure 5.17. In both cases, the first plate consisted purely of Cu with no Fe, similar to the results obtained in the Ethaline only experiment. As the experiments progress there is a small amount of Fe appearing on the plates in both cases, however significantly less than for the Ethaline only experiment. The Ethaline + 20 wt % Oxaline 100 experiment showed the most promise, with minimal Fe present (<1.6 at%) on the cathode even after 5 repeats.

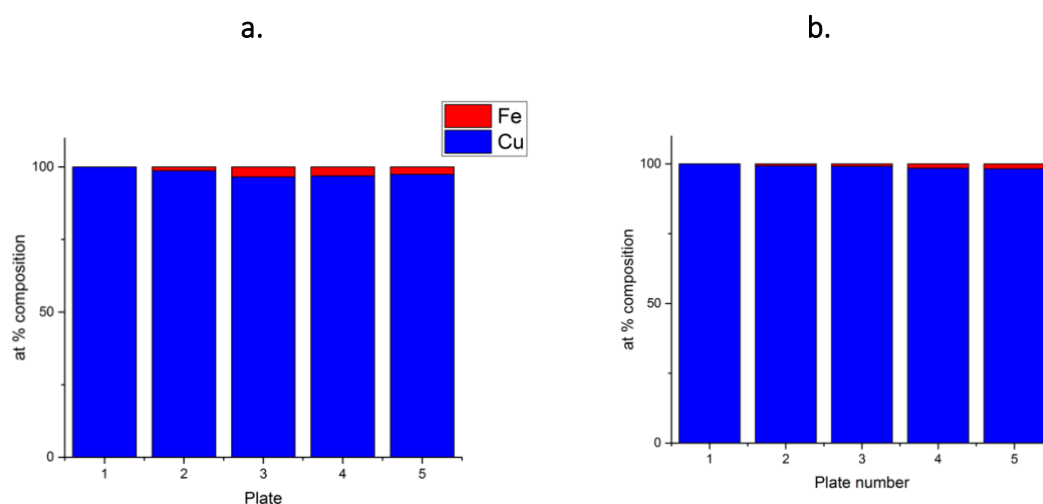


Figure 5.17: Fe:Cu composition of 5 consecutive Ni cathodes (each 5 mA for 24 hours) from the 20 wt % **a.** Reline or **b.** Oxaline in Ethaline, respectively.

Something to note about the Ni cathodes in the 20 % Reline experiment is how much thinner the coatings appeared in general, compared to the 20 % Oxaline experiments. This is visible in both the images and the SEM images in Figure 5.18, however this is not supported in the overall extraction masses in Table 5.4. The masses of all the plates in every experiment are shown in Table 5.4 and due to the low mass of individual plates the error will be quite large, however, it is certainly apparent that both the addition of Reline and Oxaline yielded more Cu on the cathodes overall compared to the Ethaline only experiment.

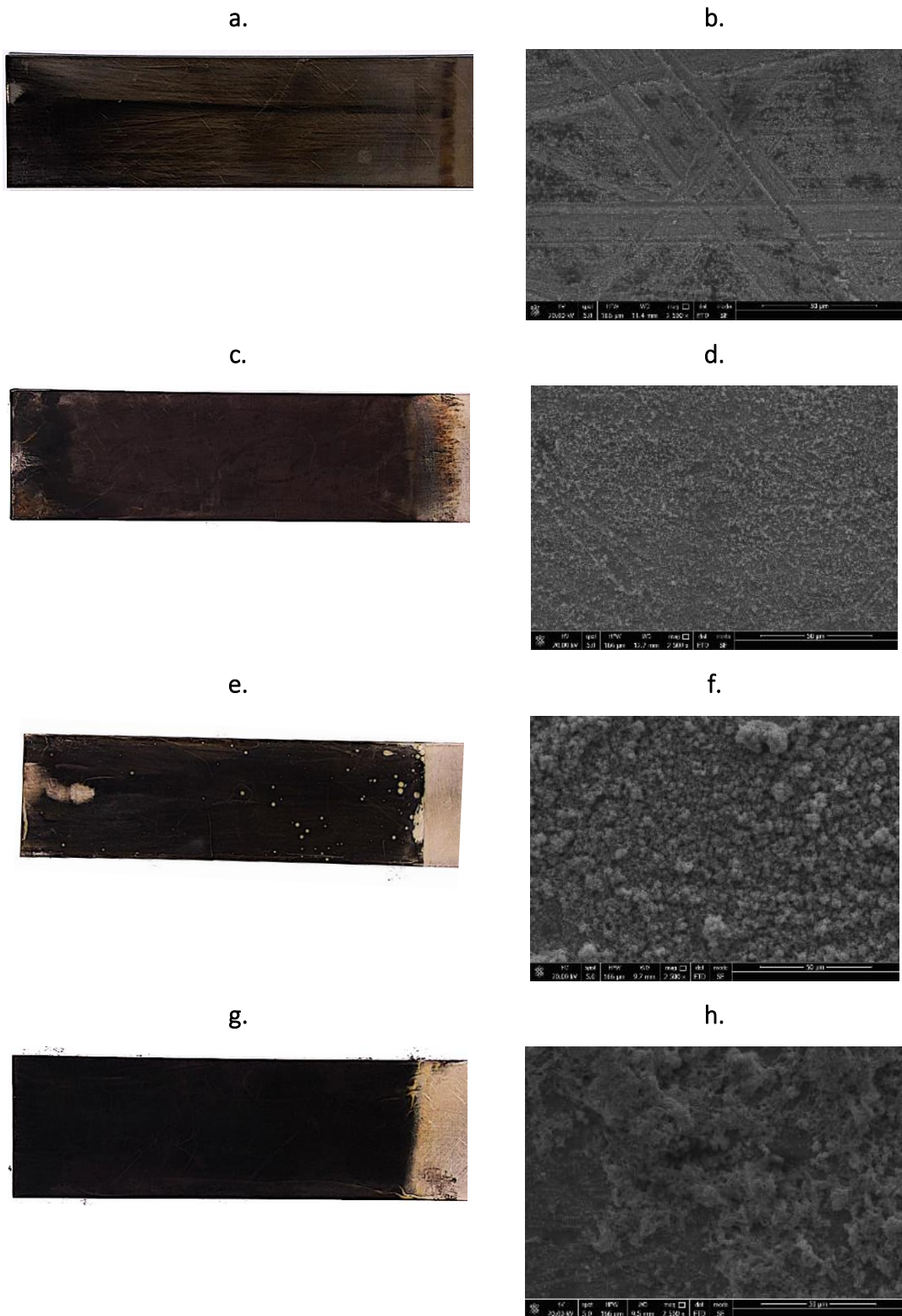


Figure 5.18: Ni cathodes from Ethaline + 20 % Reline experiments 1 & 5 (**a & c**), along with the corresponding SEM images of the surface (**b & d**). Ni cathodes from Ethaline + 20 % Oxaline experiments 1 & 5 (**e & g**), along with the corresponding SEM images of the surface (**f & h**). All cathodes are after 24 hours at 5 mA.

The crystals presented in both experiments are very different to what was observed in the Ethaline only experiment (Figure 5.13). The crystals in the SEM image in Figure 5.18b & d from the Reline experiment, show very small crystals. They are still dendritic, which as discussed earlier was expected from a fairly pure Cu deposit. The small crystals could be a result of the increased viscosity from the addition of Reline which ultimately affects the mass transport to the surface of the cathode and the rate at which the crystals form. A similar scenario is observed with the Oxaline experiment, the dendritic crystal shape is more apparent in Figure 5.18h however it remains dendritic throughout each experiment, again due to the higher purity Cu deposit.

Table 5.4: Masses and descriptions from each component of both the Reline and Oxaline experiments. Details are the same as Table 5.3.

Number	20 % Reline	20 % Oxaline	Description
1	59 g	51 g	Powdered Chalcopyrite (<1000 – 100 μm).
2	125 g	105 g	Solvent
3	0.94 g	0.7 g	Overall material on all Ni cathodes
4	71 g	62 g	Left over chalcopyrite paste with solvent
5	42 g	95 g	Liquid top layer
6	1.6 g	0.5 g	Sludge bottom layer (after wash and dry)

After each experiment a similar liquid/sludge mixture was leftover, as with the Ethaline experiment. The 20 wt% Reline and Oxaline experiments yielded a dark green and blue/grey solution, respectively, with a brown ‘sludge’ in both cases. The liquids were analysed similarly to above; however an interesting observation was that when the blue solution obtained from the 20 wt% Oxaline experiment was diluted further for UV-Vis measurements, the solution turned bright yellow. This has been attributed to the addition of a chloride rich solvent resulting in a ligand exchange between H_2O or oxalate (oxygen donor) and Cl.

The sludge present in both cases at the bottom of the cell after being washed and dried was less than for the Ethaline only experiment (1.6 g and 0.5 g respectively). The at % of each element are presented in Table 5.5. Although the overall amounts of Cu and O seem

to be increased in the sludge, it is actually reasonably similar to the pure Ethaline experiment due to the mass difference (i.e. For Cu there is 0.22 g in the Ethaline experiment, 0.46 g with Reline and 0.34 g with Oxaline leftover in the sludge). A key point to note is the significant reduction in the presence of S in the sludge, and to an extent Fe, in both cases but most noticeably in the Oxaline experiment. There also appears to be a trend relating the at % of Fe and S in all cases, suggesting that Fe sulfides are precipitating in some form. The Cu is possibly in some form of oxalate which under certain conditions can be quite insoluble, (shown by a precipitate forming when CuCl_2 at concentrations higher than 10mM are dissolved in Oxaline). Interestingly, the XRD of the sludge from the Reline experiment was similar to the Ethaline only experiment from previously, however the Oxaline sludge presented reflects that are similar to a chalcopyrite pattern. It is likely that this is due to an error in the experiment where some chalcopyrite escaped the basket. Clearly, this is not supported in the EDAX data and therefore is likely to be a mixed amorphous sludge along with a small amount of chalcopyrite.

Table 5.5: EDAX composition of sludge/bottom layer leftover from each 5 day electrowinning experiment changing Ni cathode every 24 hours (constant 5 mA).

Experiment	Cu at%	Fe at%	S at%	O at%	Mass (after drying) g
Ethaline only	10.5	17.1	36.2	36.2	2.1
Ethaline + 20	28.9	11.7	2.8	56.6	1.6
% Reline					
Ethaline + 20	67.5	6.6	1.1	24.8	0.5
% Oxaline					

5.5 Analysing the experiment design

5.5.1 Green metrics

It is generally accepted that in smaller scale experiments such as the ones shown in this Chapter, LCA's are unnecessary, not to mention time consuming and therefore not suitable.³⁶ Instead a selection of different equations can be applied to provide an overall

metric of the 'greenness' of an experiment. Due to the nature of the samples some metrics are either not useful or difficult to complete. To begin with the reaction mass efficiency takes into account the atom economy and the yield and can be used in 2 different forms (Equation 5.3 and 5.4):

$$\text{Mass efficiency} = \frac{\text{Molecular weight of product} \times \text{yield}}{\text{Molecular weight of reactant}} \quad \text{Equation 5.3}$$

$$\text{Mass efficiency} = \frac{\text{Mass of product} \times 100 \%}{\text{Mass of reactants}} \quad \text{Equation 5.4}$$

In the case of this experiment, the second version of the equation was used. The data presented for the Ethaline + 20 % Oxaline experiment was used as it showed the best results for consistency and purity, whereby the overall weight of the deposit collected on the Ni cathodes over 5 experiments was 0.7 g. The overall mass of the chalcopyrite sample in the tube to begin with was 51 g, therefore the reaction mass efficiency was calculated to be 1.37 %. This can be compared to the cell used by Al-Bassam in the recovery of metals from Jarosite. In this case the overall deposit obtained on the Cu cathodes after 13 days (6 separate cathodes) was 3.76 g from 500 g of jarosite. The reaction mass efficiency calculated from this is 0.75 %. It is interesting to compare this to the effective mass yield as well, where only the non-benign reagents are considered in the equation (Equation 5.5).

$$\text{Effective mass yield} = \frac{\text{Mass of product} \times 100 \%}{\text{Mass of non - benign reagents}} \quad \text{Equation 5.5}$$

If the purity of the sample is taken as the mass of the non-benign reagents, then it would be 41 g (80.5 % of 51 g) therefore the effective mass yield would now be 1.7 %. A similar analysis of the purity of the jarosite was not carried out as it was not suitable in that case due to the nature of jarosite. Overall, these metrics are only suitable in determining the environmental impact of a single reaction and not of a process as a whole. A more

suitable metric to establish the overall level of how green a process is, is the Environmental factor (E-Factor), which is calculated by Equation 5.6.

$$\text{E factor} = \frac{\text{Total mass of waste from process}}{\text{Mass of product}} \quad \text{Equation 5.6}$$

It is difficult to determine what waste is involved in the current experiment, simply because the solvent is still able to be used and the chalcopyrite sample shows no sign of slowing dissolution/extraction. One aspect that is determined to be completely wasted is the Ethaline lost on each Ni cathode when it is removed from the experiment. An experiment conducted to determine how much solvent is lost during each cathode replacement revealed that on average 0.82 g (4.1 g per 5 cathodes) of solvent is wasted. The sludge remaining at the bottom of the cell can also be considered as waste because the electrode is not in contact with this material. The solid material in the 20 % Oxaline experiment had a mass of 0.5 g. From this and comparing to the 0.7 g of product achieved from the experiment the E factor is 6.6. The E factor calculated in this case is in line with the waste: product ratio expected in a fine chemicals plant.³⁷ However, there is still likely to be other waste to deal with eventually, i.e. the benign material contained in the mineral sample, solvent that can no longer be re-used and any additional material that may precipitate at the bottom.

5.5.2 Cell design problems/improvements

This section deals with the overall problems presented by this cell design and some suggested improvements that could be made in future work. Clearly one of the biggest problems is the lack of material that is actually being extracted from the chalcopyrite in each experiment. It has already been discussed that this is primarily due to the very low current that is applied throughout the experiment. This was a necessity in the present cell to prevent solvent degradation, however, in future cell designs it is necessary to consider that a much higher current is required. The previous sections have shown key steps in improving the purity of the extracted Cu and decreasing or preventing the electrodeposition or precipitation of Fe or Fe complexes during electrowinning. Of the

potential improvements that could be made to these dissolution and recovery processes, three stand out, and will be discussed:

- Further improvements to cell design, e.g. by changing the anode/cathode set up and the location of the mineral material in order to increase surface area contact with the electrode and most importantly be able to increase the applied current.
- The inclusion of some degree of agitation or movement in order to aid the mass transport and maintain contact between DES and the surface of the chalcopyrite.
- Further hybridisation of the DES system, e.g. by addition of water^{38,39}

The cell design shown in Figure 5.12 cannot be accurately compared to the previous cell design by Al-Bassam as different material was used. The extraction methods that were used by Al-Bassam also differed from Cu extraction from chalcopyrite, in the sense that Pb, Fe and Zn were all being extracted at the same time. For this reason, extra room was required to accommodate the piece of Zn used in the cementation of Pb as well as the anode and cathode for electro recovery. The current cell design presented in Figure 5.12 has room for improvement in terms of increasing contact between the mineral, electrodes and electrolyte. The suggested improved design is shown in Figure 5.19. For this design the placement of the electrodes are different to the original design in Figure 5.12. The Ir coated Ti mesh anode is bent into a cylindrical shape with a circumference between that of the inner and outer tube. The idea behind this is to maximise the contact with the chalcopyrite and the mineral to reduce the effect of the passivation layer or shrinking core model. The inner porous tube contains the Ni cathode and is covered with the nylon material from the previous cell. Again, the purpose of switching the electrodes and location of the chalcopyrite is to increase the surface area of the anode that is in close proximity to the chalcopyrite and therefore should allow an even chance of electroplating the Cu. In order to utilise a larger current, a bigger electrode is required in order to reduce the current density. Currently the current density is 0.21 mA cm^2 , if the Ni cathodes used are larger, a larger current can ultimately be applied. To achieve this, one idea is to use a mesh cathode as opposed to a solid Ni sheet.

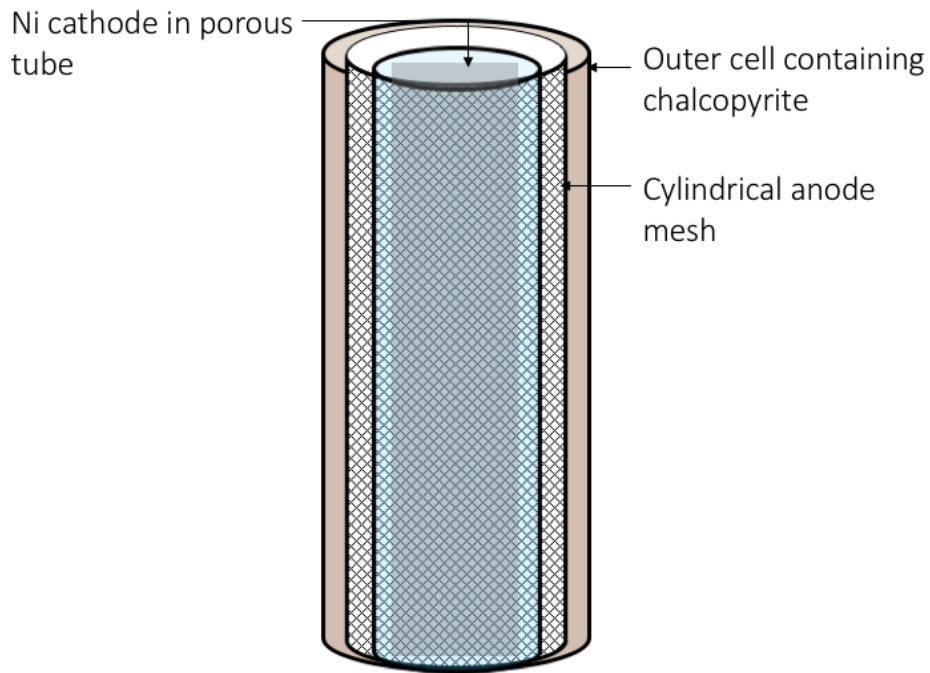


Figure 5.19: New and improved cell design idea, consisting of outer tube containing powdered mineral and large mesh anode parallel to the outer tube. Ni cathode is contained in a porous centre tube.

Another method of improving the efficiency and the general process of extraction is by agitating or moving the material/electrode in order to constantly renew the material at the anode surface. The continual renewal of material is particularly useful in this case and has been shown to be successful in other work with chalcopyrite to reduce the passivating effects on the electrode surface.⁴⁰ In the previous study by Al-Bassam, an orbital shaker plate was used in order to agitate the entire mixture, as opposed to using a stirrer bar which would not necessarily be effective throughout the cell.²⁴ A stirrer bar is also unsuitable for this application due to the use of a ferromagnetic Ni cathode. The concept of using an orbital shaker in this current experiment does not work as well because of the space restrictions between the inner cell, the cathode and the outer cell meaning the cathode would intermittently touch the either side of the cell causing deposit to fall off. Instead the idea with this cell could be to have some sort of overhead stirred electrode system. This way, the anode would be able to act as a stirrer, agitating the Ethaline that surrounds it, while in turn agitating the chalcopyrite paste in the outer

cell. This is likely to work better than a stirrer bar at the bottom of the cell as it should result in even stirring throughout the cell. Typically, overhead stirrers are deemed a more suitable alternative for larger volumes, more viscous liquids, and as a better replica for larger batch processes.⁴¹ Another option would be to apply ultrasound as another way to mechanically agitate the system.

Finally, the hybridisation of the DES is an interesting point of improvement. Chalcopyrite is notoriously refractory to leaching, both chemically and electrochemically. This presents problems that cannot be fixed solely by changing the cell design and although the hybrid DESs presented in this section have shown an improvement to the process, there is more that can be investigated. One option is to add varying degrees of water to the already hybrid DESs to improve the viscosity and therefore possibly improve aspects of the process. It has been shown previously by Al-Murshedi, that the addition of water aided in the electroplating of Cu. It was shown that the addition of small amounts of water (10-20 %) were beneficial for Cu metal deposition due to the effect on mass transport and increasing diffusion coefficients of Cu species in solution.³⁹ Additionally the increased water content altered anodic reactions, by shifting the onset potential to a less positive value.³⁹ Water also has the effect of reducing the viscosity of DESs therefore allowing easier treatment of them before, during and after the experiment. As a simple demonstration of this, sand was mixed with equivalent volumes of Ethaline and Ethaline + 20 wt % water. The mixtures were then passed through a Buchner funnel and the mass of the collected solvent was measured after an hour in both cases. 89.2 % of the Ethaline + 20 % water was recovered compared to 75.8 % of the Ethaline only solvent.

5.6 Conclusions

In this phase of the project, the electrochemistry of a more complex sulfide mineral was investigated. There are often problems associated with the hydrometallurgical processing of chalcopyrite as a result of passivation and subsequent lower reactivity rates. In this chapter it was shown that the paint casting of chalcopyrite was possible and a reasonable voltammogram was achieved. It was noted that the voltammogram looked very reminiscent of the CuS/Cu₂S from Chapter 3 and that it was not possible to

distinguish between the Cu and Fe redox couples that you would expect to be present. The use of the paint casting technique to achieve dissolution revealed that the solution colours were considerably less intense than the CuS/Cu₂S, likely demonstrating the slower dissolution rate, nevertheless, it was the characteristic yellow colour of the Cu sulfide dissolution from Chapter 3.

The cell that was utilised in the recovery experiments was the next generation in the series of cells that was reported in a previous thesis. The main problems with these designs was the separating membrane that was used (glass frit) became blocked by the formation of a precipitate which caused a drop, in efficiency. This was rectified to an extent in this cell by utilising a membrane with a much larger surface area to prevent the effect of inhibiting the ion movement. There are however problems associated with the passivation onto the electrode surface which reduces the available contact between the chalcopyrite and the anode. Whilst using the cell designed in this phase, the use of Ethaline resulted in a steady increase in the % of Fe being extracted on each plate. The use of hybrid DESs was investigated after its potential was proven in the EAF dust experiment explained previously. The use of 20 % Reline in Ethaline and 20 % Oxaline in Ethaline was trialled with better success in both cases. Overall the use of 20 % Oxaline in Ethaline was the most valuable as after 5 repeats, the purity of copper remained at no less than 98%. The use of 100 % Oxaline was inadvisable, as firstly the viscosity is too high and caused a lot of resistance when analysing the electrochemical behaviour. Secondly, and more importantly, the acidity of Oxaline led to the production of H₂S gas on electrolysing the chalcopyrite. It was tested that with only 20 % Oxaline no H₂S gas was generated and therefore containment issues were no longer a problem.

The main problem going forward is the cell design needs a great deal more work in order to increase the extraction efficiency of the Cu. Overall, the applied current needs to be increased in order to allow more material to be dissolved and more Cu to be electrodeposited. This can be achieved, but the cell design needs to be altered in order to allow a larger cathode, to ultimately reduce the current density and therefore apply a larger current.

5.7 References

1. Schlesinger, M. E., Kind, M. J., Sole, K. C., Davenport, W. G., (2011) Extractive Metallurgy of Copper, 5th Ed., Elsevier, Netherlands.
2. Baba, A. A., Ayinla, K. I., Adekola, F. A., Ghosh, M. K., Ayanada, O. S., Bale, R. B., Sheik, A. R., Pradhan, S. R., (2012) A Review on Novel Techniques for Chalcopyrite Ore Processing, *Int. J. Mining Eng. and Minl Proc*, **1**, 1-16.
3. Li, Y., Kawashima, N., Li, J., Chandra, A. P., Gerson, A. R., (2013) A Review of the Structure, and Fundamental Mechanisms and Kinetics of the Leaching of Chalcopyrite, *Adv. Colloid and Interface Sci.* **197-198**, 1-32
4. Pearce, C. I., Patrrick, R.A.D., Vaughan, D.J., Henderson, C.M.B., van der Laan, G., (2006) Copper Oxidation State in Chalcopyrite: Mixed Cu d9 and d10 Characteristics, *Geochimica et Cosmochimica Acta*, **70**, 4635–4642
5. Shuey, R. T. (1975) Semiconducting Ore Minerals, 1st Ed., Elsevier, The Netherlands
6. Bowden, J. L., Young, C. A., (2016) Xanthate Chemisorption at Copper and Chalcopyrite Surfaces, *The Journal of the Southern African Institute of Mining and Metallurgy*, **116**, 503-508
7. Adebayo, A.O., Ipinmoroti, K.O., Ajayi, O. O., (2003) Dissolution Kinetics of Chalcopyrite with Hydrogen Peroxide in Sulfuric Acid Medium, *Chem. Biochem. Eng. Q.*, **17**, 213-218.
8. Zhao, H., Hu, M., Li, Y., Zhu, S., Qin, W., Qiu, G., Wang, J., (2015) Comparison of Electrochemical Dissolution of Chalcopyrite and Bornite in Acid Culture Medium, *Trans. Nonferrous Metals Soc. China*, **25**, 303-313
9. Lundstrom, M., Aromaa, J., Forsen, O., Barker, M .H., (2013) Reaction Product Layer on Chalcopyrite in Cupric Chloride Leaching, *Canadian Metallurgical Quarterly*, **47**, 245-252.

10. Watling, H. R., (2013) Chalcopyrite Hydrometallurgy at Atmospheric Pressure:1. Review of Acidic Sulfate, Sulfate-Chloride and Sulfate Nitrate Process Options, *Hydromet.*, **140**, 163-180.
11. Batty, J. D., Rorke, G. V., (2006) Development and Commercial Demonstration of the BioCOP Thermophile Process, *Hydromet.*, **83**, 83-89
12. Dixon, D. G., Mayne, D. D., Baxter, K. G., (2008) Galvanox: A Novel Galvanically Assisted Atmospheric Leaching Technology for Copper Concentrates, *Can. Metall Quarterly*, **47**, 327-336
13. Kuzmina, O., Symianakis, E., Godfrey, D., Albrecht, T., Welton, T., (2017) Ionic Liquids for Metal Extraction from Chalcopyrite: Solid, Liquid and Gas Phase Studies, *Phys. Chem. Chem. Phys.*, **19**, 21556-21564.
14. Dong, T., Hua, Y., Zhang, Q., Zhou, D., (2009) Leaching of Chalcopyrite with Bronsted Acidic Ionic Liquids, *Hydromet.*, **99**, 33-38.
15. Whitehead, J. A., Zhang, J., Pereira, N., McCluskey, A., Lawrance, G. A., (2007) Application of 1-alkyl-3-methyl-imidazolium Ionic Liquids in the Oxidative Leaching of Sulfidic Copper, Gold and Silver Ores, *Hydromet.*, **88**, 109-120
16. Carlesi, C., Cortes, E., Dibernardi, G., Morales, J., Muñoz, E., (2016) Ionic Liquids as Additives for Acid Leaching of Cu from Sulfidic Ores, *Hydromet.*, **161**, 29-33
17. Al-Zubeidi, A., Godfrey, D., Albrecht, T., (2018) Disentangling Chemical Effects in Ionic Liquid Based Cu Leaching from Chalcopyrite, *J. Electroanal. Chem.*, **819**, 130-135
18. Hu, J., Tian, G., Zi, F., Hu, X., (2017) Leaching of Chalcopyrite with Hydrogen Peroxide in 1-Hexyl-3-Methyl Imidazolium Hydrogen Sulfate Ionic Liquid Aqueous Solution, *Hydromet.*, **169**, 1-8.
19. Safari, V., Arzpeyma, G., Raschi, F., Mostoufi, N., (2009) A Shrinking Particle-Shrinking Core Model for Leaching of a Zinc Ore Containing Silica, *Int. J. Miner. Process.*, **93**, 79-83

20. Hackl, R. P., (1977) BSc Thesis: University of British Columbia, Reduction Leaching of Chalcopyrite
21. Abbott, A. P., Al-Bassam, A. Z. M., Goddard, A., Harris, R. C., Jenkin, G. T. J., Nisbet, F., Wieland, M., (2017) Dissolution of Pyrite and Other Fe-S-As Minerals using Deep Eutectic Solvents, *Green Chem.*, **19**, 2225-2233
22. Manan, N. S. A., Aldous, L., Alias, Y., Murray, P., Yellowlees, L. J., Lagunas, M C., Hardacre, C., (2011) Electrochemistry of Sulfur and Polysulfides in Ionic Liquids, *J. Phys. Chem. B.*, **115**, 13873-13879
23. Parker, A. J., Paul, R. L., Power, G. P., (1981) Electrochemistry of the Oxidative Leaching of Copper from Chalcopyrite, *J. Electroanal. Chem.*, **118**, 305-316.
24. Al-Bassam, A. Z. M. H., (2018) PhD Thesis: University of Leicester, Mineral Processing using Deep Eutectic Solvents
25. Hartley, J. M., Ip, C. M., Forrest, G. C. H., Singh, K., Gurman, S. J., Ryder, K. S., Abbott, A. P., Frisch, G., (2014) EXAFS Study into the Speciation of Metal Salts Dissolved in Ionic Liquids and Deep Eutectic Solvents, *Inorg. Chem.*, **53**, 6280-6288
26. Hartley, J. (2013) PhD Thesis: University of Leicester, Ionometallurgy: The Processing of Metals Using Ionic Liquids.
27. Al-Murshedi, A. Y. M., (2018) PhD Thesis: University of Leicester, Deep Eutectic Solvent- Water Mixtures.
28. Abbott, A. P., Capper, G., Swain, B., Wheeler, D., (2005) Electropolishing of Stainless Steel in an Ionic Liquid, *Trans. Inst. Metal Finish*, **82**, 51-53
29. Abbott, A. P., Capper, G., McKenzie, K. J., Ryder, K. S., (2006) Voltammetric and Impedance Studies of the Electropolishing of Type 316 Stainless Steel in a Choline Chloride Based Ionic Liquid, *Electrochim. Acta*, **51**, 4420-4425.
30. Abbott, A. P., Capper, G., Davies, D. L., Rasheed, R., Shikotra, P., (2005) Use of Deep Eutectic Solvents for the Selective Extraction of Metals from Mixed Oxide Matrices, *Inorg. Chem.*, **44**, 6497-6499.

31. Abbott, A. P., Capper, G., Davies, D. L., McKenzie, K. J., Obi, S. U., (2006) Solubility of Metal Oxides in Deep Eutectic Solvents Based on Choline Chloride, *J. Chem. & Eng. Data*, **51**, 1280-1282
32. Abbott, A. P., Capper, G., Davies, D. L., Shikotra, P., (2006) Processing Metal Oxides using Ionic Liquids, *Mineral Processing and Extractive Metallurgy*, **115**, 15-18
33. Alabdullah, S. S. (2018) PhD Thesis: University of Leicester, pH Measurements in Ionic Liquids.
34. Abbott, A. P., Ahmed, E. I., Harris, R. C., Ryder, K. S., (2014) Evaluating Water Miscible Deep Eutectic Solvents (DESs) and Ionic Liquids as Potential Lubricants, *Green Chem.*, **16**, 4156-4161
35. Endres, F., Abbott, A. P., MacFarlane, D., (2008) *Electrodeposition from Ionic Liquids*, 1st Ed., Wiley-VCH,
36. McElroy, C. R., Constantinos, A., Jones, L. C., Summerton, L., Clark, J. H., (2015) Towards a Holistic Approach to Metrics for the 21st Century Pharmaceutical Industry, *Green Chem.*, **17**, 3111-3121.
37. Isac-García, J., Dobado, J. A., Calvo-Flores, F. G., Martínez-García, H., (2016) *Experimental Organic Chemistry*, 1st Ed. Academic Press, UK.
38. Azaga, R. M. M., (2018) PhD Thesis: University of Leicester, Surfactant Aggregation in DESs.
39. AL-Murshedi, A. Y. M., (2018) PhD Thesis: University of Leicester, Deep Eutectic Solvent- Water Mixtures.
40. Zhao, H., Wang, J., Qin, W., Hu, M., Qiu, G., (2015) Electrochemical Dissolution of Chalcopyrite Concentrate in Stirred Reactor in the Presence of Acidithiobacillus Ferrooxidans, *Int. J. Electrochem. Sci.*, **10**, 848-858
41. <https://www.caframolabsolutions.com/application/dissolving/magnetic-or-overhead-stirrer/> (accessed 4/06/19)

CHAPTER 6: CONCLUSIONS AND FUTURE WORK

Table of Contents

6.1 Conclusions..... 198

6.2 Suggestions for future work..... 202

6.1 Conclusions

The purpose of this study was to investigate the electrochemical behaviour of metal chalcogenides in DESs with the aim of separating the two components and electro-recovering the metals. While Fe sulfide minerals have been studied previously, the main aim was to solubilise them enabling recovery of more valuable elements which they might encapsulate. It was proposed that extraction methods using DESs could provide an alternative route of treatment to the typical hydro- and pyro-metallurgical processing commonly used for most minerals. The aim is to develop a process that does not lead to noxious gas formation such as SO_x or H_2S , H_2Se and H_2Te .

The work on sulfide minerals in the present study is centred around Cu due to its important and extensive uses around the world. Three separate Cu minerals were analysed; the simple Cu sulfides covellite and chalcocite were investigated together with the more common multi metallic sulfide, chalcopyrite, CuFeS_2 . Both covellite and chalcocite had similar voltammetry and were both easy to leach and recover copper from.

In Chapter 3 the novel paint casting method was demonstrated using galena (PbS) together with covellite and chalcocite. Paint casting functioned successfully within a limited mass loading range presumably due to the resistivity caused by the mineral layer on the electrode. Synthetic CuS was used initially and different parameters were altered within the paint casting experiments to determine the capabilities of the technique. The scan rate, temperature, water content, mass loading and purity were all investigated, and it was ultimately determined that the behaviour, although affected by each of these parameters could still be analysed within a wide range. It was also found through altering the mass applied to the surface of the electrode and the purity of the sample (through adding varying amounts of an inert material) the results from paint casting were semi-quantitative. This technique could provide a quick and easy initial study of a mineral to determine an approximate metal content in the mineral. Paint casting was carried out on mineral samples of covellite, chalcocite and chalcopyrite of high purity ($\sim 80\%$) as well as a sample of galena. These results showed that it was possible to obtain reasonable results from natural materials that corresponded closely to that of the pure synthetic material.

Moving on from this, Chapter 3 looked at the ability of paint casting to leach and ultimately extract the Cu (and Pb) contained within these materials. The Cu sulfides as well as Cu selenide and telluride were electrolysed, and, in all cases, Cu ended up being leached into the electrolyte and ultimately a Cu coating was extracted onto a Ni cathode. Interestingly, EXAFS and UV-Vis studies revealed the speciation in the solutions from the different Cu compounds differed, e.g. the Cu sulfides resulted in CuCl_4^{2-} ions in solution, whereas the Cu selenides produced solutions containing a mixture of CuCl_2^- and CuCl_3^{2-} . Cu_2Te resulted in solutions that could not be easily analysed by EXAFS and it was suggested that the Cu was coordinated to an O which was also possibly associated with the Te in the form of a tellurate or tellurite. In Chapter 5 the same dissolution was carried out on the chalcopyrite sample to reveal the same speciation as was observed with Cu^I present in solution as it was from the Cu_2Se solutions. In the same extraction experiment, the chalcopyrite resulted in a material that was mainly Cu with a small amount of FeS_2 also present.

Chalcopyrite, as mentioned previously is currently the main source of Cu worldwide. Hence making it the focus for an investigation into metal extraction in the final stages of this study. The investigation was taken beyond that investigated in Chapter 3 by increasing the size of the extraction vessel by over 10 times. The experiment using this new cell design built on a previous investigation into the recovery of metals from jarosite (a common mining waste). The same cell could not be used in both experiments due to the unnecessarily large vessel used in the jarosite study. The main concern raised in the previous study was that any separating material that was used to section the anodic and cathodic areas of the cell were causing a decrease in efficiency over time. Also, the orientation of the cell was causing a build-up of solid material that was increasing the blockage of the separator. A vertically orientated cell was developed with the main aim of improving the separator material and ultimately prevent the build-up of material which results in an overall decrease in efficiency. The cell design consisted of a central basket that contained both the chalcopyrite and the anode, this was surrounded with a nylon mesh that enabled metal ions in solution to pass through but prevented any solid material leaving the basket. This basket was then contained within a glass tube which also contained the Ni anode and was filled with Ethaline (the electrolyte). The nylon mesh

differed from previous separating materials such as filter paper and a glass frit, firstly because of its larger pore size and secondly the large surface area that was available for diffusion. In the previous cells, the area that was provided for diffusion of metal ions was small in comparison to the cell size. The cell in the present study was used for 5 consecutive experiments, replacing the cathode but nothing else, with no apparent loss of efficiency.

The difficulty with processing chalcopyrite is its inherent refractory nature which makes leaching it very slow with the efficiency of leaching decreasing over time due to the formation of a passivation layer. This possibly contributed to the low level of extraction however, this was ultimately the result of using a very low current. This is one of the biggest areas for future work which was discussed in more depth in Chapter 5. Aside from altering the cell design, the development of solvent choice was also applied. It has been shown in previous studies that different DESs alter the speciation and solubility of different metals and that their properties can be tuned by mixing varying DESs to make a so-called hybrid DES. In the present study, Ethaline was mixed with 20 % Reline and then with 20 % Oxaline. The main differences noted in these experiments compared to the Ethaline only experiment was that on the 5 consecutive cathode replacements the Ethaline only experiment resulted in increasing amounts of Fe on the surface of the cathodes. Whereas, with the addition of Reline and even more so the addition of Oxaline, the cathodes remained with a fairly pure Cu coating throughout the entire experiment.

The other main focus of this study was on the other chalcogens and chalcogenides aside from sulfur. Tellurium and selenium are important elements and their compounds with other metals are increasingly more in demand through the growing demand in technologies including solar cells. Both Te and Se are widely dispersed and not very abundant in the Earth's crust, therefore mining for them is not a suitable option. Instead they are both most often recovered as by-products from anode slimes, most specifically from the Cu mining industry. Currently, Te and Se and their associated metals found in solar cells are not recycled and recovered, and that is one focus that drives this section of the study. It was thought that obtaining electrochemical behaviour information from these compounds could provide the groundwork to develop an extraction and recovery method to be able to re-use the elements in further solar panels. The tellurides and

selenides that were investigated were Cd and Zn for their properties that make them key players in the solar cell industry as well as Cu and Ag for comparison purposes. It had been hypothesised that the rate of dissolution was controlled by the conductivity of the materials.

In Chapter 4 the paint casting technique that was analysed in Chapter 3 was trialled with a range of materials of varying conductivities. It was noted in this chapter that although it was possible to study low conducting materials there was a limit. ZnS, although able to provide a CV, did not present any characteristic peaks. In this particular chapter, only one natural mineral was investigated, sphalerite (ZnS). Sphalerite is the most common ore of Zn and it is one of the most common sulfide minerals in existence. It is often found in a very wide variety of colours, all dependent on the levels of Fe also contained in the mineral. In the paint casting investigation, 2 samples were analysed, a light (low or no Fe) and a dark (high Fe) sample. The light sample presented a CV similar to that of pure ZnS whereas the dark Fe sample produced a CV that looked very similar to a previous CV on pyrite (FeS_2). As another application of paint casting, this is a quick and easy method to determine rough compositions of a sphalerite sample, without the need for longer more laborious analysis. In the remaining paint casting investigation, CdS, CdSe, CdTe, ZnTe, ZnSe, Ag_2S , Ag_2Se and Ag_2Te were also analysed. The charge that was passed in each CV was also plotted against their direct band gap as a method of analysing the rate of dissolution. It was hypothesised that the charge would increase in relation to the band gap decreasing and therefore the material being more conductive. This hypothesis was supported by the data from the Zn and Ag chalcogenides however, the Cd telluride result exhibited a very low charge with respect to the selenide.

A 24-hour electrochemical dissolution was carried out and the speciation of the solutions was analysed by a variety of techniques, spot tests and HPLC-ICP-MS were in agreement of the presence of tellurate/tellurite and selenate/selenite species in solution with the corresponding metals likely forming chloride salts. From here, the bulk electrolysis experiment that was carried out in Chapter 3 and at the beginning of Chapter 5 for the extraction of Cu from its various sulfides, selenides and tellurides was carried out on each of the metal tellurides and selenides. This was with limited success with only the Ag_2Te presenting a pure Ag coating on the cathode. There is a lot of extra investigation

that can be done for this section of work and this is discussed in much more depth in the next section.

6.2 Suggestions for future work

This study has shown that metal chalcogenides can be processed using DESs and prevent most of the noxious gases produced by hydro- and pyro-metallurgy. There are, however, many important aspects of the DES based approach that still need to be investigated. The main aim was to develop a method to recover selenium and tellurium. While the speciation in solution was identified, a method of recovering these elements was not completed. It would still be interesting to obtain a greater depth of information regarding the speciation of Se and Te, as well as the metals Cd, Zn and Ag using EXAFS, and comparing them against standard compounds to further understand the leaching process. It would also be interesting to construct a Pourbaix diagram for species in DESs, but this will require thermodynamic data on the compounds in DESs which could be obtained using calorimetry.

As for the recovery of Te and Se, extraction of chalcogenides back to the elemental chalcogen has been demonstrated using spot tests, utilising strong reducing agents. An important area of research would be to study what types of chemical reducing agents could be sustainably and economically used to reduce selenate, selenite, tellurate and tellurite to their elemental forms.

Initially, an aim of the project was to demonstrate the extractive technology using CdTe from waste solar cells. The inefficiency of the chalcopyrite process in Chapter 5 meant that it was not worth scaling up with CdTe due to the toxicity of the material and its constituents. Another question that needs to be investigated is whether metals could be directly recovered by reduction. It has already been shown that copper oxide can be directly electroreduced in DESs to produce metallic copper, but it could be interesting to see if the same could be carried out for other metal chalcogenides.

It has been observed, not only in this study, but in more numerous electrodeposition studies, that metal deposition in DESs can lead to deposits with limiting thickness. This could be due to passivation of the electrodeposit or depletion of the solution to such an

extent that the metal no longer deposits. This is a known phenomenon with DESs but the causes are not fully understood. Rotating disc electrode experiments could inform about mass transport issues, and electrochemical impedance spectroscopy could provide evidence of passivation and film formation. This could help with improved design for the electrolysis cell. Improved mass transport could be obtained through electrode oscillation or through the application of ultrasound or solution pumping. Experiments in the group have used an overflow cell for metal plating of chromium and these have overcome limiting metal thickness issues. The majority of the experiments described in this thesis used constant potential, whereas most electrowinning experiments are carried out at constant current, as the reduction potential will decrease in a Nernstian manner as the concentration of metal decreases.

To increase the rate of mineral digestion a fluidised bed could be used with a source of agitation (mechanical, gas or ultrasound). The level of agitation will need to be optimised to enable sufficient time for the minerals to be oxidised before the bed is refreshed.

An important issue that needs to be quantified is the mass and energy balance of the process. It is essential to quantify the solvent loss onto the gangue mineral and methods of recovering any DES absorbed on the material. It is also important to use less solvent and develop an efficient method of recovering the DES at the end of the process. It is important to compare the electrodeposition efficiency of metal recovery and the overall energy balance of the process compared to classical hydrometallurgy.

CHAPTER 7: APPENDIX

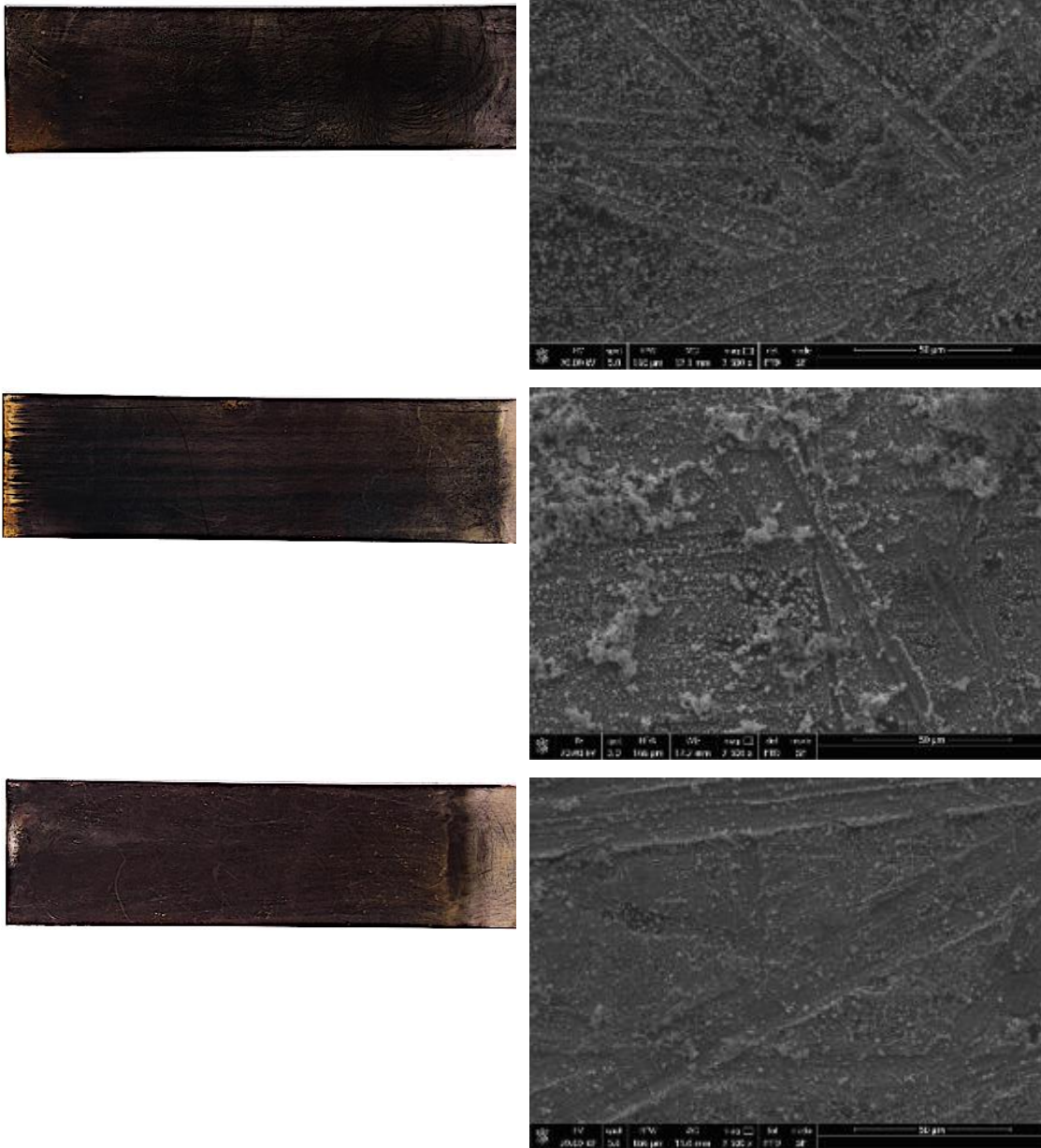


Figure 7.1: Experiment 2,3 & 4 Ni cathodes and SEM images from Chapter 5 Ethaline + 20 % Reline experiment. Each plate is a result of subsequent 24 hour experiments at 0.05 A.

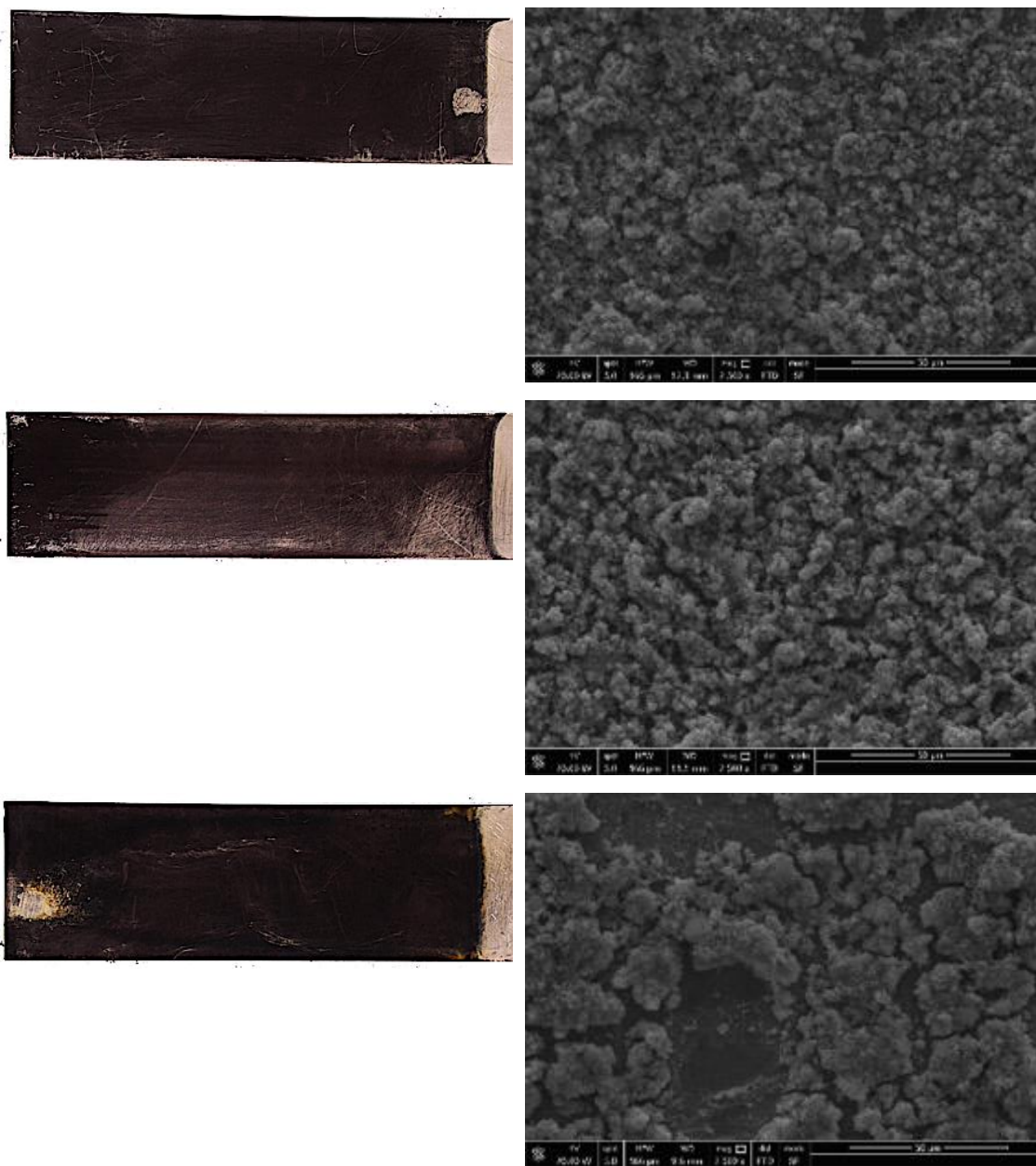


Figure 7.2: Experiment 2,3 & 4 Ni cathodes and SEM images from Chapter 5 Ethaline + 20 % Oxaline experiment. Each plate is a result of subsequent 24 hour experiments at 0.05 A.

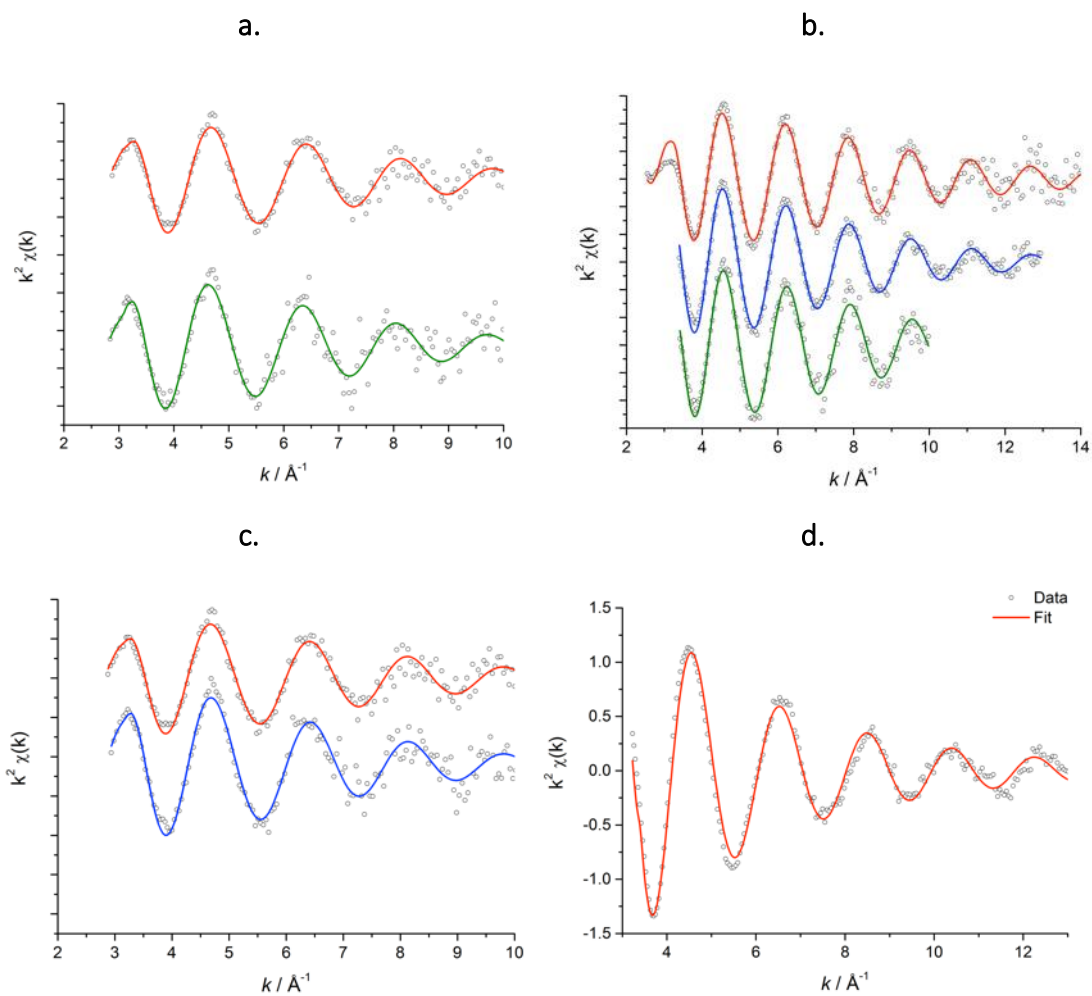


Figure 7.3: EXAFS results from Chapter 3 and 5. **a.** Chalcopyrite, **b.** CuS and Cu₂S, **c.** Cu₂Se and **d.** Cu₂Te. All solutions obtained from electrochemical dissolution for 24 hours at 1.5 V in Ethaline with IrO₂ coated electrodes.

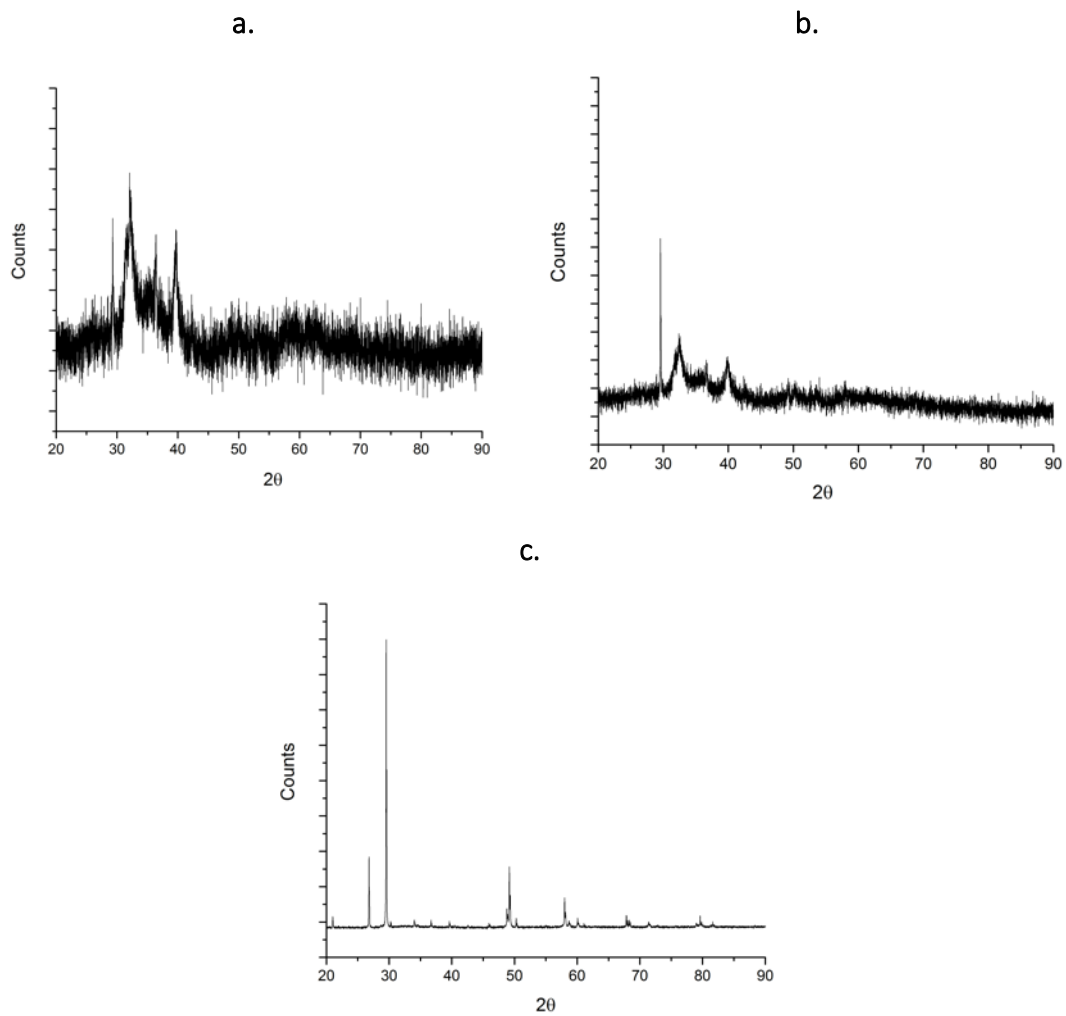


Figure 7.4: XRD of the bottom layer from the cell in Chapter 5 chalcopyrite experiment after 5 consecutive 24 hour experiments at 0.05 A. **a.** 100 % Ethaline, **b.** Ethaline + 20 % Reline, **c.** Ethaline + 20 % Oxaline.

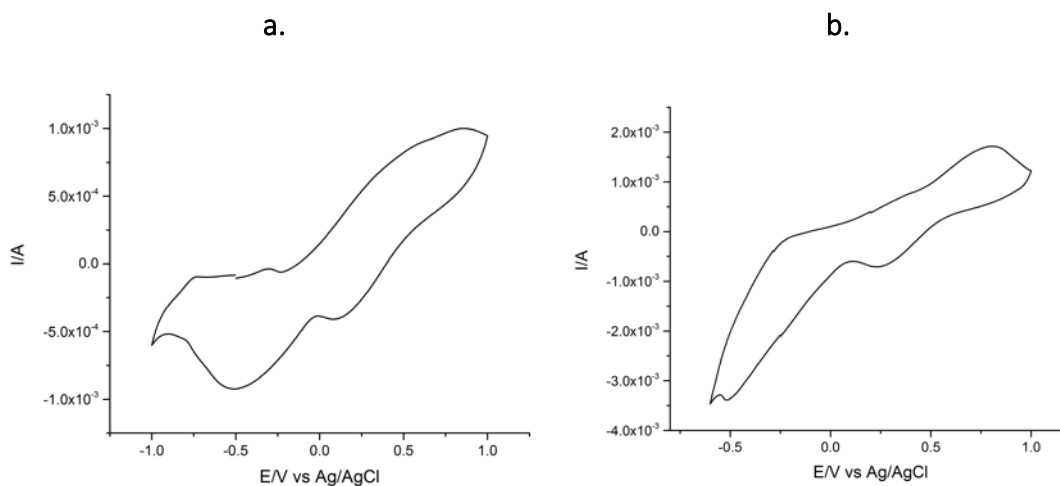


Figure 7.5: Paint casting CV of CuS in **a.** Reline electrolyte and **b.** Oxaline electrolyte. Both voltammograms conducted with 1 cm^2 Pt flag working and counter electrode and an Ag/AgCl [0.1 M in Ethaline] reference electrode at a scan rate of 5 mVs^{-1} .

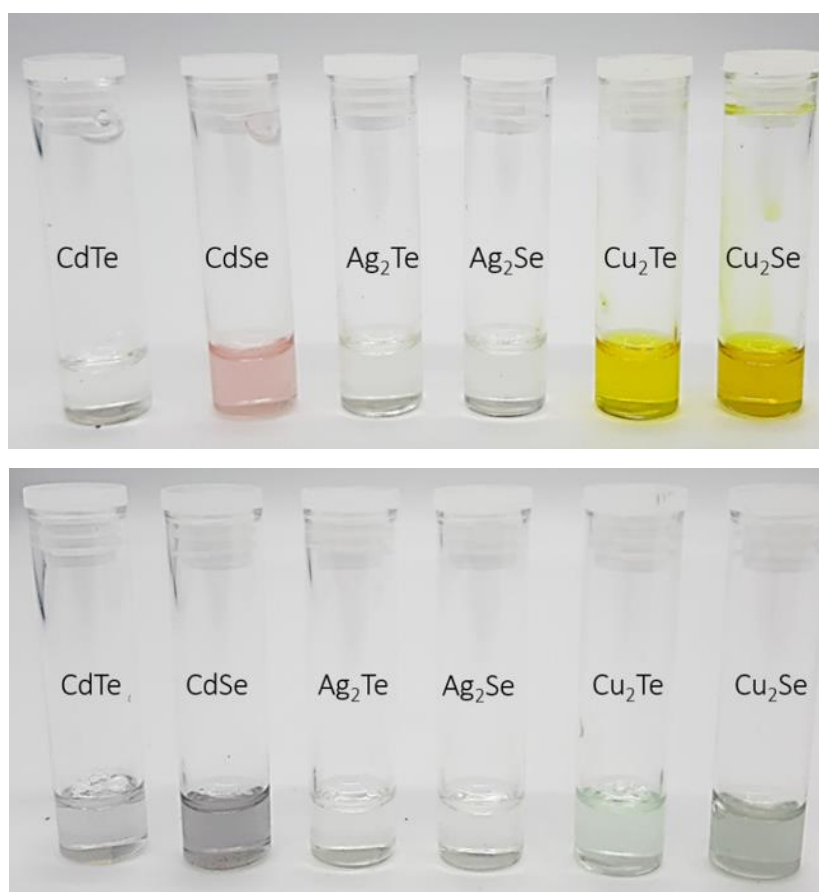


Figure 7.6: The resultant solutions from the 48 hour chemical dissolution in oxaline (top row) and in ethaline (bottom row).